AD-A140 767 LASER PROBES OF PROPELLANT COMBUSTION CHEMISTRY(U) SRI INTERNATIONAL MENLO PARK CA D R CROSLEY ET AL. 29 MAR 84 SRI-MP-84-053 ARO-17416.9-CH DAAG29-80-K-0049 1/3

UNCLASSIFIED F/G 7/4 NL

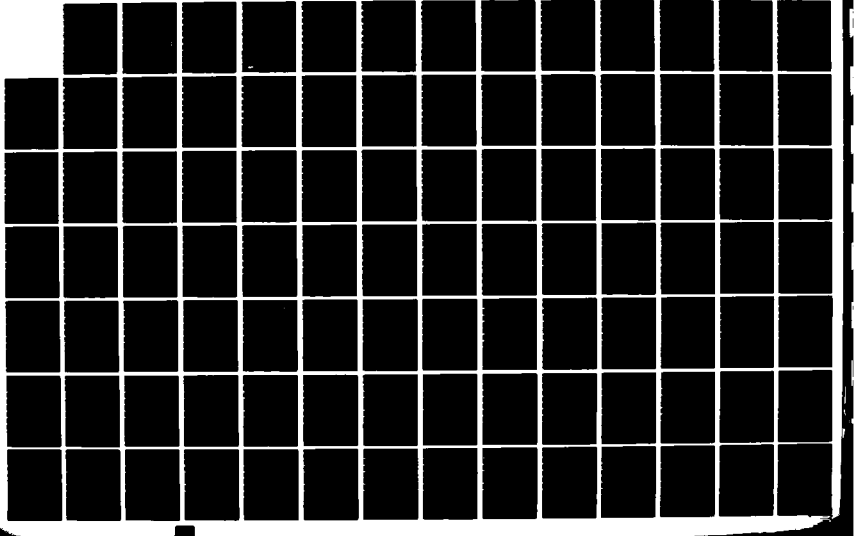

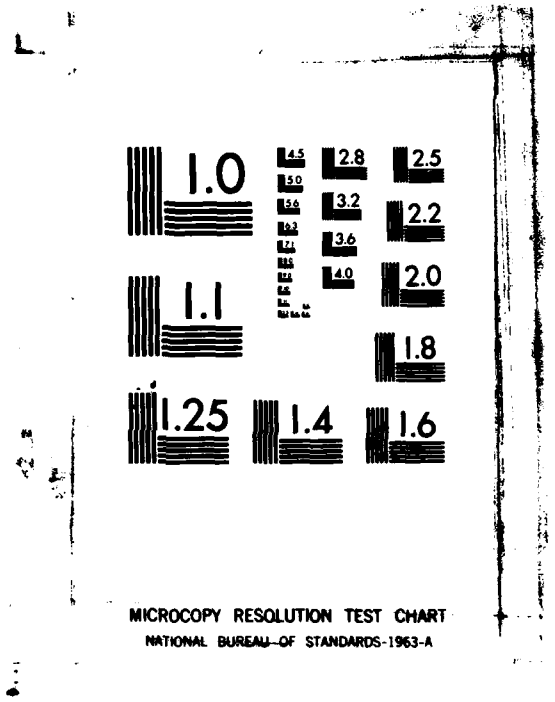
1.0
1.1
1.25
1.4
1.6
1.8
2.0
2.2
2.5
2.8
3.2
3.6
4.0
4.5
5.0
5.6
6.3
MICROCOPY RESOLUTION TEST CHART
NATIONAL BUREAU OF STANDARDS-1963-A

(2)

SECURITY CLASSIFICATION OF THIS PAGE (When Data Entered)

REPORT DOCUMENTATION PAGE	READ INSTRUCTIONS BEFORE COMPLETING FORM
1. REPORT NUMBER: ARO 17416.9-CH	2. GOVT ACCESSION NO.: AD-A140 767
	3. RECIPIENT'S CATALOG NUMBER
4. TITLE (and Subtitle): LASER PROBES OF PROPELLANT COMBUSTION CHEMISTRY	5. TYPE OF REPORT & PERIOD COVERED: Final, ~~1 October 1980~~ 30 Sep 80 to 31 January 1984
	6. PERFORMING ORG. REPORT NUMBER
7. AUTHOR(s): David R. Crosley, Gregory P. Smith, and David M. Golden	8. CONTRACT OR GRANT NUMBER(s): DAAG29-80-K-0049
9. PERFORMING ORGANIZATION NAME AND ADDRESS: SRI International, 333 Ravenswood Avenue, Menlo Park, California 94025	10. PROGRAM ELEMENT, PROJECT, TASK AREA & WORK UNIT NUMBERS
11. CONTROLLING OFFICE NAME AND ADDRESS: U.S. Army Research Office, P.O. Box 12211, Research Triangle Park, NC 27709	12. REPORT DATE: March 29, 1984
	13. NUMBER OF PAGES: 198
14. MONITORING AGENCY NAME & ADDRESS(if different from Controlling Office)	15. SECURITY CLASS (of this report): Unclassified
	15a. DECLASSIFICATION DOWNGRADING SCHEDULE

16. DISTRIBUTION STATEMENT (of this Report)

Approved for public release; distribution unlimited.

17. DISTRIBUTION STATEMENT (of the abstract entered in Block 20, if different from Report)

N/A

18. SUPPLEMENTARY NOTES

The view, opinions, and/or findings contained in this report are those of the author(s) and should not be construed as an official Department of the Army position, policy, or decision, unless so designated by other documentation.

19. KEY WORDS (Continue on reverse side if necessary and identify by block number)

Laser induced fluorescence, combustion chemistry, free radicals, laser pyrolysis, laser combustion diagnostics, collisional quenching, rate constants, modelling

20. ABSTRACT (Continue on reverse side if necessary and identify by block number)

Laser-induced fluorescence (LIF) can be used to measure the atomic, diatomic, and triatomic free radicals that are the intermediates in combustion chemistry. Coupled with detailed models, which incorporate a sound and consistent set of reaction rate constants, such measurements can lead to an understanding of that chemistry, having predictive value for use under experimentally difficult conditions.

DD FORM 1 JAN 73 1473 EDITION OF 1 NOV 65 IS OBSOLETE

SECURITY CLASSIFICATION OF THIS PAGE (When Data Entered)

This report describes the development of LIF techniques, the applications of such techniques to flames and to laser pyrolysis/laser fluorescence kinetics experiments, studies of rate constant estimations and detailed modeling of combustion chemistry. The chemistry studied is that of combusting mixtures of CH_4/N_2O, CH_2O/N_2O, CH_2O/NO_2, and related compounds. These contain the chemical networks, individual reactions, and radical species present in the gas-phase combustion of nitramine propellants, such as HMX and RDX.

The tasks described are LIF diagnostic studies on O, N, OH, NCO, and NH_2 in flow systems and flames, rate constant estimation studies for unimolecular decomposition of CH_2O and several hydrocarbons, modelling of the CH_2O/N_2O flame, and laser pyrolysis/laser fluorescence studies of CH_4/N_2O and CH_2O/N_2O chemistry.

ARO 17416.9-CH

SRI International

March 29, 1984

Final Report

LASER PROBES OF PROPELLANT COMBUSTION CHEMISTRY

By: D. R. Crosley, G. P. Smith, and D. M. Golden

Prepared for:

U.S. ARMY RESEARCH OFFICE
P.O. Box 12211
Research Triangle Park, NC 27709

Attn: Dr. G. M. Wyman

Contract No. DAAG29-80-K-0049
SRI Project No. 2230
MP 84-053

Approved:

D. C. Lorents, Director
Chemical Physics Department

G. R. Abrahamson
Vice President
Physical Sciences Division

SRI International®
333 Ravenswood Ave. • Menlo Park, CA 94025
(415) 326-6200 • TWX: 910-373-2046 • Telex: 334-486

ABSTRACT

Laser-induced fluorescence (LIF) can be used to measure the atomic, diatomic, and triatomic free radicals that are the intermediates in combustion chemistry. Coupled with detailed models, which incorporate a sound and consistent set of reaction rate constants, such measurements can lead to an understanding of that chemistry, having predictive value for use under experimentally difficult conditions.

This report describes the development of LIF techniques, the applications of such techniques to flames and to laser pyrolysis/laser fluorescence kinetics experiments, studies of rate constant estimations and detailed modeling of combustion chemistry. The chemistry studied is that of combusting mixtures of CH_4/N_2O, CH_2O/N_2O, CH_2O/NO_2, and related compounds. These contain the chemical networks, individual reactions, and radical species present in the gas-phase combustion of nitramine propellants, such as HMX and RDX.

The tasks described are LIF diagnostic studies on O, N, OH, NCO, and NH_2 in flow systems and flames, rate constant estimation studies for unimolecular decomposition of CH_2O and several hydrocarbons, modelling of the CH_2O/N_2O flame, and laser pyrolysis/laser fluorescence studies of CH_4/N_2O and CH_2O/N_2O chemistry.

CONTENTS

I INTRODUCTION

A knowledge of the detailed chemistry that occurs in a combustion process can be useful in several ways in describing the behavior of an overall system that includes that combustion. First, knowledge of the chemistry allows control of those aspects where the chemical kinetics itself can dominate (e.g., in ignition processes). Second, such knowledge allows understanding of the effects of additives or modifiers on the combustion process. Third, an observable, that is readily measured in a complex system (e.g., the emission of light in some wavelength region as a function of time) can be related to the behavior and progress of the overall process.

To understand the details of the combustion chemistry on a microscopic basis, it is necessary to measure and relate to each other the concentrations of the free radical intermediates that are formed and converted during the reaction network. The method of laser-induced fluorescence (LIF) is the member of the family of laser spectroscopic probe methods[1,2] best suited for measuring those free radical intermediates. Nonintrusive, possessing high sensitivity and selectivity, and furnishing excellent spatial and temporal resolution, LIF can be used to detect some 30 atomic, diatomic, and triatomic combustion chemical intermediates. When LIF is coupled with comprehensive computer models of the chemical networks and methods to measure or estimate accurately the pertinent reaction rate constants, these transient species can be determined and, in turn, greatly further our understanding of the detailed chemical pathways. Such a coupling can be performed for flames themselves, or for other systems, such as our recently developed laser pyrolysis/laser fluorescence (LP/LF) experiment,[3] designed to probe combustion chemistry under less complex conditions than those found in flames.

During the past three years, we have studied, under Army Research Office support, the development and use of LIF methods and the formulation of chemical models and rate constant estimation techniques for flames containing the chemistry expected to be present in the gas-phase combustion of nitramine propellants. Particular focus has been on flames of CH_4/N_2O and CH_2O/N_2O.

A key initial finding on this project was the first observation, using LIF, of ground-state NH radicals in CH_4/N_2O flames. Their presence in significant quantity raised for the first time important questions concerning the participation of nitrogen-containing radicals in the chemistry of such flames. These radicals may be even more important in the nitramines themselves, which as monopropellants are heavily fuel-rich. The detection of nitrogen-containing radicals in CH_4/N_2O flames was refined and extended in burner experiments at the Ballistic Research Laboratory (BRL), where copious quantities of NCO, CN, and NH were found in these flames using LIF. The research on the SRI project has emphasized the development of LIF spectroscopic methods, the use of the LP/LF technique, and modeling studies of the possible flame chemistry.

In the following sections, we describe first some aspects of nitramine chemistry, indicating the potential importance of the reactions and species to be studied, together with comments on how the laser probes and chemical models might be used to infer some understanding about the experimentally difficult problem of actual nitramine combustion. Then we detail the progress that has been made during this project, its significance for nitramine combustion, and its links to Army Laboratory programs addressing this topic.

II NITRAMINE COMBUSTION CHEMISTRY

The class of propellants known as nitramines (cyclic nitroorganic compounds, especially HMX and RDX) possesses a number of desirable properties, such as high energy release coupled with low vulnerability. However, they also have disadvantages, including low burn rate and breaks in the slopes of the curves of burn rate versus pressure. Ideally, through the addition of modifiers, these characteristics can be altered to minimize the undesirable behavior while not degrading the good qualities of the propellants.

The mechanisms by which the modifiers act, or the propellants themselves ignite and burn, are not at all well understood. Part of the problem is the high pressure and hostile environment under which actual propellants burn, making detailed experiments extremely difficult. For example, the distance scales involved pose special barriers. The fizz zone, or flame zone, near the propellant surface is at most tens of micrometers thick at the lowest pressures at which the propellants burn. Even though in principle this zone can be probed with sufficient spatial resolution using laser techniques, the surface irregularities are larger than this thickness, in effect rendering undefinable the appropriate length scales. Consequently, information on propellant ignition and combustion must come from a variety of separate sources, each involving experiments that often do not entail the direct burning of the propellants but provide detailed results in a more tractable way.

Those experiments that <u>can</u> be performed on actual propellants are valuable; these include final or intermediate product determinations by gas chromatography or molecular-beam mass spectrometric sampling. The presence of reactive intermediates can sometimes be detected by means of their emission spectra. Fitting these observations into a detailed chemical description of the propellant combustion requires separate experiments to develop and validate the flame chemistry; such experiments are the subject of this research.

The gas-phase part of nitramine flames forms an important part of the propellant combustion. Simple chemical considerations show that the majority

of the heat release occurs in the gas phase. It is this energy, fed back to the surface, that controls the initial vaporization and decomposition processes in the condensed phase. Also, gas-phase processes are probably crucial in ignition by convective heating. Preliminary results are available from an experiment at BRL on ignition of RDX in a flow of hot nitrogen.[4] They indicate that ignition occurs in the gaseous wake, probably in reactants that have formed from pyrolysis of gaseous species evolved from the solid; the flame then propagates back to the surface. In a study at much higher temperature,[5] ignition was also found to occur in the gas phase. In both instances, presence of oxygen in the hot gas stream altered the ignition characteristics, sometimes dramatically.

What are the constituents of these gas-phase flames? Although many experiments have been performed on the thermal decomposition of nitramines, the results with different measurement techniques and under different conditions are often in disagreement. Schroeder[6] reviewed the literature in this area and concluded that the point(s) of bond cleavage in the cyclic compounds are not known. A great variety of decomposition products has been found. Molecular-beam mass spectrometric sampling methods[7,8] indicated the presence of considerable quantities of CH_2O and N_2O on decomposition. Infrared measurements,[4] in the wake of convectively heated but unignited RDX, showed NO_2, N_2O, HCN, and some CO_2. (CH_2O was not detectable in this experiment.) On the other hand, qualitative results at the Large Caliber Weapons Systems Laboratory (LCWSL) from a coherent anti-Stokes Raman-scattering (CARS) experiment in the dark zone of an atmospheric pressure RDX flame[9] indicated that considerable amounts of CO, CO_2, H_2, and HCN exist near the surface. CH_4, CH_2O, and NO were observed in minor quantity, but N_2O and NO_2 were not observed. Low pressure pyrolysis experiments,[10] conducted on a previous project in the Department of Chemical Kinetics at SRI, indicated that the molecular elimination of HONO was a major pathway.

In view of this array of results, it is impossible to select a particular flame that will mimic the gas-phase combustion of the nitramines. What can be done is to study the appropriate sequences of chemical reactions and to establish a means of identifying those intermediate species present in the combustion of these several combinations. Many of these reactions and species are common to all; an understanding of each system on a fundamental basis is

crucial in an examination of differences that depend on the mode of breakup of the nitramine.

We have chosen, as a reasonable starting point, flames of CH_4/N_2O and CH_2O/N_2O because they contain pertinent and representative chemical sequences; these flames, their kinetics, and the LIF spectroscopy of their intermediate species have been the subject of study in the first three years of this project. CH_4/N_2O flames are also now being investigated using Raman-scattering, CARS, and LIF at BRL and with CARS at LCWSL. The flames of these compounds were chosen for study because they contain much of the chemical networks anticipated to occur in nitramine flames but constitute simpler, more experimentally tractable systems than the propellant flames themselves, in which to gain a firm understanding of that chemistry.

III PROGRESS AND RESULTS

The research has been concerned with species detection and chemical reaction rates and mechanisms in flames of CH_4/N_2O and CH_2O/N_2O. In this section we describe the progress and findings. Reprints of pertinent articles, reports, and conference abstracts are attached.

A. Nitrogen-Containing Radicals in CH_4/N_2O Flames

In earlier studies of flames of CH_2O/N_2O burning at low pressure[11] and at one atmosphere,[12] emissions from NH, NH_2, and CN were seen. Such species can arise only if the N-N bond in the N_2O is broken, suggesting different chemical pathways than if only the N-O bond dissociates. However, the presence of emission does not necessarily denote significant amounts of ground-state molecules because the emission may result from direct chemical production of a small concentration of chemiluminescent, electronically excited species. Thus, at the onset of the project, the initial step was to determine the ground-state concentration of at least one such species using LIF. This was performed for NH in CH_4/N_2O flame.[13] Because quenching rates for the excited state of NH were not known, the simple estimate was made that they were the same as for the electronically similar OH molecule. This led to an approximate ratio $[NH]/[OH] \approx 0.04$ in the reaction zone of this flame, which is a high enough concentration of NH for it to be chemically significant.

This simple, semiquantitative experiment thus provided the key information that nitrogen-containing radicals may be important in the chemistry of these flames. The next step was the consideration of possible chemical mechanisms to seek the mode of formation of the NH (probably through the $H + N_2O$ reaction) and the subsequent reactions it undergoes. This procedure led to the identification of the NCO radical as another potential key intermediate, and a study was begun of its laser spectroscopy in flow systems.

At BRL, more extensive and accurate measurements were made on NH and OH in a CH_4/N_2O flame,[14] using absorption measurements to obtain the absolute NH concentration. The results, an [NH]/[OH] ratio of 0.02, were very close to the initial estimate using approximate quench rates, and they fully support

the major conclusion about nitrogen-containing radical chemistry. In further probes of this same flame at BRL, the NCO radical was found to exist in copious quantities,[15] and significant amounts of C_2 and CN have also been found.[16]

At SRI, we began to study the spectroscopy of NCO shortly before it was detected in a flame at BRL. The experiments, performed in a low pressure discharge flow, have yielded several valuable pieces of information. Further information -- including wavelengths for excitation, intensities of fluorescence, absorption coefficients, and quenching rate constants for both the $A^2\Sigma^+ - X^2\Pi_i$ and $B^2\Pi_i - X^2\Pi_i$ electronic systems -- is needed to relate LIF flame measurements to actual concentrations. A study of the fluorescence spectrum obtained on excitation of the B-state has yielded for the first time accurate values of ground-state vibrational frequencies, important in understanding the structure of the molecule and its thermochemical parameters.

Radiative lifetime measurements were also made on the $B^2\Pi_i$ state.[17] These show a lifetime decreasing from 65 ns in the (000) vibrational level to $\lesssim$ 10 ns in the (100) vibrational level. The difference was ascribed to predissociation of the B-state to $N(^2D) + CO$. This sets a new, lower dissociation energy for NCO and a value of its heat of formation that is 14 kcal/mol higher than that currently used in the literature. It also leads to a higher value for the heat of formation of HNCO. These results can significantly alter ideas about the participation of NCO in certain flame chemical reactions -- for example, as in a recent discussion[18] of the products of the HCN + OH reaction based on the old ΔH_f^o values. Different values of ΔH_f also mean different values of the equilibrium constants of reactions in which NCO and HNCO take part, and correspondingly alter reverse reaction rates inferred from forward reaction rate values. Hence this spectroscopic experiment, which yields a thermodynamic result, can have a significant impact on flame models in which these species play a role. The remainder of the NCO data is still being analyzed and results will be published later.

The conclusion from this work, together with the complementary BRL burner experiments, is that considerable chemical activity occurs following breakage of the N-N bond in N_2O. The nature of the pathways is not clear, due in large part because of a lack of pertinent rate constants, but further research is needed to understand their role and significance in the flame chemistry.

B. Diagnostics on O, N, OH and CH

Oxygen and perhaps nitrogen atoms are also important participants in flames burning in N_2O. However, these atomic species are not detectable with standard LIF techniques because their absorption lies in the vacuum ultraviolet. Even if lasers could be made to operate in the appropriate wavelength region, absorption by atmospheric and flame gases would preclude their use for flame diagnostics. To detect these species, we have developed a method of two-photon LIF.[19] The atoms are excited by two-photon absorption to the first excited state of the same symmetry as that of the ground state, which then radiates in an infrared transition terminating on another excited state. Our experiments, performed in a low pressure flow discharge, indicated good sensitivity under flame conditions from measurement of two-photon absorption coefficients, lifetimes, and quenching rate constants.

With these methods, O-atoms have now been detected in flames of C_2H_2/O_2[20] and CH_4/N_2O.[21] The latter study was performed at BRL where the effects of laser-induced chemistry, which may complicate the detection in this flame, are under investigation. Our two-photon method has opened up an important new category of species -- O-, N-, H-, and C-atoms -- to detection in flames by laser methods and will be useful in propellant combustion as well as many other systems.

The OH radical remains of prime importance in the flames under study here and in many other applications. Although the OH spectroscopic data base for LIF detection is much better established than that for other molecules, there remain some questions concerning the collisional behavior of the excited state that are important for flame probing.

This problem has been considered first in the compilation of information on collisional effects in LIF flame probing, with special emphasis on OH. This study culminated in the writing of an invited review article that appeared in a special issue of Optical Engineering[13] and contained a comprehensive and critical discussion of collision data and outstanding questions.

One of these questions is the extrapolation to flame temperatures of electronic quenching rate constants usually obtained at room temperature in

flow systems. For OH, at least, the large cross sections suggested that the mechanism leading to the quenching involved attractive forces interacting between the $A^2\Sigma^+$ OH and the collision partner. Using our LP/LF method,[3] we measured collisional quenching rate constants k_Q for 11 collisional partners of combustion interest, at temperatures near 1200 K.[22] The key finding was that the cross sections were smaller than those at room temperature, clearly indicating that attractive forces were important and rendering a simple $T^{1/2}$ extrapolation invalid for diagnostics purposes. The experimental results were then compared with calculated cross sections where the theoretical picture incorporated a multipole interaction between the OH and its collision partner, plus a repulsive centrifugal barrier. For 8 of the 11 collision partners studied, excellent correlation between measured and calculated values was obtained, providing further evidence for the role of attractive forces in quenching collisions.

Although the experimental k_Q values may be directly used for LIF studies of OH, the theoretical correlations have wider implications for flame diagnostics as well as for fundamental collision dynamics. For most other radical species, k_Q values have been measured for only a few collision partners and then usually only at room temperature. Assuming that attractive forces play an important role in the quenching of other radicals, we can now estimate k_Q values for a variety of collision partners and as a function of temperature. Direct determinations of k_Q would still be necessary for accurate LIF measurement of other radicals, but as in the case of the [NH]/[OH] ratio in CH_4/N_2O flames, crucial information can be gained from measurements where k_Q is only estimated.

Preliminary measurements have been made on energy transfer pathways for electronically excited CH in atmosphere pressure flames of CH_4/N_2O. A laser pumps specific rotational levels in $v' = 0$ of the $A^2\Delta$ state and fluorescence from $v' = 1$ and 0 is measured, showing that rotational excitation enhances the upward $0 \rightarrow 1$ collisional transfer probability. This work will be presented at the 1984 Molecular Spectroscopy Symposium, in Columbus.[23]

C. LIF of NCO and NH_2 Radicals in Flames

LIF has been useful in measuring several atomic and diatomic free radicals of importance in flame chemistry. Although the flame chemistry

involves many larger radicals as well, no previous studies exist of the LIF spectroscopy of triatomic or larger species under flame conditions. We undertook a study of the LIF of the NCO radical in CH_4/N_2O flames, and the NH_2 radical in NH_3/O_2 and NH_3/N_2O flames,[24] all burning at atmospheric pressure. As noted above, the NCO radical has been seen in such flames at BRL using the coincidence of the fixed frequency line of an Ar^+ laser;[15] although convenient, this is not necessarily an optimum method for a given set of conditions nor can it be relied on as general for other molecules.

The excitation spectrum for NCO is quite complex, consisting of a large number of bands just to the blue of the 000–000 band at 440 nm. We have assigned a few of these but have devoted most of our attention to hot bands arising from vibrationally excited NCO further to the red, where the spectrum is much less complex. We have identified 16 individual bands and selected optimum detection wavelengths. From the bandhead positions, we have fit rotational constant and spin-orbit splitting values, providing information on the stretching-vibration dependence of the latter constants. Fermi resonance interaction can explain some of the differences seen. These spectroscopic results on NCO will be presented at the 1984 Molecular Spectroscopy Symposium in Columbus.[25]

In the case of NH_2, 8 different bands have been excited over a wide wavelength region.[24] In the flames studied, chemiluminescent emission from the NH_2 provides a background that interferes with the LIF signals. In addition, the many hot bands present lead to a very congested spectrum throughout the regions of excitation, with recognizable features resting on a near continuum background of similar intensity.

D. Modeling of Formaldehyde/Nitrous Oxide Flame Chemistry

Detailed modeling of the chemistry of the H_2CO/N_2O combustion chemistry system began with a simple isothermal model in which time is the only variable. Though far from representing a flame itself, the model has permitted us to gain insight into the important chemistry occurring. The starting point was a 19-step, 14-species, semiglobal mechanism proposed by Dean[26] for describing shock-heated mixtures of dilute formaldehyde in O_2 or N_2O. This mechanism ignores the participation of several nitrogen-containing species

that are observable with LIF and that have been found to exist in significant quantity in flames of methane in nitrous oxide.

We briefly examined Dean's rate constants and found them reasonable. Our RRKM calculations of the rate constant for formaldehyde pyrolysis (with use of the 1970 thermochemical data for formyl radical[27]) support Dean's contention that previously reported values are ten times too high. Also, Dean suggests that the rate constant for OH + HCHO → H_2O + CHO is a factor of ten slower than that previously reported in the literature. Comparison with the rate constant for H + HCHO and the use of transition theory estimates suggest Dean's value is sensible. Therefore, Dean's mechanism was used as the basic network to which were added reactions involving the nitrogen-containing radicals.

The isothermal modeling was performed at 2500 K because the flame studies at BRL showed the relatively rapid attainment of such temperatures. Rate constants were obtained from the literature[28] with no extensive attempt (as yet) at individual evaluation, and concentration profiles for many species were computed and plotted.

We found that appreciable concentrations of some nitrogen-containing species, 10^{13} to 10^{16} molecules/cm^3, can be realistically generated during the H_2CO/N_2O chemical sequence at high temperature. This is very encouraging for linking of the LIF measurements with the chemical mechanism, although the reaction set included in the model is far from complete enough to compare with experiments.

Interestingly, the NH/OH ratio at the appropriate times mimics the reported values of ~ 2-4% from our own studies and those of BRL. One problem encountered was that by adding several more reactions suggested by others,[29] we could change many of the species profiles drastically. The [NH]/[OH] ratio could be varied one to two orders of magnitude using realistic estimates of rate constants for these additional reactions.

This sort of variation is completely unacceptable. The goal of this modeling is the establishment of a predictive tool. This is especially important in the case of understanding nitramine propellant burning under conditions approaching practical reality, because laboratory experimental data will require extensive extrapolation to approach the pressures and temper-

atures at which propellants burn in actual systems.

E. Rate Constant Estimation and Correlation

From the above discussion, it is clear that any serious modeling effort must be preceded by the establishment of criteria for the critical evaluation of rate data to be used in the simulation. We have made the global understanding of individual rate constants the focus of some of our research activities. This has allowed us to begin to establish these necessary criteria. Some of the ideas involved have been discussed in the literature,[30] but we have amplified and developed others during this work. A status report is given below in terms of classes of reactions.

Bimolecular Reactions. Simple bimolecular reactions involve the transfer of atoms in a simple metathesis. They are described by simple transition-state theory and are expected to be independent of pressure with a temperature dependence best described by the form $k = AT^B \exp(-C/T)$. Often this is described by a form in which $B = 0$; these two-parameter "Arrhenius" descriptions will almost always fail over a wide temperature range. If experimental values have been determined at temperatures very different than those of the intended application, the computed k will be wrong.

The context of theory also allows sample evaluation of the quantity A in the above expression. This quantity, related to transition-state entropy values, must be larger for atom-molecule reactions than for related diatom-molecule reactions, which in turn have higher A-values than polyatomic-molecule reactions. This is due to the successive loss of rotational degrees of freedom in forming a transition state in the above processes. We have identified important families of simple bimolecular reactions, such as $OH + H_2CO \rightarrow H_2O + HCO$ and $H + H_2CO \rightarrow H_2 + HCO$, where these notions of consistent A-factors should be applied in choosing rate constants for modeling studies.

Unimolecular Reactions. These reactions are both pressure and temperature dependent. There is extensive literature concerning these processes.[31] Detailed understanding and proper modeling require use of RRKM theory and knowledge of molecular parameters. In addition, because unimolecular processes always reflect the competition between chemical and energy-transfer processes, knowledge of these latter processes is also important.

Currently, k(P,T) can be calculated with a rather cumbersome numerical apparatus. Troe[32] has developed a formalism for the analytical mimicking of RRKM results in terms of parameters that may be calculated once and then listed for each individual process. Most of our effort concerning rate constant determination has been spent in casting the Troe scheme into a usable format. The goal is to list a given reaction and the appropriate parameters that can be used with the stored analytical function to compute k(P,T) for models of combustion chemistry. Examples include the initiation reactions $H_2CO \rightarrow H + HCO$ and $N_2O \rightarrow N_2 + O$. This study was described at the Western States Combustion Meeting in Los Angeles, California, in October 1983 and is being submitted to Combustion and Flame.

Apparent Bimolecular Reactions. These reactions are the most difficult to deal with and the least often recognized. They are written as if they were simple bimolecular processes; thus,

$$CO + OH \rightarrow H + CO_2$$

However, we now know that this reaction is not a simple metathesis; it undoubtedly involves the formation of an intermediate HOCO radical. The radical is "born" with internal energy, and its lifetime is thus also pressure dependent. Hence, any analytical form for rate constants of this type must account for both pressure and temperature dependence. Currently, we do not have any simple methods for incorporating such processes into a model. If we treat them as bimolecular, we must be very careful to use data obtained under conditions similar to those simulated in the model; simple extrapolation without a better understanding can produce severe discrepancies. However, it will prove very difficult to find much data that will be easily transferred to flame conditions.

In the CH_2O/N_2O system, we have used the models to identify several reactions in this category that are likely to be crucial in reactions of the nitrogen-containing radicals:

$$H + N_2O \rightarrow OH + N_2$$

$$\rightarrow NH + NO$$

$$NH + CO \rightarrow \rightarrow H + NCO$$

$$\rightarrow \rightarrow CN + OH$$

These processes may occur through intermediates -- for example, NNOH and HNNO for the first reaction and HNCO or NCOH for the second. A proper treatment of this important class of reactions, including the branching ratio as a function of pressure and temperature, requires knowledge of the intermediates and application of unimolecular rate theory. (We have studied the first of these systems in depth as part of contracted work with DoE concerning NH_3/O_2 flames.)

F. Laser Pyrolysis/Laser Fluorescence Experiments

In the LP/LF method,[3] a mixture of SF_6, radical precursor, and reactant or quenching gas is heated by a pulsed CO_2 laser whose radiation is absorbed by the SF_6. In experiments to date, the precursor has been H_2O_2, which decomposes to OH radicals that are then detected using LIF. Temperatures between 800 and 1400 K have been attained, and the method has been used to measure quenching rates for $A^2\Sigma^+$ OH described above,[22] as well as (on another project) reaction rate constants of OH with hydrocarbons.

The original purpose of the LP/LF method was twofold: to measure bimolecular processes, such as the quenching and reaction rate constants at elevated temperature, and to produce combustion chemical networks under elevated temperature conditions but without the complications due to gas dynamics, transport, and limited stoichiometric range that occur in direct flame studies. Several preliminary experiments have been performed in this latter mode.

Mixtures of C_2H_2/O_2 and CH_4/O_2 have been pyrolyzed, both with and without added H_2O_2. A short (100-μs-long) combustion process is occurring, as evidenced by emission from OH, CH, and C_2, which can be seen following the CO_2 laser pulse. In the case of CH_4/O_2, LIF signals of ground-state OH, formed and then removed during the chemical sequence, could be seen. Pyrolysis of a mixture of CH_4/N_2O also produced emission, but LIF signals have not yet been

detected; the failure was likely due to the high quenching rate of N_2O for the excited OH and the low signal levels during that particular period of experimentation.

Formaldehyde/nitrous oxide mixtures have also been pyrolyzed. In an LP apparatus, outfitted with a mass spectrometer (but not having LIF probe capabilities), a mixture of CD_2O, N_2O, and SF_6 was irradiated with the CO_2 laser. (CD_2O was used to obtain more definitive identification of certain fragment masses that would be confusing with CH_2O.) Destruction of reactants and formation of stable products (H_2O, CO) could be observed with the mass spectrometer, summing over several laser pulses. The LP/LF setup was used to detect light emission during the laser pyrolysis of this same mixture. The emission begins shortly (~ 10 μs) after the CO_2 pulse, peaks near 200 μs, and persists for nearly a millisecond in some cases. Bands of OD, ND, CN, CD, and C_2 were observed, corresponding to the species seen in the CH_2O/N_2O flame.[12] Those of CN were especially strong. The rise and decay times varied with conditions and to some degree with species, indicating that they contain useful kinetic information on readily measured time scales. LIF detection of the ground-state radicals is the logical next step.

In each of these cases, it is possible that the reaction-initiating step is due to a trace amount of F-atoms formed from minor decomposition of the SF_6 at these temperatures, although no HF was detected mass spectrometrically. Also, quantitative measurements have not yet been made. Nonetheless, these preliminary results indicate the feasibility of LP/LF experiments on the chemical networks found in flames pertinent to nitramine combustion. Because of the lack of gas dynamic considerations, such experiments are much more amenable to simple chemical modeling and will provide a key link between the models and the laser diagnostic measurements. Moreover, because the pulsed CO_2 laser can be used to heat the mixture more rapidly than the time scales of the chemical reactions themselves we can obtain time-resolved information on the radical concentrations that will be very important in comparing the experimental results with model calculations.

IV REFERENCES

1. D. R. Crosley, Ed., Laser Probes for Combustion Chemistry, Amer. Chem. Soc. Symposium Series, Vol. 134, 1980.

2. J. H. Bechtel, C. J. Dasch, and R. E. Teets, "Combustion Research with Lasers," to appear in Laser Applications, R. K. Erf and J. F. Ready, Eds. (Academic Press, New York, 1983).

3. P. W. Fairchild, G. P. Smith, and D. R. Crosley, Nineteenth Symposium (International) on Combustion (The Combustion Institute, Pittsburgh, 1982), p. 107.

4. R. A. Beyer, M. A. DeWilde, and W. J. Scott, Eastern Section Meeting of the Combustion Institute, Providence, Rhode Island, November 1983.

5. A. Birk, L. H. Caveny, and W. A. Serignano, Eastern Section Meeting of the Combustion Institute, Atlanta, Georgia, November 1979.

6. M. A. Schroeder, Ballistic Research Laboratory Memorandum Report ARBRL-MR-3181 (June 1982).

7. R. A. Beyer, Eastern Section Meeting of the Combustion Institute, East Hartford, Connecticut (November 1977).

8. B. B. Goshgarian, Rocket Propulsion Laboratory Report AFRPL-TR-78-76 (October 1978).

9. K. Aron and L. E. Haris, private communication (1983).

10. D. F. McMillen, J. R. Barker, K. E. Lewis, P. L. Trevor, and D. M. Golden, Final Report on SRI Project 5787 (June 1979).

11. A. G. Gayton and H. G. Wolfhard, Third Symposium (International) on Combustion (The Combustion Institute, Pittsburgh, PA, 1949), p. 504.

12. M. A. DeWilde, L. J. Decker, and D. R. Crosley, unpublished results, 1979.

13. D. R. Crosley, Opt. Engr., 20, 511 (1981).

14. W. R. Anderson, L. J. Decker, and A. J. Kotlar, Comb. Flame 48, 163, 179 (1982); 51, 125 (1983).

15. W. R. Anderson, J. A. Vanderhoff, A. J. Kotlar, M. A. DeWilde, and R. A. Beyer, J. Chem. Phys., 77, 1677 (1982).

16. J. A. Vanderhoff, R. A. Beyer, A. J. Kotlar, and W. R. Anderson, Comb. Flame, submitted.

17. B. J. Sullivan, G. P. Smith, and D. R. Crosley, Chem. Phys. Lett., 96, 307 (1983).

18. D. Puechberty and M. J. Cottereau, Comb. Flame, 51, 299 (1983).

19. W. K. Bischel, B. E. Perry, and D. R. Crosley, Chem. Phys. Lett., 82, 85 (1981); Appl. Opt., 21, 1419 (1982).

20. M. Alden, H. Edner, P. Grafstrom, and S. Svanberg, Opt. Comm., 42, 244 (1982).

21. A. Miziolek, private communication (1983).

22. P. W. Fairchild, G. P. Smith, and D. R. Crosley, J. Chem. Phys., 79, 1795 (1983).

23. N. L. Garland and D. R. Crosley, submitted to Molecular Spectroscopy Symposium, Columbus Ohio, June 1984.

24. R. A. Copeland, D. R. Crosley and G. P. Smith, Twentieth Symposium (International) on Combustion, Ann Arbor, Michigan, August 1984.

25. R. A. Copeland and D. R. Crosley, submitted to Molecular Spectroscopy Symposium, Columbus Ohio, June 1984.

26. A. M. Dean, R. L. Johnson, and D. C. Steiner, Comb. Flame, 37, 41 (1980).

27. JANAF Thermochemical Tables, U.S. National Bureau of Standards, NSRDS-NBS 37 and Supplements, D. R. Stull and H. Prophet, Eds. (1971).

28. C. W. Westbrook, Comb. Flame, 46, 191-210 (1982); J. A. Miller, M. C. Branch, and R. J. Kee, Comb. Flame, 43, 81-98 (1981); A. M. Dean and R. L. Johnson, Comb. Flame, 37, 109 (1980).

29. W. M. Shaub and S. H. Bauer, Comb. Flame, 32, 35-55 (1978); D. L. Baulch, D. D. Drysdale, D. G. Horne, and A. C. Lloyd, Evaluated Kinetic Data for High-Temperature Reactions (Butterworth, London, 1972), Vol. 1; A. M. Dean, J. E. Hardy, and R. K. Lyon, Nineteenth Symposium on Combustion (The Combustion Institute, 1982), pp. 97-105.

30. D. M. Golden, J. Phys. Chem., 83, 108 (1979); "Measurement and Estimation of Rate Constants," in Dynamics and Modeling of Reactive Systems, W. E. Stewart, W. H. Ray, and C. C. Conley, Eds. (Academic Press, New York, 1980), pp. 315-331; "Measurement and Estimation of Rate Constants for Modeling Reactive Systems," in Modeling of Chemical Reaction Systems, Proceedings of an International Workshop, Heidelberg, Fed. Rep. of Germany, 1-5 September 1980, K. H. Ebert, P. Deuflhard, and W. Jager, Eds. (Springer-Verlag, Berlin, 1981), pp. 148-161.

31. P. J. Robinson and K. A. Holbrook, Unimolecular Reactions (Wiley-Interscience, London, 1972).

32. J. Troe, J. Phys. Chem., 83, 114 (1979); J. Chem. Phys., 66, 4745 (1977).

V. PUBLICATIONS

The journal articles, report, and conference presentations supported by this contract are listed below. Reprints are attached.

A. Journal Articles

1. D. R. Crosley, "Collisional Effects on Laser-Induced Fluorescence Flame Measurements," Opt. Engr., 20, 511 (1981).

2. W. K. Bischel, B. E. Perry, and D. R. Crosley, "Two-Photon Laser-Induced Fluorescence in Oxygen and Nitrogen Atoms," Chem. Phys. Lett., 82, 85 (1981).

3. W. K. Bischel, B. E. Perry, and D. R. Crosley, "Detection of Fluorescence from O and N Atoms Induced by Two-Photon Absorption," Appl. Opt., 21, 1419 (1982).

4. D. R. Crosley, "Laser-Induced Fluorescence in Spectroscopy, Dynamics, and Diagnostics," J. Chem. Educ., 59, 446 (1982).

5. B. J. Sullivan, G. P. Smith, and D. R. Crosley, "Lifetimes in the $B^2\Pi$ State and the Heat of Formation of NCO," Chem. Phys. Lett., 96, 307 (1983).

6. P. W. Fairchild, G. P. Smith, and D. R. Crosley, "Collisional Quenching of $A^2\Sigma^+$OH at Elevated Temperature," J. Chem. Phys., 79, 1795 (1983).

7. D. R. Crosley and G. P. Smith, "Laser-Induced Fluorescence Spectroscopy for Combustion Diagnostics," Opt. Engr., 22, 1795 (1983).

8. D. M. Golden and C. W. Larson, "Rate Constants for use in Modelling," Twentieth Symposium (International) on Combustion, Ann Arbor, Michigan, August 1984.

9. R. A. Copeland, R. Crosley and G. P. Smith, "Laser-Induced Fluorescence Spectroscopy of NCO and NH_2 in Atmospheric Pressure Flames," Twentieth Symposium (International) on Combustion, Ann Arbor, Michigan, August 1984.

B. Report

C. W. Larson and D. M. Golden, "Modelling the Chemical Network of the N_2O/CH_2O Flame," Interim Progress Report, SRI Project 2230, September 1983.

C. Conference Presentations

1. W. K. Bischel, B. E. Perry, and D. R. Crosley, "Detection of O and N Atoms by Two-Photon Laser-Induced Fluorescence," IEEE JQE, 17, (12, PT. 2), 120 (1981).

2. D. R. Crosley, "Laser-Induced Fluorescence in Spectroscopy, Dynamics, and Diagnostics," American Chemical Society Meeting, New York, August 1981.

3. B. J. Sullivan, G. P. Smith, D. R. Crosley, and G. Black, "Laser-Induced Fluorescence Studies of the NCO Molecule," Eastern Section Meeting, Combustion Institute, Pittsburgh, Pennsylvania, October 1981.

4. D. M. Golden, "The Effect of Pressure on Combustion Processes," American Chemical Society Meeting, Las Vegas, Nevada, March 1982.

5. D. R. Crosley, "Laser-Induced Fluorescence in Combustion Chemical Kinetics," American Chemical Society Meeting, Las Vegas, Nevada, March 1982.

6. B. J. Sullivan, G. P. Smith, and D. R. Crosley, "Laser-Induced Fluorescence Studies of the A-X and B-X Systems of the NCO Radical," Paper RC8, Symposium on Molecular Spectroscopy, Columbus, Ohio, June 1982.

7. B. J. Sullivan, G. P. Smith, and D. R. Crosley, "Laser Fluorescence Spectroscopy of NCO," XV Informal Conference on Photochemistry, Stanford, California, June 1982.

8. G. P. Smith, K. E. Lewis, D. M. Golden, P. W. Fairchild, and D. R. Crosley, "Laser Pyrolysis of Unimolecular and Bimolecular Reactions over 1000 K," Seventh International Symposium on Gas Kinetics, Göttingen, West Germany, August 1982.

9. P. W. Fairchild, G. P. Smith, and D. R. Crosley, "Bimolecular Quenching Rate Measurements for OH at High Temperatures," Paper 82-47, Western State Meeting, The Combustion Institute, Livermore, California, October 1982.

10. D. R. Crosley, "Laser-Induced Fluorescence Spectroscopy in Combustion Research," Bull. Amer. Phys. Soc., 27, 862 (1982).

11. P. W. Fairchild, G. P. Smith, and D. R. Crosley, "Quenching of the $A^2\Sigma^+$ State of OH at ~ 1100 K," Paper WH2, Molecular Spectroscopy Symposium, Columbus, Ohio, June 1983.

12. C. W. Larson and D. M. Golden, "Pressure and Temperature Dependence of Unimolecular Processes: An Approach for Combustion Modelers," Western States Meeting, The Combustion Institute, Los Angeles, California, October 1983.

13. D. R. Crosley, "Laser-Induced Fluorescence for Combustion Chemistry," American Physical Society Meeting, San Francisco, California, November 1983.

14. D. R. Crosley, "Laser Flame Diagnostics," The Pittsburgh Conference, Atlantic City, New Jersey, March 1984.

15. R. A. Copeland and D. R. Crosley, "Laser-Induced Fluorescence Measurement of Spin-Splittings in Excited Vibrational Levels of NCO ($X^2\Pi_i$)," submitted to Molecular Spectroscopy Symposium, Columbus, Ohio, June 1984.

16. N. L. Garland and D. R. Crosley, "Energy Transfer Pathways for $A^2\Delta$ CH in an Atmospheric Pressure Flame," submitted to Molecular Spectroscopy Symposium, Columbus, Ohio, June 1984.

17. D. M. Golden and C. W. Larson, "Rate Constants for use in Modelling," Twentieth Symposium (International) on Combustion, Ann Arbor, Michigan, August 1984.

18. R. A. Copeland, R. Crosley and G. P. Smith, "Laser-Induced Fluorescence Spectroscopy of NCO and NH_2 in Atmospheric Pressure Flames," Twentieth Symposium (International) on Combustion, Ann Arbor, Michigan, August 1984.

Collisional effects on laser-induced fluorescence flame measurements

David R. Crosley
SRI International
Molecular Physics Laboratory
Menlo Park, California 94025

Abstract. Laser-induced fluorescence (LIF) is a method of considerable utility for the measurement of the transient free radicals which are the keys to the chemistry of flames. Collisions experienced by the electronically excited state can alter the magnitude and the spectral form of the fluorescence signals. Recent studies on both quenching and energy transfer collisions, and their influence on LIF measurements, are treated in this review; special emphasis is given to the important and popular OH molecule. Different solutions to the problem of accounting for quenching are considered, and both effects and exploitation of energy transfer within the excited state are discussed. Although further research is needed to better quantify these collisional effects, LIF can currently provide data significant for the understanding of combustion chemistry.

Keywords: combustion and analysis; laser-induced fluorescence; quenching; energy transfer; spectroscopy; hydroxyl radical.

Optical Engineering 20(4), 511-521 (July/August 1981).

CONTENTS

1. INTRODUCTION

The past few years have seen a significant effort in the development and early application of lasers as probes of combustion processes.[1] Several methods termed laser spectroscopic probes provide concentrations and temperatures (population distributions over internal energy levels) of identifiable molecular species. Chief among these are spontaneous and coherent Raman scattering and laser-induced fluorescence (LIF), all of which share a number of common attributes. Each has excellent spatial and temporal resolution and is nonintrusive in nature. This last feature means not only that the gas flow and chemical kinetics are unperturbed, but also that the laser probes may be used in environments too hostile (high temperatures or corrosive atmospheres) to permit the insertion of a physical probe such as a thermocouple or sampling nozzle.

LIF and the Raman methods complement one another quite well in providing a wide range of molecules which can be probed. The Raman scattering methods yield a relatively easily analyzed determination of the majority species present in a combustion process, that is, the fuel, oxidant, main exhaust gases and, in an air flame, N_2. However, because of signal level considerations, they are generally unable to detect transient species (often free radicals) present at low concentration. LIF is considerably more sensitive than the Raman methods and can furnish a measurement of the concentration of those trace species, crucial to an understanding of the combustion chemistry. LIF, however, depends on the existence of appropriately separated electronic states of the molecule in question, and because of this is generally inapplicable to the closed-shell molecules for which the Raman methods are well suited. Hence, for a full description of the combustion processes, both LIF and Raman methods are necessary.

As noted, LIF has very high sensitivity. For example, under favorable conditions, OH in an atmospheric pressure flame can be detected at sub-part-per-billion concentration levels with 1 mm^3 spatial and 10 nsec temporal resolution, producing a signal level of ~100 photoelectrons. This sensitivity arises from the fact that LIF, unlike the Raman techniques which rely on scattering phenomena, involves the creation of a real electronically excited state through absorption of the laser photons. Concomitant with this sensitivity, however, arises the chief disadvantage to LIF: because the real excited state possesses a finite radiative lifetime, collisions of the excited molecule with the flame gases affect both the magnitude and spectral distribution of the fluorescence signals.

Invited Paper EP-104 received Feb. 18, 1981; accepted for publication March 11, 1981; received by Managing Editor March 19, 1981.

In this paper, we shall consider collisional effects on LIF measurements in combustion systems, with particular attention paid to the important and popular OH molecule. Both quenching (removal from the electronically excited state) and energy transfer among internal levels (rotational and/or vibrational) of the excited state will be addressed.

As we shall see, it is important to properly include collisional effects in the quantitative employment of LIF. This is most easily done in the case of OH, for which there exist relatively abundant collision data, and especially in air flames, where N_2 is often the most probable collision partner, although further research is still needed for a fully quantitative characterization over a wide-ranging set of conditions. We shall also find that, even in the absence of a complete set of collisional data, the effects introduced by quenching and energy transfer do not diminish the considerable utility of LIF as a flame probe. Even if collision rates must be estimated, LIF can still provide results of significance for the understanding of, and insight into, the chemistry of combustion.

2. MOLECULAR COLLISIONS UNDER FLAME CONDITIONS

2.1. General considerations

In laser-induced fluorescence, the laser is tuned such that its wavelength matches that of some (identifiable) absorption line of the desired species (see Fig. 1). The molecule is elevated to a particular

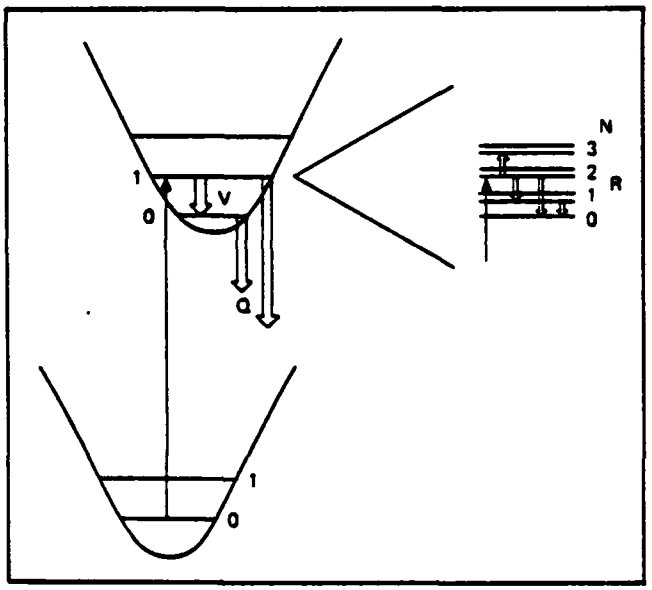

Fig. 1. A schematic diagram of pertinent energy transfer processes associated with LIF measurements, pertinent to a $^2\Sigma^+$ excited state as in OH. The laser excites (upward arrow) a specific level ($P_2(2)$ here) in $v' = 1$. Some of the rotational transfer (R) routes are shown as are vibrational transfer (V) and quenching (Q).

rotational level (perhaps one particular component, if electronic fine structure exists) of a particular vibrational level of some electronically excited state. The quantum numbers v' (vibration), N' (rotation), and J' (total angular momentum) will generally serve to identify a distinct level in this sense. As the laser is tuned through a series of absorption lines and the fluorescence monitored as a function of laser wavelength, a so-called excitation scan is produced. Figure 2, to be described further below, displays a small portion of such excitation scans for OH and NH, with one particular line designated in each case. In essence, the excitation scan is an absorption spectrum of the molecule of interest, except that detection is via the positive fluorescence signal on a null background instead of the much less sensitive decrease in transmitted light in a conventional absorption measurement.

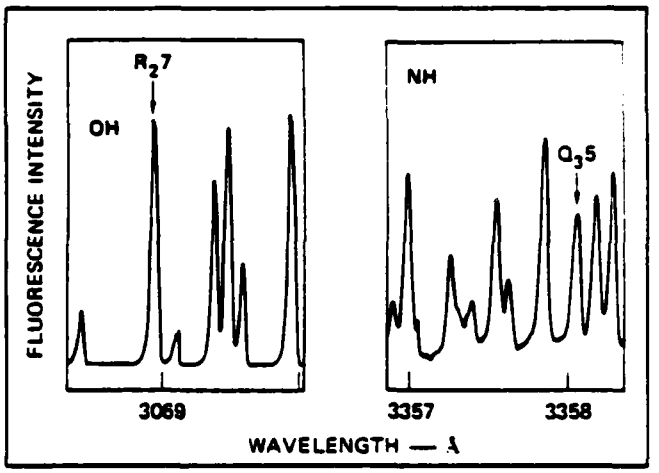

Fig. 2. Excitation scans through portions of the (0, 0) bands of the $A^2\Sigma^+ - X^2\Pi_i$ system of OH and the $A^3\Pi_i - X^3\Sigma^-$ system of NH. The medium is the reaction zone of a CH_4/N_2O flame at atmospheric pressure. From the relative intensities and an estimate that Q/A is the same for each species, it was found that [NH]/[OH] ≈ 0.04.

Because typical molecular radiative rates are of the order of $10^7\ sec^{-1}$, whereas typically rates for collisions causing a change in energy level are $\gtrsim 10^9\ sec^{-1}$ at 1 atm, the most likely fate for an excited molecule is to undergo collisional transfer to some other level. The collisions are qualitatively separated into two categories: (i) quenching collisions, with rate Q, which remove the molecule from the electronically excited state as a whole (usually, but not necessarily, into the electronic ground state) so that it does not fluoresce; (ii) energy transfer collisions (vibrational with rate V, or rotational with rate R) transferring into a different level of the electronically excited state which can then either undergo further collisions or emit a photon (see Fig. 1). As we shall see, each of these energy transfer rates is in general specific to the initial and final quantum states. The rates, in sec^{-1} units, are sums, over all possible collision partners i, of rate constants k times number densities n, e.g.,

$$V = \Sigma_i k_V(i) n_i . \tag{1}$$

An important parameter is the size of R and/or V relative to Q. If $R, V \gg Q$, an excited molecule will undergo many energy transfer collisions before quenching. Thus the excited state will attain some broad distribution (perhaps thermal-like) over its internal energy levels, and the resulting fluorescence spectrum will reflect this wide distribution. If, on the other hand, $Q \gg R, V$, the initially excited molecules will mostly be quenched before undergoing energy transfer, and the fluorescence spectrum will be dominated by large peaks corresponding to lines emitted from that level directly pumped by the laser. This situation has been termed "arrested relaxation" or "frozen excitation."

In either case it is the ratio of quenching rate to radiative rate (Einstein spontaneous emission coefficient) A which determines the total fluorescence yield Φ_t:

$$\Phi_t = \frac{A}{A+Q} \approx \frac{A}{Q} \tag{2}$$

which is the number of photons emitted per molecule initially excited by the laser.[a] The approximate equality holds at pressures of the order of 1 atm where $Q \gg A$. The effective quantum yield Φ_e for a given experiment, however, contains effects of energy transfer if (as is

[a]The situation is somewhat more complex if energy transfer occurs and A or Q varies with level. Although this often does occur to some degree, the corrections are usually minor ones and will be ignored for purposes of discussion in the paper.

often the case) the fluorescence from only a particular set of excited state levels is detected. For example, suppose OH were excited to $v' = 1$. Then if emission in the (1,0) band were detected,

$$\Phi_e = \frac{A(1,0)}{Q+V}; \tag{3}$$

whereas if emission from molecules which have undergone vibrational energy transfer to $v' = 1$ were observed,

$$\Phi_e = \frac{A(0,0)V}{Q(Q+V)}. \tag{4}$$

(Here, A(i,j) is the radiative rate into the (i,j) band and any variation of Q and V with level is ignored).

In considering the effects of energy transfer, it should be borne in mind that energy transfer within excited states often occurs quite rapidly. Even vibrational energy transfer cross sections can be similar to or in excess of gas kinetic values, such that V, R and Q are of the same magnitude. This may be due to the role played by attractive forces during such collisions,[2,3] or perhaps communication with energy levels belonging to other electronic states.[4] Whatever the reason, the excited state behavior can be quite different from that of ground states, where generally $R \gg V$.

2.2. Individual species

In Table I is given a list of species which have been observed using LIF in flow systems and/or in flames, and which arise as "natural"[b] intermediates in the combustion process. The effects of the energy transfer and quenching collisions vary from species to species in Table I, though they may be loosely categorized.

TABLE I. Combustion Intermediates Which Have Been Observed Using LIF.

O, N
OH*
CH*, CN*, C_2*, CO
NH*, NH_2
NO*, NO_2*, HNO
S_2*, SH*, SO*, SO_2*
CS, CS_2
C_2O, C_3, HCN
CH_3O, CH_2O

* Denotes that detection has been performed in a flame.

In the case of O and N atoms, whose fluorescence has been excited in a flow discharge using two-photon excitation,[5] the situation should be relatively simple. Only the quenching of one electronic state, and possibly transfer among fine structure levels, need be considered.

The diatomic hydrides have widely spaced energy levels so that only a tractably small number is of importance. However, this same large spacing may preclude rapid thermalization in the excited state and especially emphasize state-specific effects, compared to the heavier diatomics.

As one proceeds to larger molecules, the effects of collisions may be expected to generally become more severe. This is basically a consequence of the larger number of energy levels available as final states for either energy transfer or quenching. The energy transfer spreads the excited molecules over a wide distribution of internal levels, resulting in an extensive emission spectrum and reduction of the emission into any given wavelength, i.e., Φ_e, whereas the quenching reduces the overall Φ_t. This, together with a larger ground state partition function (and thus a smaller fraction of molecules in the level pumped by the laser) will tend to render LIF less sensitive for the larger species. For example, the NH_2 molecule has been readily excited in many low pressure flow system experiments, and it has been detected via laser absorption in a flame.[6] However, its observation by LIF in atmospheric pressure flames has thus far eluded efforts at several laboratories, including our own.

The effects of energy transfer within the excited state have been observed in some detail for OH and are discussed below. Additionally, nonthermal population distributions following laser excitation in flames have been seen for CH,[7,8] NH,[9,10] and CN.[8] (A published spectrum for C_2[11] appears more thermal-like but is not conclusive.) While none of the data on these other species has been treated quantitatively, it is apparent that effects similar to those in OH are occurring and that qualitative generalizations can be made from the hydroxyl results.

For molecules other than OH, bimolecular collision data (for both quenching and energy transfer) exist in a spotty fashion, and seldom at flame temperatures. LIF experiments performed under controlled (sub-atmospheric) pressure conditions constitute the best means of obtaining the collision rate constants, because of the single-level excited state preparation inherent in LIF. Quenching is typically measured by pressure effects on excited state lifetimes (using real-time or scanning gated integrator detection) while energy transfer is investigated by spectroscopic discrimination of emission from different levels, although the two must sometimes be coupled. Even so, obtaining data at temperatures corresponding to those of flames remains a problem.

At the present time (and likely in the future) the OH molecule occupies a premier place in the field of LIF combustion probing. It is an ubiquitous and important reactive intermediate, so that its presence can serve to signify the occurrence of combustion, a sort of index of the degree of reaction. It possesses a well-established spectroscopic data base and the wavelength regions required are particularly convenient from an experimentalist's viewpoint. The collisional data base for OH, while containing some gaps, is relatively well established. Quenching has been investigated extensively (a term not necessarily synonymous with "conclusively") while both rotational and vibrational excited state energy transfer have been studied in detail. Because of this, OH has also come to serve as a test molecule for concepts concerning collisional effects and for the quantitative pursuit of new ideas such as saturation spectroscopy and energy transfer thermometry. Much of the remainder of this paper, particularly the energy transfer section, will deal with collisional effects on OH LIF measurements.

3. QUENCHING

Quenching of the excited state determines the overall fluorescence yield Φ_t [Eq. (2)] and its value is obviously crucial in relating the observed fluorescence signals to the desired concentrations. There are several ways of dealing with the problem of accounting for the quenching: (i) calculation of Q using previously measured or estimated bimolecular rate constants; (ii) calibration of the fluorescence signals and extrapolation of energy transfer rates; (iii) direct measurement of Q *in situ*; and (iv) optical saturation. Each has advantages and limitations depending on conditions and the problems addressed, and each will be discussed in turn.

3.1. Calculation or estimation of quenching rates

In this straightforward approach, Q is calculated as in Eq. (1) using previously measured bimolecular collision rate constants and absolute number densities of collision partners in the flame. This presupposes, of course, that each of these is known for the major contributors; this situation varies with probed species and flame conditions.

In the case of OH there exists a number of measurements of k_Q values for some flame gases, although nearly all of them have been

[b] Thus a number of species such as metal atoms, their oxides and halides, which are observable with LIF but usually obtained in flames through seeding, are not included. Also excluded is a considerable number of larger organic molecules, e.g., benzene, acetone, benzyl radicals, etc.

made at room temperature. Schofield[12] presents a useful compilation of collision rate constants for excited OH (as well as several other species); only one measurement[13] has appeared subsequently.[c] Disagreement is evident: there are nine modern values for $k_Q(H_2O)$ differing by a factor of three. In our opinion, the most reliable values arise from recent LIF experiments where a single level is initially excited; these are summarized in Table II. The *agreement* evident in

TABLE II. Quenching Rate Constants for $v' = 0$, $A^2\Sigma^+$ OH from LIF Measurements. Units are 10^{-11} cm^3 sec^{-1}. All values have been corrected to a radiative lifetime of 0.69 μsec; all determinations were made at room temperature.

Reference	2	13	14	15	16
Collision Partner					
N_2	4.0	2.8	2.3	2.5	—
O_2	—	9.1	8.1	—	—
H_2O	—	37	56	—	—
H_2	7.8	—	11.9	13.7	8.4
D_2	10.9	—	—	—	—
Ar	—	—	—	0.037	0.06
He	—	—	—	0.008	—
H	—	—	—	—	60

Table II, among independent measurements in separate laboratories, is noteworthy when set against the full range of OH rate constants, and within the field of energy transfer in general, in which there usually exists far higher precision than accuracy. Nonetheless, discrepancies are evident, and there are no modern (LIF) data for the important gases CO_2, CO, or fuel molecules. Furthermore, there are little data at flame temperatures; a value of $k_Q(N_2)$ in a flame[17] is larger than expected for a simple $T^{1/2}$ extrapolation from room temperature.[12] In considering the important H_2/O_2 flames, including those with Ar diluent, it should be noted that[16] $k_Q(H) = 6 \times 10^{-10}$ cm^3 sec^{-1}; $k_Q(O)$ and $k_Q(OH)$ have never been measured.

Using such rate constants, Bechtel and Teets[18] calculated quench rates at each flame position to reduce their LIF data on OH in an atmospheric pressure CH_4/air flame. Number densities of the principal collision partners were determined, at each flame position, by Raman profiles for the major species. The absolute OH concentration is normalized to laser absorption measurements in the post-flame gases. The resulting profile of OH through the reaction zone (where the absorption is too weak to measure) is in good agreement with the predictions for a theoretical model of this flame. These results are encouraging regarding the use of calculated quenching rates for the reduction of OH LIF measurements.

Morley[19] has measured profiles of LIF signals for OH, CN, NH and NO in H_2/O_2/Ar flames doped with CH_3CN. The radical concentrations are deduced using previously determined or estimated quenching rate constants and calculated values of collision partner densities. The results fit realistically into a model of the chemistry, again suggesting proper (at least adequate) handling of the quenching.

Under some conditions, even a rather crude estimation of the quenching rate can provide valuable information. As an example consider measurements which we have made in a CH_4/N_2O flame. Because the N-N bond strength in N_2O is 4.93 eV, while the N-O bond strength is 1.68 eV, the obvious chemical mechanism would involve the splitting off of the oxygen atom and subsequent oxidation of the hydrocarbon. The emission spectrum of this flame shows bands due to NH, NH_2, NO and CN, all of which arise through breakage of the N-N bond. However because of the possibility of chemiluminescent excitation within the flame, the existence of emission does not necessarily denote a significant concentration of these radicals in the chemically relevant ground state.

Such information can be supplied with LIF. Figure 2 shows a section of the excitation scans through particular regions of the OH and NH spectrum; the laser was focused into the luminous reaction zone of the flame. In each case the identified line is used to calculate the relative concentrations of NH and OH. Given the near-total absence of quenching information for NH, the ratio Q/A is taken the same for both species. This results in a ratio [NH]/[OH] ~ 0.04 in the reaction zone of this flame. A separate absorption measurement shows OH to be present in typically large amount, $\sim 7 \times 10^{15}$ cm^{-3}. Thus the concentration of NH is $\sim 3 \times 10^{14}$ cm^{-3}, high enough to be of chemical significance. This finding, using an obviously very simple approach to the quenching problem, is important in setting the stage for consideration of the chemistry of this flame, a model for which must address the potential role of nitrogen-containing molecules in the chain reactions.

Subsequent to this simple experiment and analysis, the measurement was repeated by Anderson and coworkers[10] in a more thorough and careful way, taking profiles through the flame. They found the NH concentration to reach a maximum in the reaction zone; calibrating with an absorption measurement, $[NH] = (3.8 \pm 1.3) \times 10^{14}$ cm^{-3} in that region. Our approximate value agrees with this careful determination more closely than our assumption on Q/A warrants; but it demonstrates that useful information on flames *can* be obtained without undue concern as to quenching.

3.2. Calibration and extrapolation of energy transfer rates

This method, due to Steinberg and Schofield,[20] does not incorporate absolute collision rates but rather only their temperature dependence. A narrow bandwidth detector senses only emission from the initially pumped level, so that the effective quantum yield in their experiment is determined by the sum Q+V+R [compare Eq. (3)]:

$$\Phi_e = A/(Q+V+R) . \tag{5}$$

Now this rate for total collisional transfer from the initially excited level is large and *probably* does not involve energy barriers, so that the rate constants scale as $T^{1/2}$ from the mean velocity variation. The number density of collision partners varies as T^{-1} at constant pressure, so that for two positions at different temperatures within the flame

$$\Phi_e(x_1)/\Phi_e(x_2) = [T(x_1)/T(x_2)]^{1/2} . \tag{6}$$

The position x_2 is chosen to be downstream, at a point where the concentrations of all desired fluorescing species can be confidently calculated from chemical equilibrium considerations. Then, with S denoting fluorescence signals,

$$\begin{aligned} n(x_1) &= S(x_1)\Phi(x_2)n(x_2)/S(x_2)\Phi(x_1) \\ &= [S(x_1)n(x_2)/S(x_2)]\,[T(x_2)/T(x_1)]^{1/2} . \end{aligned} \tag{7}$$

(Alternatively, the concentration at x_2 could be determined by an absorption measurement, as in Refs. 10 and 18, if sufficient absorption were present). The technique was used to obtain profiles of OH, SH, S_2, SO and SO_2 in the post-flame gases of H_2, O_2, N_2 flames seeded with H_2S, so as to investigate sulfur chemistry in flames.

This is an attractive technique for laboratory flames for both its simple handling of the quenching problem and built-in calibration of the detection system and geometrical factors. Selection of the initially excited level and an isolated transition is possible in general, but perhaps must be done at the expense of signal level and hence sensitivity. It is most useful through the post-flame region as employed in Ref. 20, because neither temperature nor the molecular composition of the collision environment is varying drastically. As one approaches the reaction zone, the method is on a less sure

[c] It should be noted that all of Schofield's rate constants for OH should be multiplied by 1.10 because of his use of 0.76 μsec as the radiative lifetime instead of a preferred value of 0.69 μsec.

footing: relative values of k_Q, k_V, and k_R vary from one collision partner to another, and a temperature dependence more complex than $T^{1/2}$ may become noticeable over a larger temperature range. As more energy transfer rate constants, and especially their temperature dependence, become available, this method will become useful over a broader set of conditions.

3.3. Direct lifetime measurements

Under certain conditions it is possible to directly measure the quenching rate of the laser-excited molecules *in situ*. Consider a short laser pulse creating an initial excited state population[d] n_o at time $t = 0$. The excited state will then decay exponentially as

$$n(t) = n_o \exp[-(Q+A)t]. \tag{8}$$

Thus a measurement of the time-dependent decay curve of the fluorescence furnishes Q + A. This is the typical method for the LIF measurement of radiative lifetimes and quenching rate constants such as those of Table II.

The limitation on this method is the requirement that $Q+A<\tau_L^{-1}$, where τ_L is the laser pulse length. (If this were not the case, the excited state would decay rapidly following excitation, and the time dependence of the signal would simply follow the laser temporal pulse shape.) For a typical $\tau_L \sim 10$ nsec, this then limits the maximum $Q+A$ to $\sim 3\times 10^7$ sec^{-1} for usable signals. For OH, this would correspond to a maximum pressure of $N_2 \sim 100$ torr at flame temperatures, and less if H_2O is present. Hence, this method is not useful for atmospheric flames.[e]

The method is, however, eminently suitable for low-pressure flames. It has been applied to flames of propane-oxygen at total pressures ~20 torr by Stepowski and Cottereau.[21,22] Quenching rates, ranging from 2.5 to 3.1×10^7 sec^{-1}, were measured at three different stoichiometries, in good agreement with those calculated from bimolecular k_Q values. An important and somewhat surprising result[22] is the nearly constant value of Q found to exist throughout the entire luminous zone and into the burnt gas region. The authors attribute this to an early rapid increase in the concentration of the efficient quencher H_2O, and a lack of sensitivity of the quenching rate to temperature.

Stepowski and Cottereau also point out[21] that, for a short-pulse laser $\tau_L > Q+A$, the absolute concentration can be obtained from the peak value n_o and knowledge of τ_L, although use of the integrated signal

$$\int_0^\infty n(t)dt$$

and the directly measured decay rate should provide more accurate results.

For flame conditions such that it is experimentally tractable, this direct determination of Q is the decidedly preferable method, relying on no assumptions about rate constants, their temperature dependence, or the gas composition. It also serves as an important means of investigating with low-pressure flames the validity of calculated or estimated quenching rates for use at higher pressure; this will be particularly valuable for high temperature conditions, as with the existing results for propane/oxygen through the flame front.

[d] In concept, we are here summing over all excited state internal levels and assuming Q and A independent of level in the sense of Eq. (2) for present discussion. In practice one must often consider effective quenching rates including energy transfer, as in Eq. (3), but this is readily incorporated.

[e] In principle, picosecond lasers and fast detection methods could increase the useful pressure range. However, the necessary technology is too cumbersome at the present time to consider this a currently practical extension.

3.4. Saturated LIF

This method was first suggested by Piepmeier[23] for detection of atoms in flames, and later extended by Daily[24] to consider LIF probing of combustion intermediates. The essential impetus which has driven development of this technique is a desire to make accurate absolute time-resolved measurements in systems whose temperature, composition and density vary with time, such as one encounters in turbulent combustion or in detonations. In such situations, the instantaneous collisional environment may be very poorly characterized, so that Q cannot be calculated or estimated with confidence. The saturation method seeks to circumvent this by operation at high enough laser intensity that the signal level is independent of Q.

In concept the method is elegant and simple. Figure 3(a) illustrates the situation for a two-level system. The signal level in this case

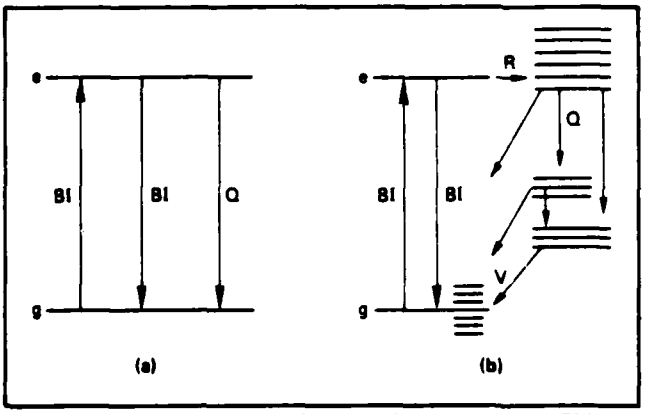

Fig. 3. Schematic level diagram for saturation spectroscopy. BI is the absorption/stimulated emission rate for laser intensity I. (a) Idealized two level system. (b) Molecular system with internal levels. In general, energy transfer rates in the ground state are slower than those in the excited state.

in given by[f]

$$S = \frac{AB I n_g}{Q+A+2BI} \tag{9}$$

where $B = \lambda^3 A/2hc^3$ is the Einstein absorption coefficient. The presence of the term 2BI in the denominator arises from the fact that at sufficiently high laser intensity, stimulated emission at a rate BIn_e constitutes a significant process for returning the atom from e to g. At very high laser intensity, where $BI \gg Q+A \approx Q$, S approaches the asymptotic value $An_g/2$, independent of Q. (At low values $BI \ll Q$, Eq. (9) reduces to Eq. (2) because $\Phi_t = S/BIn_g$ by definition.)

Thus a measurement of the absolute signal as $I \to \infty$ furnishes an absolute concentration n_g, requiring for the analysis only an independently measured value of A. Relative measurements of S, as a function of I measured absolutely, yield the quench rate Q; inverting Eq. (9) one obtains

$$S^{-1} \propto [2+(Q+A)/BI] \tag{10}$$

so that a plot of S^{-1} versus I^{-1} yields Q (in terms of a known A and calculable B) from the slope to intercept ratio.[25]

Saturation behavior in flames was first observed for C_2 by Baronavski and McDonald.[26] It has also been studied experimentally for Na,[25,27-32] MgO,[30] CH and CN,[33] and OH.[34] It became apparent that spatial and temporal profiles of the laser beam must be considered[31,35] for quantitative results. Creation of a significant excited

[f] Neglecting geometrical factors, detection efficiencies, etc., assuming for simplicity equal degeneracies in each state, and using a steady-state approximation.

state population can result in perturbations in the chemistry and total concentration of the probed species,[29] if the electronically excited state processes different reaction rate constants from those of the ground state. Such laser-induced chemistry does not occur under all flame conditions, however,[6] and can often be avoided through the use of sufficiently short (10 nsec) laser pulses.

More important, within the context of this review, is the fact that energy transfer among the internal vibrational and rotational levels of molecules can greatly modify the situation, compared to the two-level system picture. Figure 3(b) schematically illustrates such effects. The laser strongly couples a pair of levels e and g, equalizing their population at high I. However, collisional processes transfer population from e to other excited state levels; these as well as e itself may be quenched to some distribution over ground state energy levels. Because energy transfer rates (especially vibrational) in the ground state are generally slower than those in the excited state, the population of level g is collisionally repleted more slowly than the population of e is depleted. The net result is that during the laser pulse, a fraction of the population in the pair of levels e and g connected by the laser is transferred into other levels. The relationship between the population in the pair, which determines the measured signal level, and the total molecular population depends sharply on the relative energy transfer rates.

There exist two limiting cases in which the energy transfer can be treated simply.[30] If quenching of e directly back to g is much more rapid than energy transfer out of e, there is no communication with other levels and the system behaves like a two-level system. The quench rate Q obtained from the S^{-1} versus I^{-1} plot [Eq. (10)] would be the correct value. Although considerable quenching directly back to g is unrealistic for a true molecule, this limit will be approached if $Q \gg R, V$. Conversely, if $R, V \gg Q$, the upper state will thermalize before quenching. Then the apparent quench rate plot based on Eq. (10) would be Q times the upper state partition function. For example, the reported[26] Q for C_2 was $1.2 \times 10^{12}\,sec^{-1}$; if the excited C_2 were to fully thermalize this would correspond to an actual Q of $1.7 \times 10^{8}\,sec^{-1}$. A value $Q \sim 10^{9}\,sec^{-1}$ is physically realistic, suggesting significant relaxation occurs before quenching in this molecule.

The intermediate situation, when $Q \approx R, V$, has been considered in a numerical model of the response of OH to laser excitation, under conditions approaching optical saturation and in a collision environment at 2000 K corresponding to the burnt gases of an atmospheric pressure methane-air flame.[16] The model, a solution of time-dependent equations, describes excited-state energy transfer based on previously measured state-specific rate constants,[17] and includes ground-state energy transfer with estimated rate constants. The spirit of the model was not the provision of a quantitative means of analyzing saturated LIF in OH, but rather an exploration of the above qualitative concepts using realistic parameters. The chief findings were several. First, the steady-state approximation is not fully valid for 10 nsec laser pulses in an atmospheric pressure flame. This has received qualitative confirmation in the experiments of Lucht, Sweeney and Laurendeau[34] who observe a slight time dependence in the emission from laser-excited OH apart from that which simply follows the laser pulse. Second, the apparent quench rate tends toward the qualitative limits as the "true" Q is artificially varied relative to R, V. Finally, the importance of ground-state relaxation is clear. Using an estimated but realistic $V(\text{ground}) = 2 \times 10^{8}\,sec^{-1}$, it was found that 40% of the population was tied up in other ground state vibrational levels, and that significant alteration of the ground state rotational distribution occurred.

Several other models[35–40] of this process have also been constructed. These generally consider the molecular internal structure in terms of a highly truncated number of levels, so that the energy transfer may be described by a small number of parameters. This is a sensible approach and is probably ultimately realizable, at least for some range of conditions. However, the present truncated level models do not, in our opinion, realistically consider ground state relaxation, in that they leave out the slow vibrational transfer. Until that issue is addressed, through experimental rate constant determination, it will be difficult to assess the validity of various truncated-level approaches.

The rate constants needed to develop saturated LIF into a quantitative method generally encompass those needed for the means of accounting for quenching in Sections 1 and 2. Thus, for molecules, it does not appear that saturation spectroscopy possesses inherent advantages with regard to accuracy. In laboratory flames, where there exists the leisure to characterize the collision environment, calibrate the fluorescence signal, etc., operation in a nonsaturation regime appears preferable. However, when that is not possible, for example in turbulent combustion, the saturation method remains promising and warrants continued development. Such further study should concentrate on OH, which will probably command the bulk of the LIF attention in nonlaboratory flames. Of course, saturation experiments on other species, performed under controlled conditions, can be an important tool in developing the technique and understanding the energy transfer itself.

4. ENERGY TRANSFER

As we have seen, quenching modifies the overall signal levels and total quantum yield for LIF. Collisions which cause energy transfer among the vibrational levels of the excited state, on the other hand, alter the spectral shape of the fluorescence and determine the effective quantum yield Φ_e into a given detector bandwidth.

The value of Φ_e is obviously needed to determine concentrations from the LIF measurements. In addition, if Φ_e varies with energy level from within the excited state, the energy transfer can significantly influence the value of the temperature determined by relative intensity measurements as in an excitation scan. Knowledge of the temperature is required in order to reduce the LIF concentration data, in the relationship between total molecular population and the population in the ground state level responsible for the absorption of the laser radiation. Of course, the temperature can be obtained by other means, although its determination using LIF ensures ready spatial coincidence with the concentration measurement.

The growing evidence from many regimes that much molecular energy transfer is state-specific, that is, the rates are dependent on the individual quantum states involved, suggests that its influence must be considered in some detail. In fact, observations on state-resolved energy transfer in flames are important in providing information on high temperature collision dynamics which supplements the more typical low-pressure flow system energy transfer experiments, usually performed at room temperature. Additionally, of direct interest for combustion itself is the description of how molecules with excess energy (e.g., as formed in an exoergic chemical reaction) approach thermal equilibrium.

The first laser-based measurements of state-specific energy transfer in flames involved single- and double-photon excitation of several electronic states of Na in C_2H_2/air.[32] The intensities of fluorescence from four levels were measured following initial excitation of one of them with the laser, and the measurements were repeated with each of the four levels being initially excited. Determination of the relative populations permitted the extraction of energy transfer rates specific to initial and final states. The results showed that the Na relaxed in a stepwise fashion, preferentially to nearby levels, experiencing a significant degree of population of intermediate levels before returning to the ground state. A similar, independent study[41] soon followed; in it rates were not deduced although the observations were consistent with the results in Ref. 32.

The first measurements of state-specific energy transfer, however, well pre-date the laser era. Carrington[42] used atomic line excitation of a single level in OH in low-pressure and atmospheric flames. He observed a nonthermal rotational distribution and deduced a ratio $R/Q \approx 2.2$. This important experiment showed that neither the rapid quenching nor the thermalization limit applied for OH and that the energy transfer must be considered on a detailed basis.

[6] See, e.g., the discussion comments following Ref. 32.

As noted above, nonthermal distributions following single-level laser excitation have been observed for a number of species. Only for OH, however, do quantitative results exist, and this molecule is the subject of the remainder of this section. For reference, individual rotational levels for $v' = 0$, 1 and 2 of the $A^2\Sigma^+$ excited state are shown in Fig. 4. N' labels the rotational quantum number. Each level (save that with $N' = 0$) is a closely spaced doublet; these are labeled by $F_1(N')$ and $F_2(N')$. An F_1 level has $J' = N' + 1/2$ and an F_2 level has $J' = N' - 1/2$, where J' is the total angular momentum, composed of N' and the spin angular momentum S'; thus in an F_1 level S' is more or less parallel to N' whereas in an F_2 level they are more or less antiparallel.

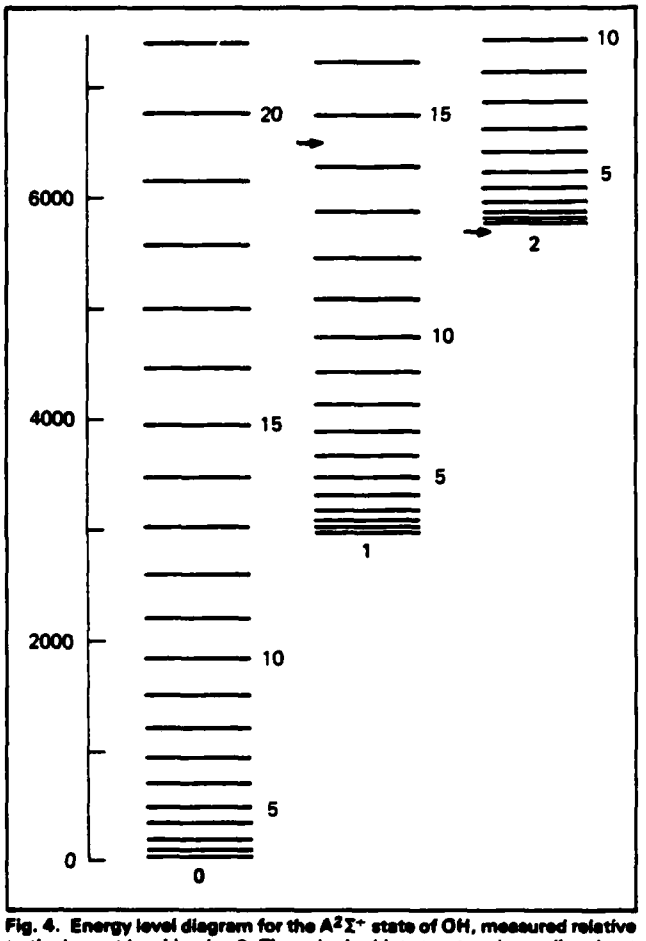

Fig. 4. Energy level diagram for the $A^2\Sigma^+$ state of OH, measured relative to the lowest level in $v' = 0$. The spin doublet structure is small and not shown. The numbers to the right of each stack denote N' and the values below each are v'. The arrows mark the predissociation limits in each vibrational level.

4.1. Rotational energy transfer

Most of the experiments on energy transfer are performed in a similar way: the laser is tuned to excite a specific level, and the fluorescence is dispersed through a spectrometer. From the intensities of the rotationally resolved lines are obtained relative populations in each level. In some cases a study of the time dependence of the observed signals provides the desired information.

Several groups have studied rotational energy transfer within the $v' = 0$ level of electronically excited OH, and the results are generally quite consistent. The observations reveal distinctly state-specific behavior, which is reasonably well described using a rate constant model based on room temperature measurements.

Smith and Crosley[43] performed measurements in the burnt gases ($T \approx 1900$ K) of a methane/air flame at atmospheric pressure; rotational level population distributions were determined for initial excitation of the $F_1(1)$, $F_1(5)$, $F_2(5)$, $F_1(10)$, $F_2(10)$ and $F_2(15)$ levels.

The observed distributions exhibit the following features: (i) The total amount of rotational transfer which occurs decreases with increasing N'; this will be discussed in more detail below. (ii) Transfer upward from the pumped level is described by a thermal-like distribution, although the apparent temperature is an artificial one whose value increases with N'. (iii) Downward transfer is described by a statistical distribution, proportional to the final-state degeneracy, with little or no energy dependence. (iv) Transfer to the same spin component ($F-F_1$ and F_2-F_2) is favored over F_1-F_2 for $|\Delta N'| \lesssim 4$. (v) In general, transfer to nearby levels (small $\Delta N'$) is favored but multiquantum ($|\Delta N'| > 1$) transfer in a single collision clearly takes place.

These features are generally what would be expected from consideration of the room-temperature, state-specific rotational energy transfer rate constants of N_2 collisions,[37] where similar behavior is seen. A computational prediction[36] of the distributions utilizes an information theoretic[44] form of those experimental rate constants constructed for extrapolation to high temperatures. It is in good qualitative agreement with the experiments, although in particular the observed propensity for F_1, F_2 conservation is larger than the model suggests.

Chan and Daily[45] have performed similar experiments pumping a series of lower-lying levels ($N' = 1$ to 5). They use a more sophisticated form of the state-specific transfer rates, again based on the experimental results of Ref. 37. A fit of the model to ~40 observed populations is in very good agreement (~20% typical) with, pleasingly, little sensitivity to the precise values of additional parameters introduced beyond the information theoretic form.

Stepowski and Cottereau[46] have performed experiments in a low pressure flame, where $Q \ll \tau_L^{-1}$. The $F_1(7)$ level is pumped and rotationally resolved fluorescence is observed at successive time delays following the exciting laser pulse. This permits the determination of the time evolution of the population distribution governed by the same state-specific rate constants. Again, similar features are noted, including good agreement for the total energy transfer rate with the low-temperature Ar results,[37] using a flame diluted with that gas.

In an even more recent experiment,[47] the excitation is to a mixture of $F_1(1)$, $F_2(1)$ and $P_1(3)$. Upward transfer to very high levels ($N' > 8$) is described by a thermal distribution having a derived temperature close to that of the flame. This result is not inconsistent with those of Ref. 43, in which transfer to such high levels was not measured for $N' = 1$ excitation.

As discussed above, the ratio Q/R forms a simple measure of the degree of thermalization which occurs in the excited state prior to emission. A very simple interpretation of the energy transfer data permits the determination of this quantity. Consider that rotational energy transfer, at rate R, transfers molecules from the initially excited level e into all other levels, o, as schematically illustrated in Fig. 5. Levels o are then quenched at the rate Q; back-transfer into e is ignored. A steady state approximation is applied to N_o, the population of the pumped levels:

$$dn_o/dt = 0 = Rn_e - Qn_o \tag{11}$$

and

$$n_e/n_o = Q/R. \tag{12}$$

The results for Q/R determined in this way from several investigations are presented in Fig. 6 as a function of the rotational quantum number N' of the initially pumped level. (The value of the Chan and Daily experiments is from our analysis of a spectrum published earlier[48] by those authors, and the value for the computational model[36] arises from a similar treatment of the model predictions as if it were experimental data.) The error bars, where shown, are the estimates of the original authors. There exists impressive agreement

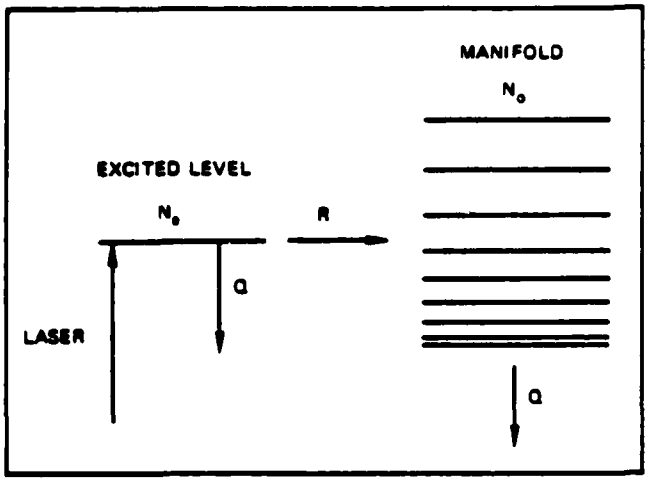

Fig. 5. Diagram defining levels and rates for the simplified analysis yielding Q/R as a function of N'.

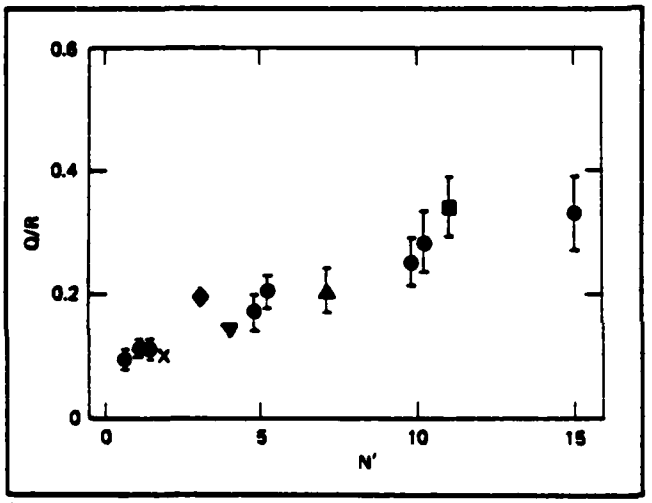

Fig. 6. Q/R as a function of N' in v' = 0. Circles, Ref. 43; X, Ref. 47; Diamond, Ref. 38; Inverted Triangle, Ref. 48; Triangle, Ref. 46; Square, Ref. 42.

among the different experiments; although different flames were used in some cases, the measurements were all made in the burnt gases where a similar collisional environment exists.

The increase in the ratio Q/R with increasing N' is strikingly evident. Because quenching is an exoergic process, transferring large amounts of energy away from the OH, it is not a probable candidate for N' variation. More likely to vary is R, because transfer with small $|\Delta N|$ is preferred and the energy separation between adjacent levels does increase linearly with N'. The only direct (single-collision) measurements offer little guidance. These, available for room temperature and low N', show both quenching [14] and rotational energy transfer[37] to be constant over the range N' = 1 to 6.

This variation must be included in any type of truncated-level approach[30-40] for treating saturated LIF. Even the state-specific computational models[36,45,49] of the rotational distributions have assumed a constant value for this ratio, based on the room-temperature experiments, and must be amended to provide a microscopically realistic description.

Rotational energy transfer in v' = 1 has not yet been determined quantitatively. Because the degree of thermalization is there governed by the ratio R/(V + Q), even less rotational transfer is expected to occur. This is borne out by qualitative consideration of fluorescence spectra[50] obtained pumping a series of levels in v' = 1. Of particular interest is a marked decrease in the amount of rotational transfer for levels above the predissociation limit (see Fig. 4), compared with the amount for levels below this limit. Additionally, a smaller amount of vibrational transfer occurs for the higher levels (see next section). Thus, for these very high levels, the behavior of OH is tending more toward the frozen excitation limit. Whether this is directly associated with the predissociation, or simply the large level spacing in this region, is not yet known.

4.2. Vibrational energy transfer

The only study of vibrational energy transfer in flames is that of Smith and Crosley.[50] The levels N' = 1, 5, 10 and 15 of v' = 1 were pumped, and fluorescence scans taken.

The rotational population distribution in v' = 1 is dominated by the initially pumped level, so that the measured vibrational transfer rate V can be ascribed to that level. The results exhibited a marked decrease in V with increasing N' of v' = 1 (see Fig. 7). An even larger

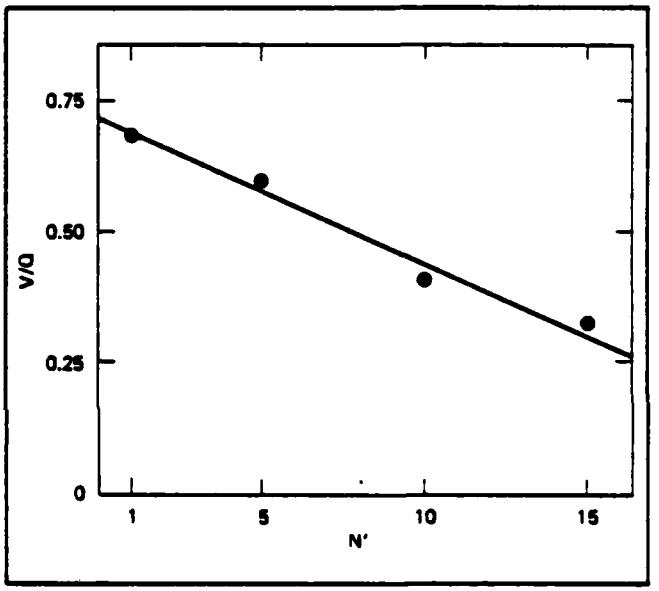

Fig. 7. V/Q as a function of N' in v' = 1. The line is drawn to emphasize the linear behavior observed, but there exists no fundamental reason known for such a relationship.

decrease was observed in room temperature experiments;[2] the comparison provides further (though not definitive) evidence for a rotationally dependent barrier on the potential energy surface on which occurs the vibrational energy transfer.

The rotational distribution for the molecules which underwent transfer to v' = 0 was measured. For an initial N' = 1, 5 and 10 in v' = 1, a thermal distribution over N' in v' = 0 was found, with T ~ 2200 K agreeing for each within experimental error of ~100 K. This is slightly higher than the flame temperature of 1900 K. Perhaps excess rotational energy results from the loss of vibrational energy. Thermal distributions with T higher than the ambient temperature, but independent of initial N' in v' = 1, were also found in the low temperature experiments.

A higher temperature (3300 ± 300 K) was determined for the distribution for the initial level N' = 15. Again, whether this is directly related to the predissociation is unknown.

4.3. Energy transfer effects on LIF signals

Because of the rather coarse rotational structure of the OH spectrum, a bandpass of 15 to 30 Å for an LIF experiment using spectrometer detection, which is a typical experimental configuration, will moni-

tor only certain upper state levels. For example, a finite bandpass centered near the intense Q_2 head of the (0,0) band will discriminate against P and Q branches of high N'. Due to the rotational energy transfer, which mostly populates nearby levels, the set of levels of high N' contain a greater portion of the entire upper state population when a level with high N' is pumped by the laser. Thus the ground-state populations for levels of high N' will appear anomalously low. If an excitation scan across a series of rotational lines is made, the resulting temperatures derived from a Boltzmann plot would be too low due to this effect. Similarly, the OH concentration obtained from excitation of an individual line could be systematically in error.

The influence of energy transfer on temperatures determined by LIF with narrowband detection has been qualitatively investigated for a single set of flame conditions.[51] The "true" temperature of a CH_4/air is determined using excitation scans with a broadband detector unaffected by the energy transfer considerations. Smoothed rotational population distributions obtained from Ref. 43 were used to generate a synthetic spectrum for each level pumped, and to calculate relative values of Φ_e for a defined detector center wavelength and bandpass. The model predictions were then compared with experiment using the same detector parameters; the results are shown as Boltzmann plots in Fig. 8. It is to be emphasized that the

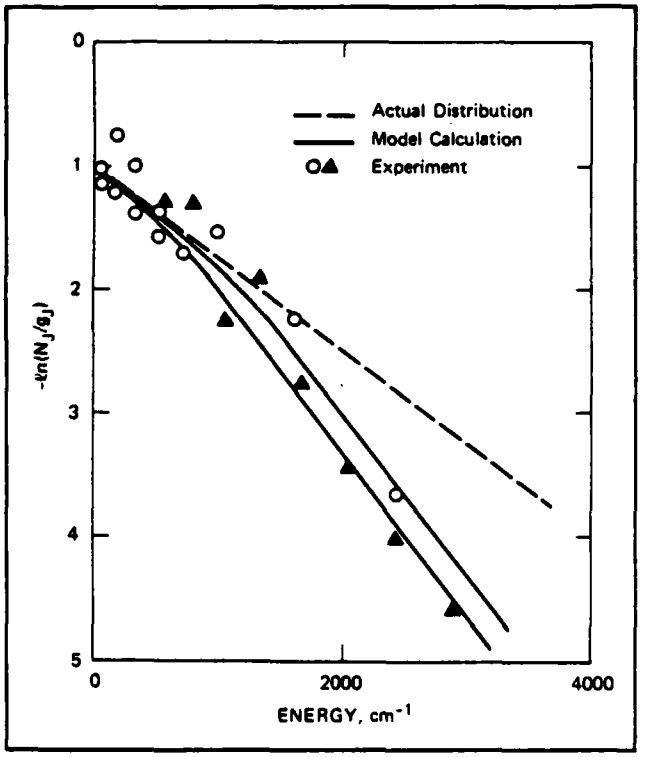

Fig. 8. The effects of rotational energy transfer on temperatures measured by LIF in OH are shown in the Boltzmann plot of apparent population. The distribution observed experimentally by the broadband runs is given by the dotted line. The rotational energy distributions are used to create a synthetic spectrum and predict the apparent populations for a narrowband run. The corresponding narrowband experiment is shown by the data points. The actual temperature (dashed line) is 1900 K while the apparent temperature from the narrowband run (points) is 1200 K.

model predictions arise from measurements of the rotational distributions, independent of the plotted experimental points. That is, no fitted parameters are involved, and the influence of the rotational energy transfer can be clearly seen. Using narrowband detection can lead to errors of several hundred degrees, if the transfer is not accounted for. An obvious conclusion is to use wideband detection, although in some cases narrowband detection may be necessary because of interfering species or to reduce the background flame luminosity.

Vibrational transfer can affect signal levels in a similar way.[50] Excitation to $v' = 1$ and observation of emission from molecules collisionally transferred to $v' = 0$ is a convenient way to avoid scattered laser light. However, the rate of vibrational transfer V and hence the effective quantum yield Φ_e for this scheme depends on N' (see Fig. 7). Again, errors of several hundred degrees can result depending on the range of N' covered in the experiment.

An examination[51] of previously published determinations[52-55] of temperatures from LIF in OH did not reveal direct evidence of possible energy transfer bias, beyond data scatter, except perhaps in Ref. 52. In fact agreement with temperatures measured by other means was achieved in some cases. Nonetheless it would appear prudent, in the light of the results expressed in Figs. 7 and 8, to consider possible errors during experiment design stages. In an experiment on NH in a CH_4/N_2O flame, using a 10 Å detection bandwidth, observed non-Boltzmann distributions from an excitation scan have been ascribed to energy transfer.[10]

Cattolica[56] has developed the method of two-line fluorescence, in order to circumvent problems due to both quenching and energy transfer in temperature determinations by LIF. In this method, the molecule is excited to the same upper level fom two different ground state levels. Thus any excited state collisional effects will cancel out in taking the ratio of the fluorescence intensities, which then directly yields the ratio of the two level populations. The two ground state levels may differ in rotational spacing, with $\Delta N = 2$ possible in OH using a satellite line as one pump transition, or they may belong to different vibrational levels; the choice depends on the temperature range to be probed. However, if OH concentrations, and not just temperatures, are to be deduced from the same measurements, the collision effects must be considered.

4.4. Energy transfer as a flame thermometer

Two attempts have been made to change energy transfer from a possible complication into a useful tool. Each seeks to exploit the energy transfer to determine the temperature simultaneously with the OH concentration, in a single laser shot. Such information correlating the temperature with the OH density will be useful in validating models of reactive time dependent flow. (As in Cattolica's two-line method, which is also suitable for single shot measurements of temperatures, rates must be known to determine absolute concentrations.)

Chan and Daily[49] measured the fluorescence spectrum following excitation of a single rotational level in $v' = 0$. The spectra were fit to the model[45] mentioned above, in which Chan and Daily added several parameters to a surprisal theory extension of the low temperature rate constants. In this study, the temperature was considered as a parameter determined by fitting the observed spectrum to the model. The sensitivity of the derived temperature to the results arises mostly through populations of levels with high N'; these are populated through upward transfer with rate constants related to those of the downward process by detailed balancing. Good agreement with thermocouple measurements over the range 1880 to 2010 K was achieved. Although the fluorescence spectrum was obtained by scanning the spectrometer and averaging over many laser pulses, single shot results could be achieved using an optical multichannel analyzer to record the entire spectrum at once.

Crosley and Smith[57] have investigated vibrational energy transfer as a flame thermometer. Here, $v' = 0$ is pumped. A few of the molecules undergo transfer upwards to $v' = 1$, with a rate given by $V\exp(-\Delta E, kT)$. This is obtained from detailed balancing on the downward rate, V, and expressed in terms of the vibrational spacing ΔE. The molecules in $v' = 1$ are collisionally removed at a rate $V + Q$, so a steady state balance on n_1 yields

$$n_1(V + Q) = n_0 V\exp(-\Delta E\ kT)\,. \tag{13}$$

This leads to an expression for the temperature

$$T = -\frac{\Delta E}{k}\left\{\ln\left[\frac{n_1}{n_0}\left(1+\frac{Q}{V}\right)\right]\right\}^{-1} \quad (14)$$

in terms of the measured ratio n_1/n_0 and the quantity Q/V. Using an average value of $V/Q = 2.2$ from measurements of downward transfer led to a temperature in good agreement with that from a rotational excitation scan.[36,b] The use of detailed balancing, even when $v' = 0$ is not in rotational thermal equilibrium under these conditions,[43] is validated by the observation[36] of common thermal distributions in $v' = 0$ following downward transfer from $v' = 1$.

The vibrational transfer experiment, though actually performed by averaging over several laser pulses, is also suitable for single-shot measurements using only two filtered photomultipliers. This requires much less data storage and fitting than does the rotational transfer thermometry, and may thus be advantageous for the collision of many single-shot measurements in a turbulent system. Additionally, no complex model is required. On the other hand, any two-point measurement is inherently less accurate than one which possesses considerable data redundancy, as in the rotational transfer thermometry experiment, and a value for Q/V is required.

4.5. Polarization of the fluorescence

In LIF measurements on flames, the fluorescent signals are collected with some particular detection geometry (usually 90° with respect to the exciting beam). This anisotropy can affect the effective quantum yields,[38] particularly if the exciting laser is polarized. Essentially, the emission transition dipole is parallel to the absorption transition dipole in a collision-free environment. Molecular rotation reduces the degree of anisotropy but does not remove it. Calculations of the degree of anisotropy have been performed for OH,[38] and they show that the effects can be large in the absence of collisions. For example, consider pumping a Q-branch for low J with polarized light and 90° detection. The Q-branches emitted by the pumped level have about 1.4 times the intensity expected for fully isotropic conditions, while the R and P branches appear some fifteen percent smaller.

Collisions generally reduce the level of polarization (i.e., degree of anisotropy) of the fluorescence, in two ways. First, elastic dephasing collisions destroy the directional polarization effects while leaving the molecule in the same level. The rate constant for this process for OH in the $F_1(1)$ level of $v' = 0$, colliding with H_2, has been determined[37] to be $2.4\,k_Q(H_2)$ from a combination of energy transfer[37] and Hanle effect measurements.[39] Second, collisions causing transfer to other levels can dephase at the same time. In the case of OH colliding with N_2, it was found[37] that emission from transferred levels was completely depolarized (isotropic) even when that from the initially pumped level was highly polarized. This is not, however, a universal situation. For example, rotational energy transfer in excited S_2 molecules caused by collisions with He still preserves at least eighty percent of the polarization per collision.[40]

In a way similar to the effects of energy transfer, the effects of polarized excitation and anisotropic detection on Φ_e depend on the ratio of the depolarizing (dephasing) rate compared to that of quenching. If the former is not much larger, and the Q, P and R branches are observed separately or with different detector efficiency, the fluorescence signals can be systematically different from the levels expected assuming isotropic conditions. Thus errors can be introduced, although they will probably be small.

Stepowski and Cottereau[46] have observed differences in apparent line strengths, in qualitative accord with the predictions,[39] for rotationally resolved fluorescence is their low-pressure (20 torr) flame. Polarization of LIF in an atmospheric pressure flame has not been measured.

[b]The value reported in Ref. 37 was based on $V/Q = 0.6$, estimated from bimolecular rate constants, and is erroneous. Apparently CO and CO_2 rapidly quench but cause little vibrational transfer.

5. CONCLUSIONS

In this review we have attempted to consider, in a fairly comprehensive way, collisional effects which are known (or at least conjectured) to influence the magnitude and/or spectral form of LIF signals in combustion systems. We have seen that a quantitative treatment must account for quenching and, for some situations, include a state-to-state description of energy transfer. In some cases this may be very difficult, due to the lack of certain rate constants or a detailed characterization of the collisional environment.

These considerations are important and further research is needed to place them on a still firmer foundation. However, in spite of them, LIF remains a very powerful and useful tool for combustion studies. Quenching can be treated in laboratory flames through calculation, calibration, or direct lifetime measurements. In the future we expect that saturation spectroscopy in OH can be made reasonably quantitative for certain definable ranges of conditions, if the ground state energy transfer is addressed experimentally.

In particular, it is important to recognize that LIF is predominately a tool for the understanding of combustion chemistry. Most investigations of this topic are (and should be) performed in laboratory flames, where the collisional environment can usually be characterized if necessary. However, even when it is unable to furnish accurate *absolute* concentration measurements, LIF can still provide crucial information about, and insight into, the pertinent chemical networks. The evidence may be ratios of concentrations of two or more intermediates, relative profiles or rates of change in certain zones, or just the detection of some key species even with large error bars. A simple example is the [NH]/[OH] measurement in CH_4/N_2O flames. Clearly, with the proper design of the experimental questions, useful and important results can be obtained well in advance of a full quantative characterization of all the collisional effects.

6. ACKNOWLEDGMENTS

Our studies of energy transfer in flames have been the result of a collaboration with Dr. Gregory P. Smith, whose participation in both the experiments and in countless discussions is acknowledged with pleasure. Support for that research was provided by internal research and development funds of SRI International; the preparation of this review was supported by the U.S. Army Research Office.

7. REFERENCES

1. D. R. Crosley, Ed., Laser Probes for Combustion Chemistry, Amer. Chem. Soc. Symposium Series, Vol. 134(1980).
2. R. K. Lengel and D. R. Crosley, Chem. Phys. Lett. 32, 261 (1975); J. Chem. Phys. 68, 5309(1978).
3. H. M. Lin, M. Seaver, K. Y. Tang, A. E. W. Knight and C. S. Parmenter, J. Chem. Phys. 70, 5442(1979).
4. D. H. Katayama, T. A. Miller and V. E. Bondybey, J. Chem. Phys. 72, 5469(1980).
5. W. K. Bischel, B. E. Perry and D. R. Crosley, Bull. Amer. Phys. Soc. 26, 23(1981); Chem. Phys. Lett. (submitted).
6. R. M. Green, Paper FA3, Molecular Spectroscopy Symposium, Columbus, Ohio, June 1980.
7. R. H. Barnes, C. E. Moeller, J. F. Kircher and C. M. Verber, Appl. Opt. 12, 2531(1973).
8. A. C. Eckbreth, in Ref. 1, p. 271.
9. D. R. Crosley, in Ref. 1, p. 3.
10. W. R. Anderson, L. J. Decker and A. J. Kotlar, Paper 67, Eastern Section Meeting of the Combustion Institute, Princeton, New Jersey, November 1980.
11. C. J. Vear, P. J. Hendra and J. J. McFarlane, J. C. S. Chem. Comm. 1972, 381.
12. K. Schofield, J. Phys. Chem. Ref. Data 8, 723(1979).
13. P. M. Selzer and C. C. Wang, J. Chem. Phys. 71, 3786(1979).
14. K. R. German, J. Chem. Phys. 64, 4065(1976).
15. P. Hogan and D. D. Davis, J. Chem. Phys. 62, 4574(1975); 64, 3901(1976).
16. K. H. Becker, D. Haaks and T. Tatarczyk, Chem. Phys. Lett. 25, 564(1974).
17. H. P. Hooymayers and C. Th. J. Alkemade, JQSRT 7, 495(1967).
18. J. H. Bechtel and R. E. Teets, Appl. Opt. 18, 4138(1979).
19. C. Morley, Eighteenth Symposium (International) on Combustion, Waterloo, Ontario, August 1980.
20. C. H. Muller III, K. Schofield, M. Steinberg and H. P. Broida, Seventeenth Symposium (International) on Combustion (1979), p. 367; C. H. Muller III, K. Schofield and M. Steinberg, in Ref. 1, p. 103.
21. D. Stepowski and M. J. Cottereau, Appl. Opt. 18, 354(1979).

22. M. J. Cottereau and D. Stepowski, in Ref. 1, p. 131; D. Stepowski and M. J. Cottereau, Combust. Flame 40, 65(1981).
23. E. H. Piepmeier, Spectrochim. Acta 27B, 431(1972).
24. J. W. Daily, Appl. Opt. 16, 568(1977); in Ref. 1, p. 61.
25. J. E. Allen, Jr., W. R. Anderson and D. R. Crosley, Opt. Lett. 1, 118(1977).
26. A. P. Baronavski and J. R. McDonald, J. Chem. Phys. 66, 3300(1977); Appl. Opt. 16, 1897(1977).
27. B. Smith, J. D. Winefordner and N. Omonetto, J. Appl. Phys. 48, 2676(1977).
28. J. W. Daily and C. Chan, Combust. Flame 33, 47(1978).
29. C. H. Muller III, K. Schofield and M. Steinberg, Chem. Phys. Lett. 57, 364(1978); 61, 212(1979); J. Chem. Phys. 72, 6620(1980).
30. L. Pasternack, A. P. Baronavski and J. R. McDonald, J. Chem. Phys. 69, 4830(1978).
31. R. A. VanCalcar, M. J. M. Van de Ben, B. K. Vitert, K. J. Biervenga, Tj. Hollander and C. Th. J. Alkemade, JQSRT 21, 11(1979).
32. J. E. Allen, W. R. Anderson, D. R. Crosley and T. D. Fansler, Seventeenth Symposium (International) on Combustion, 1979, p. 797.
33. P. A. Bonczyk and J. A. Shirley, Combust. Flame 34, 253(1979).
34. R. P. Lucht, D. W. Sweeney and N. M. Laurendeau, in Ref. 1, p. 145.
35. J. W. Daily, Appl. Opt. 17, 225(1978).
36. A. J. Kotlar, A. Gelb and D. R. Crosley, in Ref. 1, p. 137.
37. R. K. Lengel and D. R. Crosley, J. Chem. Phys. 67, 2085(1977).
38. R. P. Lucht and N. M. Laurendeau, Appl. Opt. 18, 856(1979).
39. J. O. Berg and W. L. Schackleford, Appl. Opt. 18, 2093(1979).
40. R. P. Lucht, D. W. Sweeney and N. M. Laurendeau, Appl. Opt. 19, 3295(1980).
41. C. A. Van Dijk, P. J. Th. Zeegers, G. Nienhius and C. Th. J. Alkemade, JQRST 20, 55(1978).
42. T. Carrington, J. Chem. Phys. 31, 1418(1959); Eighth Symposium (International) on Combustion, 1962, p. 257.
43. G. P. Smith and D. R. Crosley, Eighteenth Symposium (International) on Combustion, Waterloo, Ontario, August 1980.
44. R. K. Lengel, Ph. D. Thesis, Univ. of Wisconsin, 1977; R. K. Lengel and D. R. Crosley, J. Chem. Phys. (to be published).
45. C. Chan and J. W. Daily, Appl. Opt. 19, 1357(1980).
46. D. Stepowski and M. J. Cottereau, J. Chem. Phys. (submitted).
47. G. Zizak, J. J. Horvath and J. D. Winefordner, Appl. Spectr. (submitted).
48. C. Chan and J. W. Daily, Paper 79-20, Western States Meeting of the Combustion Institute, Provo, Utah, April 1979.
49. C. Chan and J. W. Daily, Appl. Opt. 19, 1963(1980).
50. D. R. Crosley and G. P. Smith, Paper 69, Eastern Section Meeting of the Combustion Institute, Princeton, New Jersey, November 1980; G. P. Smith and D. R. Crosley, J. Chem. Phys. (to be published).
51. D. R. Crosley and G. P. Smith, Combust. Flame (submitted).
52. C. C. Wang and L. I. Davis, Jr., Appl. Phys. Lett. 25, 34(1974).
53. J. H. Bechtel, Appl. Opt. 18, 3100(1979).
54. R. J. Cattolica, Paper 78-18, Western States Meeting of the Combustion Intitute, Boulder, Colorado, April 1978.
55. W. R. Anderson, Paper 3, Eastern Section Meeting of the Combustion Institute, Atlanta, Georgia, November 1979; W. R. Anderson, R. A. Beyer and J. A. Vanderhoff, Paper FA1, Molecular Spectroscopy Symposium, Columbus, Ohio, June 1980.
56. R. J. Cattolica, Appl. Opt. 20, 1156 (1981).
57. D. R. Crosley and G. P. Smith, Appl. Opt. 19, 517(1980).
58. D. R. Crosley, Report LSR-2, SRI International, August 1981.
59. K. R. German, R. H. Bergemann, E. M. Weinstock and R. N. Zare, J. Chem. Phys. 58, 4304(1973).
60. T. A. Caughey and D. R. Crosley, Chem. Phys. 20, 467(1977).

TWO-PHOTON LASER-INDUCED FLUORESCENCE IN OXYGEN AND NITROGEN ATOMS

William K. BISCHEL, Bryce E. PERRY * and David R. CROSLEY
Molecular Physics Laboratory, SRI International, Menlo Park, California 94025, USA

Received 8 May 1981

Two-photon absorption is used to populate the $3p\ ^3P$ state of O and the $2s^2 2p^2 3p\ ^4D^o$ state of N in a flow discharge. Exciting photons are produced by anti-Stokes Raman frequency conversion of tunable UV laser radiation; the resulting near IR fluorescence from the excited state yielded lifetimes, quenching rates, and relative two-photon transition probabilities.

New methods for the selective excitation of high-lying states in atoms continue to become possible with the ever-increasing variety of laser sources and techniques. These state-selective excitation techniques allow the determination of a variety of new fundamental information concerning the spectroscopic and collisional properties of atoms. We describe here the first observation of laser-induced fluorescence in oxygen and nitrogen atoms, excited by two-photon absorption in the ultraviolet. Although two-photon absorption has been previously used to excite high-lying states in atoms [1–3], the recent availability of widely-tunable narrow-band radiation in the UV, as exploited in this study, opens up the possibility of experiments on a broad number of atomic and molecular species and excited states. In particular, this technique of two-photon laser-induced fluorescence can provide structural and collisional information about the excited states of important atomic radicals. For example, lifetimes, quenching rates and relative two-photon transition probabilities are determined here for excited states in O and N atoms. In addition, the technique holds considerable promise as a diagnostic tool for detecting these elusive atomic species at low concentration in systems such as flames and plasmas. One example of this application is the proposal [4,5] to remotely detect oxygen atoms in the upper atmosphere using the two-photon transition experimentally observed here.

In fig. 1 are shown the energy levels [6] involved in the experiment for both O and N. In each case, the

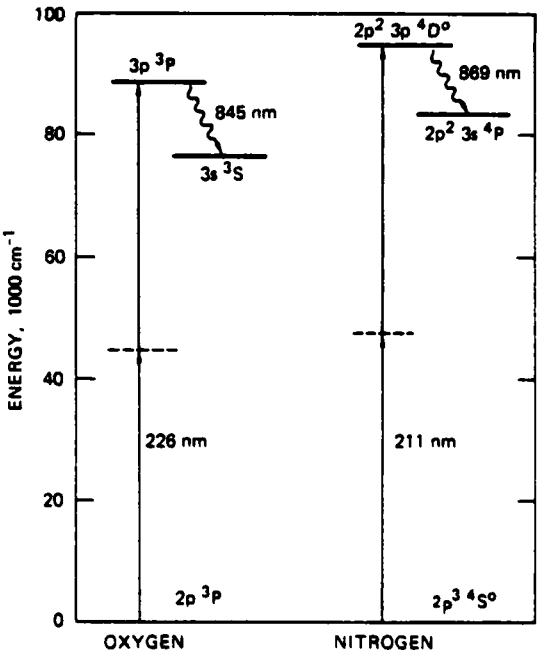

Fig. 1. Relevant energy levels for the two-photon excitation of atomic oxygen and nitrogen.

* Present address: Quanta-Ray, Inc., Mountain View, California, USA.

atom is raised to the first electronically excited state of the same symmetry and multiplicity as the ground state, through the absorption of two ultraviolet photons of equal wavelength. The atom then emits an infrared photon in a transition terminating on an excited state of opposite symmetry; in this case it happens to be the upper state of the main resonance line of the species. Detection of this photon forms the observed signal. Similar schemes can be designed for other atoms (e.g. H, C, S, F) and for higher-lying electronic states.

The laser radiation at the required wavelengths is provided by anti-Stokes Raman shifting [7] of frequency doubled, tunable dye laser radiation. Radiation of energy ≈20 mJ per 8 ns pulse at 314 nm (O atoms) or 286 nm (N atoms) is directed into a cell containing ≈10 atm of H_2. A Pellin–Brocha prism separates the several shifted wavelengths, and the desired third anti-Stokes component at 226 nm (O atoms) or 211 nm (N atoms), having ≈30 μJ pulse energy, is focused into the experimental cell. Here, N atoms are produced by a standard flow discharge, dissociating N_2 in a He + SF_6 buffer gas mixture at ≈10 Torr total pressure. O atoms are produced by a downstream titration [8] of the N atoms with NO. The atom densities are estimated from the titration to be $(1-5)\times 10^{14}$ cm^{-3}. Wavelength calibration and measurement of the linewidth of the Raman-shifted radiation is furnished by single-photon excitation scans of the (0,0) band of the γ system of NO. The linewidth of the third anti-Stokes component of the Raman shifted laser was measured from the excitation lineshape to be ≈0.3 cm^{-1}.

The UV radiation is focused into the experimental cell using a 6 inch suprasil lens, and is then monitored by a fast photodiode to provide an intensity normalization for the near IR fluoresence signal.

The near IR fluorescence from the two-photon excited state is focused ($f/2$ collection optics) through a filter ($T \approx 50\%$) into a photomultiplier having high (≈15%) quantum efficiency in the 850 nm region. Following preamplification, a fast gated integrator (2 ns gate) averages the signal over typically 10 pulses; the results are read out on a chart recorder. Typical signal levels for ≈10 μJ of incident third anti-Stokes laser light were ≈100 photons/pulse integrated over the lifetime of the excited state and scale as the square of the laser intensity.

The two-photon absorption cross section may be written [9], for a transition from the ground state with angular momentum J_g to an excited state J_e, as

$$\alpha = \frac{(2\pi)^3}{\hbar c^2}\,\nu_Q \left| \sum_i \frac{\langle J_e|r|J_i\rangle\langle J_i|r|J_g\rangle}{\Delta E_i} \right|^2 g(2\nu_Q), \qquad (1)$$

where the term i runs over all single-photon-accessible states, ν_Q and $g(2\nu_Q)$ are the laser frequency and normalized lineshape function for the atomic transition, respectively, and $\Delta E_i = E_i - h\nu_Q$. If the laser linewidth, $\Delta\nu_Q$, is much larger than the atomic Doppler width, then $g(2\nu_Q)$ can be approximated [10] by $(2^{1/2}\,\Delta\nu_Q)^{-1}$. For the P → P transition in O, the intermediate state could be either an S or a D state but for N, which is S → D, it must be a P state. Because of the energy denominator ΔE_i and the strong oscillator strengths involved in the pertinent single-photon transitions, the bulk of the intermediate state contribution comes in each case from the same state which is the terminus of the infrared emission (see fig. 1). The assumption that this constitutes the entire contribution permits the calculation of α for different fine-structure components, using standard angular momentum coupling schemes.

For O, the ground-state fine-structure components are well-separated on the scale of $\Delta\nu_Q$, but the upper-state splitting is of the order of $\Delta\nu_Q$ and is thus unresolved. Fig. 2 exhibits excitation scans originating from $J_g = 0$, 1 and 2 of the ground ^{3}P state. We consider the states to be thermally populated and determine the temperature within the discharge using the excitation scan in NO. The integrated intensities from fig. 2 then yield equal two-photon absorption cross sections for the three fine-structure ground states within our experimental error of ≈10%. The simple coupling scheme predicts equal intensities, as does the more sophisticated treatment [4] which also estimates contributions from other J_i to be ≈5%.

For N, there exists only one ground-state component but four resolved upper-state levels of ^{4}D, $J = 7/2$, $5/2$, $3/2$ and $1/2$. Because the intermediate state must be ^{4}P, the simple calculations should apply; they yield α_J values in respective ratios 4 : 3 : 2 : 1. The values for the relative transition probabilities measured in our experiment agree with this prediction to better than 10%.

Considering only the single intermediate state and

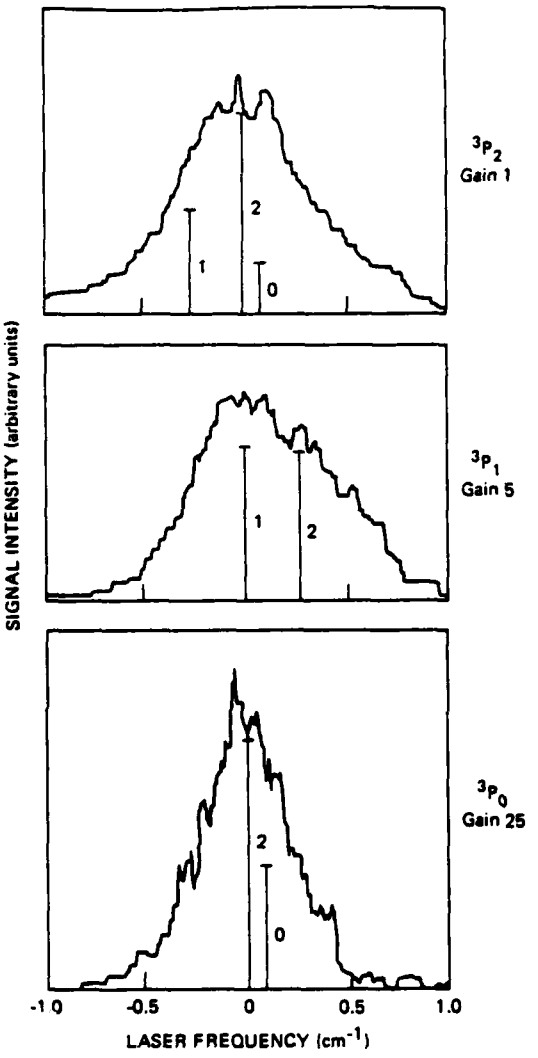

Fig. 2. Typical signals obtained by scanning the oxygen atom fine-structure two-photon transitions. The asymmetry observed in the line profiles is due to the fact that the upper-state fine structure is unresolved. The strengths and positions of these unresolved transitions are indicated by the bar graph.

using tabulated transition moments [11], an effective α for our $\Delta\nu = 0.3$ cm^{-1} can be theoretically estimated from eq. (1) to be $\alpha \approx 3 \times 10^{-28}$ cm^4/W for O atoms for the $^3P_2 \rightarrow {}^3P_{2,1,0}$ two-photon transition. This value is consistent with the value given in ref. [4] for this transition. For nitrogen atoms, we estimate a cross section for the $^4S_{3/2} \rightarrow {}^4D_{7/2}$ two-photon transition of $\alpha_N = 2.4 \times 10^{-28}$ cm^4/W, when the $^4P \rightarrow {}^4D^o$ transition moment is derived from our measured $^4D^o$ excited-state lifetime of 20 ns. This leads to a theoretical cross section ratio $\alpha_N/\alpha_O = 0.85$, while experimentally we observe a ratio of $\approx$0.5. This is good agreement for our estimated experimental error of ±25%.

Absolute signal estimates, assuming gaussian beam propagation, a two-photon absorption cross section from eq. (1), and a simple rate equation model [3] for the excited-state density, give signal levels which are a factor of 10–100 larger than the observed levels. This discrepancy is currently under investigation and probably results from poor third anti-Stokes beam quality.

The use of the gated integrator in the scanning mode allowed measurements of the excited-state lifetime. Such measurements have been made for both atoms. The laser pulse width was separately scanned using the signal from a fast photodiode so that its effects could be deconvoluted from signals with fast time decays. In fig. 3 is shown a plot of the effective

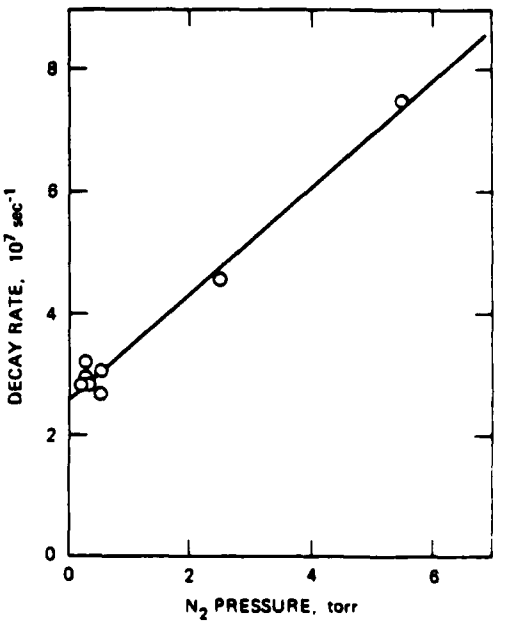

Fig. 3. Plot of the inverse of the excited-state lifetime for oxygen as a function of pressure of N_2.

decay rate of the $3p\,^3P$ state of O as a function of N_2 pressure. For O atoms, the intercept gives a radiative lifetime of $\tau = 39.1 \pm 1.4$ ns which can be favorably compared to a tabulated value [11] of 36 ns. The slope yields a quenching rate for collisions with N_2, $k_Q = (2.5 \pm 0.1) \times 10^{-10}$ cm^3/s. Similar measurements on the $3p\,^4D^o_{7/2}$ state of N result in a lifetime $\tau = 27 \pm 3$ ns and a quenching rate of $k_Q(N_2) = (2.4 \pm 0.6) \times 10^{-10}$ cm^3/s. Comparing to the tabulated [11] N-atom lifetime of $\tau = 52.3$ ns, we see that the value measured in this experiment is considerably smaller. Other sources for quenching the excited state, such as the 10 Torr helium buffer, have been checked and found to have no effect on the excited-state lifetime. Since the measurement of the oxygen atom lifetime gave the tabulated result for similar experimental conditions, we have confidence in our measured value.

It is clear that this method of two-photon excitation of fluorescence can be extended to other states and to other species as well, for the determination of structural, radiative and collisional properties. For example, excitation of each ^4D_J state of N in conjunction with spectrally resolved emission to ^4P_J would permit the measurement of state-to-state collision cross sections, as has been done for Na using two-photon excitation in bulb experiments [12] and flames [13].

Important also is the potential which this method possesses as a diagnostic tool for the sensitive detection of transient atomic species present at low concentration, as in plasmas and flames. It would be particularly useful for experimental conditions which render atomic detection by VUV resonance fluorescence impossible to implement due to absorption of the VUV light. The wavelengths used here readily propagate through the atmosphere and through flame gases.

Oxygen atom profiles at concentrations of $\approx 10^{17}$ cm^{-3} have recently been determined in a hydrogen/oxygen flame using spontaneous Raman scattering [14] and even more recently using coherent anti-Stokes Raman scattering [15]. Oxygen atoms have also been observed at 10^{15}–10^{16} cm^{-3} in a discharge flow, using intracavity dye-laser absorption on the $^3P_{1,2} \rightarrow {}^1D_2$ transition [16]. Two-photon excitation can be considerably more sensitive than these methods. From the signal strengths observed in our experiments and the measured quench rates with N_2, we estimate that a modest improvement in beam quality and laser energy to ≈ 1 mJ/pulse would permit part-per-million level of detection of O and N atoms in atmospheric pressure flames, and allow concentration of $\approx 10^{11}$ cm^{-3} to be detected under low-pressure conditions.

In summary, we have used tunable, Raman-frequency-shifted laser excitation for the two-photon excitation of fluorescence in O and N atoms. The method is a general one both promising fundamental information on a number of species and possessing considerable potential as a diagnostic tool.

We thank Tom Slanger for assistance concerning the production of the atoms and Greg Smith for useful discussions. This research was supported in part by SRI International internal research funds and in part by the US Army Research Office.

References

[1] T.W. Hänsch, S.A. Lee, R. Wallenstein and C. Weiman, Phys. Rev. Letters 34 (1975) 307.
[2] F. Birben, B. Cognac and G. Grynberg, Phys. Rev. Letters 32 (1974) 643;
M.D. Levenson and N. Bloembergen, Phys. Rev. Letters 32 (1974) 645;
D. Pritchard, J. Apt and T.W. Ducas, Phys. Rev. Letters 32 (1974) 641.
[3] W.K. Bischel, J. Bokor, D.J. Klizer and C.K. Rhodes, IEE J. Quantum Electron. QE-15 (1979) 380.
[4] M.S. Pindzola, Phys. Rev. A17 (1978) 1021.
[5] T.J. McIlrath, R. Hudson, A. Aiken and T.D. Wilkerson, Appl. Opt. 18 (1979) 316.
[6] C.E. Moore, Atomic Energy Levels, Vol. 1, NSRDS-NBS 35 (US Govt. Printing Office, Washington, 1971).
[7] V. Wilke and W. Schmidt, Appl. Phys. 18 (1979) 177.
[8] M.F. Golde and B.A. Thrush, Rept. Progr. Phys. 36 (1973) 1285.
[9] V.S. Letokhov and V.P. Chebotayev, Nonlinear laser spectroscopy (Springer, Berlin, 1977) ch. 4.
[10] B.R. Marx, J. Simons and L. Allen, J. Phys. B11 (1978) L273.
[11] W.L. Wiese, M.N. Smith and B.M. Glennon, Atomic Transition Probabilities, NSRDS-NBS4 (US Govt. Printing Office, Washington, 1966).
[12] T.F. Gallagher, W.E. Cooke and S.A. Edelstein, Phys. Rev. A17 (1978) 125.
[13] J.E. Allen Jr., W.R. Anderson, D.R. Crosley and T.D. Fansler, Seventeenth Symposium (International) on Combustion (The Combustion Institute, Pittsburgh, 1979) p. 797.
[14] C.J. Dasch and J.H. Bechtel, Opt. Letters 6 (1981) 36.
[15] J.H. Bechtel and R. Teets, private communication.
[16] S.J. Harris and A.M. Weiner, Opt. Letters 6 (1981) 142.

Reprinted from Applied Optics, Vol. 21, page 1419, April 15, 1982

Detection of fluorescence from O and N atoms induced by two-photon absorption

William K. Bischel, Bryce E. Perry, and David R. Crosley

The $3p\ ^3P$ state of O and the $2s^22p^23p\ ^4D^0$ states of N are populated by two-photon absorption at 226 and 211 nm, respectively, and the resulting near-IR fluorescence is detected. The exciting photons are provided by stimulated Raman frequency shifting, and the experiments are performed in a flow discharge. The measured lifetime of 39 (O) and 27 (N) nsec and quenching rate constants of 2.5×10^{-10} cm^{-3} sec^{-1} for collisions of N_2 with each atom indicate promise for this method as a diagnostic tool in flames and plasmas.

I. Introduction

Oxygen and nitrogen atoms play an important role in the chemistry of a number of processes, such as combustion, plasmas, and the atmosphere. It would, therefore, be desirable to detect them in their ground electronic states using optical means. Doing so by conventional resonance absorption or fluorescence techniques poses a severe problem, however, for their first resonance transitions fall far into the VUV and can be observed only in cells specially constructed to pass such wavelengths. Atmospheric and flame gases and quartz windows are opaque to such radiation.

Oxygen possesses several low-lying electronic states: a ground ^3P_J state and a $^1D_2$ state ~2 eV higher. This structure has recently been exploited for detection pertinent to combustion studies. Both spontaneous[1] and coherent[2] Raman scattering on the $^3P_2 \rightarrow {}^3P_{1,0}$ levels have been observed for O atoms in an H_2/O_2 flame, and intracavity laser absorption on the forbidden $^3P_{2,1} \rightarrow {}^1D_2$ transition[3] has been detected in a flow system. Each of these pioneering experiments demonstrates the capability of nonintrusive *in situ* monitoring of O characteristic of many laser diagnostic methods[4] but does possess some limitations. In the Raman techniques, low signal levels and interference from O_2 (and potentially other species) make necessary long acquisition times, and the intracavity absorption is a line-of-sight technique.

Nitrogen atoms, on the other hand, possess no nearby electronic states furnishing the possibility of either Raman or intracavity detection.

We describe here a new means of detection of both O and N, minor modifications of which are suitable for other species, including H, C, and F. (Pertinent wavelengths for these atoms are tabulated in Table I, and others are given in Ref. 5.) The scheme is illustrated in Fig. 1. Two-photon absorption from a UV laser beam is used to populate the first excited state of the same symmetry as the ground state, which then radiates in the near IR and is thus detected. This two-photon absorption transition in O has been treated theoretically,[6,7] and the scheme has been proposed for lidar detection of stratospheric O from a balloon platform.[8] Briefer accounts of our own studies have appeared elsewhere,[9] and similar experiments have now been performed on hydrogen[10] and carbon.[11]

The experiments were performed in a low-pressure flow discharge. Lifetimes and quench rates for collisions with N_2 were measured to determine the feasibility of the two-photon excitation as a diagnostic technique. We estimate that (realistic) improvements in beam quality and energy would permit detection down to perhaps parts per million levels at atmospheric pressure, apparently much more sensitive than for the Raman or intracavity absorption methods. On the other hand, the creation of a real emitting excited state with a finite lifetime demands that the collisional quenching rate, within the system probed, be known for accurate concentration measurements. This poses limitations on absolute accuracy, although the situation is likely to be more favorable for atom detection than for molecular measurements.[12]

The exciting photons are provided by stimulated Raman frequency shifting[13] of relatively intense tunable UV laser radiation. Although the necessary wavelength

When this work was done all authors were with SRI International Molecular Physics Laboratory, Menlo Park, California 94025; Bryce Perry is now at Quanta Ray, Inc., Mountain View, California 94043.

Received 16 December 1981.
0003-6935/82/081419-11$01.00/0.

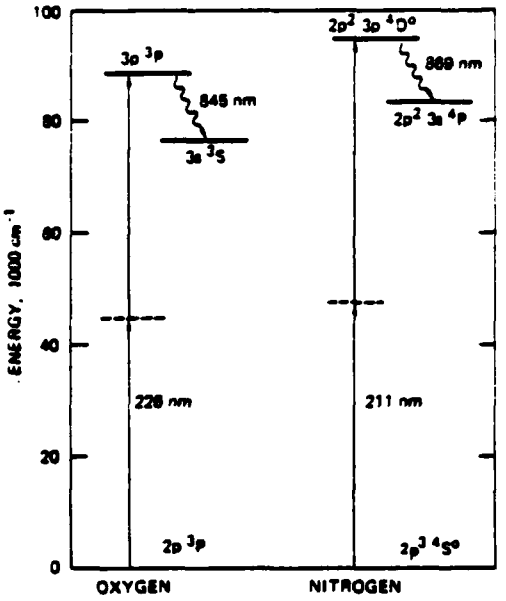

Fig. 1. States and wavelengths involved in the detection scheme. Fine state splittings are too small to show on this scale.

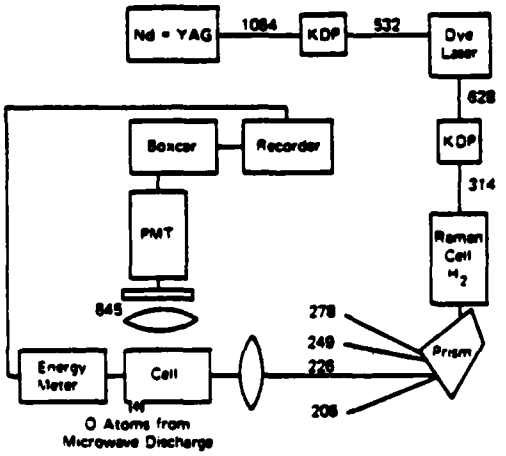

Fig. 2. Schematic diagram of the experiment. The wavelengths (nm) shown are those pertinent to O atoms, which are produced in the reaction $NO + N \rightarrow N_2 + O$. Stokes beams (not shown) are also present in the Raman cell output.

for O (226 nm) could be generated by direct frequency doubling or mixing in crystals, that needed for the N atoms (211 nm) is beyond the absorption edge of the standard crystals. Thus these experiments additionally demonstrate the utility of the Raman shifting method, which we anticipate will be increasingly exploited for the generation of these and shorter wavelengths in the near future.

II. Experimental Details

In this section we describe the apparatus used for the experiment and the measurements made. Figure 2 is a schematic diagram of the overall setup showing the laser wavelengths pertinent to the oxygen atom experiments.

A. Flow System and Atom Production

The discharge flow cell used is standard for such atom production. A mixture of N_2 seeded into ~10-Torr He is passed through a 2450-MHz discharge to produce N atoms. It was found that soiling the He by addition of 5–10 mTorr of SF_6 enhanced the N atom production efficiency considerably in accord with the general lore for this technique. In the experiments on the N atoms themselves, the products of the discharge passed through ~1 m of glass tubing into a blackened Wood's horn cell containing an exit window for the laser radiation; a moderate speed pump maintained a continuous flow. Gas pressures were measured with a Baratron gauge.

For the O atom experiments, NO was added a few centimeters downstream of the discharge. The reaction $NO + N \rightarrow O + N_2$ is used to produce the oxygen atoms quantitatively, and it can be followed by chemiluminescence: a red glow due to N + N radiative recombination dominates below the titration point (where the concentration of added NO equals the initial N concentration); a very faint deep violet color due to NO near the titration point; and a bright greenish yellow glow from $O + NO \rightarrow NO_2^*$ in the presence of excess NO. These characteristics corresponded well to the disappearance of the N atom signal observed in the experiments. From the value of the amount of added NO at the titration point, we obtain the atom concentrations; most of the experiments were conducted at atom concentrations of $3–10 \times 10^{13}$ cm^{-3}.

For the measurement of O fine structure transition probabilities, it was necessary to know the temperature within the flow system. For this purpose, NO was added in excess, and the IR filter used for the atom fluorescence was replaced by a UV filter. A few angstroms from the O atom wavelengths lies the P_2 head of the (0,0) band of the γ system ($A^2\Sigma^+ - X^2\Pi$) of NO. An excitation scan through this head and neighboring P_2 and Q_2 lines is shown in Fig. 3. These intensities were used to obtain a rotational temperature for the NO; the results confirmed that the flow gases were at room temperature with the microwave discharge either on or off.

B. Frequency Conversion

The UV wavelengths used in these experiments were generated using stimulated Raman shifting, also known as multiwave parametric Raman scattering. This technique is based on many-order anti-Stokes (AS) stimulated Raman scattering in molecular hydrogen and has been recently studied experimentally in our laboratory[13,14] and elsewhere as well as theoretically.[15,16] These experimental studies have demonstrated good conversion efficiencies in the UV for such a high-order

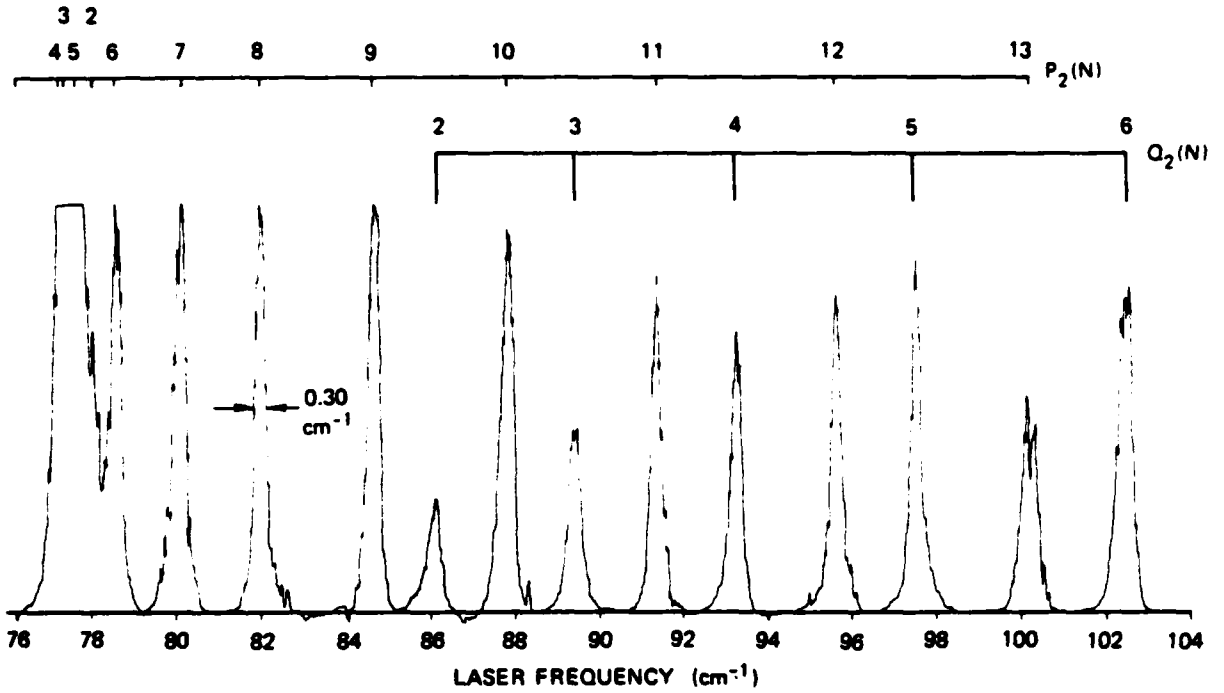

Fig. 3. Excitation scan through the P_2 and Q_2 branches of the (0,0) band of the NO γ system near 2263 Å, showing the linewidth of the third anti-Stokes component as well as serving as a thermometer. The frequency given is −44000.

nonlinear process and indicate that the technique holds promise for the routine production of VUV radiation. In this section we present a brief description of the frequency conversion process along with details of our experience with it.

A high-power doubled dye laser operating at 314 nm is focused into a cell containing hydrogen at ~6–8 atm (Fig. 1), and the resulting nonlinear process produces a series of lines separated from the pump wavelength by the fundamental vibrational frequency of the H_2 (ν_R = 4155 cm^{-1}). The conversion efficiency into these sidebands can be very high, and in many cases the pump energy is depleted by more than 50%. The light emerging from the cell is recollimated, and the various Stokes/anti-Stokes orders are separated for use in experiments using a quartz Pellin-Broca prism. The process can be divided into two parts: generation of the first Stokes wave $\nu_s = (\nu_p - \nu_R)$ by stimulated Raman scattering, and the generation of the anti-Stokes wave by four-wave mixing $\nu_{as} = (\nu_p + \nu_R)$. The Stokes wave is produced in a gain process that builds up from noise and hence has a threshold dependence on laser pump energy. Once this wave has developed an intensity comparable with the pump, it can interact with the pump frequency via the third-order nonlinear susceptibility χ^3 to produce the anti-Stokes beam in a four-wave mixing process. Stokes orders are also produced by this process. It can be shown that this latter process does not have a threshold, and in the low-gain limit the anti-Stokes intensity in proportional to $|\chi^3|^2 I_p^2 I_s$. Once the anti-Stokes wave becomes strong, it can mix with the pump to produce the second anti-Stokes wave and so on. Theoretical analysis of this process[15] becomes extremely complicated when many waves are involved in the problem. For example, in a system containing eight anti-Stokes and three Stokes orders, the frequency of the third anti-Stokes line can, in principle, result from twenty-two different mixing processes among waves propagating in the medium.

Our experimental application uses the third anti-Stokes order for the detection of both O and N atoms. For a pump laser energy of 15–20 mJ at 314 nm we typically obtain 50–100 μJ at 226 nm. This conversion efficiency of ~0.5% into the third order is critically dependent on the pump laser beam quality. If considerable care is taken in the laser alignment, we can attain over 1% conversion efficiency with our commercial system. We have observed the interesting and useful fact that the above conversion efficiency was obtained when both the doubled dye (15 mJ) and the dye fundamental beams (70 mJ) were focused into the hydrogen cell.[17] If only the doubled dye is focused into the cell at the same energy, the conversion efficiency drops by a factor of 3–5. This dependence of the conversion efficiency on the presence of a high-intensity nonresonant wave is not understood at this time. Theoretical treatments of this process (nonlinear mixing)[15,16] indicate that the conversion efficiency depends on all injected waves and that it perhaps is enhanced by the presence of an additional nonresonant wave.

It is of primary importance to know the bandwidth of the anti-Stokes emission if this radiation is to be used

in practical experiments. From a consideration of the four-wave mixing processes, the bandwidth should be the same as the UV pump laser bandwidth, unless some other nonlinear mechanism such as self-phase modulation broadens the frequency spectrum of the AS waves. We have addressed this question by scanning the third AS order at 226 nm through the bands of NO. This scan has been given in Fig. 3. We observe a FWHM of 0.30 cm^{-1} for an isolated rotational line that should have a Doppler width of 0.10 cm^{-1}. If we assume a Gaussian distribution for the laser linewidth, we can extract the laser linewidth using the deconvolution formula $\Delta\nu_L = (\Delta\nu_{exp}^2 - \Delta\nu_D^2)^{1/2} = 0.28\ cm^{-1}$. This laser linewidth is the same as we have measured for the doubled dye laser by scanning it through an isolated absorption line in OH at 314 nm. We, therefore, conclude that for a resolution limit of ~0.1 cm^{-1}, we see no broadening of the anti-Stokes emission. This measured linewidth of 0.3 cm^{-1} gives an effective resolution for the two-photon experiments of 0.5 cm^{-1}, in agreement with our obeervations.

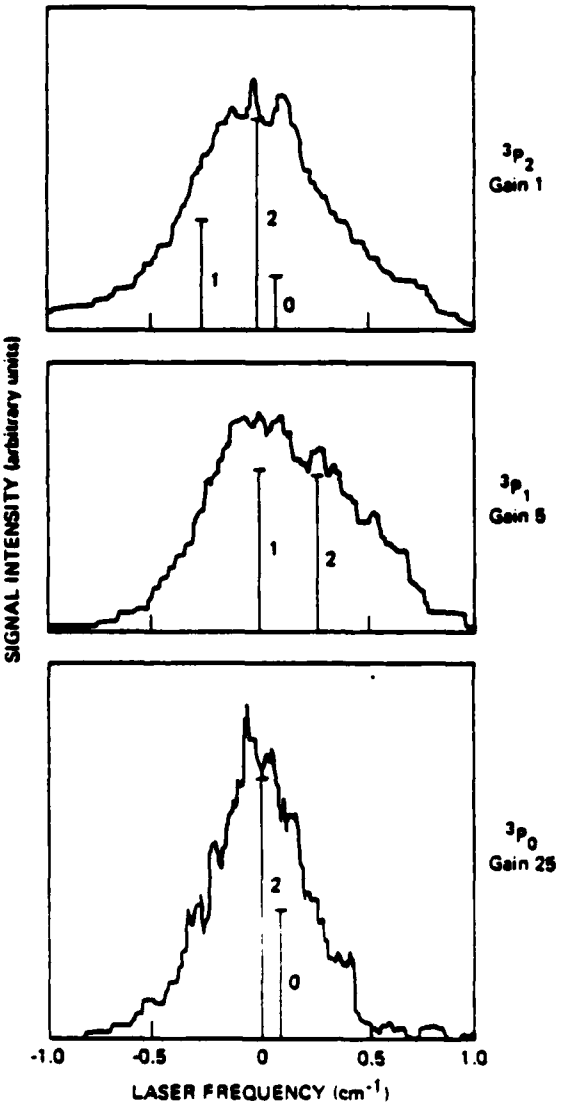

Fig. 4. Excitation scans through each of the O ^3P_J transitions. The stick diagrams correspond to the expected positions of the upper state components. The laser frequency is in cm^{-1}; note that the gain increases from top to bottom.

It is important to remember that the two-photon absorption cross section depends linearly on the laser linewidth when it is much larger than the linewidth in the two-photon transition. If the UV pump at 226 nm is created by mixing doubled dye with the fundamental YAG at 1060 nm, care must be taken to ensure that the YAG laser has a linewidth comparable with the dye laser to obtain the highest O atom detection sensitivity.

C. Fluorescence Measurements

The fluorescence was collected from the cell at right angles to the laser beam with a fast ($f/2$) Suprasil lens and focused through a filter onto a photomultiplier with high near-IR sensitivity (RCA C31034A). In some early experiments, a small (0.35-m) monochromator served as the filter; this was scanned to verify that the observed fluorescence was at the proper wavelengths. In later runs the monochromator was replaced by appropriately chosen glass or interference filters with ~20% transmission at the fluorescence wavelengths.

The signal passed through a fast gain-10 preamplifier and into a boxcar integrator with narrow-gate capability (PAR model 165). Used in a gate scanning mode, this permitted lifetime determinations down to the limit where the laser UV pulse length—separately obtained from fast photodiode measurements to be 7 nsec—precluded measurement of more rapid decays. A portion of the laser beam which passed through the cell was split off into the photodiode, and the resulting signal was fed to the other boxcar channel to serve as a laser amplitude monitor. Because of the nonlinear dependence of the signal level on laser power, electronic ratioing was not undertaken; rather runs were scrapped when the drift in laser power over a scan precluded quantitative results.

Figure 4 shows an excitation scan over each of the three fine structure components of the O atom transition. Here, as with most of the intensity runs, an average over 60 pulses (6-sec time constant) was used. Very little background was observed (~1% of the peak signal); the noise arises from laser power fluctuations. A small variation in the original Nd:YAG IR amplitude causes a large variation in the signal due to the nonlinear nature of the several frequency conversion steps (Fig. 2) and the two-photon absorption itself.

The laser beam was attenuated with a series of screens for a measurement of the dependence of the $^3P_2$ signal on laser power. The results are shown in the form of a log–log plot in Fig. 5. The fitted slope is 2.6 ± 0.2 (the steeper line in the figure), although the errors associated with each datum do not preclude a quadratic

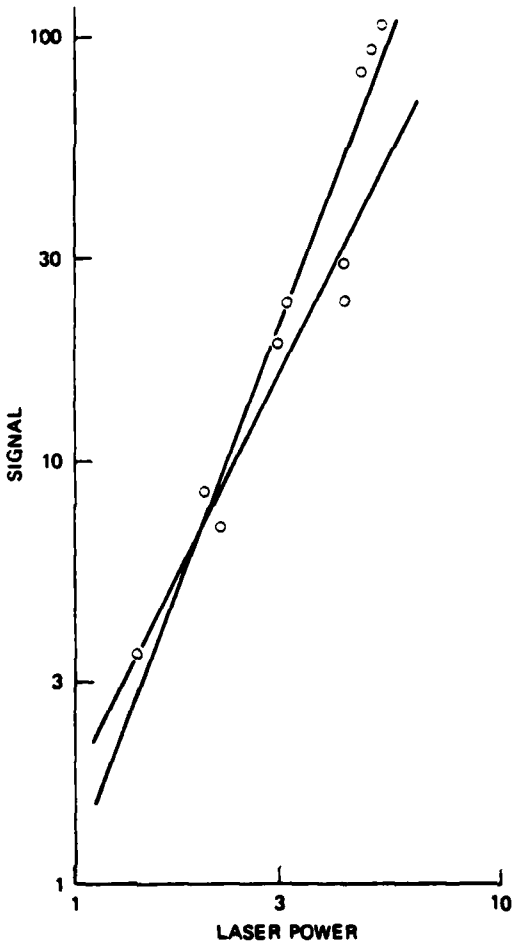

Fig. 5. Relative signal vs relative laser intensity for the O ($^3P_2$) excitation. The two lines are at the fitted slope 2.6 ± 0.2 and a slope of 2 corresponding to strictly quadratic behavior.

dependence (the other line). Even though one more UV laser photon is easily able to ionize either atom from its excited state, Fig. 5 shows that laser ionization does not constitute an appreciable removal rate in our experiment; if that had been the case, a slope between linear and quadratic would have been obtained. We also see that we are not appreciably saturating the transition, a result which places an upper limit on the two-photon pump rate of $\lesssim 10^8$ sec^{-1} under our conditions.

Although the fitted slope in Fig. 5 is not 2, the quadratic dependence expected theoretically is used to normalize results at different laser power. An example is the determination of relative integrated intensities from Fig. 4, where the UV laser energy varied ~20% due to variations in the gain of the dye laser.

A lifetime run for the N atom state and its logarithmic plot to obtain a lifetime are shown in Fig. 6. The increase at short times is due to the laser pulse length and pumping rate, slightly stretched by the 2-nsec gate, but the decay fits clearly to a single exponential.

III. Results and Discussion

The two-photon cross section for a transition from a ground state g to an excited state e may be written[18]

$$\alpha_{ef} = \frac{(2\pi)^3}{hc}\nu_l|P_{eg}|^2 g(2\nu_l) \qquad P_{eg} = \sum_i \frac{\langle e|\mu|i\rangle\langle i|\mu|g\rangle}{\Delta E_{eg} - h\nu_l}, \quad (1)$$

where the sum runs over all virtual states i accessible by a one-photon transition from both g and e, ν_l is the laser frequency, and g is the two-photon absorption line shape. If we assume that there exists a single intermediate state (still denoted by i) which forms the dominant contribution to P_{eg} and include the effects of laser linewidth,[19] α may be written

$$\alpha(J_e,J_g) = \frac{a\nu_l|P^i_{eg}|^2}{\Delta E^2_{il}(2\Delta\nu^2_D + \Delta\nu^2_l)^{1/2}} \quad (2)$$

for a transition from a particular ground state angular momentum component J_g to a particular excited state component J_e. Here ΔE_{il} is the difference in energy between that of the laser and that of state i, $\Delta\nu_D$ is the FWHM Doppler width, and $\Delta\nu_l$ FWHM the laser linewidth. The matrix elements of P^i_{eg} may be split into radial and angular integrals:

$$|P^i_{eg}|^2 = \langle\phi^{n'}_e(r)|r|\phi^{n'}_i(r)\rangle\langle\phi^{n'}_i(r)|r|\phi^{n'}_g(r)\rangle|^2 \times \frac{1}{2J_g+1}\sum_{m_g,m_e}\left|\sum_{J_i,m_i}\langle J_e m_e|\cos\theta|J_i m_i\rangle \times \langle J_i m_i|\cos\theta|J_g m_g\rangle\right|^2. \quad (3)$$

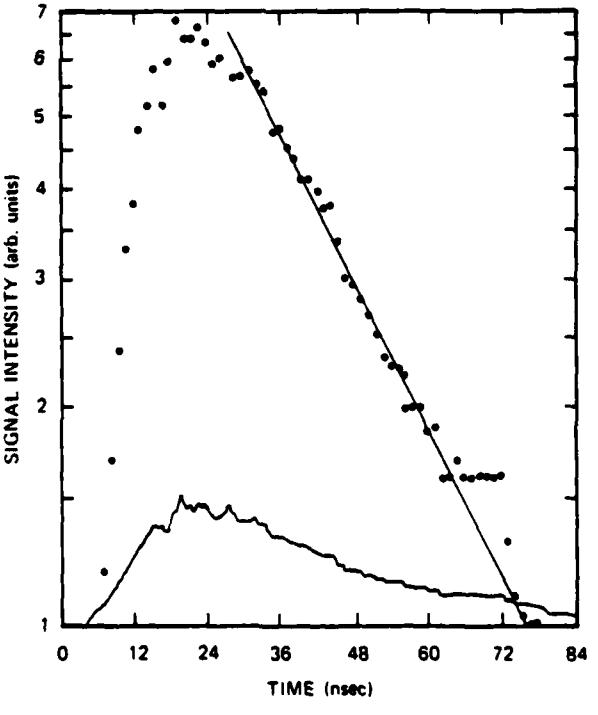

Fig. 6. (Bottom curve) experimental data on a linear scale for the time dependence of the N ($^4D_{7/2}$) signal. (Top) a fit of the decay portion to an exponential. This exemplary run was made at 0.28-Torr N_2, 0.06-Torr NO, and 9.4-Torr He, yielding τ = 26.2 nsec.

Table I. Two-Photon Excitation Parameters

Atom	Ground state	Intermediate state (cm^{-1})	Final state (cm^{-1})	$\lvert\mu_{ri}\rvert^2$ (D^2)	$\lvert\mu_{ig}\rvert^2$ (D^2)	$\Delta\nu_D$ (cm^{-1})	$\alpha 10^{-27}$ (cm^4/W)	k_r (10^7 sec)	λ_{exc} (nm)	λ_{fluor} (nm)
H[a]	^2S	$^2p^0$	^2D							
		82258	97492	3.6[d]	59[d]	1.2	0.5	6.6[d]	206	656
C[b]	$^3P_0$	^3P	^3P							
		60353	71386	6.0[d]	6.0[d]	0.25	5	2.5[d]	280	909
N[c]	$^4S^0$	^4P	$^4D^0$							
		83366	94883	1.1[d]	104[d]	0.31	0.9	3.7[c]	211	869
O[b,e]	^3p	^3S	^3P							
		76795	88631	2.6[d]	54[d]	0.27	1.2	2.6[c]	226	845
F	$^2p^0$	^2P	$^2D^0$							
		104732	117624	3.7[d]	52[d]	0.33	0.8	3.5[c]	170	776

[a] Observed in Ref. 10. [b] Observed in Ref. 11. [c] This work. [d] Values from Ref. 20. [e] Value from Ref. 32.

The angular matrix element here is expressed for linearly polarized light, whose polarization vector defines the axis of quantization. The radial integrals in Eq. (3) determine the absolute value of α, whereas the angular integrals are responsible for the relative values of α among the fine structure components of the transition.

In Eq. (2), if ΔE_{il} is expressed in cm^{-1} and the matrix elements in debyes, a numerical value 6.2×10^{-25} for the constant a yields α in cm^4/W.

The two-photon pumping rate W_{eg} (sec^{-1}) is then expressed as

$$W_{eg} = \alpha_{eg} I_l^2 / h\nu_l, \tag{4}$$

where I_l is the laser intensity in W/cm^2; the time dependence of the excited state number density is

$$\frac{dN_e}{dt} = W_{eg} N_g - (k_r + k_Q n) N_e \tag{5}$$

in the absence of appreciable photoionization or saturation. Here k_r is the radiative decay rate, k_Q is a collisional quenching rate constant, and n is the total number density. (For a mixture of gases, $k_Q n$ would be replaced by the appropriate sum over all species present.) All these quantities, the relative and absolute values of α plus k_r and k_Q, are needed in the diagnostic application of two-photon laser-induced fluorescence. Their measurement (including a presumably representative k_Q for N_2 collisions) has formed the subject of this study.

A. Absolute Two-Photon Absorption Cross Sections

Absolute two-photon cross sections for atomic transitions of interest can be estimated if the single intermediate state approximation is made. This approximation is very reasonable for all the two-photon transitions considered in this paper since the intermediate defined by the resonance transition has most of the oscillator strength. The two terms in α, that describing the radial wave functions (assumed to be constant for all fine structure states of the multiple) and that describing the angular momentum factors, are explicitly written in Eq. (3). The second term is dealt with in the next section; we describe here the calculation of absolute cross sections for the multiplet transitions.

Using Eq. (2) and the transition moment for the multiplets obtained from Wiese *et al.*,[20] we can calculate the two-photon absorption cross sections for a number of atoms of interest assuming a Doppler limited linewidth for the two-photon transition. These calculations, along with the relevant parameters for the two-photon transitions considered, are given in Table I. Note that all the listed values of α are of the order of magnitude 10^{-27} cm^4/W. These cross sections must be multiplied by an angular momentum factor of the order of 0.5 (as discussed in the next section) to obtain an experimentally measured cross section.

There is one theoretical calculation that includes all the relevant intermediate states available for comparison with these estimates. Pindzola[6] has calculated for the atomic oxygen the cross section for the two-photon transition listed in Table I. Because he has used the natural linewidth (derived from the radiative lifetime of $\tau = 36$ nsec the upper ^3P state) instead of the Doppler width in his formulation of $g(\nu)$ in his version of Eq. (1), his value of the average cross section for the multiplet transition ($\langle \mathcal{J}_c^{HF} \rangle = 2.3 \times 10^{-43}$ cm^4 sec) must be adjusted for our line shape function. For consistency, we have used Pindzola's line shape function [given in his Eq. (14)] to obtain his peak value for $g(2\nu_l)$. The cross section can now be compared using the conversion equation

$$\alpha(cm^4/W) = \langle \mathcal{J}_c^{HF} \rangle \frac{0.94\pi}{2\tau \Delta\nu_D h\nu}. \tag{6}$$

This gives an *ab initio* value for the multiplet transition of $\alpha = 1.2 \times 10^{-27}$ cm^4/W identical to our simple single intermediate calculation. It is also quite close to the values of McIlrath *et al.*[8] This good agreement gives us confidence that the rest of the cross sections given in Table I have a similar accuracy.

We have attempted to obtain an order of magnitude estimate of this cross section from our signal levels for the case of oxygen atom detection. The largest uncertainty in this type of measurement is knowing the laser

Table II. Relative Values of $\alpha(J_g, J_e)$

J_g	J_e	Three-state calculation	*Ab initio* velocity[a]	*Ab initio* length[a]
0	0	333	542	599
	1	0	0	0
	2	667	458	401
1	0	0	0	0
	1	500	656	700
	2	500	344	300
2	0	133	92	80
	1	300	206	180
	2	567	702	739

[a] Pindzola.[6]

intensity in the focal volume. We present here calculations for the signal intensity assuming a diffraction-limited Gaussian beam.

The excited state density produced by two-photon absorption can be calculated by integrating Eqs. (2) and (3). Assuming a square pulse in time of length T_p, much shorter than the quenched lifetime of the excited state, the excited state density at the end of the pulse can be written

$$N^e(t = T_p) = \frac{\alpha I^2}{h\nu} N_0 T_p, \tag{7}$$

where N_0 is the initial atom density in the ground state.

To obtain the total number of excited states created N_T^e, Eq. (4) must be integrated over the spatial distribution of the laser intensity within the observation volume. This integration is particularly simple for the assumed Gaussian beam. If the observation volume is limited to one confocal parameter,[21] the integration of Eq. (4) leads to

$$N_T^e = \frac{\pi}{2} N_0 \frac{\alpha}{hc} \frac{E^2}{T_p}, \tag{8}$$

where E is the total energy in the laser pulse. Note that this particularly simple expression is independent of the focusing conditions as long as the observation region is larger than one confocal parameter.

For a laser energy of 50 μJ with a pulse length $T_p \sim 10^{-8}$ nsec exciting the $^3P_2 \rightarrow {}^3P_{210}$ two-photon transition, we obtain a signal corresponding to $\sim N_T^e = 10^5$ excited states total for $N_0(^3P_2) = 7 \times 10^{13}$ cm^{-3}. Using Eq. (5), this leads to an experimental value of $\alpha \simeq 10^{-30}$ cm^4/W. Scaling the value for α given in Table I to include the angular factors ($\sim$1/3) and compensating for the laser linewidth ($\sim$1/2) lead to an expected effective cross section of approximately $\alpha \sim 2 \times 10^{-28}$ cm^4/W. This is over 100 times larger than the value calculated from the experimental signal. At the present time we believe that this discrepancy is partly because we have neither a diffraction-limited beam nor a near Gaussian spatial distribution. At the conclusion of the experiments we discovered that damage had occurred to the Pellin-Broca prism; this would have affected the beam quality, although we do not know the prism's actual condition at the time the absolute intensities were measured. Also subsequent experiments[22] investigating the use of Raman scattering as an intensity standard have been performed on a different system. These have indicated that our estimated collection and detection efficiencies may have been low here by a factor of as much as 10, which would account for part of the discrepancy. An accurate determination of the cross section with a diffraction-limited beam would be extremely useful because it would indicate a potentially much higher sensitivity for O atom detection than found in these experiments.

B. Relative Fine-Structure Transition Probabilities

The O atom possesses three ground state fine structure components $^3P_2$, $^3P_1$, and $^3P_0$ at energies of 0, 158.5, and 226.5 cm^{-1}, respectively. The three components of the upper $3p$ ^3P state are packed more closely with separations of 0.54 and 0.16 cm^{-1}. Consequently the laser can easily discriminate between the ground state J values but is too broad to resolve the upper state splitting. In Fig. 4 the stick diagrams correspond to the relative positions and intensities of each expected component, labeled by its value of J_e. It can be seen that the breadth of each excitation corresponds well to these expectations. The integrated intensity $I(J_g)$ from the data in Fig. 4 can be expressed in terms of the two-photon cross section $\alpha(J_g)$ for that component and its population $N(J_g)$:

$$I(J_g) \propto \alpha(J_g) N(J_g); \tag{9}$$

$$\alpha(J_g) \propto \sum_{J_e} \alpha(J_e, J_g); \tag{10}$$

and the results compared to theoretical calculations.

For the ^3P–^3P transition in O, the one-photon allowed intermediate state i may be either a $^3S^0$ or $^3D^0$. Although a sum must be taken over all possible states i, as indicated in Eq. (1), we expect that the $2s^22p^33s$ $^3S^0$ state at 76800 cm^{-1} (which is also the terminal state for the fluorescence as shown in Fig. 1) yields the bulk of the contribution. It is the only allowed intermediate between g and e; most important, it possesses a high reasonable oscillator strength (value of μ) in each step. The detailed theoretical calculation by Pindzola,[6] which employs *ab initio* wave functions, indicates that this state contributes some 97% of the value of α. We consequently restrict our considerations to the $3s$ $^3S^0$ as the sole intermediate.

The wave functions are expressed in terms of their spin and orbital angular momentum components

$$|Jm_J\rangle = \sum_{m_S} C(LSJ; m_L m_S m_J) |L, m_L\rangle |Sm_S\rangle \tag{11}$$

for each $|e\rangle$, $|i\rangle$, and $|g\rangle$. The laser may be taken as linearly polarized in the direction of quantization without loss of generality, so that the opeartor μ has the selection rule $\Delta m_L = 0$. $\alpha(J_g)$ is then obtained by calculating the matrix elements using Eqs. (3) and (11), summing over the m_J values of states i and e and over the J values of $|e\rangle$, and finally averaging over the m_J values for $|g\rangle$. The results of the calculation are collected in Table II, where they are compared with

Pindzola's results[6] using both velocity and length representations of the transition moment operator and Hartree-Fock wave functions, which include correlation. Although the results for each $J_g \rightarrow J_e$ component differ among the calculations, the values of $\alpha(J_g)$ summed over J_e are the same for each.

The predicted values of $I(J_g)$ may then be calculated from Eq. (4) using populations $N(J_g)$ from a Boltzmann distribution at room temperature as ascertained from the NO excitation scan in Fig. 3. The comparison between predicted and measured values is shown in Fig. 7. The fitted line is not constrained to pass through the origin but does so within two standard deviations, as it should do. (The fitted intercept is 0.035 ± 0.021.)

It would be interesting to measure the J_e dependence of the $\alpha(J_e,J_g)$ values, so as to discern among the different possible representations of the transition probability (Table II). Such an experiment, impossible here due to our $\Delta\nu_I$ of 0.3 cm^{-1} and a $\Delta\nu_D$ of 0.27 cm^{-1}, could be performed in a Doppler-free (counterpropagating beams) excitation with a narrower bandwidth laser.

In the case of the N atoms, there is only one ground state component $^4S_{3/2}$ but now four upper state components of ^4D, with J_e ranging from 1/2 to 7/2 over a total energy difference of 110 cm^{-1}. Each of these is readily resolved by the laser, and again the intensities may be compared with calculated values. Here the intermediate state must be a $^4P^o$; the wave functions are expressed using Eq. (11), and the calculation proceeds as before to obtain $\alpha(J_e)$. The results are that the intensities should be in the ratio 1:2:3:4 for $J = 1/2:3/2:5/2:7/2$; that is, the intensity should be proportional to the final state degeneracy $2J_e + 1$. The experimental results are shown in Fig. 8, again in the form of a plot measured vs calculated values. The fitted intercept here is 0.066 ± 0.078.

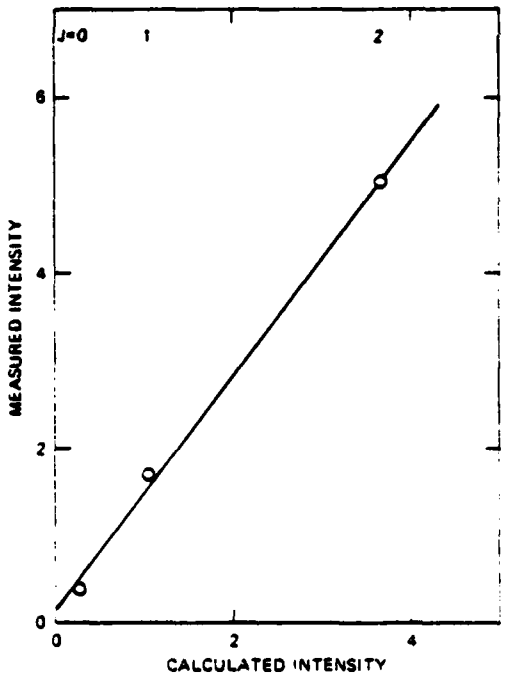

Fig. 7. Measured vs calculated intensity (both arbitrary units) for the three fine structure components of the O atom transition shown in Fig. 4. The line is fitted and not constrained to pass through 0.

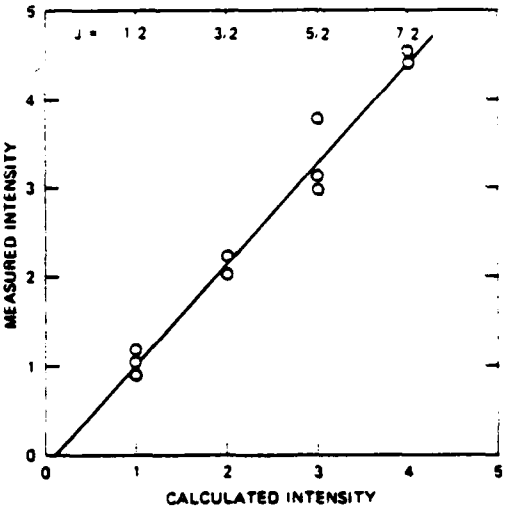

Fig. 8. As Fig. 7 for the four components of the N atom transition.

The results in Figs. 7 and 8 may be taken essentially as an experimental demonstration that we understand well the angular momentum coupling nature of two-photon excitation in atoms. While this is unsurprising, it does constitute a pleasing experimental confirmation of the fact and may be furthermore considered as an indication that the experiment itself is behaving properly.

C. Lifetime and Quenching Rates

The excited state decay rates k_d measured using the scanning gated integrator were plotted as a function of N_2 pressure according to the equation

$$k_d = k_r + k_Q n. \tag{12}$$

The results for O are shown in Fig. 9, where each point is that for one run. The N_2 pressure was never quite 0 because of the small amount added to the discharge for the production of N atoms. A few runs at varying pressures of He, NO, and SF_6 showed no discernible effect on the measured lifetimes at the pressures of these gases normally used.

A least squares fit yields for the intercept $k_r = (2.56 \pm 0.09) \times 10^7$ sec^{-1} or a radiative lifetime 39.1 ± 1.4 nsec. From the slope is obtained $k_Q(N_2) = (2.45 \pm 0.12) \times 10^{-10}$ cm^3 sec^{-1}, corresponding to a cross section of 31 ± 2 $Å^2$. These quoted error bars are from the fit, whereas the spread in points at the same pressure is more of the order of ±10% (Fig. 9).

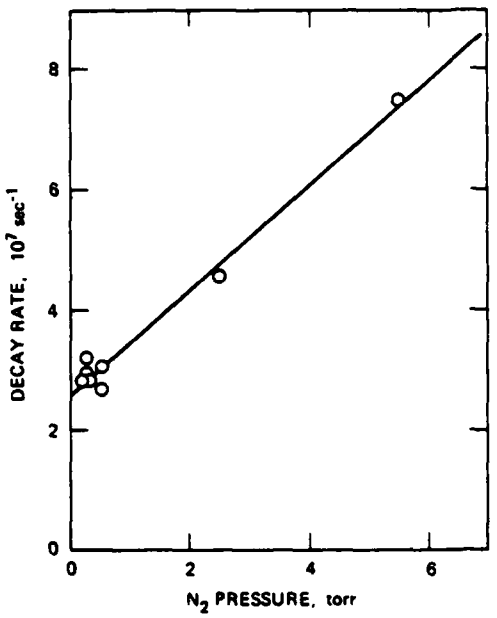

Fig. 9. Decay rate of the O atoms as a function of total pressure of N_2. Each point is an individual run.

The lifetime for this transition in O has been studied rather extensively in the past. Solarski and Wiese[23] obtained a value $k_r = 2.6 \times 10^7$ sec^{-1} with error bars of 27% from intensity measurements in a stabilized arc under equilibrium conditions. In a critical comparison with results of previous experimental and theoretical determinations for this and other oxygen multiplets, they concluded that there existed here a rare case of good agreement among independent determinations and recommended an averaged value of 2.80×10^7 with 10% uncertainty. The present results push this toward the lower end, in excellent agreement with the experimental values[23,24] of 2.6 and 2.5 ± 10^7.

Following the Solarski and Wiese assessment, there have appeared two further experimental determinations. In a study of lifetimes for VUV transitions in O induced by pulsed electron beam dissociation of oxygen-containing molecules Lawrence[25] observed a long tail on the 1304-Å transition. He ascribed this to filling of the $3s\ ^3S$ level from $3p\ ^3P$ at a rate given by $k_r(^3P)$, since $k_r(^3S)$ is much faster. The result is $(2.86 \pm 0.08) \times 10^7$ sec^{-1}, with which our value agrees well. A yet more recent measurement has been performed by Quickenden *et al.*[26] using pulsed electron beam dissociation of H_2O. They obtained $k_r = (5.1 \pm 1.0) \times 10^7$ sec^{-1} in disagreement with our and other[23,24] values, and we feel that the latter are definitely preferable.

The *N* lifetime data showed considerably more scatter. The reasons are not apparent to us, but perhaps by the time this series of runs was made the Pellin-Brocha prism had become damaged and was causing noise problems not present in the O measurements. Twenty-five separate determinations were made at zero added N_2, that is, the presence of N_2 entering only through the discharge. The standard deviation on the average was ±18%, a spread which includes 21 of the 25 data. Similar uncertainties were encountered at other pressures, although far fewer data were taken.

We have chosen to plot in Fig. 10 the averages and errors bars at each pressure rather than the individual data. The results correspond to $k_r = 3.7 \pm 10^7$ sec^{-1} or a lifetime of 27 nsec and $k_Q(N_2) = 2.4 \times 10^{-10}$ cm^3 sec^{-1} or a cross section of 30 Å^2. From the fit and the spread in the data we estimate a 15% uncertainty in k_r and a 30% uncertainty in k_Q. Neither He nor SF_6 was found to have an effect on the measured lifetimes within the data scatter; NO was not checked as it was not used for the final N lifetime runs.

The present result for k_r is in serious conflict with a previous experimental determination by Richter.[27] He made intensity measurements in a nitrogen plasma (similar to the method used for O),[23] obtaining a result $k_r = 1.87 \times 10^7$ sec^{-1} or a 53-nsec lifetime, with estimated error bars of ±15%. A theoretical value using the method of Bates and Damgaard[28] is closer to our result: 2.70 ± 10^7 sec^{-1} (lifetime of 37 nsec). We shall not attempt here a critical comparison. It is true that when lifetimes are shorter they invite suspicion due to the possibility of neglected quenching effects. The O lifetime measurements performed in this same system agree with previous values as discussed, suggesting that such systematic errors are not present and lending confidence to our N lifetime. We thus feel that our value is preferable to that of Richter.

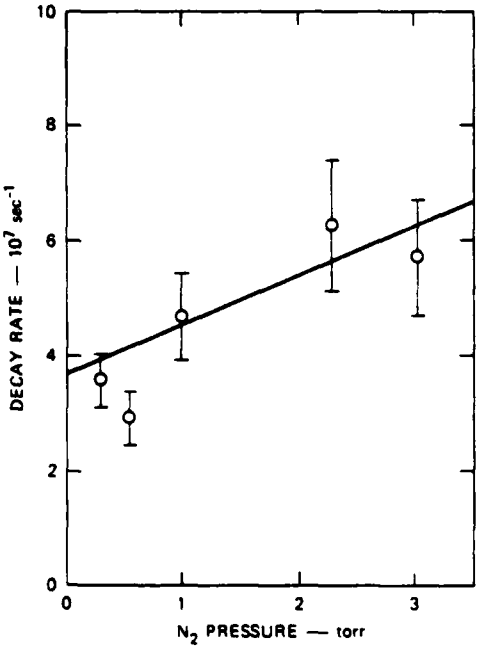

Fig. 10. Decay rates for N as a function of N_2 pressure. Each point and its error bars represent an average of the measurements at that pressure.

The cross sections of ~30 Å^2 which we obtain for collisions with N_2 are gas kinetic in size, which may be expected for quenching of high-lying atomic states. Previous measurements of these processes [$O(^3P) + N_2$, $N(^4D) + N_2$] have not been made, but two pertinent determinations do exist. The study of Quickenden *et al.*[28] included the O quench rate with water; they obtained $k_Q(H_2O) + (9.4 \pm 1.5) \times 10^{-10}$ cm^3 sec^{-1}. Catherinot and Sy[29] have used a laser to single-photon-pump the $3p\ ^4S$ state of N from the $3s\ ^4P$ present in a discharge and measured lifetimes. This ^4S state lies just above (~0.25 eV) the ^4D state we studied. They conclude, from considerations of the energies of possible exit channels of a quenching collision, that only N_2 in vibrationally excited states with $v \geq 2$ can quench the ^4S state. Estimating the concentration of excited N_2 in their discharge, they derive a $k_Q = 6.5 \times 10^{-9}$ cm^3 sec^{-1} for collisions with the excited molecules. Our measurements were made at room temperature where all the N_2 is in the ground vibrational state, and our k_Q is due to $v = 0$ molecules only.

IV. Conclusions

These experiments have demonstrated the viability of two-photon excitation of fluorescence emitted by atomic states lying far above the normal VUV cutoff. The method is straightforward and applicable to a large number of atomic species. Although the laser which we used is a version with relatively high power, so as to make possible the necessary chain of frequency conversion steps, it is a commercially available system, that is, a custom rig is not required.

From the results of this work we can project good detectivities when this method is used as a flame diagnostic tool. If other gases collisionally quench the excited states with the same efficiency as does N_2 and if those rate constants are independent of temperature, reasonable assumptions for estimation purposes since the measured rate constant was gas kinetic, the quenching rate at 1 atm, and 2000 K is ~10^9 sec^{-1}. This corresponds to a fluorescence quantum yield for O of 0.026 and for N of 0.039. The flow system measurements were performed at ~10^{14} atoms cm^{-3}. Because the absorption rate is quadratic in laser intensity, the same signal levels as observed here would then be attained for 1 ppm of atoms in an atmospheric pressure flame, given an increase in laser power by a factor of ~30 over that used here. This laser power, ~1 mJ/pulse, is a demanding but realistic value at 226 nm, and one could obtain perhaps 300 μJ/pulse at 211 nm.

In fact the required laser power to detect parts per million levels may be lower for two reasons. First, the bulk of the noise in the observed signal levels (Fig. 4) was caused by laser fluctuations. The signal-to-background ratio in the flow system was by contrast ~100. If this background does not increase under flame conditions, a more stable laser may improve the results. A flame will have emission in the near IR, but the observed level can be decreased using sharp spectroscopic filtering (the O fluorescence emission is only 1 cm^{-1} wide) and fast gating (possibly gating of the photocathode to avoid background overloads). Second, as discussed above, our observed signal level is lower than that expected on theoretical grounds by a factor of perhaps 100. The true reason is unknown, but poor beam quality is suspected. Were this correct, a laser of better beam quality would generate larger signals at the same pulse energy with a concomitant increase in ultimate detection limits.

We thus conclude that two-photon laser-induced fluorescence of O and N atoms, although not yet successfully performed in flames, should be a feasible technique for combustion measurements at the parts per million level. This two-photon method thus adds a significant category of species, the single atoms O, N, H, and C, to the list of some twenty diatomic and triatomic free radical combustion intermediates detectable with laser-induced fluorescence.[4]

For collision-free conditions as in a low-pressure plasma, the measurable absolute concentration limit will be lower. Our initial estimate[9] of 10^{11} cm^{-3} appears conservative following the efforts of Muller *et al.*[11]; their developments aimed at such plasma diagnostics projects detectivities as low as 10^{10} cm^{-3}.

Additionally collision information of fundamental interest can be obtained using this technique. For example, the excitation of each individual ^4D_J component could be followed by spectrally resolved measurements on the $^4D_J \rightarrow {}^4P_J$ multiplet in the extraction of state-specific collision cross sections among the J values of ^4D, similar to experiments performed on Na using two-photon excitation under bulb[30] and flame[31] conditions.

We are grateful to Tom Slanger for advice on flow systems and atom production and to Greg Smith for useful discussions. This research was supported in part by SRI International internal research and development funds and in part by the U.S. Army Research Office.

References

1. C. J. Dasch and J. H. Bechtel, Opt. Lett. 6, 36 (1981).
2. R. E. Teets and J. H. Bechtel, Opt. Lett. 6, 458 (1981).
3. S. J. Harris and A. M. Weiner, Opt. Lett. 6, 142 (1981).
4. D. R. Crosley, Ed., *Laser Probes for Combustion Chemistry*, Vol. 134 (American Chemical Society, Washington, D.C., 1980).
5. K. Schofield and M. Steinberg, Opt. Eng. 20, 501 (1981).
6. M. S. Pindzola, Rev. A 17, 1021 (1978).
7. K. Omidvar, Phys. Rev. A 22, 1576 (1980).
8. T. J. McIlrath, R. Hudson, A. Aiken, and T. D. Wilkerson, Appl. Opt. 18, 316 (1979).
9. W. K. Bischel, B. E. Perry, and D. R. Crosley, Bull. Am. Phys. Soc. 26, 23 (1981); Chem. Phys. Lett. 82, 85 (1981).
10. J. Bokor, R. R. Freeman, J. C. White, and R. H. Stroz, Phys. Rev. A 24, 612 (1981).
11. C. H. Muller III, D. R. Eames, and K. H. Burrell, Bull. Am. Phys. Soc. 26, 1031 (1981); C. H. Muller III, private communication.
12. D. R. Crosley, Opt. Eng. 20, 511 (1981).
13. V. Wilke and W. Schmidt, Appl. Phys. 16, 351 (1978); 18, 177 (1979).

14. J. A. Paisner and R. S. Hargrove, in *Digest of Conference on Laser Engineering and Applications* (Optical Society of America, Washington, D.C., 1981), postdeadline paper II-4.
15. D. Eimerl, R. S. Hargrove, and J. A. Paisner, Phys. Rev. Lett. **46**, 651 (1981).
16. J. R. Ackerhalt, Phys. Rev. Lett. **46**, 922 (1981).
17. W. K. Bischel and D. R. Crosley, to be published.
18. W. K. Bischel, P. J. Kelly, and C. K. Rhodes, Phys. Rev. A **13**, 1817 (1976).
19. B. R. Marx, J. Sumons, and L. Allen, J. Phys. B **11**, L273 (1978).
20. W. L. Wiese, M. W. Smith, and B. M. Glennon, "Atomic Transition Probabilities," Nat. Stand. Ref. Data Ser. Nat. Bur. Stand. (1966).
21. H. Kogelnik and T. Li, Appl. Opt. **5**, 1550 (1965).
22. W. K. Bischel and G. Black, to be published.
23. J. E. Solarski and W. L. Wiese, Phys. Rev. A **135**, 1236 (1964).
24. L. R. Doherty, Thesis, U. Michigan (1963), quoted in Ref. 23.
25. G. M. Lawrence, Phys. Rev. A **2**, 397 (1970).
26. T. I. Quickenden, S. M. Trotman, J. A. Irvin, and D. F. Sangster, J. Chem. Phys. **71**, 497 (1979).
27. J. Richter, Z. Astrophys. **51**, 177 (1961).
28. D. R. Bates and A. Damgaard, Philos. Trans. Soc. London Ser. A **242**, 101 (1949).
29. A. Catherinot and A. Sy, Phys. Rev. A **20**, 1511 (1979).
30. T. F. Gallagher, W. E. Cooke, and S. A. Edelstein, Phys. Rev. A **17**, 125 (1978).
31. J. E. Allen, Jr., W. R. Anderson, D. R. Crosley, and T. D. Fansler, in *Seventeenth Symposium (International) on Combustion* (Combustion Institute, Pittsburgh, 1979), p. 797.
32. M. A. A. Clyne and W. S. Nip, J. Chem. Soc. Faraday Trans. 2 **73**, 1308 (1977).

Laser-Induced Fluorescence in Spectroscopy, Dynamics, and Diagnostics

David R. Crosley
Molecular Physics Laboratory, SRI International, Menlo Park, CA 94025

In the technique of laser-induced fluorescence, or LIF, a laser is tuned so that its frequency matches that of an absorption line of some atom or molecule of interest. The absorption of the laser photons by this species produces an electronically excited state which then radiates. The fluorescent emission is detected using a filter or a monochromator followed by a photomultiplier. Because a particular absorption line is selected, the excited state has definite and identifiable vibrational, rotational, and fine structure quantum numbers. This clean state preparation has significant advantages for spectroscopic and collision studies, in contrast to the congestion often found in ordinary emission spectra from, for example, a discharge. Since the lower state responsible for the absorption is also definite, considerable selectivity is provided by LIF when used as a diagnostic tool. In addition, its high degree of sensitivity, the spatial and temporal resolution available, and its non-intrusive nature are important attributes for this purpose. Finally, special LIF methods not possible in non-laser spectroscopy, such as two photon excitation, yield new information and make possible new diagnostic probes.

These features of LIF are illustrated in this paper using as examples a variety of experiments conducted in the author's laboratories. LIF as a whole has had a tremendous impact on the study of the electronic spectra of small molecules,[1] and it should be noted that the experiments discussed here form but a tiny portion of the many ways LIF has been used to further our knowledge of molecular structure and behavior. Nonetheless, it is hoped that the highly personal selection presented will serve to describe some of the important aspects of this exciting and rapidly progressing technique.

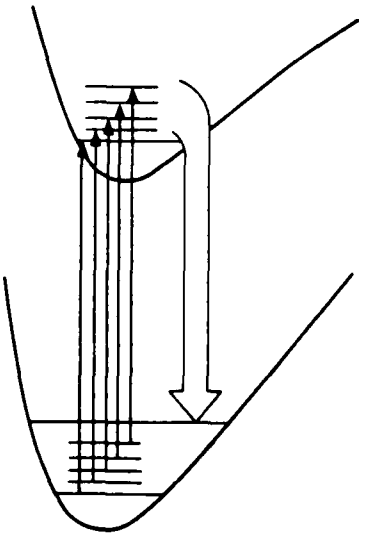

Figure 1. Schematic diagram of an excitation scan showing the potential curves (electronic states) and some levels involved. The detection system measures fluorescence (downward arrow) from any excited level; this will occur each time the laser is tuned to match the frequency of some absorption line (upward arrows). As the laser is tuned through the series of absorption lines, an excitation scan results.

LIF Experiments

Given a laser, the experimental configuration employed for most LIF studies is quite simple. The laser beam is directed into a sample, which is contained in some suitable cell if necessary. The fluorescence emitted at a right angle to the beam direction is focussed through a filter into a photoelectric detector. The filter may be at a particular wavelength (such as a glass color filter or interference filter) or scannable (i.e., a monochromator).

A single frequency laser (such as from a rare gas ion laser) may be used if its frequency happens to coincide with that of some absorption line, but clearly a tunable (dye) laser is more versatile. It permits the performance of experiments on different molecules, or on a sequence of excited levels in one species so as to compare their behavior. The most rapid growth in the number of LIF studies has coincided with the availability of commercial tunable dye lasers. Continuous duty lasers have advantages of much narrower linewidth and more stable output amplitudes, whereas pulsed lasers have higher peak powers and thus higher instantaneous signal levels, and with them is possible a variety of non-linear processes including frequency doubling and shifting methods. All of the experiments described in this paper involve pulsed lasers having repetition rates of typically 10 Hz, pulse lengths of 10 nsec or 1 μsec, and in all but one a frequency shift from the dye laser fundamental. When operating with a pulsed laser, it is generally advantageous to use a gated detection system. Also termed a boxcar integrator when used to average over a number of laser pulses, this device basically turns the detection electronics on only for a short period during or immediately after the laser pulse. Because all of the LIF signal occurs in this brief time span, gated detection greatly enhances the ratio of signal to that background which is continuously present, such as photomultiplier dark current or ordinary flame emission.

The two chief methods of spectroscopic data acquisition in an LIF experiment are excitation and fluorescence scans. In an excitation scan, depicted schematically in Figure 1, the detector and filter are chosen so that fluorescence from any excited level can be detected. The laser frequency is then scanned through the absorption region of the molecule; each time it matches that of an absorption line, fluorescence results. Thus an excitation scan mimics the absorption spectrum of the molecule. The main difference is that instead of looking at a small dip in a large transmitted signal, LIF forms a positive signal on a null background. It is thus much more sensitive: total absorptions of 10^{-6} or less can produce readily measured signals. In addition, higher selectivity can be possible than in an absorption measurement. Suppose two (or more) species are present, both absorbing at the same wavelength but fluorescing at different wavelengths. The choice

[1] Witness the fact that, of the papers in this category presented at the annual molecular spectroscopy symposium in Columbus, Ohio, each June, the fraction involving LIF has grown from less than one-tenth a decade ago to about two-thirds presently.

Reprinted from Journal of Chemical Education, Vol. 59, Page 446, June 1982.

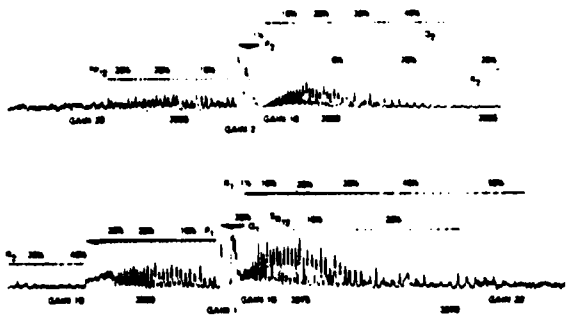

Figure 2. An excitation scan through the (0,0,1) — (0,0,0) band of the $A^2\Sigma^+$-$X^2\Pi$ system of the linear triatomic molecule NCO, near 4000 Å. Several rotational branches are marked with the ground state value of the angular momentum quantum number J'', for the $^2\Pi_{1/2}$ sub-band (top) and the $^2\Pi_{3/2}$ sub-band (bottom). The wavelength (Å) is listed under the scan, as are the regions where the amplifier sensitivity is changed.

of detector wavelength then permits the spectrum of one to be obtained with no contribution from the other.

An example of an excitation scan is shown in Figure 2. Here the laser is tuned through the (001)–(000) band of the $A^2\Sigma^+ - X^2\Pi$ system of the linear NCO molecule (*1*), which has here been produced in a flow discharge at about 1 torr total pressure. The top and bottom portions show the rotational branches, designated by the value of the total angular momentum quantum number in the ground state, for each of the two fine-structure components ($^2\Pi_{1/2}$ and $^2\Pi_{3/2}$). The details are not of concern here, but it is obvious that considerable spectroscopic information is available from such a scan.

As a monitor, an excitation scan measures populations in the ground state of the molecule. That is, the intensity of each line is proportional to the population of the ground state level responsible for that absorption. In the well resolved branches in Figure 2 one can discern an envelope reflecting a Boltzmann distribution over the rotational levels. Using such lines to obtain a population distribution, and from it a temperature, is an important aspect of the use of LIF as a combustion probe.[2]

Figure 3 shows a schematic description of a fluorescence scan. Here, the laser is parked at a particular frequency so that one individual upper state level is pumped. One now scans a monochromator so as to measure different fluorescence

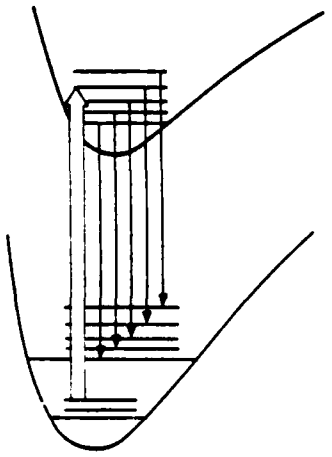

Figure 3. Schematic diagram for a fluorescence scan. Here the laser is set at some wavelength so as to pump a specific level in the excited state. Fluorescent lines emitted by the pumped level and/or by other levels populated by collisions are separated by a scanning monochromator.

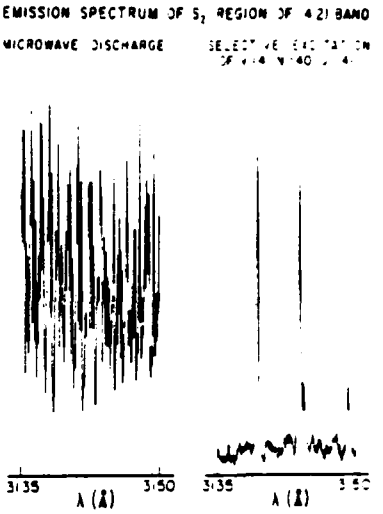

Figure 4. *Left*, Emission spectrum from the $B^3\Sigma_u^-$-$X^3\Sigma_g^-$ system of the S_2 molecule excited in an electrodeless discharge, in a small wavelength region. The zero of intensity is at the bottom of the figure; the apparent offset is due to the blending of many individual lines (above 50 of which can be distinguished) emitted by many upper state levels. *Right*, The fluorescence spectrum in the same region following excitation of the single level $v' = 4$, $N' = 40$, $J' = 41$ of the B-state. The lines are all emitted by this level and are (in order of increasing wavelength) the $R_1(39)$, $P_1(41)$, $^PR_{12}(41)$, and $^NP_{12}(43)$.

transitions. In the isolated molecule, these will be those emitted only by the pumped level. In the presence of some colliding species, other levels may be populated by collisional energy transfer and they too will emit.

The simplicity and resulting advantages of the spectrum measured are illustrated in Figure 4, which shows emission spectra from the S_2 molecule in a region containing primarily, though not exclusively, the (4,2) band of the $B^3\Sigma_u^- - X^3\Sigma_g^-$ system. On the left is the emission from an electrodeless discharge in sulfur vapor; the heavy congestion of closely spaced and often overlapping lines (there are about 50 visible in the figure, not counting blended lines) arises from the many rotational levels produced in the discharge. On the right is the fluorescence spectrum in the same region from a single level populated such as would be done[3] in an LIF experiment. Obviously here the situation is much cleaner. In particular, the two smaller lines ("satellite branches") show up clearly, whereas in the discharge spectrum they are totally masked by the strong lines ("main branches") emitted by different rotational levels. Using LIF, the relative intensities of the satellites and the main branches emitted by the single pumped level can be measured. In this case such ratios led to some new and surprising information concerning the spin-spin interaction in the B-state (*2*), which had escaped notice in earlier conventional spectroscopic studies.

In Figure 5, one sees how the presence of collisions alters the fluorescence spectrum. Here, the molecule is OH, present in a low-pressure flow system, and the $v' = 0$, $N' = 1$, $J' = 1.5$ level[4] is pumped by the laser. On the left is the emission from OH by itself, consisting of the five strong rotational branches

[2] For a system not at thermal equilibrium, so that a temperature is undefined, the population distribution itself is the desired result of interest.

[3] The actual scan from which this figure was made employed as an excitation source an atomic Zn lamp one of whose lines coincidentally overlapped an S_2 absorption line, but the experiment could be done (actually more easily) using laser excitation.

[4] In accordance with common spectroscopic notation, a single prime will be used to denote the upper state and a double prime for the ground state; also, when a transition is referred to, the upper state is always written first (e.g., the 6,0 band means $v' = 6$, $v'' = 0$).

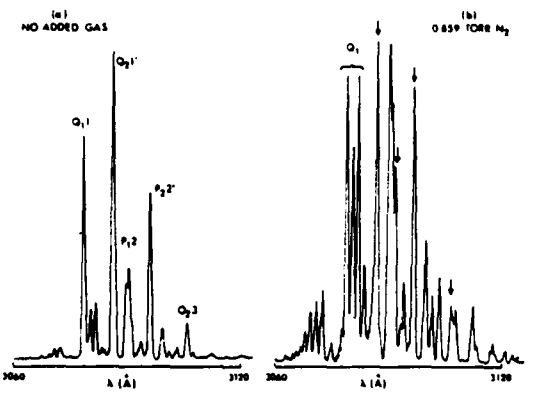

Figure 5. Fluorescence scans of the (0,0) band of the $A^2\Sigma^+$-$X^2\Pi_i$ system of the OH molecule, following pumping of the $N' = 1$, $J' = 1\frac{1}{2}$ level. *a*, No added gas. The five rotational lines marked are those emitted by the pumped level (a few small lines are due to collisions with the background gases H_2O and NO_2; also, laser scatter is partially responsible for the width of the feature in the $P_1(2)$ region). *b*, Spectrum with added N_2, at 0.86 torr. The Q_1 series is marked as are (with arrows) the remaining four branches noted in (*a*). The new features are lines emitted by other rotational levels within $v' = 0$, populated by energy transfer collisions with the N_2. [Reprinted from the *Journal of Chemical Physics*]

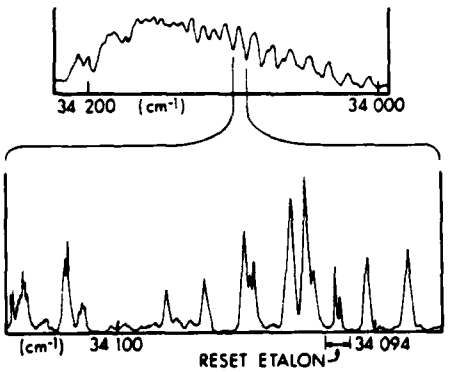

Figure 6. Excitation scans of the (6,0) band of the B-X system of S_2 near 2930 Å. *Top*, Scan across the entire red-shaded band, showing double heads on the left and some structure in the high-J regions to the right. The laser bandwidth is here 12 cm^{-1}. *Bottom*, Scan of a small region at narrower laser bandwidth, 0.3 cm^{-1}, showing individual rotational lines which constitute the feature near 34100 cm^{-1} in the upper scan. The region marked "reset etalon" is an artifact of the scanning mechanism. [Reprinted from the *Journal of Chemical Physics*]

as marked. (A few smaller lines are due to collisions with background gases H_2O and NO_2 used to produce the OH, but they shall be ignored here; some scatter from the exciting laser is responsible for the breadth in the P_12 region.) When 0.86 torr of N_2 is added, the spectrum on the right is obtained. The Q_1 series is marked, as are (with arrows) the other four branches noted in (*a*). The new lines are fluorescence emitted from other rotational levels, populated by energy transfer collisions of the excited OH with the N_2 present.

From relative intensities of the lines in scans such as these, taken at several pressures of the collision partner, individual energy transfer rate constants (or cross-sections) between the initially pumped level and each final rotational level can be obtained. The laser is then tuned to pump a different initial level, and the process repeated. In this way is determined the entire matrix of state-to-state rotational energy transfer cross sections for the upper electronic state (*3*).

The populations deduced from fluorescence scans such as those in Figure 5 reflect excited state behavior, in contrast to the ground state populations deducible from the excitation scan intensities. Each type of spectrum of course contains spectroscopic information about both the upper and lower states connected in the transition.

When LIF is used as a diagnostic monitor the laser and detection wavelengths generally remain fixed while some other parameter pertinent to the behavior of the probed system is varied. This could, for example, be the distance above a burner in a flame study, or the time delay between two lasers as described below for a laser pyrolysis experiment. Of course, the laser frequency would be varied for population determinations at each point in the flame or at a particular delay time.

If the upper state radiative lifetime is longer than the laser pulse length, useful information can be obtained from its measurement. This could be done in principle from an oscilloscope trace of the time dependence of one fluorescence decay. It is usually accomplished in practice using the gated integrator to average over a number of pulses at a given time after the laser pulse, and then systematically scanning that time difference.

Franck-Condon Factors in S_2

In this experiment, the laser excites a particular v' vibrational level of the $B^3\Sigma_u^-$ state of S_2, which then radiates to a large number of v'' levels in the $X^3\Sigma_g^-$ ground state. In a fluorescence scan the intensity $I_{v'v''}$ of each $v' \rightarrow v''$ term is measured as a function of v''; from it may be extracted the Franck-Condon factor

$$q_{v'v''} = |\int \psi_{v'}(r)\psi_{v''}(r)dr|^2 \qquad (1)$$

which is the square of the integral of the upper and lower state vibrational wavefunctions taken over the internuclear distance r. $q_{v'v''}$ is proportional to the measured $I_{v'v''}$. Tuning the laser so that a different v' is excited, and repeating the fluorescence scan, permit the full matrix $q_{v'v''}$ to be obtained. This, we shall see, provides a simple pictorial description of the $\psi_{v'}(r)$.

The S_2 is contained in a small cell, and is produced by heating liquid sulfur in a reservoir to about 100°C. This yields a pressure of some 50 mTorr total of sulfur which exists predominantly in the form of S_6 and S_8, plus some S_4 and S_2. The body of the cell is kept much hotter, about 600°C, by a separate heater coil; at this temperature the equilibrium constants for the reactions among the several species are such that nearly all of the sulfur is in the form of S_2.

The first part of the experiment consists of an excitation scan so as to select a particular line. We begin by operating the laser in a wide bandwidth (12 cm^{-1}) mode and scan across an entire vibrational band. This is shown in the upper trace in Figure 6, in which $v' = 6$ is excited. The laser operation is shifted to narrow bandwidth (0.3 cm^{-1}), and a small portion of the band is now scanned (lower trace in Fig. 6); the unresolved feature in the first scan is seen to actually consist of a series of individual rotational lines.

The laser is now set to excite one line, and a fluorescence scan is made (see Fig. 7). This is first done over a small wavelength region covering the rotational structure of a particular $v' \rightarrow v''$ term, as shown in Figure 7a for (6,1). This pattern is the same as that in Figure 4, except that one of the satellites is here blended with the line marked P_1. From the rotational branch pattern and the R-P splitting (3.85 Å here), we can determine the rotational and fine structure quantum numbers of the level excited, although they are not important for the current purpose.

A scan over the entire region of emission, extending from the ultraviolet well into the visible, is now made (Fig. 7b). Each peak corresponds to a particular v''. The full $v' = 6 \rightarrow v''$ pattern can be seen, beginning with the (6,0) band marked with the asterisk and corresponding to the excitation, out to the (6,26) band on the far right. Each of the terms contains the same rotational structure as in Figure 7a.

The ability of LIF to clean up an emission spectrum is at-

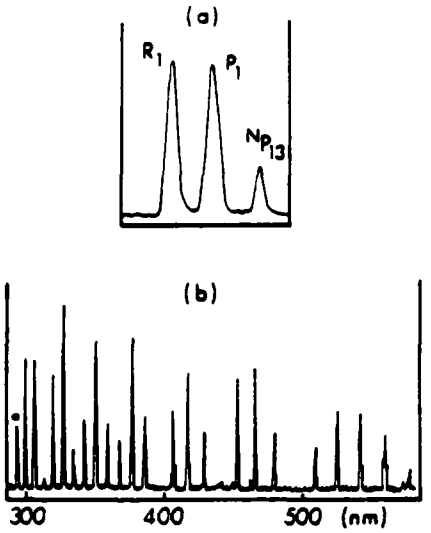

Figure 7. Fluorescence scans obtained upon excitation of the $v' = 6$, $N' = 36$, $J' = 37$ level. *a*, Scan of the rotational line structure of the (6,1) band; the R_1–P_1 splitting is 3.85 Å. *b*, Scan of the entire fluorescence progression emitted by $v' = 6$. The asterisk marks the (6,0) band where the laser pumps. Bands are visible here out to $v'' = 26$; each peak consists of the same rotational line pattern shown in (*a*). [Reprinted from the *Journal of Chemical Physics*]

tested to by the fact that of the 27 terms belonging to $v' = 6$ seen in this study, only nine had been previously reported in the conventional spectroscopic literature, due primarily to overlapping by other bands. An examination of Figure 7b reveals a very regular pattern to the intensities as the wavelength and hence v'' increases. An undulating envelope having seven maxima can be easily discerned. This pattern is subject to a very simple explanation, through the Franck-Condon principle, clearly illustrating the validity of a wavelike picture of vibrational motion.

The Franck-Condon principle, which governs the intensities, may be stated in a classical formulation to require that neither the internuclear distance nor the instantaneous value of the momentum is altered during an electronic transition (which occurs much more rapidly than nuclear motion takes place). Quantum mechanically, these two requirements must be satisfied simultaneously, as reflected in the integral of eqn. (1). In Figure 8 on the left are shown schematic wavefunctions for S_2 for a single v' and several v''. Consider the overlap with $v'' = 20$. The rapid oscillations in the center of the $v'' = 20$ wavefunction will yield alternating positive and negative values when multiplied by the more slowly varying upper state wavefunction. Consequently the contributions to the integral from the central region of internuclear distance will tend to cancel, and the integral will be dominated by the slowly varying lobe of $\psi_{v''}$ near the right hand part of the potential.

This argument is extended graphically in the right hand side of Figure 8, where the effective $\psi_{v''}$ has been replaced by a function which is zero except for a gate, or delta function, attached to the ground state potential at the right hand turning point[5] $r_{v''}$. In this approximation one may write the Franck-Condon factor as

$$q_{v'v''} = |\int \psi_{v'}(r)\delta(r_{v''})dr|^2 = |\psi_{v'}(r_{v''})|^2 \qquad (2)$$

i.e., it represents the square of the probability amplitude of the upper state wavefunction evaluated at $r_{v''}$. Since $r_{v''}$ increases smoothly with v'', the spectrum in Figure 7b reflects the value of $|\psi_{v'}(r)|^2$ with r increasing. Recalling the harmonic oscillator wavefunctions for $v' = 6$, the meaning of the seven lobes is now clear.

[5] The two turning points are those values of r where the total energy of the vibrational state is potential, that is, where the energy level cuts the potential curve.

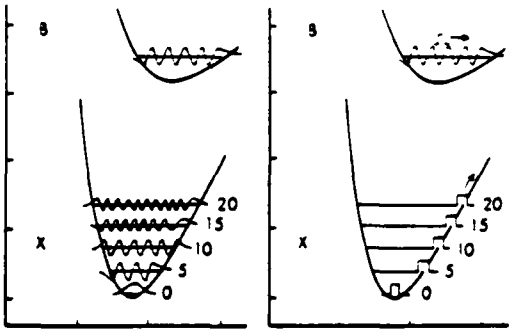

Figure 8. Potential curves and vibrational wavefunctions for the B and X states of S_2. *Left*, Wavefunction for $v' = 9$ and several ground state levels. *Right*, Schematic replacement of the ground state wavefunctions by a gate attached at each right-hand turning point. Increasing v'' effectively scans the gate to larger internuclear distance r, tracing out $|\psi_{v''}|^2$ as a function of r. [Reprinted from the *Journal of Chemical Physics*]

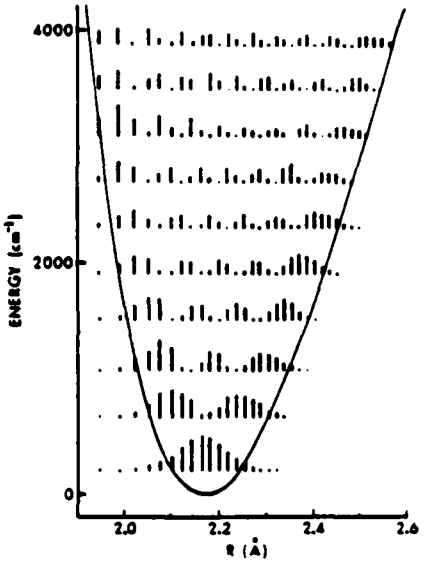

Figure 9. A plot of the experimental $q_{v'v''}$ versus ground state right hand turning point $r_{v''}$. This yields in effect a plot of each $|\psi_{v'}(r)|^2$, as rationalized in the text. The potential curve is the B-state potential curve, superimposed independently. Expected features of these "experimental wavefunctions" which can be seen are $v + 1$ lobes and v nodes, and a wavelength inversely related to the instantaneous kinetic energy. [Reprinted from the *Journal of Chemical Physics*]

The values of $r_{v''}$ can be obtained from the spectral constants of the ground state, and a plot of $q_{v'v''}$ vs. $r_{v''}$ should (within the spirit of the approximation in eqn. (2)) yield directly the probability distribution of $\psi_{v''}$ as a function of internuclear distance. Measurements have been made on all ten bound vibrational levels of $B^3\Sigma_u^-$; half of these were made using LIF (4) and half by the pre-laser counterpart of excitation by a coincidentally overlapping atomic line (5).

The results are displayed in Figure 9. For each v', and $q_{v'v''}$ are plotted as a function of $r_{v''}$ with zero at the corresponding energy level (that is, the way vibrational wavefunctions are often drawn). Superimposed on the $q_{v'v''}$ pattern is the potential curve for the B electronic state: it is to be emphasized

that the potential curve plot and the $q_{v'v''}$ plots are entirely independent of one another.

The assumptions involved in the use of eqn. (2) preclude attaching a full quantitative significance to Figure 9; nonetheless, the results are instructive. The "wave functions" exhibit the proper number of lobes and span the expected region of internuclear separation with reasonable centering. The undulations in the center (where the kinetic energy is high) have a shorter effective wavelength than those near the turning points, and there is some finite though small amplitude in the classically forbidden region outside the potential. In any event, these results form a compelling reminder that molecular vibration is indeed described by a wavelike picture; in fact, the essence of this is contained in the raw intensity data of Figure 7b.

Vibrational Energy Transfer in OH

We have seen that LIF can provide spectroscopic (i.e., structural) information about isolated molecules. It is also invaluable as a state preparation method for collisional energy transfer studies. As an illustration, we consider vibrational energy transfer in the OH molecule (*6*).

The OH is produced in a flow system by the reaction H + NO_2; the H atoms are formed by a microwave discharge in H_2 vapor. Controlled amounts of other gases are added as collision partners. The OH is excited by the laser to a specific fine structure component of a particular rotational level in $v' = 1$ of the $A^2\Sigma^+$ excited state. Emission in the (1,1) band will identify molecules within this initially excited vibrational level. If the presence of added gas is high enough that collisions occur before the OH fluoresces, some of the molecules may be transferred downward to $v' = 0$ of the excited state, losing ~3000 cm^{-1} of vibrational energy. These collisionally transferred molecules can be measured by the fluorescence in the (0,0) band.

Figure 10 exhibits the experimental results. As signified in the top scan, emission to the left of the short vertical line at 3124 Å is the (0,0) band, while the (1,1) band lies to the right. Here, the $N' = 3, J' = 3\frac{1}{2}$ level in $v' = 1$ is pumped by the laser. In scan (a), only OH molecules are present and the spectrum consists of the six marked rotational branches emitted by this level. (A small number of weaker lines is also present; as in Figure 5 these are due to collisions with the ever-present H_2O and NO_2, and will be ignored.) In the absence of collisions, there is no OH in $v' = 0$ and the (0,0) band region is dark.

In scan (b), about 1 torr He has been added. In the (1,1) region, we see not only the distinctive pattern emitted by the pumped level, but also additional lines due to other rotational levels within $v' = 1$, which have been populated by rotational energy transfer due to collisions with the He. A very small amount of fluorescence is seen in (0,0), coming from OH molecules which have been collisionally transferred downward into $v' = 0$. Now the separation between adjacent rotational levels in $v' = 1$ is some tens of cm^{-1}, much smaller than the vibrational energy difference. Energy transfer is expected to occur less efficiently for a larger energy defect. For He as a collision partner, the weaker fluorescence from $v' = 0$, compared to that from rotationally transferred molecules within $v' = 1$, is in accord with this notion.

H_2 is a light molecule and, although it does have internal vibrational and rotational energy levels, they are widely spaced, so that one might expect it to behave not unlike He as a collision partner. However, Figure 10c, which shows the fluorescence spectrum obtained in the presence of ~1 torr H_2, is strikingly different. The (1,1) band again shows the lines emitted by the pumped level, plus some due to rotational transfer, but less rotational transfer has occurred than with He. The amount of vibrational transfer, as seen by the relative intensity of (0,0), is, however, much larger. Here the rate of vibrational transfer is actually faster than rotational transfer. The surprising result does appear to be linked with the internal structure of the H_2, which provides, compared with He, extra channels in which to deposit the excess energy. The full series of experiments (*6*) include Ar, N_2 and D_2 as a collision partner, OD as the pumped molecule, transfer from $v' = 2$, and measurements of the rotational distribution of the collisionally transferred OH. These all point to the conclusion that the vibrational energy transfer, for diatomics as a collision partner, occurs as a result of a long-lived collision involving attractive interactions.

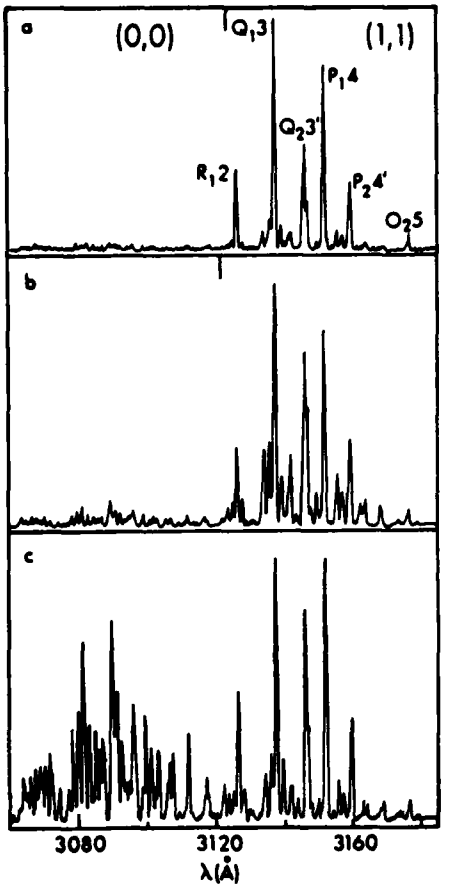

Figure 10. Fluorescence scans of OH excited to the $v' = 1$, $N' = 3$, $J' = 3\frac{1}{2}$ level of the A-state. To the left ($\lambda < 3124$ Å) lies emission in the (0,0) band and to the right emission in (1,1). *a*, No added gas. The rotational lines emitted in the (1,1) band by the pumped level are marked (a few small features are due to collisions with background gases as in Fig. 5). With no collisions occurring, there is no population in $v' = 0$ and consequently no emission in the (0,0) band. *b*, ~1 torr He added. In addition to the lines emitted by the pumped level, other rotational lines in the (1,1) band arise through collisional rotational energy transfer within $v' = 1$. The emission in (0,0) originates from molecules which have undergone vibrational transfer collisions to $v' = 0$. The relative intensities show that the vibrational transfer, which has a much larger energy difference, occurs more slowly than rotational transfer, for the collisions. *c*, ~ 1 torr H_2 added. Here, much more vibrational transfer occurs, as indicated by the (0,0) intensity; it actually is faster than rotational transfer within $v' = 1$ for collisions with H_2. [Reprinted from the *Journal of Chemical Physics*]

Yet another important and surprising result can be obtained from the data, exploiting the tunability of the laser. Consider again Figure 10c. The rotational branch pattern in the (1,1) band shows that most of the molecules in $v' = 1$ are in the initially pumped rotational level. This means that the molecules which are transferred to $v' = 0$ originated from that same level. That is, the vibrational transfer which has occurred is specific to the initially pumped rotational level. We can measure the vibrational transfer rate constant (or cross section) from the (0,0) to (1,1) intensity ratio as a function of

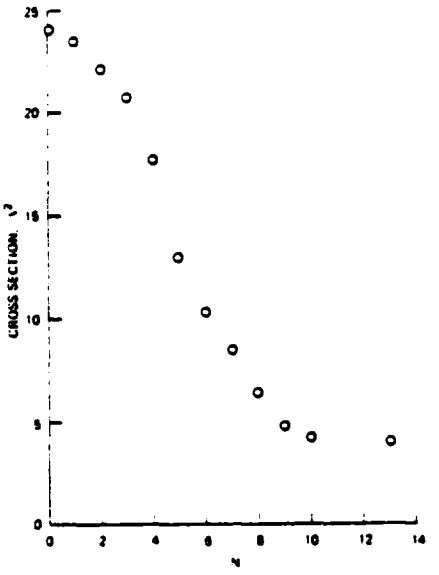

Figure 11. Cross section for $v' = 1 \rightarrow v = 0$ collisional energy transfer in $A^2\Sigma^+$, as a function of initial rotational quantum number N' in $v' = 1$. These results are for N_2 as a collision partner.

Combustion Intermediates Detected by LIF

O,N	S_2, SH, SO, SO_2
OH	CS, CS_2
CH, CN, C_2, CO	HCN, NCO
NH, NH_2	C_2O, C_3
NO, NO_2, HNO	CH_2O, CH_3O

pressure of the collision partner. Tuning the laser so as to pump a sequence of rotational levels then will provide the initial rotational level dependence of the vibrational transfer rate.

The prior expectation is to find little or no dependence on N'. The results, shown in Figure 11 for N_2 as a collision partner, demonstrate quite the opposite—a very noticeable variation with initial rotational level. This is not a matter of energy differences, or resonant exchange of any kind. Rather, it appears that the initial collision dynamics, in the entrance channel to the long-lived complex, are responsible. The attractive forces leading to the complex are anisotropic with respect to the OH (as befits its strong dipolar character). As the OH rotates, approaching velocities not unlike that of the collision pair, the anisotropy would be washed out and the ease of formation of the complex reduced.

The results in Figure 11 *do not* demand this explanation but it is plausible. At the very least, they demonstrate that molecular collisions, when investigated on a detailed basis, exhibit features and behavior far richer in variety and complexity that previously supposed. It is through the clean state preparation afforded by LIF, and its ability to pump a sequence of levels so as to compare results, that such details can emerge.

Diagnostics for Combustion Chemistry

Besides providing fundamental spectroscopic and collisional information, LIF is also becoming of more practical importance, notably as a tool for the study of flames. It is one of a family of laser spectroscopic probes whose development has been the subject of a significant effort within the past few years (*7*).

By spectroscopic probes is meant those methods which provide concentrations and temperatures (population distributions over internal levels) of identifiable molecular species. Chief among these are spontaneous and coherent Raman scattering and LIF, all of which share a number of common attributes. Each has a high degree of spatial resolution, achievable by focussing the laser beam to a diameter of 100 μ or less and imaging the signal through a slit in front of the detector. This is necessary when probing a flame at atmospheric pressure, where the flame thickness, or region over which significant chemical conversion and hence steep concentration gradients occur, is often less than 1 mm. The use of pulsed lasers and single-shot data acquisition means a time resolution of 10 nsec, much faster than flow times or chemical activity can distort a given spatial region in a time-dependent system such as a turbulent flame or detonation. Importantly, the laser methods are non-intrusive; that is, they do not perturb the gas flow and/or chemistry such as can occur when a physical probe such as a thermocouple or sampling nozzle is inserted into the flame. Also, they can be used in environments too hostile (high temperature or corrosive atmospheres) to permit the insertion of such physical probes.

The information obtained from the laser methods are typically in the form of profiles of species concentrations and temperatures through the flame, which are then compared with models of the flame structure. LIF and the Raman methods complement one another well in providing a wide range of molecules which can be studied. The Raman scattering methods yield a relatively easily analyzed measure of the majority species present, that is, the fuel, oxidant, main exhaust gases, and, in an air flame, N_2. However, signal strength considerations limit typical detectivities to about 0.5–1 mole per cent, and the Raman methods generally cannot measure the transient species (often free radicals) present at low concentration. LIF has the needed sensitivity and can furnish a measurement of the concentration of these intermediates, crucial to an understanding of the chemistry of the combustion process. On the other hand, most of the closed-shell majority species cannot be made to fluoresce (due often to a predissociative nature of the lowest accessible excited state). Hence, both the Raman techniques and LIF are needed for a full characterization of the combustion process using laser spectroscopic methods.

As noted, LIF has high sensitivity. For example, under favorable conditions, OH in an atmospheric pressure flame can be detected at sub-part-per-billion concentration levels with 1 mm^{-1} spatial resolution and during a single 10 nsec laser shot, producing a signal level of ~100 photoelectrons. Averaging over a number of pulses, as one would typically do in the study of a flame in the laboratory,[6] would permit extending the sensitivity or tightening the spatial resolution.

Clearly, LIF is sensitive enough to detect transient species. For it to work, however, one must have suitably separated electronic states, the lower of which absorbs the laser light and the upper of which fluoresces. Serendipitously, many of the key intermediates in combustion chemistry can be made to fluoresce following laser excitation. In Table 1 are listed those molecules which have been observed using LIF in flow systems and/or in flames, and which arise as "natural"[7] intermediates in the combustion process. Of these, the OH molecule is by far the most popular for probing in flames via LIF, for several reasons. It is an ubiquitous and important reaction intermediate, so that its presence can serve to signify the occurrence of combustion, a sort of index of the degree of reaction. The spectroscopic data base is well established, and the necessary laser wavelengths are especially convenient for the experi-

[6] The single-shot figure of merit is directly applicable to probing a time-dependent flame, such as a turbulent one, where the data must be collected and analyzed on a shot-by-shot basis.

[7] Thus a number of species such as metal atoms and their oxides and halides, which can be detected with LIF but are usually obtained in flames by seeding, are not listed. Also excluded is a considerable number of large organic molecules such as benzene, acetone, benzyl radicals, etc.

mentalist. A complete picture of a combustion chemical network of course requires measurements on other species as well, comparing the profiles of different intermediates as they appear and disappear through the flame.

The high sensitivity of LIF arises because one creates with the laser a real electronically excited state, in contrast to the virtual states involved in the Raman scattering methods. Concomitant with this sensitivity is, however, the chief disadvantage of LIF as a combustion probe: because the excited state possesses a finite lifetime, it is subject to collision processes which affect both the magnitude and spectral form of the observed fluorescence signals (*8*).

The types of collisions can be separated into two categories. Energy transfer collisions move the excited molecule to different levels of the excited state and alter the fluorescence spectrum. This is readily apparent in Figures 5 and 10 for OH. If the energy transfer cross section is a function of the excited level, as we have seen to be the case for vibrational transfer in OH, the spectrum will be different for different pumped levels. This can easily be accounted for if cognizance of the effect is taken; but if unnoticed under typical operating conditions it can lead to, for example, significant (several hundred degrees) systematic errors in temperatures deduced from excitation scans (*9*).

Of more concern, and harder to account for, is the occurrence of quenching collisions which return the excited molecule to the ground state nonradiatively. The observed fluorescence signal is proportional to the excited state population N_e which can be related to the (desired) ground state population N_g through a simple steady state balance[8]

$$N_e = \frac{\alpha N_g}{A + Q} \qquad (3)$$

Hence, α is the excitation rate due to absorption of the laser photons, A is the radiative rate, and Q is the collisional quenching rate, all in sec^{-1} units. For OH, $A \sim 1.4 \times 10^6\ sec^{-1}$ while in typical flame gases at atmospheric pressure Q exceeds $10^9\ sec^{-1}$, so that only about one in a thousand excited OH molecules radiates. Thus an accurate determination of absolute values of N_g requires accurate values for Q—a tall order given the complexity, and variation with position, of the composition of flame gases. Several approaches are under development to attack this problem, as reviewed in reference (*8*); although more work remains to be done, the outlook appears promising, especially for measurements in laboratory flames where the collision environment can be characterized.

Even when one lacks information concerning the quenching rates, significant and important information can be obtained using even coarse estimates. This is illustrated with a very simple experiment involving the flame of CH_4 burning in N_2O, which has been under study in our laboratory.

The N—N bond strength in N_2O is 4.93 eV while the N—O bond strength is 1.68 eV. Therefore the obvious chemical mechanism would involve a splitting off of the oxygen atom and subsequent oxidation of the hydrocarbon with the N_2 an inert bystander, much as in a CH_4/air flame. The conventional emission spectrum of the CH_4/N_2O flame shows bands due to NH, NH_2, NO and CN (plus the omnipresent OH); all of these can be formed only through breakage of the N—N bond. However, because of the possibility of chemiluminescent excitation occurring within the flame, the existence of emission does not necessarily denote significant concentrations of these radicals in their chemically relevant ground states.

LIF, on the other hand, can provide the needed information. Excitation scans were made in the A-X system of the OH molecule near 3080 Å and the $A^3\Pi_i$-$X^3\Sigma^-$ system of the NH molecule near 3360 Å, with the laser directed into the flame near the most intensely luminous portion. There exists a near-total absence of information on quenching rate constants for the excited state of NH, so the ratio Q/A was simply estimated to be the same for both species. Using this guess, the experimental results yield a ratio [NH]/[OH] ~ 0.04 for the reaction zone of this flame. In a separate experiment, the OH concentration was shown to be present in a typically large amount, $\sim 7 \times 10^{15}\ cm^{-3}$. Thus the NH concentration is $\sim 3 \times 10^{14}\ cm^{-3}$, high enough to be of considerable chemical significance.

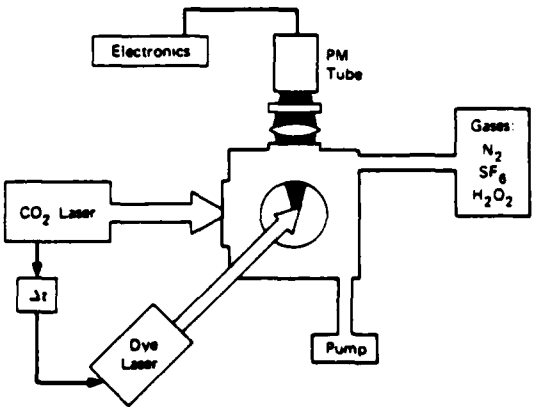

Figure 12. Schematic diagram of the apparatus used for isothermal laser pyrolysis with LIF detection. A mixture of N_2 as bath gas, SF_6 as absorber, and H_2O_2 as sample flows slowly through the cell. The pulsed CO_2 laser radiation is absorbed by the SF_6, rapidly heating the mixture and causing the H_2O_2 to decompose into OH radicals. These are detected via LIF, excited by a pulsed laser fired a time Δt after the CO_2 pulse.

Because of the need to estimate Q/A, these results are not accurate enough to provide any quantitative comparison with assumed mechanisms. They do, however, contain a crucial message: any model of the CH_4/N_2O flame chemistry which ignores breakage of the N—N bond is unwise. Thus the tone for the development of a mechanism is set by this simple, qualitative experiment. The next step would be to search for other species whose presence or absence in the flame answers important questions concerning that mechanism; for example, ideas about the chemistry involved have identified the NCO molecule as a possible species in this category, and this formed the impetus for the laser spectroscopic study of NCO illustrated in Figure 2.

A flame burns through a complex interplay of physical and chemical phenomena. The exoergic chemical reactions of combustion heat up the flame gases, further accelerating the rate of reaction; also considerable chain branching and sequences are involved. Transfer of mass and heat and the overall flow dynamics of the gases are intricately interwoven with the chemistry to produce the overall structure of a flame, and all of these processes must be taken together to produce a proper theoretical description. In fact, it has been suggested that a flame itself is a very poor candidate for study if one wishes to understand flame chemistry.

It would be satisfying to construct a model of the combustion chemical reaction mechanism based on rate constants determined in separate, independent experiments. This can be done to some degree using values obtained from flow system studies and shock tube results, but the temperature dependence of many reactions in the regions pertinent to flames remains lacking. We have recently carried out some preliminary measurements (*10*), combining the use of LIF with the method of isothermal laser pyrolysis (ILP). ILP, with detection using gas chromatography and mass spectroscopy, has been studied and applied at SRI within the past few years (*11*); the addition of LIF as a detection technique, should, we feel, provide a powerful tool for the measurement of rate constants and small chemical networks involving radical species.

A schematic diagram of the apparatus used is shown in Figure 12. A mixture of N_2 and SF_6 together with some sample

[8] In the limit of low laser power, that is, when no optical saturation effects are present.

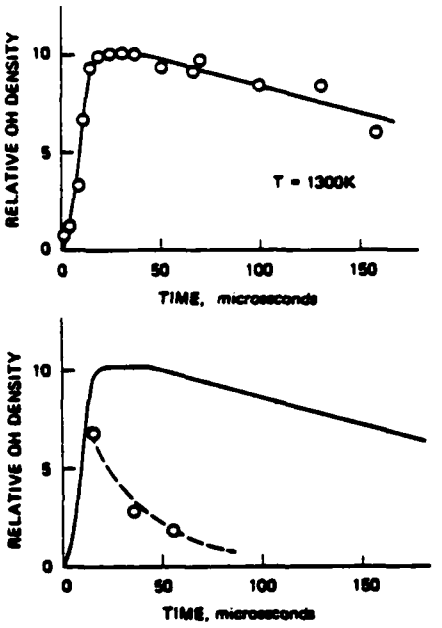

Figure 13. Results of ILP/LIF experiments, showing the OH density as a function of time after the CO_2 pulse. *a*, N_2, SF_6, and H_2O_2 in the cell. The rise is due to the decomposition of the H_2O_2, and the slow decrease at long times is because of cooling within the cell. The temperature is the ground state rotational temperature, measured using two different rotational lines at $t = 30$ μsec. *b*, CH_4 added to the mixture. The solid line represents the data in *a*, obtained with no CH_4. Here, the data points show that OH is removed by a reaction with the CH_4; from the time dependence can be obtained the reaction rate constant at 1300 K.

gas—H_2O_2, in these proof-of-principle experiments—slowly flows through a reaction cell. A pulsed CO_2 laser (~1 μsec pulse length) is fired into the mixture, and its energy is absorbed by the SF_6. Rapid transfer of the vibrational energy of the SF_6 into vibrational, rotational, and translational modes of the other gases heats the sample to some given temperature,[9] chosen by the amount of SF_6 used which dictates the amount of laser energy absorbed. In the case chosen here, the H_2O_2 pyrolyzes, falling apart into OH radicals. Following the CO_2 pulse, after a predetermined time delay which is set electronically, the dye laser is triggered and excites fluorescence in the OH.

The results of the experiment are shown in Figure 13a. The time delay is varied so that the temporal profile of the OH concentration can be followed. Here it rises as the H_2O_2 decomposes, remains steady at some plateau value, and finally falls off as the mixture begins to cool. A temperature of 1300 K in the plateau region is measured by tuning the laser to a different rotational line and obtaining a rotational temperature; obviously one could in this way follow the time dependence of the temperature as well.

In the next phase of the experiment, a little CH_4 is added to the flow. In Figure 13b, the solid line represents the same OH time-dependent concentration measured in the first experiment (i.e., in Fig. 13a). Now, however, the OH, after rising in the first 10 μsec, falls due to reaction with the CH_4, as shown by the points in Figure 13b. From these we may extract a rate constant for the OH + CH_4 reaction at 1300 K; the results are within ~20% of the best literature value at this temperature.

The preliminary experiments illustrated in Figure 13 were not carried out at a level of accuracy to warrant such a good level of agreement, but the numerical result does illustrate that the ILP/LIF method works well and holds high promise for the determination of high-temperature rate constants. The heating of the gases inside the cell avoids heterogeneous reactions sometimes encountered in wall-heated reactors; the use of a pulsed heating method can simplify situations where

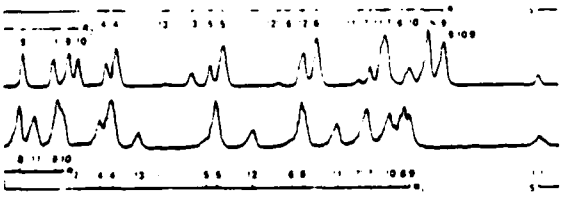

Figure 14. Excitation scans through the R-branch region of the (0,0) band of the A-X system of OH. The rotational branches are marked with the value of the ground state quantum number N''. *Top*, Single-photon excitation; *bottom*, two-photon excitation. The horizontal scale is absorbed energy (that is, $h\nu$ (single) and $2h\nu$ (double)). The differences in the spectra arise because the two types of excitation originate from opposite λ-doubling components of each rotational level of the ground $^2\Pi_i$ state.

subsequent reactions take place, if a real-time monitor such as LIF is employed. In addition to studying such bimolecular reactions such as the one described here, we plan to perform experiments in which radical species are not only reactants but also products, so that small chemical networks can be followed. With the large variety of species which can be detected with LIF (see Table 1) this should permit the detailed investigation of a large number of reactions important in combustion systems.

Two-Photon Excitation

All of the experiments described thus far involve fluorescence from the excited state following the absorption of a single laser photon. The advent of powerful commercially available dye lasers has made possible a number of non-linear experiments[10] such as two-photon excitation. Here in the excitation process the molecule absorbs two photons simultaneously, a process with a small absorption coefficient but enabled by the high photon densities available with focussed, pulsed lasers. Two-photon LIF provides us with new kinds of information and permits new diagnostic methods, as we shall now see.

The first experiment to be described (*12*) involves the now-familiar OH molecule. Instead of exciting with the frequency-doubled dye radiation in the ultraviolet, we now use the dye laser fundamental in the red. The electronic transition (the same $A^2\Sigma^+$-$X^2\Pi$, considered before) is allowed in both one and two-photon absorption because the OH has no inversion symmetry, and the detection is carried out using the single-photon fluorescence in the ultraviolet. The OH sample is produced for these experiments simply by operating in the hot burnt gas region of a CH_4/air flame—we now are using combustion to study laser spectroscopy rather than the other way around.

Compared to one-photon excitation, new selection rules are involved in a two-photon transition. The most immediately apparent difference is the occurrence of new rotational branches having $\Delta J = \pm 2$ in addition to $\Delta J = \pm 1, 0$. An interesting and useful result is due to differences in parity selection rules, as illustrated through Figure 14. This figure shows a two-photon excitation scan through the R-branch heads of the (0,0) band. Above it, on the same scale of total photon energy for comparison, is the single-photon excitation scan. The individual rotational transitions are marked; the number listed is the ground state value of N'', the angular momentum ignoring electron spin effects.[11] Note that the same rotational branches do not appear at the same energy in each scan. Further, the shift varies with N'': this can be seen for

[9] In actuality, there is first a sharp, superheating spike followed by a cooling wave, all occurring before the plateau region of Figure 13; see Reference (*11*) for details on the physics of the ILP process.

[10] We have already implicitly encountered these within the laser itself for the frequency doubling and shifting methods used.

[11] N'' is not a totally "good" quantum number but adequately identifies the lines in this transition.

example by comparing the relative positions of $R_1(5)$ and $R_1(13)$ from upper to lower trace.

The reason for this is as follows. The ground state for the transition is a $^2\Pi$ state, so that each level is actually a nearly degenerate pair termed a λ-doublet. One component of the doublet has positive parity, and the other negative, with respect to a reflection symmetry operation through the internuclear axis. The upper state is $^2\Sigma^+$, where only one parity is associated with each rotational level. A one-photon transition connects levels of opposite parity while a two-photon transition occurs between levels of the same parity. Therefore, for a particular rotational branch between two specific levels, the one-photon transition will originate from one component of the λ-doublet and the two-photon transition will originate from the other. The difference between corresponding rotational branches in Figure 14 then directly yields the λ-doublet splitting. This, as can be seen from the figure, increases with increasing value of N''. Reducing the data to the actual splitting values yields the results shown as dots in Figure 15. The solid lines are the predictions (not fits) from a theoretical study; obviously the theory of λ-doubling in OH is in good shape.

In addition to providing such fundamental information, two-photon excitation has promise from a practical viewpoint. One set of species which are important intermediates in combustion and plasmas are the atoms themselves such as H, C, N and O. These cannot be detected using single-photon LIF because their first absorption transitions lie far in the vacuum ultraviolet; even if there were lasers operating at the appropriate wavelengths, the atmosphere and flame gases are opaque in those regions. Two-photon excitation permits the use of accessible wavelengths which will propagate through the air and flames.

In our experiments on O and N atoms (*13*), the absorption of two photons with wavelengths near 2000 Å elevates each to the first excited state of the same symmetry as the ground state. This state then emits in the near infrared a photon which forms the detected signal. The details of the states and wavelengths are shown in Figure 16. These wavelengths are usable for diagnostic measurements, and similar schemes can be designed for H and C atoms.

The atoms are produced in a flow system using a microwave discharge in N_2 and He, which produces N atoms. When O atoms are desired, NO is added downstream from the discharge to form them in the reaction $N + NO \rightarrow O + N_2$. (This is a titration reaction detectable by its chemiluminescence, and can be used to measure [N] or [O]). The necessary laser radiation is produced by a string of non-linear processes. A Nd:YAG laser at 1.064 μ is frequency doubled to 5320 Å, where it is used to pump a dye in the red (for O) or yellow (for N). The dye laser radiation is frequency doubled to wavelengths in the 3000 Å vicinity. This ultraviolet radiation is then focussed into a cell containing ~10 atm of H_2. Here, stimulated Raman scattering occurs, producing intense radiation at the frequency $\omega_R = \omega_L - \omega_H$, where ω_L is the input frequency and ω_H the hydrogen vibrational frequency. The beams at ω_R and ω_L then, in the same cell, undergo a frequency mixing process producing a series of output wavelength at $\omega_L \pm n\omega_H$. With a prism, we choose the one corresponding to $n = 3$, at the wavelengths listed in Figure 16.

In order to assess the usefulness of two-photon excitation as a diagnostic, we must gain some information on the absorption coefficient and on the radiative and quenching rates of the upper state. We begin by considering relative transition probabilities for the several fine structure components of the $^3P - {}^3P$ transition in O, to compare with theoretical calculations. The ground state of O is split into three components; $^3P_2$ is the lowest while $^3P_1$ and $^3P_0$ lie at 158 and 226 cm^{-1} higher, respectively. The upper ^3P level is split by an amount of the order of the laser linewidth. Excitation scans across each of the three ground state components are shown in Figure 17. (Note that the sensitivity is different for each trace.) The expected positions of the upper state components accessible by the selection rules in each case is given by the stick diagrams. Although the upper state fine structure is not resolved, the relative breadths are in accord with expectations.

To obtain relative absorption coefficients from the integrated intensities of Figure 17, we need to know the populations of each level. This requires that the temperature in the flow cell be measured. For this purpose, we admit some excess NO and replace the infrared filter in front of the photomultiplier with an ultraviolet filter. Only a few Ångstroms from the O-atom two-photon wavelengths lies the single-photon absorption of the (0,0) band of the $A^2\Sigma^+$-$X^2\Pi$ system of NO. Excitation scans through this band quickly confirm that the system is at room temperature with the discharge either on or off. This then leads to the result of equal two-photon transition probabilities for each fine structure component, in agreement with theoretical expectations.

The radiative and quenching rates are determined by measurements of the upper state fluorescence decay as a

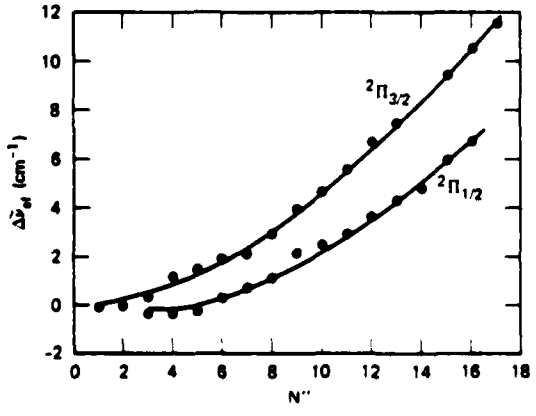

Figure 15. λ-doublet splitting as a function of N'' in the $X^2\Pi$, state of OH. *Points:* results from the data of Figures 14. *Line:* prediction from theoretical values of the splitting coefficients.

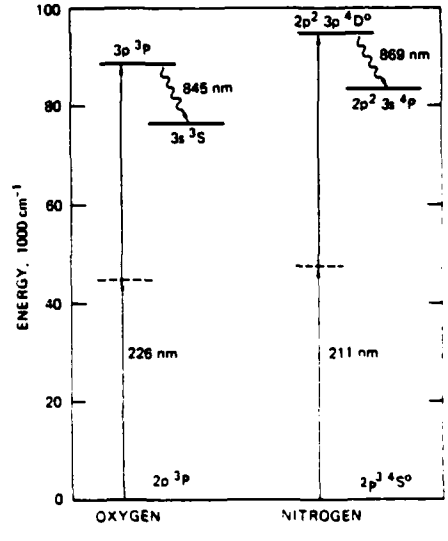

Figure 16. State designations and energies, excitation and detection wavelengths (in nm) for the two-photon LIF schemes in O and N. The excitation "lines" actually have three components for O and four for N, due to fine-structure splitting, but that does not show up on the scale of the diagram. [Reprinted from *Chemical Physics Letters*]

function of time. Figure 18 shows a short series of such runs for O. Here, a narrow gate on the gated detector is scanned from a time shortly before the laser fires till long after. Any given point in Figure 18 thus is an average over several laser pulses, although the simplest way to regard each decay is as an oscilloscope trace in real time of the fluorescence signal.

At early times the signal increases as the laser pulse, ~8 nsec long, pumps the excited state. The later decay of the fluorescence reflects the decay of the excited state population, which obeys a first-order rate law

$$N_e = N_e(t = 0) \exp(-kt) \tag{4}$$

where $k = A + Q = A + k_Q P$. k_Q is the rate constant for quenching and P the pressure. As can be seen from Figure 18, addition of N_2 to the cell (downstream from the discharge, so that the atom-production chemistry is not perturbed) causes a decrease in the excited state lifetime. A plot of k versus the pressure of added N_2 yields the radiative rate from the intercept and k_Q from the slope. In the case of the O and N atoms, we find that the values obtained portend well for the use of two-photon excitation as a diagnostic tool in flames, providing potential detectivities down toward the part-per-million level.

Concluding Remarks

It is hoped that these experiments have illustrated some of the kinds of interesting and useful information which can be obtained using laser-induced fluorescence. It is reemphasized that the selection of topics follows wholly the author's own interests and research; there have been many other LIF experiments performed in other laboratories and this paper is not meant to constitute a review of the field as a whole. Taken together, the efforts with and results from LIF experiments have greatly increased our knowledge of molecular structure and behavior, not only in quality and quantity but also in opening new levels of understanding. It is clear that this will continue in the future, especially with the extension of laser sources to cover even a greater range of wavelengths.

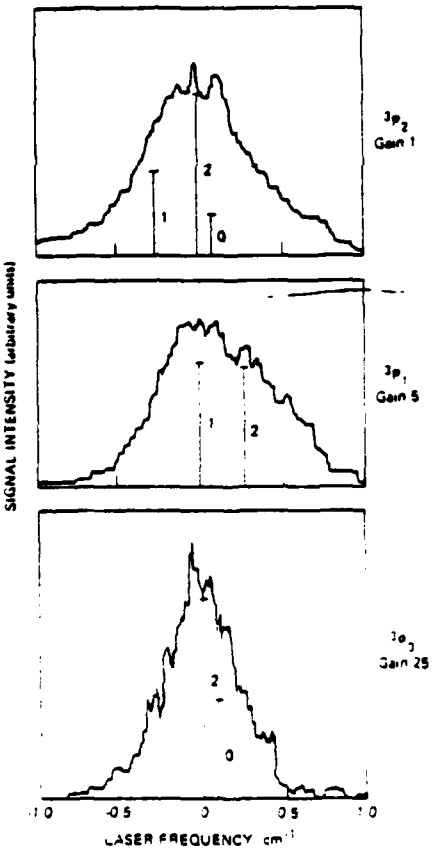

Figure 17. Excitation scans through each fine structure component in the O transition. The figures are denoted by the ^3P_J ground state level in each case; note that the gain varies. The upper state splitting is not resolved by the laser; the theoretically expected positions and relative intensities due to each is indicated by the stick diagrams, which are labelled by the upper state value of J. (The lower two scans have only two contributing upper state components each due to selection rules.) [Reprinted from *Chemical Physics Letters*]

Acknowledgment

The experiments described in this paper have been performed over several years and have involved a large number of colleagues. It is my pleasure to acknowledge John Allen, Bill Anderson, Bill Bischel, Rus Lengel, Keith Meyer, Bryce Perry, Greg Smith, and Brian Sullivan for their invaluable contributions to this research. I am also grateful for support for this research, which is currently provided by the U.S. Army Research Office, the National Science Foundation, the Department of Energy, and the Air Force Wright Aeronautical Laboratories.

Literature Cited

(1) Sullivan, B. J., Smith, G. P., and Crosley, D. R., *to be published.*
(2) Meyer, K. A. and Crosley, D. R., *Can. J. Phys.*, 51, 2119 (1973).
(3) Lengel, R. K. and Crosley, D. R., *J. Chem. Phys.*, 67, 2085 (1977).
(4) Anderson, W. R., Crosley, D. R., and Allen, Jr., J. E., *J. Chem. Phys.*, 71, 821 (1979).
(5) Meyer, K. A. and Crosley, D. R., *J. Chem. Phys.*, 58, 3153 (1973).
(6) Lengel, R. K. and Crosley, D. R., *J. Chem. Phys.*, 68, 5309 (1978).
(7) Crosley, D. R., (*Editor*), "Laser Probes for Combustion Chemistry," *Amer. Chem. Soc. Symposium Series*, Vol. 134 (1980).
(8) Crosley, D. R., *Opt. Engr.*, 20, 511 (1981).
(9) Crosley, D. R. and Smith, G. P., *Combust. Flame*, 44, 27 (1982).
(10) Smith, G. P. and Crosley, D. R., *to be published.*
(11) McMillen, D. F., Lewis, K. E., Smith, G. P., and Golden, D. M., *J. Phys. Chem.*, 86, 709 (1982).
(12) Crosley, D. R., Smith, G. P., and Bischel, W. K., *to be published.*
(13) Bischel, W. K., Perry, B. E., and Crosley, D. R., *Chem. Phys. Lett.*, 82, 85 (1981).

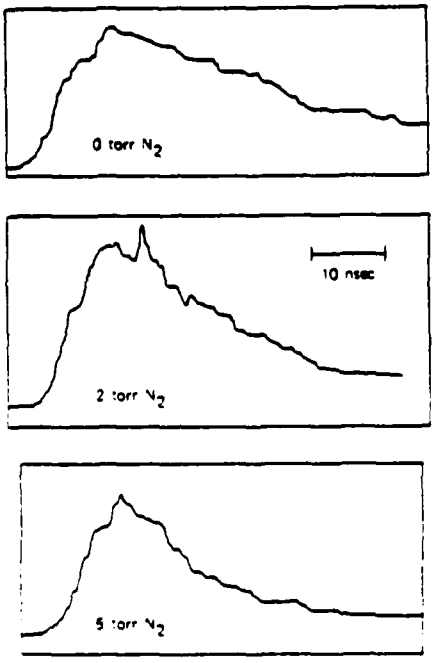

Figure 18. Lifetime scans for the $3p\ ^3P$ state of oxygen. The laser pumps the excited state but shuts off after ~8 nsec, leaving the excited state to fluoresce at its characteristic decay rate. The top scan is in the absence of added gas, and the middle and bottom scans are with 2 and 5 torr of N_2 added, respectively. From these data are obtained the radiative lifetime of the state and cross section for its collisional quenching by N_2.

LIFETIMES IN THE B $^2\Pi_i$ STATE AND THE HEAT OF FORMATION OF NCO

Brian J. SULLIVAN *, Gregory P. SMITH and David R. CROSLEY
Molecular Physics Laboratory, SRI International, Menlo Park, California 94025, USA

Received 22 December 1982; in final form 31 January 1983

Using laser-induced fluorescence in a low-pressure flow system, the lifetimes of the 00^10 and 10^10 vibrational levels of the B $^2\Pi_i$ state of NCO have been measured. The results, 63 and ≤10 ns respectively, indicate that the dissociation limit to N(^{2}D) + CO lies between these levels. This corresponds to a dissociation energy $D_0^0 \leq 1.68$ eV and an enthalpy of formation $\Delta H^0_{f,298} \geq 48$ kcal/mole for NCO, and $\Delta H^0_{f,298}$ (HNCO) ≥ −14 kcal/mole.

1. Introduction

The NCO free radical has been proposed as a possible intermediate in the oxidation of HCN and in the production of NO in the combustion of nitrogen-containing fuels [1], and also in the C_2N_2/O_2 flame [2]. It has been detected by laser-induced fluorescence as a product of the CN + O_2 reaction [3] and, in copious quantity, in the reaction zone of a CH_4/N_2O flame [4]. Consequently, values of its thermochemical parameters are of interest for incorporating NCO into reaction schemes for such systems. The value of the heat of formation, $\Delta H^0_{f,298}$, generally used is 34 ± 3 kcal/mole from Okabe's study [5] of photodissociation thresholds in HNCO.

As part of a laser spectroscopic study of the $A\,^2\Sigma^+$–$X\,^2\Pi_i$ and $B\,^2\Pi_i$–$X\,^2\Pi_i$ systems of NCO [6], we have made measurements of radiative lifetimes in the B state. These differ sharply between the 00^10 and 10^10 vibrational levels, indicating a significantly lower dissociation limit and higher ΔH^0_f than given by Okabe.

2. Experimental details and results

The NCO was produced by the gas-phase reaction F + HNCO and/or HOCN. The acid vapor was formed in a small reaction vessel containing KOCN and stearic acid at ≈80°C, picked up in a He carrier and injected into a glass flow system of moderate pumping speed. The fluorine atoms were created by a microwave discharge in CF_4 in ≈1 Torr He. The exciting radiation was provided by a frequency-doubled Nd : YAG-pumped dye laser, with bandwidth ≈0.3 cm^{-1} and pulse length ≈8 ns in the ultraviolet. The fluorescence emitted at right angles to the laser beam was focused onto the slit of a 0.35 m monochromator; for the lifetime measurements, a resolution of 40 Å was used. The signal from the photomultiplier was processed with a scannable boxcar integrator and strip chart recorder.

Excitations from the 00^10 level of $X\,^2\Pi_i$ to the 00^10 and 10^10 vibrational levels of the $B\,^2\Pi_i$ state were identified from Dixon's absorption spectra of the B–X system [7]. In the case of the 00^10 level, the R_1 and R_2 bandheads near 315 nm were easily discerned in excitation scans but the other weak rotational lines exhibited no obvious pattern, in accord with Dixon's conclusion that the level is perturbed. For the 10^10 level, excited near 305 nm, the rotational pattern of P_1, P_2, R_1 and R_2 lines could be readily assigned following Dixon's analysis. Other lines visible in Dixon's spectrogram but unassigned by him could also be seen in our excitation scans. Fluorescence scans for each level exhibit long progressions in the ground-state stretching frequencies as well as weaker transitions to Π components of even-num-

* Present address: IBM Research Laboratory, San Jose, California 95193, USA.

0 009-2614/83/0000–0000/$ 03.00

bered bending vibrational levels. (These weaker transitions show intensity differences depending on which spin component, $^2\Pi_{1/2}$ or $^2\Pi_{3/2}$, of the B state is excited; the analysis of this is still in progress [6].) For the lifetime measurements, strong bands of the B–X emission were chosen from the fluorescence scans; these were $00^10 \rightarrow 10^10$ at 328 nm and $10^10 \rightarrow 00^11$ at 326 nm.

Several measurements were made of the decay lifetime of the 00^10 level, both in the presence and absence of added collision partners. The zero-pressure result is 63 ± 3 ns, independent of fine-structure component. It is shorter than the values of ≈400 ns we measured for several vibrational levels of the A state [6], which are in good agreement with the A-state results of Reisler et al. [3] but ≈15% longer than the recent measurements of Charlton et al. [8].

In the case of the 10^10 level, the time dependence of the fluorescence decay is identical to that of the laser pulse itself, ≈17 ns when stretched by the photomultiplier and electronics. This was determined by tuning the laser off the absorption line and setting the spectrometer to detect scattered laser light (the signal at 326 nm vanished when the laser was tuned off the line). The pressure was reduced to the lowest value (≈110 mTorr) at which a signal could be observed, with no change in the decay shape. We conclude that the lifetime of 10^10 is <10 ns, considerably shorter than that of 00^10.

The overall fluorescence intensity of the 10^10 level was measured to be ≈0.1 of that from 00^10, whereas Dixon found the absorptions to each level to be approximately equal. These results indicate that a dissociation limit of NCO lies somewhere between the 00^10 and 10^10 levels of B $^2\Pi_i$, with the latter level decaying mainly through the non-radiative route. Attempts were also made to excite the 20^10 level, but no fluorescence was observed.

3. Discussion

Fig. 1 shows the term values for NCO. The first dissociation limit is to N(^{4}S) + CO($^1\Sigma^+$), which lies well below the energies involved in the present experiment. This limit correlates with a $^4\Sigma^-$ state so that predissociation to it is spin-forbidden. Although doublet–quartet predissociation has been observed in other

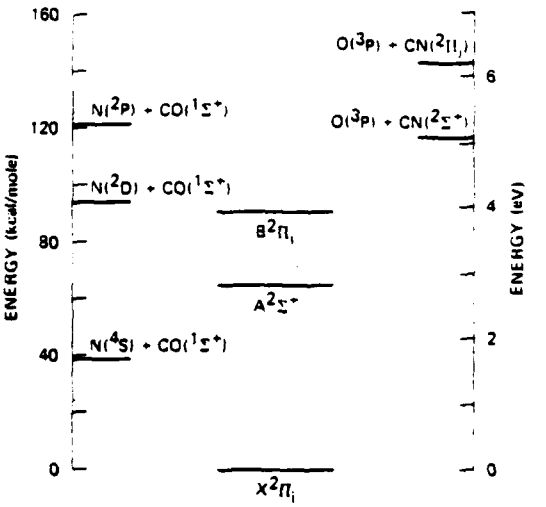

Fig. 1. Term diagram for the electronic states and dissociation limits of the NCO molecule. Only the X, A and B states of NCO have been spectroscopically identified.

molecules, such mixing would not only have to be strong but also vary sharply in strength between the two vibrational levels in question in order to explain the lifetime differences. A mechanism by which that might occur is a large difference in Franck–Condon overlap between the $^4\Sigma^-$ state and each of the 00^10 and 10^10 vibrational levels. This seems unlikely in that the B state lies high above the bottom of the repulsive $^4\Sigma^-$ potential, so that the latter's wavefunctions do not vary much in form with energy; it would require that the $^4\Sigma^-$ curve cut that of the ν_1(B) stretch close to the 10^10 level. The observed diffuseness in the 00^11 band of the B–X system [7] would require a similar coincidence in the ν_3 stretch surface.

We conclude that the dissociation observed here is to N(^{2}D) + CO($^1\Sigma^+$), lying 19230 cm^{-1} above the first, spin-forbidden, limit. Dixon [7] assigns the molecular predissociating state correlating to this limit as $^2\Sigma^-$ in character. This limit lies ≤32820 cm^{-1} above 00^10 of X $^2\Pi_i$, and the dissociation limit D_0^0 to ground-state nitrogen atoms then has an upper limit of 1.68 eV. The heat of formation of NCO at room temperature may then be determined from

$$\Delta H^0_{f,298}(\mathrm{NCO}) = -D_0^0 + \Delta H^0_{f,298}(\mathrm{N}) + \Delta H^0_{f,298}(\mathrm{CO}). \quad (1)$$

The value obtained is $\Delta H^0_{f,298}(NCO) \geq 47.8$ kcal/mole; the value at 0 K, $\Delta H^0_{f,0}$, is <0.1 kcal lower [9].

These values are based on the reasonable assignment of the non-radiative process to a spin-allowed predissociation. However, the inability to assign the rotational lines in the 00^10–00^10 transition and the observed irregularities in the $B\,^2\Pi_i$ fine structure splitting make it clear that the state is perturbed [7]. We must thus also consider this perturbation as a possible cause of the lifetime variation. That the vibrational levels in question are correctly identified is indicated by the B–X absorption spectrum observed in matrix isolation spectroscopy [10]. Mixing could occur with the $X\,^2\Pi_i$ state, the $A\,^2\Sigma^+$ state, or any bound levels of the $^2\Sigma^-$ state correlating with the limit. However, the level density of none of these states increases by the factor of six or more over this 1000 cm^{-1} interval, as would be necessary to account for the observed fluorescence lifetime variation. The A state has a shorter overall N–O distance and slightly steeper potentials [7,11] so it is unlikely that the vibrational overlap with B will be significantly greater for 10^10 than 00^10. (In fact, no A–X fluorescence was observed upon excitation of the B state.) In the $A\,^2\Sigma^+$ state, a much shorter 10^00 lifetime in a matrix laser-induced fluorescence study [12] was attributed to Fermi resonance with 02^00 but effects of a similar magnitude do not occur in the gas phase [6,8]. (The A-state lifetimes in the matrix are less than half of those in the gas phase, suggesting environmental effects in general.) The similarities in the fluorescence spectra for both 10^10 and 00^10 levels [6] suggest that mixing with other electronic or vibrational levels is not occurring to an appreciable degree.

Dixon [7] observed diffuse features above 33700 cm^{-1} in absorption, which he attributed to dissociation to $N(^2D) + CO(^1\Sigma^+)$, corresponding to $D^0_0 \leq 1.8$ eV. He noted, however, that the diffuseness might be unresolved groups of lines. The present results imply that the interpretation in terms of dissociation is correct.

Okabe's values [5] were obtained by measuring the photodissociation thresholds for HNCO to CO + $NH(c\,^1\Pi)$, and $H + NCO(A\,^2\Sigma^+)$. (These results form the basis of the current JANAF values [9].) The heat of formation of HNCO was first determined from

$$\Delta H^0_{f,298}(HNCO) = -D^0_0(NH–CO) + \Delta H^0_{f,298}(NH) + \Delta H^0_{f,298}(CO)\,, \quad (2)$$

with D^0_0 related to the measured threshold of $c\,^1\Pi$ emission by the $c\,^1\Pi$–$X\,^3\Sigma^-$ energy difference in NH. Using recent values for $\Delta H^0_{f,298}(NH)$ [13] and the $a\,^1\Delta$–$X\,^3\Sigma^-$ energy difference [14], Okabe's measurements yield $\Delta H^0_{f,298}(HNCO) \geq -22.1$ kcal/mole. The value of the heat of formation of NCO was then obtained from the threshold for $A\,^2\Sigma^+$ emission by

$$\Delta H^0_{f,298}(HNCO) + D^0_0(H–NCO) = \Delta H^0_{f,298}(H) + \Delta H^0_{f,298}(NCO)\,. \quad (3)$$

Okabe's value is $\Delta H^0_{f,298}(NCO) \geq 39$ kcal/mole, using $\Delta H^0_{f,298}(HNCO) = -22.1$ kcal/mole. Okabe's result corresponds to a dissociation limit for NCO $D^0_0 \leq 2.14$ eV, and he concluded that Dixon's apparent diffuseness was due to unresolved lines.

Our results for $\Delta H^0_{f,298}(NCO)$ can be combined with Okabe's H–NCO dissociation threshold measurement to obtain a new value for the heat of formation of HNCO, using eq. (3). This leads to $\Delta H^0_{f,298}(HNCO) \geq -14.3$ kcal/mole. It is considerably higher than that obtained by Okabe using the NH–CO threshold and eq. (2). Consistency demands that Okabe's value for the H–NCO threshold is too low, or that for the NH–CO threshold is too high, by 0.34 eV. Examination of the figure in his paper indicates the first possibility is ruled out, but the second is possible as the lower threshold would be at 1472 Å in a region of very low HNCO absorption. (A threshold at 1472 Å is the one consistent with $\Delta H^0_{f,298} = -14.3$ kcal/mole.)

The dissociation limit for NCO to O + CN can also be calculated from our values. The heat of formation of CN is subject to some uncertainty [15]. Adopting a value $\Delta H^0_{f,298}(CN) = 103.7$ kcal/mole, the dissociation limit for NCO to $O(^3P) + CN(^2\Sigma^+)$ is 0.92 eV higher than the limit to $N(^2D) + CO(^1\Sigma^+)$ seen here. Thus the present results are consistent with Milligan and Jacox's failure to observe CN upon irradiation of NCO in a matrix with the 2537 Å Hg line [10], which lies 0.82 eV above our $N(^2D)$ + CO limit.

4. Summary

Lifetime measurements in the $B\,^2\Pi_i$ state of NCO suggest that the dissociation limit lies at or below the 10^10 vibrational level of this state. This leads to the following results: $D_0^0(\mathrm{NCO}) \geq 1.68$ eV; $\Delta H^0_{f,298}(\mathrm{NCO}) \geq 47.8$ kcal/mole ($\Delta H^0_{f,0}(\mathrm{NCO}) \geq 47.7$ kcal/mole); $\Delta H^0_{f,298}(\mathrm{HNCO}) \geq -14.3$ kcal/mole ($\Delta H^0_{f,0}(\mathrm{HNCO}) \geq -13.8$ kcal/mole).

Acknowledgement

This work was supported by the US Army Research Office.

References

[1] B.S. Haynes, D. Iverach and N.Y. Kirov, 15th Symposium (International) on Combustion (1975) pp. 1103; C.P. Fenimore, Combustion Flame 26 (1976) 249; C. Morely, Combustion Flame 27 (1976) 189.

[2] J.N. Mulvihill and L.F. Phillips, 15th Symposium (International) on Combustion (1975) pp. 113.

[3] H. Reisler, M. Mangir and C. Wittig, Chem. Phys. 47 (1980) 49.

[4] W.R. Anderson, J.A. Vanderhoff, A.J. Kotlar, M.A. DeWilde and R.A. Beyer, J. Chem. Phys. 77 (1982) 1677.

[5] H. Okabe, J. Chem. Phys. 53 (1970) 3507.

[6] B.J. Sullivan, G.P. Smith and D.R. Crosley, to be published.

[7] R.N. Dixon, Can. J. Phys. 38 (1960) 10.

[8] T.R. Charlton, T. Okamura and B.A. Thrush, Chem. Phys. Letters 89 (1982) 98.

[9] D.R. Stull, ed., JANAF Thermochemical Tables (Dow Chemical, Midland, MI, 1974) addenda.

[10] D.E. Milligan and M.E. Jacox, J. Chem. Phys. 47 (1967) 5157.

[11] R.N. Dixon, Phil. Trans. Roy. Soc. (London) A252 (1960) 165.

[12] V.E. Bondybey and J.H. English, J. Chem. Phys. 67 (1977) 2868.

[13] L. Piper, J. Chem. Phys. 70 (1979) 3417.

[14] J. Masanet, A. Gilles and C. Vermeil, J. Photochem. 3 (1974/75) 417.

[15] K.P. Huber and G. Herzberg, Constants of diatomic molecules (Van Nostrand, Princeton, 1979).

Collisional quenching of $A\,^2\Sigma^+$ OH at elevated temperatures

Paul W. Fairchild, Gregory P. Smith, and David R. Crosley

Molecular Physics Laboratory, SRI International, Menlo Park, California 94025
(Received 11 April 1983; accepted 10 May 1983)

Thermally averaged cross sections σ_Q for collisional quenching of the $A\,^2\Sigma^+$ state of the OH molecule have been measured near 1100 K. The OH was produced and detected in a laser pyrolysis/laser fluorescence experiment, in which a mixture of SF_6, H_2O_2, and the collision partner M was heated by a pulsed CO_2 laser. Thermal decomposition of the peroxide produces OH which is then excited by a tunable laser; the real-time decay of the fluorescence signal at different pressures of M furnishes σ_Q. These σ_Q at elevated temperatures are generally less than the room temperature values. This result, the size of σ_Q, and its variation with M suggest the importance of attractive forces in the collisional quenching. The experimental results have been compared with a theoretical calculation of σ_Q based on multipole attractive forces with a repulsive centrifugal barrier. Good correlation is obtained for eight of the 11 quenchers studied; the experimental values of σ_Q for N_2 and SF_6 are conspicuously low.

I. INTRODUCTION

Quenching collisions are those in which an electronically excited molecule A* is deactivated to the ground state by interaction with some partner M. Recent experiments, and particularly theoretical correlations, show strong indications that attractive interactions between A* and M play a major role in the collisional quenching process. This is suggested first by the sizes of quenching cross sections σ_Q, which are typically as large as gas kinetic values. More detailed theoretical comparisons form further support. Parmenter and coworkers[1] considered an A*–M intermediate collision pair in equilibrium with the separated species. A calculation of its concentration from partition functions led to a linear relationship between $\ln\sigma_Q$ and ϵ_{A^*M}/kT, where ϵ_{A^*M} is the depth of the attractive well in the A*–M interaction. Taking $\epsilon_{A^*M} \propto \sqrt{\epsilon_{MM}}$ for a given excited species A* furnished a correlation of σ_Q for a series of collision partners. This was successful for a number of different excited species and collisional processes. Lee and co-workers[2] have examined their SO_2 quenching data for a large series of M using a σ_Q calculated as the sum of cross sections for a series of attractive multipole interactions—dipole–dipole, dipole–quadrupole, dispersion, etc.—and a repulsive centrifugal barrier. Multipole moments were taken from the literature or estimated. Very good agreement between experimental and calculated values was achieved.

In the case of the $A\,^2\Sigma^+$ state of the OH molecule, the size of previously measured room temperature σ_Q values also suggests the role of attractive forces in quenching. Several aspects of vibrational energy transfer ($v' = 1 \rightarrow 0$ and $v' = 2 \rightarrow 1, 0$) in this state, for the collision partners H_2, D_2, and N_2, are also strongly indicative of attractive interactions.[3]

We have performed measurements of σ_Q for the $v' = 0$ level of $A\,^2\Sigma^+$ OH for a series of 11 collision partners at elevated temperatures. The measurements were made in a laser pyrolysis/laser fluorescence (LP/LF) system,[4] in which a CO_2 laser pulse absorbed by SF_6 rapidly heats a sample containing H_2O_2 and the chosen M. The peroxide pyrolyzes to OH which is detected by laser-induced fluorescence (LIF); σ_Q is determined by direct decay time measurements at different pressures of M. The objective of the experiments was to provide two kinds of information bearing on the role of attractive forces. First are the measurements for the series of partners and a correlation with pertinent molecular parameters. The second is a comparison with room temperature σ_Q values. If governed by attractive interactions, σ_Q should decrease with increasing temperature; this is so basically because the A*–M complex can more rapidly dissociate to the original A* and M before remaining captured long enough to deexcite the A*.

The results show σ_Q values mostly lower than those at 300 K (where comparisons exist) and a general ordering with type of M indicating the role of attractive forces in many cases (though the σ_Q's for N_2 and SF_6 are conspiciously small). In order to examine the results more quantitatively, we have reformulated the approach taken by Lee and coworkers. Instead of summing analytically obtained cross sections for each segment of the potential independently, we numerically calculate the single full potential and a resulting σ_Q as a function of energy, which is then thermally averaged. A reasonable correlation between experiment and calculation is obtained for 8 of the 11 M investigated.

In addition to some insight into fundamental characteristics of energy exchange, the present results furnish some applications to the areas of LIF diagnostics of the important OH radical. These fields are atmospheric monitoring and, especially, combustion, where the OH exists at elevated temperatures and in a complex collisional environment.[5] Values of σ_Q are needed to relate the observed LIF signal to the desired ground-state OH concentration, i.e., to obtain the fluorescence quantum yield. Generally, quenching rate constants k_Q in flames have been taken simply as proportional to $T^{1/2}$ through the relationship $k_Q = \bar{v}\sigma_Q$, where $\bar{v}$ is the mean velocity and σ_Q is assumed to be constant with temperature. The decrease in σ_Q at elevated temperatures found here, as well as the correlation with collision partner M, have important implications for LIF diagnostics experiments.

 0021-9606/83/161795-13$02.10

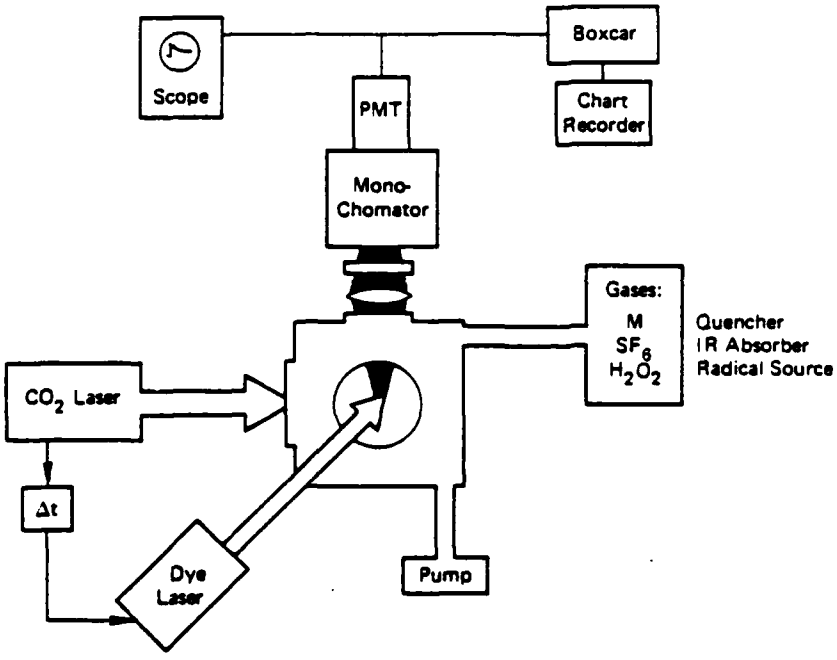

FIG. 1. Schematic diagram of the laser pyrolysis/laser fluorescence apparatus.

II. LASER PYROLYSIS/LASER FLUORESCENCE

A. Description

The LP/LF method has been described in detail.[6] Those aspects of the technique relevant to the present quenching measurements are discussed here.

The LP/LF method involves irradiating a gas mixture containing an infrared absorber (SF_6), radical precursor (H_2O_2/H_2O), and some quenching molecule (M) with a pulsed (~1 μs) CO_2 laser. The SF_6 absorbs the infrared laser radiation. Collisions during and shortly after the CO_2 laser pulse transfer this energy to the surrounding gas, and thermal decomposition of the H_2O_2 to OH begins. Experiments described later illustrate that for our conditions complete thermalization occurs within a few microseconds. The heated cyclindrical volume, now at a higher pressure, will expand and cool. A compression wave travels outward through the cool surrounding gas, slightly heating and compressing it. Simultaneously, an expansion wave propagates first inward to the center and then outward again, producing a two-stage cooling of the initially heated region. At this point the expansion of the heated region ceases, the temperature and density remain constant, and the pressure across the interface between hot and cool regions is equal (at roughly the initial value). A further slow cooling due to thermal conductivity occurs, but it is small on the < 100 μs time scales of these experiments. It is this steady temperature and density region which is suitable for bimolecular quenching or reaction measurements.

Thermal decomposition of H_2O_2 has a high activation energy and thus OH will only be produced during the initial hottest period, before the expansion cooling (from 1400 to 1200 K in a typical experiment). The temperature is controlled by the CO_2 laser fluence and SF_6 pressure. Care must be taken, however, to avoid an optically thick cell that may produce axial temperature inhomogeneities.

At a fixed time delay following the CO_2 laser pulse, a pulsed dye laser, tuned to an absorption line of the OH $A\,^2\Sigma^+ - X\,^2\Pi_i$ (0, 0) transition, is fired. The amount of detected fluorescence is proportional to the number density of OH in the absorbing rotational level. The rotational temperature is deduced by measuring the relative population distribution of several rotational levels of $v'' = 0$ using LIF.

A wide range of temperatures is accessible with LP LF. We have observed OH fluorescence for post-expansion temperatures as low as 750 K and as high as 1500 K. Measurements at lower temperatures are difficult to attain since not enough OH is produced by H_2O_2 decomposition to yield a measurable signal. Higher temperatures are possible by increasing the CO_2 laser fluence or adding more SF_6, although the latter method is limited since increased absorption is offset by an increased total heat capacity. Another kinetic and temperature limiting complication occurs at the higher temperatures ($T_{\text{initial}} \gtrsim 1750$ K), when thermal decomposition of the SF_6 begins. Complete SF_6 decomposition occurs for initial temperatures above 2000 K. SiF_4 is not a suitable substitute infrared absorber in these experiments due to SiF_4 hydrolysis that will take place with the H_2O_2 and water present.

B. Experimental details

The apparatus is illustrated in Fig. 1. It consists of a 10 cm diameter cylindrical aluminum gas cell fitted

with KCl windows for transmission of the infrared radiation, and perpendicular suprasil windows for transmission of the dye laser radiation and ultraviolet fluorescence. Gas flows through the cell were regulated by Matheson flow meters and measured with Hastings mass flow meters. In all of the decay measurements except those with added N_2, SF_6 made up the largest percentage of gas flowing through the cell ($\gtrsim 90\%$). For the decay measurements with N_2, SF_6 was only ~50% at the higher N_2 pressures used. Before entering the cell the gases flowed through a bubbler containing a solution of ~80% H_2O_2 in H_2O at 0 °C. This produced a vapor phase of approximately 1/3 H_2O_2 and 2/3 H_2O, which were present as background quenchers in all of the experiments. All quenching gases but water were directly added through flowmeters; for the water quenching measurements, a separate flow of H_2O vapor entrained in SF_6 was used.

The TEA CO_2 laser (Lumonics K-921 with curved 5 m radius rear reflector and 50% reflecting output coupler) used to heat the gas mixture provides a fluence of 1 J/cm^2 in pulses of ~1 μs duration, at 10.6 μm, every 1.6 s. The beam is apertured; its central 1.0 cm diameter area passes through the cell along a 1.0 cm path length and is reflected back through nearly the same volume to insure uniform heating along the axis. This permits up to 50% of the CO_2 laser energy to be absorbed while minimizing temperature inhomogeneities associated with optical thickness. The resulting spread in temperature across the probed volume is $\lesssim 30$ K, less than the error in the measured temperature.

The frequency doubled output of a Quantel 10 Hz Nd: YAG pumped dye laser generates 8 ns ultraviolet pulses of ~1 mJ in energy with a 0.2 cm^{-1} bandwidth, and is used to excite various rotational lines of the 0–0 band of the OH A–X transition at ~308 nm. The UV beam diameter, and thus the spatial resolution, was 2 mm. Fluorescence along a 2 mm path of the dye laser beam was focused (1:1) through a monochromator (set at $\lambda = 309$ nm, $\Delta\lambda = 2$ nm) onto a photomultiplier tube (EMI 9558QA). Both the dye and CO_2 laser power levels were monitored and recorded continually on a strip chart recorder. For the quenching measurements, the time delay between the CO_2 laser and dye laser was set at 32 μs.

The output of the PMT was processed by a boxcar integrator, triggered at the repetition rate of the CO_2 laser, to record excitation scans for the temperature determinations. The fluorescence decay traces were displayed in real time on an oscilloscope. Scope photographs were manually digitized with a Houston Instruments "HI PAD" interfaced to a PDP-11/40 computer.

C. Diagnostics

Once the gas has been heated, a series of gas dynamic processes begin. We have carried out both experimental and computational studies to characterize the spatial and temporal behavior of the temperature and density in the cell. For a typical condition of 3:1 N_2 and SF_6 heated initially to 1300 K, calculations indicate the center of the cell stays at 1300 K for ~10 μs, at which point the expansion wave (Mach 1.0) drops the temperature to ~1000 K. At the same time the compression wave travels outward at roughly Mach 1.6. Since the speed of sound is faster in the heated region, the expansion wave, after reflecting at the center of the cell, will eventually nearly catch up with the compression wave. For the conditions mentioned this will occur after ~25 μs, in the large volume beyond the heated region. By this time the pressures on either side of the heated boundary have equalized and the expansion is completed.

The symmetry in our experiment is cylindrical, dictated by the apertured CO_2 laser beam shape, and a full quantitative description of the heating/cooling process and pressure waves must incorporate this geometry. To help us understand the dynamics that are occuring in the cell we have made use of the PUFF code available at SRI.[6] This is a general program for the calculation of stress waves for a variety of media, geometries, and initiation mechanisms. The code results are used to determine the density after the expansion has occured.

In the earlier study,[4] we measured time histories of rotational temperatures and total OH fluorescence signals at various points in the cell, so as to verify the behavior predicted by the PUFF code. In those experiments, however, the OH signals were integrated over decay time; they thus reflected simultaneous changes in both OH density and the quenching rate which occurred as a result of the gas dynamic processes. Here the OH LIF signal was measured with a narrow boxcar gate, set shortly after the dye laser pulse before quenching appreciably reduces the signal. That is, we measured

$$\int_{t_1}^{t_2} N dt = \int_{t_1}^{t_2} N_0 \exp[-t/(A+Q)]dt\,,$$

where N_0 is the initial excited state number density, and A and Q are the Einstein emission coefficient and quench rate, respectively. For t_1 near zero and $t_2 - t_1 \ll (A+Q)^{-1}$, the signal yields N_0 which is in turn proportional to the ground state OH number density.

Figure 2 shows a plot of this signal as a function of the time delay between the two lasers. The position of the dye laser beam is the center of the heated volume, where according to the code, the most extreme variations of density occur. The gas mixture is 25% SF_6 in N_2, at a total pressure of 50 Torr. Here, $t_1 = 20$ ns, $t_2 = 30$ ns, and $(A+Q)^{-1} \geq 253$ ns. An excitation spectrum gives an initial, maximum temperature (at 12 μs delay) of 1375 ± 50 K.

The rise in the fluorescence signal reflects the production of OH from the thermal decomposition of H_2O_2. The rise is linear with a short, 2 μs induction time. Thus the rate constant for the decomposition $H_2O_2 + M \rightarrow 2OH + M$ does not vary with time. This indicates in turn that the temperature is constant during this period, i.e., the energy transfer is fast. We are thus assured that thermalization has occured at the longer delay times at which the bimolecular quenching measurements were made.

These results indicate also that thermalization is rapid in an alternate version of the laser pyrolysis method used for unimolecular reaction rate measurements.[7]

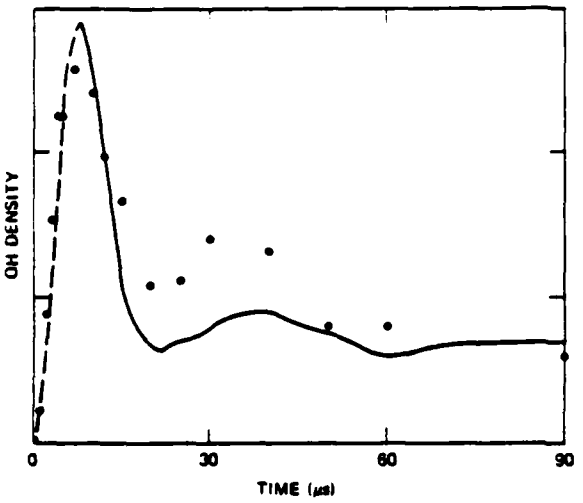

FIG. 2. Narrow gate experiment measuring the density of OH as a function of time after the CO_2 heating pulse, at the center of the pyrolysis cell. Points: Experimental results. Solid line: Predictions from computer calculation. Dashed line: Pyrolysis rate of H_2O_2 at the initial temperature.

as was already indicated by the temperature dependence of competing reactions in those experiments.

The solid line in Fig. 2 shows the density profile predicted by the code at the center of the cell. The results follow the decline and predict the final value (> 50 μs) quite well. An oscillation due to overcooling at 20–40 μs is also seen, although the measured drop is not as great as that computed by the code. Part of the discrepancy is because the experiment averages over the central 20% of the cell. This oscillatory effect is most severe at the center of the cell, where the role of acoustic waves tend to be amplified. Thus, once the main expansion wave has proceeded outward into the cold gas, a continued series of weak waves can continue to perturb the density at the center of the cell.[4]

Halfway between the cell center and the expanded edge of the heated region, the code predicts an absence of such density oscillations and fluctuations, and no initial overcooling. The previous LIF measurements[4] confirm this behavior. This is the position used for the quenching measurements.

III. EXPERIMENTAL RESULTS

A. Decay and density measurements

Both H_2O and H_2O_2 are present in small amounts as background quenchers during all decay measurements, and the concentration and composition of the H_2O/H_2O_2 mixture varied from day to day. This can be attributed to varying flow conditions through the bubbler, where the carrier gas picks up differing amounts of the H_2O/H_2O_2 vapor. In addition, changing flow conditions of the room temperature carrier gas may alter the temperature of the H_2O/H_2O_2 sample slightly from 0 °C thereby changing both the vapor pressure and the vapor composition above the liquid solution. Thus extrapolations of measured fluorescence decays to zero pressure of added gas do not correspond to the true zero pressure lifetime and must be measured for each series of experiments. The measured decays can be related to the concentration of the various gases present by the following equation:

$$\frac{1}{\tau} = \frac{1}{\tau_0} + k_Q^{SF_6}[SF_6] + k_Q^B\,[\text{BACKGROUND}] + k_Q^M[M]\,. \quad (1)$$

Typical decay traces are shown in Fig. 3(a) for pure SF_6 plus H_2O/H_2O_2 background and $SF_6 + N_2$ plus the background. Figure 3(b) shows the corresponding log, plots. Note the faster quenching by nitrogen. Decays were recorded over at least two lifetimes, starting after ~50 ns to eliminate any complication due to scattered laser light.

Temperatures were determined from OH rotational populations, measured by laser excitation scans over the $P_2 5$, $P_1 6$, $Q_2 11$, $Q_2 12$, and $Q_1 13$ lines in the (0, 0) A–X system of OH, for each quenching measurement. From the precision of these data we estimate that the error in a given temperature determination is ±50 K, in accord with the scatter in the previously determined temperature histories.[4] The measured temperature is then used in conjunction with the computer code to obtain the post-expansion gas density at the position and time of the quenching measurement. That is, $\rho = P/RT$ where, for example, the code predicts $P = 1.13P_0$ for the pure SF_6 and $P = 1.01P_0$ for the SF_6/N_2 mixture of

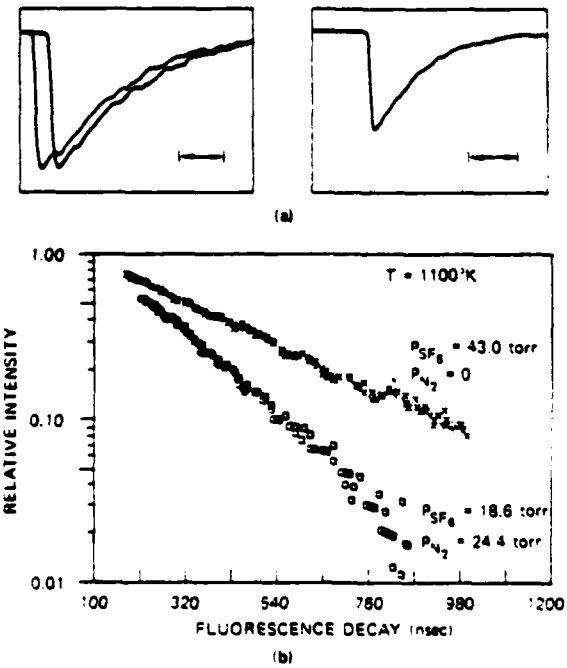

FIG. 3. (Top): Oscilloscope traces of OH fluorescence decay at 1100 K in pure SF_6 (left, two traces) and N_2–SF_6 mixture (right); 200 ns per marked interval. (Bottom): Logarithmic plots of these decays, giving lifetimes of 395 and 200 ns, and a N_2 quenching rate constant of 1.3×10^{-11} cm^3 s^{-1}.

Fig. 3; here P_0 is the initial pressure of cold gas.

Recent flow system measurements at room temperature[8] indicated a variation of σ_Q with rotational level N' in $v'=0$. The differences were most pronounced for N_2 as a collision partner, decreasing more than a factor of 2 between $N'=0$ and 3. We measured σ_Q for each of the five excited levels ($N'=4$, 5, 11, 12, and 13) with N_2 as a collision partner. No variation (< 10%) was observed in this series of runs. Fluorescence scans at moderate resolution indicate that the excited state rotational distribution of the fluorescence was independent of the level initially excited. This is presumably due to a rapid SF_6 rotational energy transfer rate. Thus these measurements reflect σ_Q for a 1200 K Boltzmann distribution in the excited state. For all the reported quenching measurements the $P_1 6$ excitation line was used, pumping $F_1(5)$ for $v'=0$ in $A\,^2\Sigma^+$.

B. Pressure dependence

Somewhat different procedures were necessary to obtain values of σ_Q for SF_6, H_2O, and N_2 in contrast to the other collision partners. Both SF_6 and H_2O/H_2O_2 from the bubbler contribute to the quenching in each measurement. The SF_6 rate is very low, and small amounts of H_2O_2, with a large quench rate, tend to dominate the quenching in SF_6 runs. Furthermore, simply varying the SF_6 pressure alters the temperature and density in the heated system and provides an inadequate solution to the problem. Similarly a water quench rate cannot be determined accurately from such data because the exact partial pressure picked up from the bubbler is uncertain. N_2 must be treated differently from the other gases because its slow rate requires replacement of the SF_6 by a significant fraction of it.

The SF_6 measurements are illustrated in Fig. 4. They were obtained by constructing a dual inlet line, so as to vary the fraction of SF_6 which passes through the bubbler and the fraction which bypasses it. The flow rate through the bubbler remained constant to ensure that the vapor pressure of the H_2O_2 that was picked up in the wet SF_6 flow was the same. By varying the fraction through the bubbler and extrapolating to 0% wet SF_6 a "pure" SF_6 decay rate can be determined. Figure 4 is a decay rate plot as a function of percentage of bubbler (wet) SF_6 for two peroxide bath temperatures. Lowering the bath temperature reduced the amount of H_2O_2 present in the vapor, but also reduced the amount of H_2O_2, OH, and thus signal level. A least squares fit of the more precise first data set gives a $k_e = 1.7\times10^{-12}$ $cm^3\,s^{-1}$ molecule^{-1} at 1125 K. A large statistical uncertainty of ~25% in the fit is attributable to the low value of this rate constant compounded by the background problem. The lower temperature data set was not used quantitatively but the values are consistent with expectations.

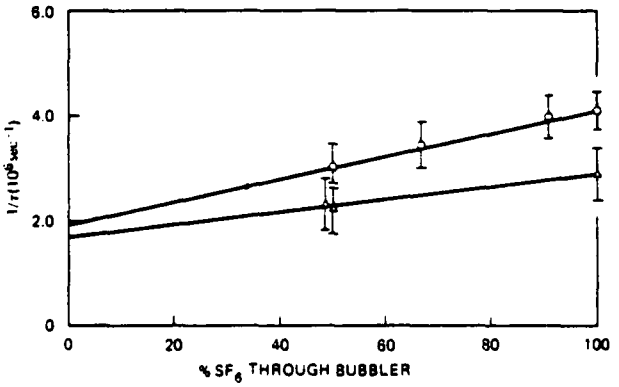

FIG. 4. Plot of OH fluorescence decay rate as a function of the percentage of SF_6 flowing through the H_2O_2 bubbler. Circles, 1130 K, 38.5 Torr. SF_6 triangles 1340 K, 58.5 Torr SF_6 colder H_2O_2 bath temperature. Lines are least squares fits. Error bars indicate decay trace standard deviations for these runs.

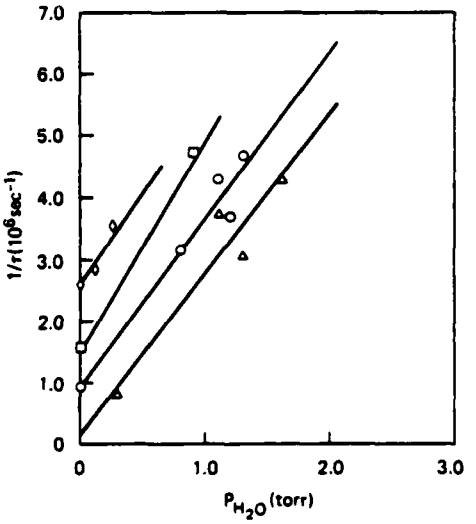

FIG. 5. Decay rate of OH fluorescence, minus contributions from SF_6 quenching and radiative decay, vs pressure of added H_2O. Squares, 1220 K in 26 Torr SF_6. Circles, 1140 K in 37 Torr SF_6. Triangles, 1430 K in 40 Torr SF_6. Diamonds, 1000 K in 16 Torr SF_6.

For the water quenching measurements, a separate flow of 3% H_2O in SF_6 (from a 15ℓ bulb containing 1 atm SF_6 saturated with water vapor) was added to the cell, bypassing the bubbler in a manner similar to the above SF_6 measurement. Figure 5 is a plot of decay rate as a function of added water pressure. The derived rate constant of 4×10^{-10} $cm^3\,s^{-1}$ molecule^{-1} assumes the added cell water pressure proportionately reflects the storage bulb condition. Possible water adsorption in the gas lines could mean that the true k_Q is in fact higher, although the gas flow was permitted to equilibrate before measurements were made. Note the different intercepts for different runs, indicative of the experimental problem of variation in bubbler H_2O_2 background concentrations. A separate water quenching determination was made by measuring a decay in a $SF_6 + H_2O/H_2O_2$ mixture under very slowly flowing conditions where the vapor should be nearly saturated. A determination of H_2O_2

concentration was made by independently measuring the vapor pressure at the ice bath and trap temperature. This single measurement yields a higher $k_Q = 7.5 \times 10^{-10}$ $cm^3 s^{-1}$, assuming that the vapor is saturated at 0.6 Torr and that H_2O_2 has a k_Q equal to that of H_2O.

Experiments for other gases were carried out by first recording the fluorescence decay due to SF_6 and H_2O_2 background, and then recording the decay in the presence of varying fractions of quenching gas. All gas mixtures for these experiments passed through the bubbler, and, except for N_2, the amount of added gas was a small fraction of the total flow. A plot for runs on two separate days for CO_2 is shown in Fig. 6; k_Q values are obtained from an application of Eq. (1) plotting τ^{-1} vs [M]. In each case it was necessary to measure the intercept (zero added gas pressure) separately due to the variation in background quenching, which is evident in Fig. 6. Occasionally, and unpredictably, the background quenching was found to be very high, as in the run shown by the dashed line in Fig. 6. This led to short and thus poorly determined lifetimes; data sets with high intercepts were discarded.

Figure 7 is a plot of decay rate vs nitrogen partial pressure. Because of its slow quench rate, significant fractions of nitrogen were required in order to significantly decrease the observed fluorescence decay lifetime. This replacement of 50%–80% of the SF_6 made

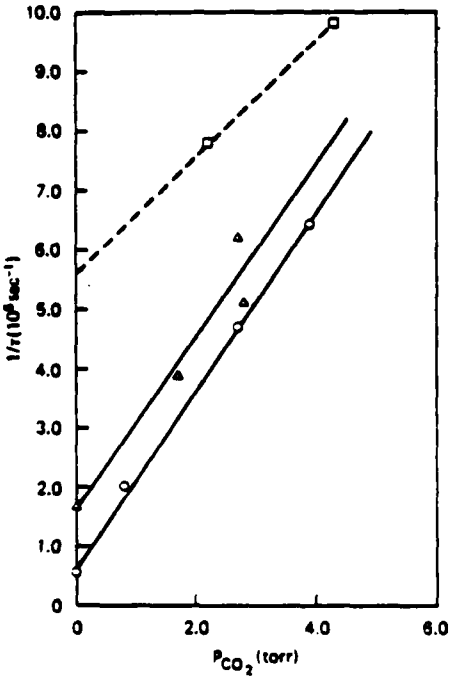

FIG. 6. Decay rate of OH fluorescence, minus contributions from SF_6 quenching and radiative decay, vs CO_2 pressure of added CO_2. Circles 1240 K, 40 Torr total pressure. Triangles 1000 K, 40 Torr total pressure. Squares 1250 K, 40 Torr total pressure, illustrating a run with unacceptably high background quenching.

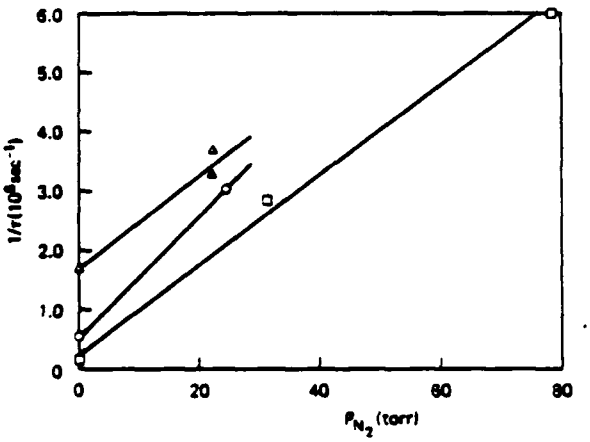

FIG. 7. Decay rate of OH fluorescence, minus contributions from radiative decay and SF_6 quenching, vs pressures of added N_2. Triangles 1030 K, 40 Torr total pressure. Circles 1110 K 43 Torr total pressure. Square 1200 K, with a constant SF_6 pressure of 20 Torr.

two adjustments necessary. First, the laser fluence had to be readjusted, and excitation scans repeated, to attain the same temperature. Second, a full analysis of the data in Fig. 7 using Eq. (1) is needed to account for the significant variation in quenching due to SF_6 as its fraction is varied. The resulting rate constant is 1.0×10^{-11} $cm^3 s^{-1}$ $molecule^{-1}$.

Measurements were made at a variety of temperatures. N_2 in particular was studied extensively, with a series of measurements over the range 900–1400 K. No temperature variation in k_Q was observed beyond the precision in the data. $\bar{v}$ increases only 25% over this temperature range so even a small decrease in σ_Q would mask a noticeable change with temperature in the measured k_Q.

The full set of results, including temperature, k_Q, and σ_Q values, is given in Table I. Because of the lack of an observable temperature dependence, we have averaged the σ_Q values regardless of temperature for later comparison with room temperature and with theoretical values.

C. Sources of error

Three general sources of error merit some discussion and estimation: Statistical, systematic, and the background H_2O_2 quenching problem. For errors in the random category, there is typically 5% scatter among the lifetimes from the three or more decay traces taken for each set of experimental conditions. Similarly, the temperature can be determined to within 50 K by the laser fluorescence excitation scans, introducing 4% uncertainty in k_Q via the density calculation ($\rho \propto 1/T$). CO_2 laser intensity variation during a given run is monitored and held to typically 3%, which generates small temperature fluctuations that ultimately show up as error in the density calculation. Finally, total pressure and mass flowmeter readings are estimated to contribute

TABLE I. Experimental and calculated cross sections.

Gas	T(K)	k_Q[a]	σ_Q[b]	$\sigma_{Q\,avg}$[b]	$\sigma_{Q\,calc}$[b,c]
N_2	1110	1.3	0.89	0.68 ± 0.16	49
	1030	1.0	0.72		
	1200	0.82	0.53		
	1040	0.85	0.59		
SF_6	1130	0.17	0.14	0.14	57
CO	1270	31	20	20	57
CO_2	1200	21	15	13 ± 3	65
	1140	19	14		
	1250	14	9.5		
H_2O	1220	39	23	26 ± 3	89
	1140	47	28		
	1430	44	23		
	1000	47	30		
	(1160)[d]	(75)	(44)		
CH_4	1440	44	23	15 ± 5	47
	1230	23	13		
	1260	21	12		
	1130	21	12		
NH_3	1470	62	32	39 ± 7	85
	1250	79	45		
O_2	1160	11	7	11 ± 3	41
	1460	22	13		
	1090	17	12		
H_2	1320	48	12	10 ± 3	36
	1330	45	11		
	1320	23	6		
NO	1110	42	28	26 ± 4	53
	1320	45	28		
	1320	35	22		
N_2O	1390	47	30	30	65

[a]Units = 10^{-11} cm^3 s^{-1}.
[b]Units: Å^2.
[c]At 1100 K using multipole approach, see the text.
[d]Single run with measured vapor pressure; see the text. Not included in average.

another 5% uncertainty.

A more systematic error can be introduced through the dependence of the derived quenching rate constants on the density values calculated by the computer code. Experience with the code[8] suggests a 5% possible inaccuracy in this value. Furthermore, the calculations indicate that up to 12% variations in the density occur at times and positions close to those chosen for these measurements. Any spatial or temporal drift, misalignment, or computational inaccuracy could thus introduce a comparable error in a rate constant. We have, however, measured OH decay times, in a 1:1 SF_6/N_2 mixture at 1040 K, at various delays from 30–100 μs, and found no significant differences, to within 10%. This indicates the density fluctuations are probably below this 12% level.

Finally, the uncertainty of the measured value of the SF_6 quench rate enters the calculation of k_Q^M, but is only significant for N_2 since such a large fraction of N_2 is used. For other gases little SF_6 is replaced by added gas, and the bulk of SF_6 quenching remains a constant factor, effectively included in the measured value of the intercept.

We noted earlier the experimental difficulty in keeping the H_2O_x quenching constant over long periods of time and the necessity of measuring the intercept lifetime with no added quench gas. For a typical run (a series of lifetimes at different pressures), a maximum possible 50 ns error in τ_Q^B would produce up to a 20% error in k_Q. Most runs, particularly for those with little H_2O_x, show less scatter. The k_Q values are obtained from a least squares analysis of the quenching plot, further reducing this error contribution.

By combining all of these possible error sources as the square root of the sum of the squares of the above percentages, we derive an approximate uncertainty of 25% in the final rate constant values. Those gases where many measurements were made generally show ~20% average deviations, again giving an error estimate of 25% after also including the density uncertainty. The reactive gases are generally harder to measure and more scatter in the data exists due to the lower overall OH concentration. The low SF_6 and N_2 values are also less precise, due to the significance of k_Q^B in all SF_6 measurements and the contribution of the $k_Q^{SF_6}$ uncertainty to the $k_Q^{N_2}$ calculation. Estimates are 40% and 30%, respectively. Finally, the H_2O rate constant is subject to additional uncertainty, since its derivation rests on assumptions that the cell water vapor concentration (or water plus peroxide) reached the values of the bulb or bubbler. Some problems of surface absorption and equilibration are evident in the scatter of the data, and particularly the background intercept values. The reported k_Q probably represents a lower limit, and more work is needed to produce a quenching rate constant within 30% accuracy.

IV. COMPARISONS AND CORRELATIONS

A. Comparison with other measurements

Only a few high temperature OH quenching cross sections are available, consisting of values deduced from flame measurements in a complex collisional environment. Hooymayers and Alkemade[9] give approximate values (in units of 10^{-11} cm^3 s^{-1} molecule^{-1}, corrected to a 0.69 μs OH radiative lifetime) of 105, 20, and 33 for H_2O, N_2, and O_2 respectively, at 1500–1800 K. The O_2 and H_2O values are ~60% higher than our values. Their N_2 value, however, is 20 times larger than our measured rate and also exceeds any reasonable extrapolations from 300 K determinations. Carrington[10] has also deduced some quench rates from measurements in low pressure C_2H_2/O_2 flames over a wide (850–1500 K) temperature range. His values (corrected for $\tau_R = 0.69$ μs) for H_2O, CO_2, and CO are 51, 20, and 9×10^{-11} cm^3 s^{-1} molecule^{-1} which agree well with our direct measurements except for CO. Recently, Morley[11] has measured relative OH quench rates in a 2000–2400 K flame for H_2O, H_2, and CO of 1.0:0.32 ± 10:1.3 ± 0.2. This compares with our values of 1.0:0.38:0.76. One possible reason for the discrepancy in the CO results may be the neglect of CO_2 quenching in analyzing the flame

TABLE II. Room temperature quenching measurements.[k]

Reference	a	b	c	d	e	f	g	h	i	j
N_2 k	4.4		4.6	2.7	2.5	1.8	1.8	2.9		2.5[l]
σ	5.7		5.8	3.8	3.5	2.3	2.3	3.6		3.2
CO k	33								56	
σ	43								72	
CO_2							14			
σ							20			
H_2O k	50			56		39		37		54
σ	65			66		45		43		63
O_2 k				8.1				9.1		10.4
σ				10.7				12.3		13.8
H_2 k	6.6	8.4	9.0	12	14					18
σ	3.5	4.5	4.8	7.0	7.3					9.6
O_2 k	4.4		11							
σ	2.8		7.4							

[a] M. Kaneko, Y. Mori, and I. Tanaka, J. Chem. Phys. 48, 4468 (1968).
[b] K. H. Becker, D. Haaks, and T. Tatarczyk, Chem. Phys. Lett. 25, 564 (1974).
[c] R. K. Lengel and D. R. Crosley, Chem. Phys. Lett. 32, 261 (1975); J. Chem. Phys. 68, 5309 (1978).
[d] K. R. German, J. Chem. Phys. 64, 4065 (1976).
[e] P. Hogan and D. D. Davis, J. Chem. Phys. 62, 4574 (1975); 64, 3901 (1976).
[f] M. A. A. Clyne and S. Down, J. Chem. Soc. Faraday Trans. 2 70, 253 (1974).
[g] E. Erler, D. Field, R. Zellner, and I. W. M. Smith, Ber. Bunsenges. Phys. Chem. 81, 22 (1977).
[h] P. M. Selzer and C. C. Wang, J. Chem. Phys. 71, 3786 (1979).
[i] M. A. A. Clyne and P. M. Holt, J. Chem. Soc. Faraday Trans. 2 75, 569 (1979).
[j] I. S. McDermid and J. B. Laudenslager, J. Chem. Phys. 76, 1824 (1982).
[k] Units: k_Q, 10^{-11} cm^3 s^{-1}, σ_Q, Å^2. All values corrected to $\tau = 0.69$ μs.
[l] k and σ were found to vary with N'. Values given are for $N' = 3$.

data. A value for CO quenching larger than that for H_2O seems unlikely, given both the 300 K results and (see below) the stronger attractive forces for H_2O as a collision partner.

Table II lists for comparison the present results and a selected set of σ_Q values for the six collision partners which have also been studied at room temperature. There have been many determinations, with a large spread, for H_2, N_2, and H_2O; in general, the values are chosen primarily from recent LIF experiments if available. It is seen that for all cases save H_2 there is a decline in σ_Q between 300 and 1100 K. This is expected if attractive forces are responsible for the quenching collisions.

The very low values of σ_Q which we obtain for N_2 and SF_6 at elevated temperatures are, however very surprising. We shall see below that the experimental results are much smaller than expected from a model involving attractive interactions. However, if quenching by N_2 is due only to the repulsive part of the potential, the large decrease in σ_Q should not occur. Although SF_6 has not been studied at room temperature, one would not expect it to behave much differently from CF_4. Yet σ_Q for the latter has been measured[12] as 16 Å^2 at 300 K in contrast to σ_Q (SF_6, 1100 K) which is less than 1% of this value.

A measurement of OH quenching by H_2O has been made[13] from the temperature dependence of the luminescence following photodissociation of H_2O vapor. It shows a k_Q (H_2O) linearly proportional to T over the range 300–600 K. Both the magnitude ($\sigma_Q = 110$ Å^2 at 600 K) and the variation with temperature are in contradiction with our results and our concept of attractive interactions as responsible, although we can offer no explanation for the discrepancy.

B. Well depth correlation

Several attempts have been made to theoretically characterize the collision-induced electronic quenching that occurs in small molecules. The goal has been to correlate the observed σ_Q's with certain molecular parameters, so as to obtain insight into the quenching process and ultimately yield predictive capabilities. Earlier approaches[14–18] considered the interaction to be due to dispersion forces. Although they contribute, they are not the dominant forces in the case of $A\,^2\Sigma^+$ OH and the collision partners measured here. This we conclude from unsuccessful attempts at correlation of our σ_Q with the pertinent parameters involving polarizability, ionization potential, and gas kinetic radius.[14–16]

A more successful approach involving a single molecular parameter was developed by Parmenter and coworkers,[1] who applied it to a number of collision processes. This model assumes that only attractive forces are responsible for the quenching and considers an A^*–M intermediate collision pair to be in equilibrium with the separated species. The $[A^*\text{–M}]$ concentration and resulting σ_Q are then calculated from partition func-

tions. Although derived differently in Ref. 1, this can be considered as an application of transition state theory to the quenching problem. The energy of the complex compared to the separated A* and M is taken as a Lennard-Jones type potential well depth, ϵ_{A^*M}. This leads to the relationship

$$\ln \sigma_Q^M = \ln C + \frac{\epsilon_{A^*M}}{kT} , \tag{2}$$

where C is a constant. Because the well depth for A* and M is unknown, the reasonable approximation

$$\epsilon_{A^*M} = \sqrt{\epsilon_{A^*A^*}\epsilon_{MM}}$$

was made. Then, with $\beta = \sqrt{\epsilon_{A^*A^*}}/kT^{\frac{1}{2}}$,

$$\ln \sigma_Q^M = \ln C + \beta\sqrt{\epsilon_{MM}/k} \tag{3}$$

furnishes a correlation between the σ_Q^M for a given A* and the well depths for the ground state M–M interactions. The ϵ_{MM} were obtained[1] from a variety of methods, including for many species a correlation with boiling point. From the slope of a plot of $\ln \sigma_Q^M$ vs $\sqrt{\epsilon_{MM}/k}$ one should obtain $\epsilon_{A^*A^*}$ which could then be used to predict σ_Q^M values at other temperatures.

Parmenter and co-workers[1] found that Eq. (3) described well a large number of excited state collision processes where large overall cross sections indicated *a priori* the importance of attractive forces. An attempt was made by them to describe the temperature dependence of glyoxal quenching using the β from a room temperature plot corresponding to Eq. (3); it was found that the decrease with T in the experimental σ_Q values was less than predicted.

A plot of the room temperature OH quenching cross section values vs $\sqrt{\epsilon_{MM}/k}$ is shown in Fig. 8(a). The σ_Q are those from Table II plus 11 of the extensive series of halocarbons measured by Clyne and Holt[12] for which ϵ_{MM} are available. A reasonable correlation is achieved, with a slope $\beta = 0.19$ and an intercept $\ln C = 0.6$. Figure 8(b) plots the σ_Q measured here at ~1100 K vs $\sqrt{\epsilon_{MM}/k}$. The correlation (ignoring the N_2 and SF_6 values) does not appear as clearly as for the room temperature results although it must be borne in mind that a slope smaller by 3/11 is expected at the higher temperature. The line is the predicted σ_Q using $\beta(1100\ \mathrm{K})$ and $\ln C$ derived from the 300 K plot; the slope is reasonable although the predicted cross sections are uniformly low.

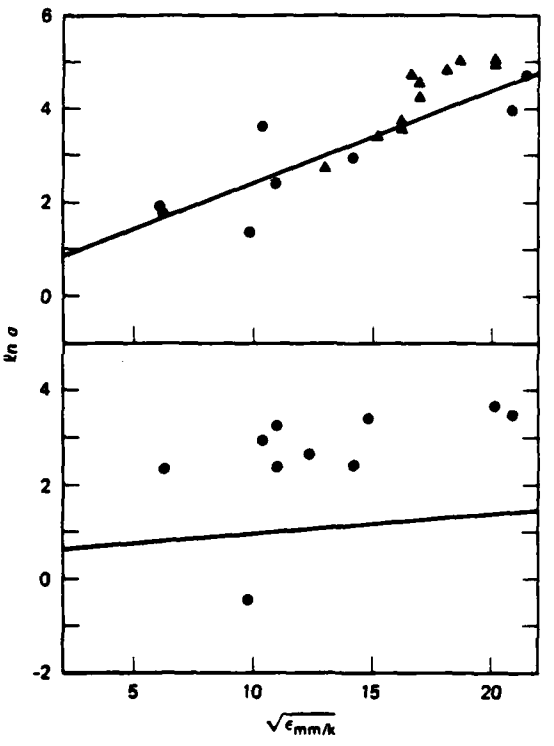

FIG. 8. Plots of $\ln \sigma_Q$ vs $(\epsilon/k)^{1/2}$ for various gases. (Top) Values at 300 K. Circles, selected from results from Table II. Triangles, halocarbon quenchers measured by Clyne and Holt (Ref. 12). Line is a fit to the results. (Bottom) Present experimental values at high temperature. Line is predicted cross sections using the 300 K values. Note that the slope is reasonable although the predicted σ_Q are uniformly low.

C. Multipole attractive forces correlation

This approach too rests on the concept of a collision complex held together by attractive forces, although the physical model for the complex formation is rather different than in the correlation with M–M well depth. Suggested earlier,[18] it was applied by Lee and co-workers[2] to quenching of SO_2, using a simplified procedure of adding analytically derived cross sections for each attractive component of the potential taken separately. We have chosen to construct the single potential with all the attractive interactions taken together, and compute the cross section numerically. We describe here the physical picture in some detail, followed by a comparison with the present σ_Q values.

The long range part of the interaction between A* and M is composed of a sum of attractive multipole interactions (dipole–dipole, dipole–quadrupole, dipole–induced-dipole, and dispersion) and a repulsive centrifugal barrier. This last term is $L^2/2\mu r^2 = (\mu v b)^2/2\mu r^2 = Eb^2/r^2$; L is the angular momentum involved in the collision at kinetic energy E and with impact parameter b. Thus, the effective potential $V(r)$ is

$$V(r) = \frac{Eb^2}{r^2} - \frac{C_3}{r^3} - \frac{C_4}{r^4} - \frac{C_6}{r^6} . \tag{3}$$

This potential for OH–H_2O collisions at $E = 1100\ \mathrm{K} = 2.18$ kcal/mol and several impact parameters is illustrated in Fig. 9. For each E and b, there is a maximum value in the potential at the separation r_0; both r_0 and $V(r_0)$ depend on both E and b (i.e., E and L).

In a collision at a particular energy E, there then exists some impact parameter b_0 where the maximum in the effective potential is just equal to E. For $b < b_0$, the barrier will be lower and the collision pair can form a complex which is bound, at least briefly, within the barrier. For $b > b_0$, the barrier is higher than E, and the pair cannot surmount it, so as to come closer than r_0 and form a complex. This impact parameter $b_0(E)$ is thus the maximum separation for which a complex

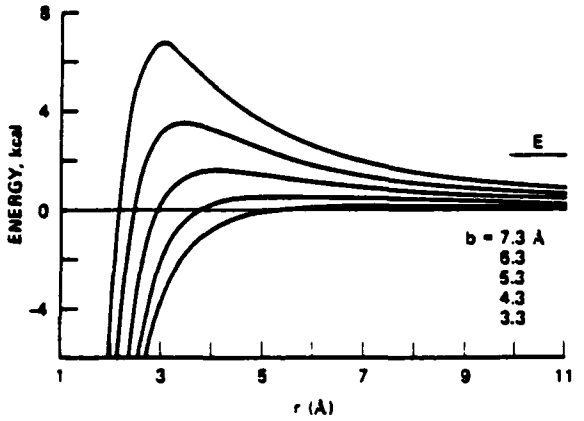

FIG. 9. The long range part of the effective potential [Eq. (3)] for OH ($A\,^2\Sigma^+$) colliding with H_2O at a collision energy of 1100 K = 2.18 kcal (shown on right). Curves are for successively larger values of impact parameter b as indicated.

can form at the collision energy E, and the cross section for complex formation at this energy can be written as

$$\sigma_{cf}(E) = \pi b_0^2(E) \,. \tag{4}$$

The cross section for quenching is that for complex formation times a probability P that quenching will occur during the residence time of the complex. We have no way of knowing P *a priori*, or how it varies among collision partners, and so will consider it a single value independent of collider. The thermally averaged cross section at T is then

$$\sigma_Q(T) = P\left(\frac{1}{kT}\right)^2 \int_0^\infty \sigma_{cf}(E)\, E \exp(-E/kT)\, dE \,. \tag{5}$$

In the case of a single attractive term, such as for CH_4 or SF_6 where only dipole-induced-dipole and dispersion forces contribute, the equations may be solved analytically. For this potential

$$V(r) = \frac{Eb^2}{r^2} - \frac{C_4}{r^4} \,.$$

r_0 is the value at which $dV/dr = 0$, leading to $r_0 = (3C_4/Eb^2)^{1/4}$ and $V(r_0) = 2E^{3/2}b^3/3^{3/2}C_4^{1/2}$. b_0 may then be evaluated by recalling that at this value of impact parameter, $V(r_0) = E$. Thus $b_0 = (3^{1/2}/2^{1/3})\,(C_4/E)^{1/4}$, which can then be used with Eqs. (4) and (5) to obtain $\sigma_Q(T)$.

For a potential with more than one multipole interaction [Eq. (3)] this simple procedure cannot be used because the derivative equation $dV/dr = 0$ at the top of the barrier leads to a more complex power series equation for r_0. We have adopted a straightforward, if tedious, numerical approach. For a given E, a small value of b is chosen. $V(r)$ is then calculated as a function of increasing r until a maximum is found; this $V(r_0)$ is compared to E. b is then incremented and the process is repeated until $V(r_0) = E$; the corresponding value of b is set equal to b_0 for that energy. The process is repeated for increased E, and the resulting set of b_0 is then numerically integrated to obtain $\sigma_Q(T)$.

This approach contrasts with that used previously for SO_2.[2] There, the approximation was made of a separate σ_Q calculated for each component of the interaction, with the total σ_Q taken as the sum of those cross sections. Actually, there is only one potential, rather than a sum of various r^{-n} potentials acting independently. Unless one multipole interaction strongly dominates, this sum of cross sections from each component can be much larger than that calculated numerically from the single potential. In the case of SO_2, excellent agreement was achieved between the calculated and experimental values. For OH, the various interactions are often of comparable magnitude, necessitating the numerical computation we have used.

The C_n coefficients may be expressed in terms of the dipole and quadrupole moments, polarizability and ionization potential of excited OH and the collision partner; the pertinent expressions are listed in Table III. The dipole moment for $A\,^2\Sigma^+$ OH has been measured; the quadrupole moment is taken as the same as for the ground state and the polarizability is estimated by that of $X\,^1\Sigma^+$ HF. These necessary approximations are reasonable; note that the same values are used for each collision partner. The molecular parameters used in the calculations are collected in Table IV. There exists an orientation dependence for some of the attractive terms; in each case the interaction is calculated at the most favorable orientation. For example, the dipole–dipole interaction is $[\mu_1 \cdot \mu_2 - (\hat{r} \cdot \mu_1)(\hat{r} \cdot \mu_2)]/r^3$ which has a maximum value of $2\,\mu_1\mu_2/r^3$. With one exception, the most favorable orientation is the same for all orientation-dependent interactions. The exception is $\mu_{OH}Q_{H_2O}$ compared with other OH–H_2O terms, but its magnitude is also quite small by comparison. The use of weaker, orientation-averaged potentials generally gave too small a calculated cross section.

The results of the calculations at a temperature of 1100 K are listed in Table I for each of the gases measured. The experimental values are compared with the calculated ones in Fig. 10. With the obvious exceptions of N_2 and SF_6, and possibly CO_2, there is a reasonable correlation between experimental and calculated values. The line drawn is a least-squares fit, constrained to go through the origin, for the eight other gases. The slope of 0.4 can be interpreted as a common, average probability P for quenching once the collision complex has been formed. Although it is not expected that P be the same for each collision partner, the experimental values

TABLE III. Multipole terms included in the calculation, at the most favorable orientation.

C_1	Dipole–Dipole	$2\mu_1\mu_2$
C_4	Dipole–Quadrupole	$3/2\,\mu_1Q_2 + 3/2\,\mu_2Q_1$
C_6	Dipole–Induced Dipole	$2\mu_1^2\alpha_2 + 2\mu_2^2\alpha_1$
	Dispersion	$3/2\,\dfrac{(\text{I. P.})_1(\text{I. P.})_2}{(\text{I. P.})_1 + (\text{I. P.})_2}\,\alpha_1\alpha_2$

TABLE IV. Parameters used in calculation.

Reference	$(\epsilon/k)^{1/2}$ a	μ (D) b	$Q\times10^{26}$ esu cm^2 c	α(Å^3) d	I. P. (eV) e
N_2	9.7	0	−1.52	1.76	15.58
SF_6	14.2	0	0	4.52	16.15
CO	10.2	0.112	−2.5	1.95	13.98
CO_2	14.0	0	−4.3	2.65	13.77
H_2O	20.7	1.85	+0.13	1.48	12.6
CH_4	12.1	0	0	2.60	12.71
NH_3	18.9	1.47	−1	2.26	10.19
O_2	10.8	0	−0.39	1.60	12.06
H_2	6.1	0	+0.66	0.79	15.43
NO	10.7	0.153	−1.8	1.74	9.25
N_2O	15.6	0.166	−3.0	3.00	12.89
OH $A\,^2\Sigma^+$		1.98[f]		(2.46[i])	9.12
$X\,^2\Pi_i$		1.66[g]	+1.8[h]		13.17

[a]H. M. Lin, M. Seaver, K. Y. Tang, A. E. Knight, and C. S. Parmenter, J. Chem. Phys. 70, 5442 (1979).
[b]From R. D. Nelson, D. R. Lide, and A. M. Maryott, *Selected Values of Electric Dipole Moments for Molecules in the Gas Phase* (U.S. GPO, Washington, D.C., 1967), Vol. 10.
[c]D. E. Stogryn and A. P. Strogryn, Mol. Phys. 11, 371 (1966).
[d]J. O. Hirschfelder, C. F. Curtiss, and R. B. Bird, *Molecular Theory of Gases and Liquids*, 2nd ed. (Wiley, New York, 1964).
[e]R. A. Beaudet and R. L. Poynter, J. Phys. Chem. Ref. Data 7, 311 (1978).
[f]E. A. Scarl and F. W. Dalby, Can. J. Phys. 49, 2825 (1971).
[g]W. L. Meerts and A. Dymanus, Chem. Phys. Lett. 23, 45 (1973).
[h]A. Khayar and J. Bonamy, J. Quant. Spectrosc. Radiat. Transfer 28, 212 (1982).
[i]Value for HF $X\,^1\Sigma^+$.

(excluding N_2, SF_6, and CO_2) do differ from the predicted ones by only 25% on the average.

The multipole interaction approach predicts a decrease in σ_Q with increasing temperature, but to a smaller degree than indicated by the Parmenter model correlating with well depth. We have calculated σ_Q at 300 K. The pertinent results are collected in Table V for the six gases studied here which have also been measured at room temperature. The experimental cross section ratio is the present result divided by the selected room temperature value listed in the table. An assessment of the level of agreement between the experimental and calculated temperature dependence is strongly influenced by the choice of σ_Q (300 K) from the range of available values. Nonetheless, except for the weak quencher N_2, and for H_2 where σ_Q (1100 K)/σ_Q (300 K)>1, the predicted dependence is essentially observed.

V. CONCLUSIONS AND QUESTIONS

Two related conclusions can be drawn from these results. The first is the direct experimental result showing the σ_Q at elevated temperatures to be lower than those at room temperature, and the second is the interpretation that attractive forces and collision complex formation play an important role in the quenching of OH by many collision partners.

For the comparison of σ_Q at room and elevated temperatures, it would have been preferrable to have measurements over the entire range in a single system, which was not possible with the LP/LF apparatus. One must consider errors in absolute σ_Q at both temperatures. The full set of σ_Q previously measured at room temperature shows considerable spread,[19] and even the selected set of recent values given in Table II exhibits differences of a factor of 2 where there exist multiple determinations. Within the context of energy transfer measurements in general, this constitutes rather respectable agreement among values obtained in different laboratories, but it does suggest the potential for systematic error in any given measurement. We have cho-

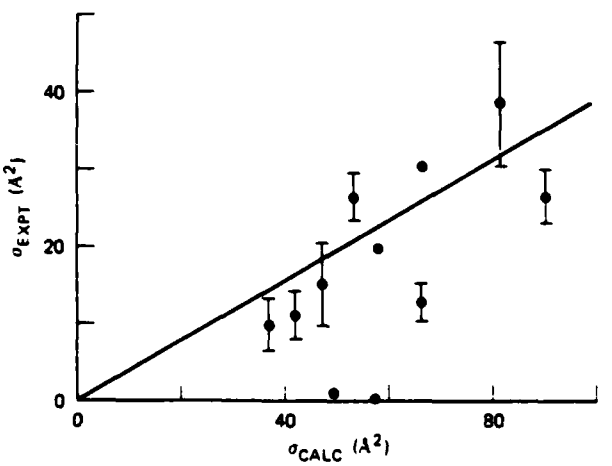

FIG. 10. Experimental cross sections vs cross sections calculated using the multipole approach. The line is a least squares fit, constrained to pass through the origin and not including the results for N_2, SF_6, and CO_2.

TABLE V. Quenching cross sections at 300 and 1100 K.

	$\sigma_Q(300)$ (Å^2)	$\sigma_Q(1100)$ (Å^2)	$\sigma_Q(1100)/\sigma_Q(300)$	
			Experiment	Multipole theory
N_2	3.7	0.7	0.19	0.60
O_2	12	11	0.92	0.62
H_2O	65	26	0.40	0.47
CO_2	20	13	0.65	0.57
H_2	7	10	1.43	0.60
CO	43	20	0.47	0.56

sen for comparison (Fig. 8 and Table V) what appear as consensus or average values. At the elevated temperatures, we recall our error estimates of ~25%. This is also the error estimated for our rate constant measurements[4] for OH + CH_4 from 800 to 1400 K, which in turn agrees well with the scatter from expected values (measurements, and extrapolations from a fit to more accurate lower temperature data).

In view of these uncertainties, it is the totality of the evidence—the ratios in Table V on which we conclude that σ_Q decreases with increasing temperature.

These results have immediate implications for experiments in which LIF is used to detect OH in flames where composition, temperature, and density vary with position. In a flame of CH_4/O_2, for example, the average σ_Q increases as the fuel and oxygen are converted to CO, CO_2, and H_2O. $\bar{v}$ increases as $T^{1/2}$ but the density varies inversely with T, and σ_Q for each gas decreases somewhat with higher T. Some model calculations[20] indicate a quenching rate (s^{-1}) and resulting fluorescence quantum yield which varies little with position, in accord with direct measurements for OH[21] and CH[22] in low-pressure flames. In the case of an air-based flame, the very low σ_Q for N_2 means higher quantum yield and better sensitivity than would have been estimated using the room temperature value. In contrast, atmospheric monitoring experiments in which OH is measured by LIF at $T < 300$ K (i.e., in cooler regions of the stratosphere) will probably be affected by higher σ_Q than the room temperature values.

This temperature dependence and the correlation between experimental and calculated cross sections shows that attractive forces are responsible for the overall size of σ_Q and its variation with collision partner. The correlations with the well depth model and the multipole interaction are of course not independent; a plot of $\ln \sigma_{eff}$ vs $\sqrt{\epsilon_{300}/kT}$ shows a correlation similar to that in Fig. 8(b) with a slope of ~0.065 at 1100 K.

The picture is still far from complete. The correlation seen in Fig. 10 suggests a similar probability P for quenching once a complex is formed, for the eight partners whose experimental values lie near the line. One might expect *a priori* quite different values given the differences in the nature of the colliding molecules. If the quenching were facilitated by some partial equipartition of energy among modes of the collision complex, large differences in P between the diatomics on the one hand and the triatomics plus ammonia on the other would seem likely. Alternatively, one might have anticipated the A–X mixing in OH to be caused by an interaction with the dipole or other moments of the collision partner, but this does not appear to be the case.

The conspiciously low values for N_2 and SF_6 are particularly puzzling. for N_2 alone, one might rationalize especially ineffective quenching once the complex is formed; note that the σ_Q at room temperature is also the lowest of all molecular gases. However, an interpretation including participation of the repulsive part of the interaction is not in accord with the results for N_2, which shows a much smaller $\sigma_Q(1100)/\sigma_Q(300)$ ratio than all other gases for which comparison is possible (Table V). The small size of σ_Q for SF_6, while welcome from the experimental point of view due to its necessary presence in the LP/LF method, is even harder to reconcile. It lacks attractive interactions with an r^{-3} and r^{-4} dependence but so does CH_4 which has a much larger cross section. Any special rationalizations involving the cloud of fluorine atoms is invalidated by the size of $\sigma_Q(300)$ for CF_4 and other halocarbons.[11] Thus the low values for these two collision partners remains a fully open question. Measurements for an even broader range of collision partners is needed to formulate a full picture of the quenching of $A\,^2\Sigma^+$ OH.

ACKNOWLEDGMENTS

We appreciate the support for this research, which was furnished by the U. S. Army Research Office under contract DAAG29-80-K-0049. We thank Charles Parmenter for useful discussions, and Edward Lee for sending us a copy of Ref. 2 in advance of its publication.

[1] H. M. Lin, M. Seaver, K. Y. Tang, A. E. W. Knight, and C. S. Parmenter, J. Chem. Phys. 70, 5442 (1979).
[2] D. L. Holtermann, E. K. C. Lee, and R. Nanes, J. Chem. Phys. 77, 5327 (1982).
[3] R. K. Lengel and D. R. Crosley, J. Chem. Phys. 68, 5309 (1978).
[4] P. W. Fairchild, G. P. Smith, and D. R. Crosley, Nineteenth Symposium (International) on Combustion, The Combustion Institute, Pittsburgh, 1982, p. 107.
[5] D. R. Crosley, Opt. Eng. 20, 511 (1981).
[6] L. Seaman, Final Report, SRI Project 6802, Menlo Park, California, August 1978.
[7] D. F. McMillen, K. E. Lewis, G. P. Smith, and D. M. Golden, J. Phys. Chem. 86, 709 (1982).
[8] I. S. McDermid and J. B. Laudenslager, J. Chem. Phys. 76, 1924 (1982).

[9]H. P. Hooymayers and C. Th. J. Alkemade, J. Quant. Spectrosc. Radiat. Transfer 7, 495 (1967).
[10]T. Carrington, J. Chem. Phys. 30, 1087 (1959).
[11]C. Morley, Combust. Flame 47, 67 (1982).
[12]M. A. A. Clyne and P. M. Holt, J. Chem. Soc. Faraday Trans. 2 75, 569 (1979).
[13]I. P. Vinogradov and F. I. Vilesov, Opt. Spectrosc. 44, 653 (1979).
[14]F. W. Byron and H. M. Foley, Phys. Rev. A 134, 625 (1964).
[15]J. E. Selwyn and J. I. Steinfeld, Chem. Phys. Lett. 4, 217 (1969).
[16]C. A. Thayer and J. T. Yardley, J. Chem. Phys. 57, 3992 (1972).
[17]C. S. Parmenter and M. Seaver, Chem. Phys. Lett. 67, 279 (1979); Chem. Phys. 53, 333 (1980).
[18]J. C. Tully, J. Chem. Phys. 61, 61 (1974); G. E. Zahr, R. K. Preston, and W. H. Miller, *ibid.* 62, 1127 (1975).
[19]K. Schofield, J. Phys. Chem. Ref. Data 8, 723 (1979).
[20]D. R. Crosley (unpublished calculations).
[21]D. Stepowski and M. J. Cottereau, Combust. Flame 40, 65 (1981).
[22]R. J. Cattolica, D. Stepowski, D. Puechberty, and M. J. Cottereau, Western States Meeting of the Combustion Institute, Salt Lake City, Utah, April, 1982.

Laser-induced fluorescence spectroscopy for combustion diagnostics

David R. Crosley
Gregory P. Smith
SRI International
Menlo Park, California 94025

Abstract. Laser-induced fluorescence can be used to detect with high sensitivity small molecular species, typically free radicals, which are the intermediates in the chemistry of combustion processes, the atmosphere, and plasmas. Using as examples recent work from our laboratory, we describe the laser spectroscopy and spectroscopically based collision studies needed for application of the laser-induced fluorescence techniques, with an emphasis on combustion diagnostics.

Keywords: fluorescence; laser-induced fluorescence; free radicals; collision studies; combustion diagnostics.

Optical Engineering 22(5), 545-553 (September/October 1983).

CONTENTS

1. INTRODUCTION

The technique of laser-induced fluorescence (LIF) of small, gas-phase molecules has found widespread application in the physical and engineering sciences. In addition to providing fundamental information on spectroscopic and collisional properties, it is proving useful as a diagnostic technique in several fields. LIF is especially suitable for the sensitive detection of a number of reactive intermediates in chemical networks, the most important example of which is OH. The areas in which LIF is increasingly used include the study of combustion phenomena, processes in the upper and lower atmosphere, the chemistry of plasmas, and laboratory measurements of chemical reaction rates.

Invited Paper F-105 received Mar. 3, 1983; revised manuscript received June 6, 1983; accepted for publication June 7, 1983; received by Managing Editor July 20, 1983.

Establishment of the ability to detect a given species with LIF requires a study of its spectroscopic characteristics. This often takes as a departure point previous, conventional (nonlaser) spectroscopic investigations, but involves further research to develop optimal detection strategies (choices of excitation and fluorescence wavelengths). This is especially true if there are potential interfering species. In many cases, further quantification of the LIF method is desirable; the extent and level of precision required vary with the species detected and processes studied. Here measurements are needed of lifetimes, transition probabilities, and a variety of collision phenomena. Finally, the development of special LIF variants such as two-photon detection requires additional spectroscopic detail.

We discuss in this paper the types of spectroscopic and collisional measurements needed to develop LIF as a diagnostic technique, using as illustrations recent experiments from our laboratory. (There are many other researchers and laboratories active in this field, and we emphasize that this paper is not to be construed as a review of work in the field in general.) Such studies form a significant portion of our research program, which has as its objective the development and application of laser methods (primarily LIF) for the understanding of the chemistry of a variety of processes. Much of our current orientation is toward combustion phenomena; the choice of species and characteristics for study and for discussion here is slanted toward that application. We note that of the nearly thirty combustion chemistry intermediates detectable by LIF, all were first studied by chemists or physicists in fundamental spectroscopic studies and not by the user community interested in applications. Hence, it is important to establish a coupling between the needs, present and anticipated, in the applied areas and an awareness of the current and possible capabilities of the fundamental studies.

2. LASER-INDUCED FLUORESCENCE AS A DIAGNOSTIC PROBE

2.1. LIF method

In laser-induced fluorescence[1] one tunes a laser so that its wavelength

matches that of some absorption line of the species of interest. The molecules absorb the laser photons, becoming elevated to an electronically excited state from which they emit light (fluoresce). The fluorescent photons then form the detected signal. As the laser is scanned across a series of absorption lines, signal is produced each time a match occurs. Such a so-called excitation scan is depicted schematically in Fig. 1. It traces out what is essentially the absorption spectrum of the molecule, but with a significant difference compared to conventional absorption spectra. In LIF one detects not a small dip in some transmitted beam of light, but rather a positive signal on a null background. This yields much higher sensitivity; absorptions less than 10^{-6} per cm can produce readily measured signals.

The rate of production of molecules in the upper level pumped by the laser is given by

$$\frac{dN_e}{dt} = BIN_a \ , \tag{1}$$

where N_e and N_a are the number densities (cm^{-3}) in the pumped and absorbing levels, B is the Einstein absorption coefficient, and I is the laser intensity (W/cm^2). (We will not consider here line shape effects; BI in Eq. (1) represents actually the convolution of the laser and absorption lines over frequency, or $\int B(\nu)I(\nu)d\nu$.) N_a is related to the total ground-state density N_g by a Boltzmann distribution:

$$N_a = N_g G_a \exp(-E_a/kT) \ , \tag{2}$$

where G_a and E_a are the degeneracy and energy of level a. The B-coefficient for a given v',v" vibrational band and J',J" rotational branch* is a product of three factors: a vibrational transition probability† $P_{v'v"}$, a rotational line strength $S_{J'J"}$, and an overall electronic transition probability, which is, in turn, inversely proportional to the radiative lifetime τ of the upper state. Thus,

$$B = \frac{P_{v'v"}S_{J'J"}\lambda^3}{8\pi hc\tau}\,\frac{G_e}{G_g} \ , \tag{3}$$

where λ is the transition wavelength, and the G's are the electronic degeneracies of the excited and ground states.

The excited state then radiates. Under collision-free conditions, and when light from all the possible fluorescent transitions is collected and integrated over time, the fluorescence signal F is given by

$$F = cAN_e = cN_e/\tau \ , \tag{4}$$

where $A = \tau^{-1}$ is the Einstein emission coefficient. c contains all the factors of geometry (solid angle, probed volume), optical losses (filters or monochromator transmission, detector quantum efficiency), and electronic gain that can be separately calibrated. If a particular $J' \rightarrow J"$, $v' \rightarrow v"$ fluorescent transition is observed, the A of Eq. (4) becomes

$$A_{v'v";J'J"} = P_{v'v"}S_{J'J"}/\tau \ . \tag{5}$$

Measurements of P, S, τ, and the energy levels of the molecule in question form the needed spectroscopic information for LIF diagnostic development.

At pressures of an atmosphere, a molecule that has been excited by the laser can suffer collisions during the time it resides in the upper state, before it radiates at the rate A characteristic of the electronic transition involved. For example, for the OH molecule in a flame at atmospheric pressure, only about 1 in each 1000 excited molecules emits a photon; the remainder are collisionally quenched back to the ground electronic state. In this case one has

$$F = cA\Phi N_e \ . \tag{6}$$

The fluorescence quantum yield Φ is related to A and the quenching rate Q by

$$\Phi = A/(A + Q) \ . \tag{7}$$

Collisions can also be of the energy-transfer type, which move the molecule from the pumped level to other radiating levels within the upper state. In this case one must consider the state-to-state dependence of these collision processes together with the specific transitions monitored in fluorescence. That is, one may have an effective quantum yield differing from that in Eq. (7), as we shall discuss later. In any event, it is clear that the study of collisional effects[2] is also an important part of LIF development research.

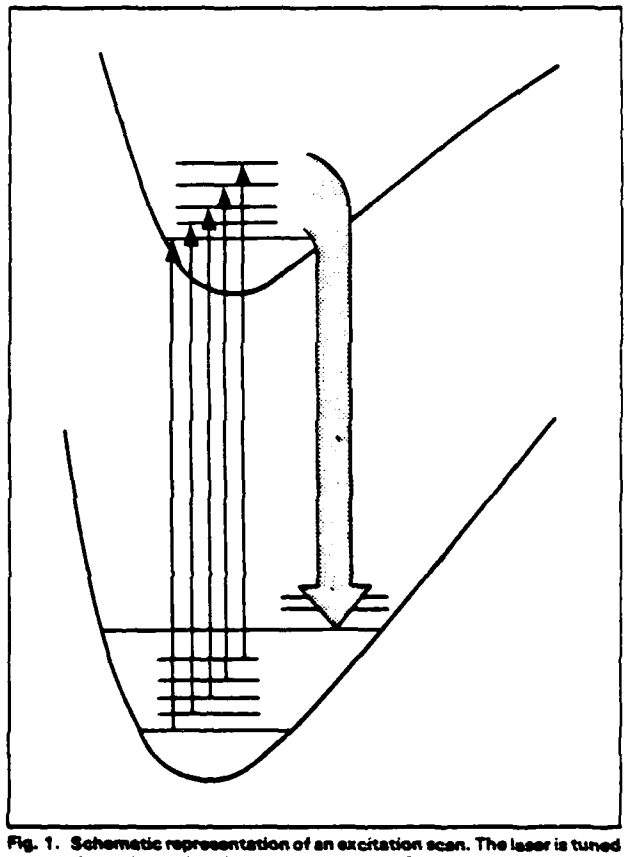

Fig. 1. Schematic representation of an excitation scan. The laser is tuned over various absorption lines (small arrows). Detection is achieved by measuring the total fluorescence intensity (large shaded arrow).

2.2. LIF in combustion measurements

LIF, together with spontaneous and coherent Raman spectroscopy, forms a family of laser spectroscopic probes[3] for the study of combustion, that is, methods providing concentrations and temperatures (through the population distribution over internal energy levels) of identifiable molecular species. The methods complement one another well in that the Raman techniques are the choices for measuring major species in a flame (the fuel, oxidant, main exhaust gases, and, in an air flame, N_2). LIF is the only method suitable for the detection of the chemical intermediates present at low concentration.

LIF has a number of attributes especially useful in combustion

* As in customary molecular spectroscopic notation, a single prime denotes the upper state and a double prime the ground state; also, when a transition is labeled, the upper state is always written first for both absorption and emission (e.g., the 6,0 band means v' = 6, v" = 0).

† For the important OH molecule, but for no others of current practical significance, P varies with J' and J" also, as discussed in Sec. 3.4.

studies. The laser can be focused and is generally pulsed, so that high spatial and temporal resolution are possible. Sample volumes of $<10^{-3}$ mm^3 can be defined, although 1 mm^3 is a more typically used value in many present studies. Most of the lasers used have pulse lengths of 10 ns, so that measurements average only over this interval. These attributes are important in atmospheric pressure flames, where significant concentration and temperature gradients can exist over spatial regions of the order of 1 mm, and under turbulent conditions, where conditions can change in times of the order of a few μs. The method is sensitive; for example, OH can be detected in 1 mm^3 volume at sub-part-per-billion concentrations, producing some 100 detected photons on a single 10 ns laser shot. Selectivity is obtained through the narrow bandwidth of the laser, which provides high spectral resolution. Even if two species absorb at the same bandwidth, they can often be distinguished by choosing different fluorescent wavelengths at which only one or the other emits. As with other optical probes, LIF is nonintrusive, so that it does not perturb the gas flows or chemical reactions. Additionally, it can be used in environments too hostile to permit the insertion of a physical probe device, such as a thermocouple or a sampling nozzle.

LIF is, in fact, the only method capable of providing sensitive, fast, spatially resolved measurements of chemical intermediates. It is, on the other hand, not general, as is mass spectrometry, for example. To be detectable with LIF, the molecule must possess a suitable electronic transition, at wavelengths accessible with available lasers, which also fluoresces. Fortunately, many important small combustion chemical intermediates fall into this category. Table I lists the "natural" combustion intermediates that have been detected with LIF in low pressure flows or cells and/or in flames. (Not included in the table are a number of metals, their oxides and halides, often obtained in flames only through seeding but sometimes found as contaminants, and many larger organic species, such as benzene, acetone, benzyl radicals, etc.)

For diagnostic applications, it is important to recognize that LIF measures the concentration of the ground electronic state of the species monitored, in contrast to the excited states seen directly from emission spectroscopy. Because the excited states are often produced through very different chemical reactions than ground states, the distributions can be very different, and only LIF furnishes information truly relevant to the overall chemistry.

Recently we have developed a new two-dimensional variant of LIF[4] which promises numerous useful applications in flames and other systems. It is a fluorescence imaging technique that furnishes a planar map of the radical concentration throughout the flame on a single laser shot. Here, the laser is focused into a thin sheet of radiation (in our experiments on OH, it was 0.5 mm thick) and passed through the flame. Wherever the OH existed in the plane cut by the laser sheet within the flame, fluorescence resulted. This was focused at right angles onto the face of a two-dimensional vidicon tube, yielding an instantaneous picture of the OH concentration. Such a spatial correlation of the concentration is important in a turbulent system, where the conditions at the sampling point can vary drastically from shot to shot. The sensitivity for the OH fluorescence imaging was very promising; using 1.5 mJ of laser energy, ~2000 counts were obtained per mm^3 of sample volume at an OH concentration of 700 ppm, on a single shot. The sensitivity for other species will vary with their spectroscopic characteristics.

TABLE I. Combustion Intermediates Observed by LIF

O*, N, H, C, S
OH*
CH*, C_2*, CN*, CO*
NH*, NH_2, NO*, NO_2*
NCO*, HCO, HNO
S_2*, SH*, SO*, SO_2*
CS, CS_2
C_2O, C_3, CH_3O
C_2H_2, CH_2O, HCN

*Denotes that detection has been performed in a flame

2.3. Spectroscopic data needs

The particular needs for an LIF data base vary with the problem addressed by the method. In some cases, relatively crude knowledge may suffice. For example, a measurement of relative signal intensities for LIF in NH and OH in a CH_4–N_2O flame was analyzed using the simple assumption that the quantum yield Φ for each was the same, given the total lack of quenching experiments on NH. The surprising result that [NH] ~ 0.04[OH] indicated a potentially important chemical role for nitrogen containing radicals in this flame; subsequent experiments[5] have confirmed the high [NH] and found large amounts of CN and NCO as well.

Similarly, an imaging experiment with only a semiquantitative analysis may provide a great deal of information and stimulus to theorists approaching the problems of turbulent reactive flow, witness the theoretical advances following visualizations of turbulent structures using Schlieren methods. At the other extreme, one may wish to fit to a chemical model a detailed set of profiles of several radical species in a laminar flame. This may require much more information to assess precisely enough the relative signal strengths from different species over the changing thermal and collisional environments encountered through the flame.

The OH radical occupies a special position among molecules detectable by LIF. It is a ubiquitous and important intermediate in nearly any flame involving oxygen and hydrogen (as well as many other networks, such as atmospheric chemical processes). Its presence can be used to signify the occurrence of oxidation reactions. The needed laser wavelengths are experimentally very convenient, and its spectroscopic and collisional data base is far better established than that of any of the other molecules in Table I. It has served as a test species on which to try new methods (e.g., the imaging) and is generally the first species to search for when studying a new flame or probing a complex system. Despite the large spectroscopic effort devoted to OH, there remain some gaps in its data base, the closing of which is warranted by the premier importance of this radical.

3. SPECTROSCOPIC MEASUREMENTS UNDER COLLISION-FREE CONDITIONS

3.1. Production of radicals

The first step in performing laser spectroscopic experiments is to obtain an adequate concentration of the molecules to be studied. If it is a stable species, such as CO or SO_2, a static cell may simply be filled at the desired pressure. Under some conditions, a static cell operated at specific conditions of temperature and pressure can lead to sufficient concentration of certain radical species; this method has been used for OH and S_2. Most of the studies of free radicals, however, have been made in discharge flow systems. A parent species is dissociated in a microwave or radio frequency discharge at total pressures of the order of 1 Torr (generally the majority gas is an inert carrier such as He or Ar). In some cases the desired radical is directly produced in the discharge; N atoms may be produced from N_2 in this way, for example. In many cases the original radical reacts with another molecule to yield the species of interest. Thus, N atoms reacting with O_2 produce O atoms, and OH may be produced from H + NO_2. These reactions proceed rapidly to completion, so they can be used to produce known quantities of the radical through the addition of measured amounts of the stable reactant, O_2 or NO_2. An attractive method for the production of many radicals is a discharge of CF_4 in a He carrier to produce F atoms; these then strip H atoms from a parent to produce radicals. We have used this method to produce the NCO radical from HNCO vapor, and it has been used for the production of alkoxy radicals (CH_3O, C_2H_5O, etc).

Lasers can also be used for radical production in several ways. Single or multiphoton dissociation through an electronically excited state of the parent species (often with an excimer laser) has been used by several groups. A CO_2 laser can be used for multiphoton infrared

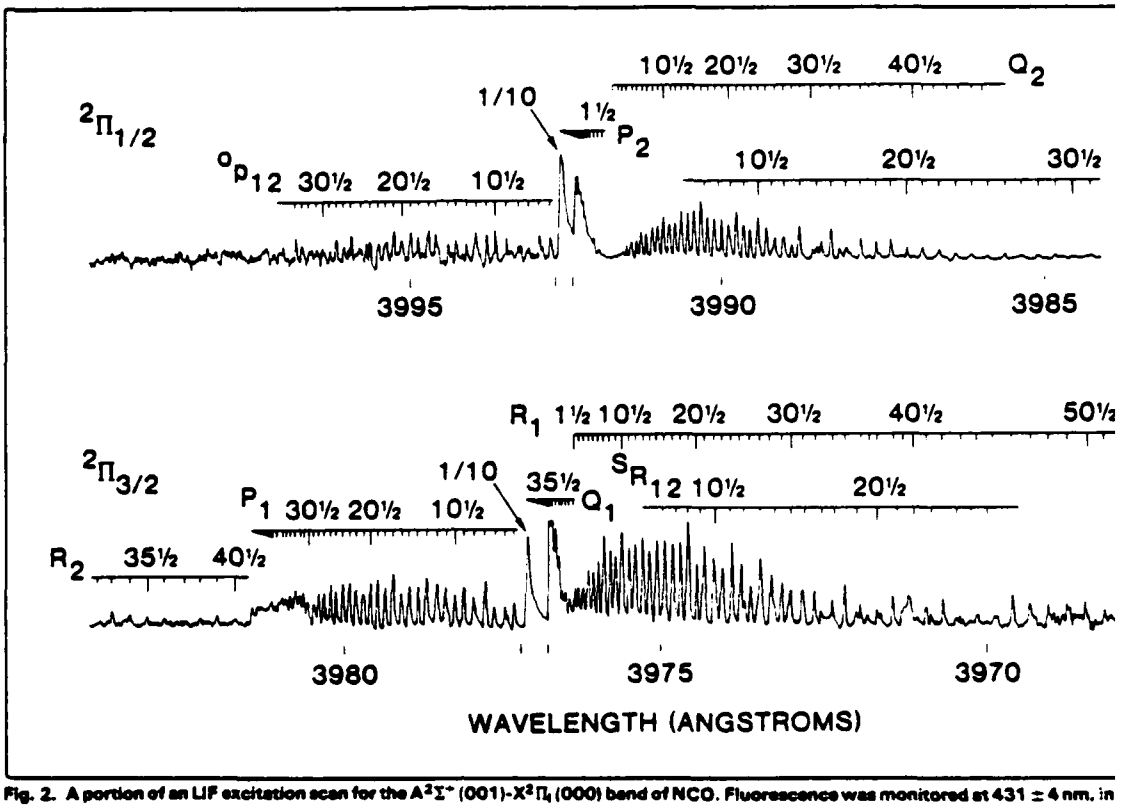

Fig. 2. A portion of an LIF excitation scan for the $A^2\Sigma^+$ (001)-$X^2\Pi_i$ (000) band of NCO. Fluorescence was monitored at 431 ± 4 nm, in

dissociation of the parent to low-lying fragment states, or as a thermal gas heating source for dissociation. We have developed a laser pyrolysis/laser fluorescence method[9] using a pulsed CO_2 laser to heat a gas sample. Here the infrared radiation is absorbed by SF_6, and collisional energy transfer rapidly heats the system to a temperature chosen by the laser pulse energy and SF_6 pressure. Our experiments have used the radical precursor H_2O_2; this pyrolyzes to form OH radicals whose LIF is then detected with a dye laser timed to fire after the CO_2 laser. So far, only OH, NH_2, and Fe atoms have been produced in this way although there are other possible candidate precursors and radicals.

The initial flow tube experiments are generally performed at low pressure and room temperature. This often yields larger signals than in a flame for two reasons: collisions do not reduce the quantum yield, and the population is distributed over a smaller number of internal levels than at high temperature. Using a flame as a radical source for initial search experiments also suffers from the disadvantages of more complex chemistry leading to interfering species, and the possible confinement of the species of interest to a very narrow spatial zone. Each of the molecules in Table I whose LIF has been observed in flames was first detected by LIF in a low pressure system.

3.2. Excitation scan studies

The next order of business after radical production is a search for the excitation scan of the molecule; that is, find the LIF signal. Again, all the molecules detectable with LIF have a common feature; such a search has used as a guide emission or absorption spectra previously obtained using conventional (nonlaser) methods. In many cases those measurements were made in flames, the medium in which the emission spectra of many radicals were first observed. Discharge emission spectra and the flash photolysis absorption studies of the 1950s and 1960s are a rich source of such data as well. Such starting points are most valuable, for an undirected search for sharp lines with a bandwidth of the same size as the laser bandwidth would be very time-consuming.

Figure 2 exhibits an excitation scan for the NC the excitation is from the 000 level[a] of the ground X level of the excited $A^2\Sigma^+$ state. The energy levels inv Fig. 3. The ground-state level is split into two compo 98 cm^{-1} by a spin-orbit interaction,[b] and the excita the resulting $^2\Pi_{1/2}$ and $^2\Pi_{3/2}$ sublevels can be seen component has associated with it an R ($\Delta J = J' - J''$ and P ($\Delta J = -1$) branch (as well as smaller O and S f $\Delta N = \pm 2$), as marked on the figure. The assignme followed from a detailed rotational analysis of abso flash photolysis experiment.[8] Excitation scans sim also been performed pumping five other vibrational state, as well as two vibrational levels of the $B^2\Pi_i$ s

The relative intensity of each line within the ba product of the line strength factor $S_{J'J''}$ and the fra N_a in the absorbing level. In this case the line strer calculated from knowledge of the angular moment interactions among them (in this case, spin-orbit). T have been assigned, the relative intensities may be rotational population distribution from which ca temperature from a plot of $\ln(N_a, G_a)$ versus E_a [Eq. is not at thermal equilibrium so that a temperature the population distribution itself is of direct interes

Clearly, obtaining the total concentration from given line requires knowledge of the temperature fractional population in the absorbing level [see Eq.

[a] This notation signifies the three vibrations $\nu_1\nu_2\nu_3$ of this linear tri ν_1 are stretches, and ν_2 is a twofold degenerate bend.

[b] Levels with $\nu_2 > 0$ have a more complex splitting pattern due to momentum of the degenerate bend which interacts with the el momentum, and the Renner-Teller splitting of the potential for

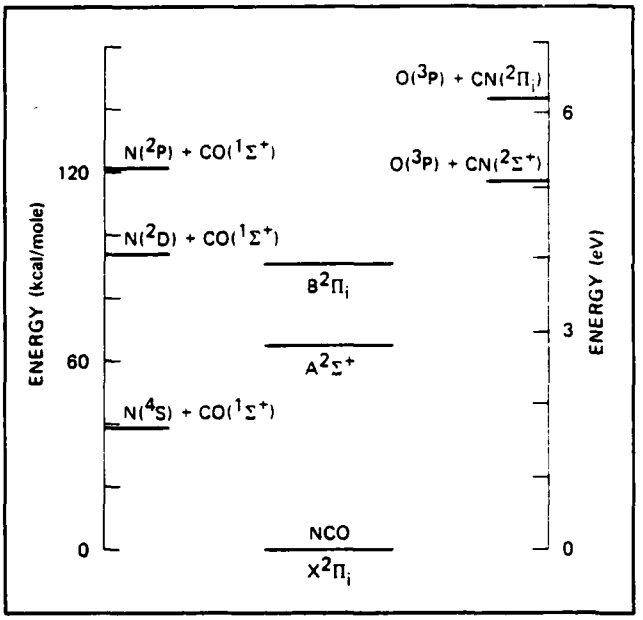

Fig. 3. Energy-level diagram for NCO showing the known electronic states and thermodynamic dissociation limits.

profiles are taken throughout a flame, it is often useful to choose a level for monitoring whose fractional population varies little over the temperatures of interest, that is, some J" for which $\partial N_a / \partial T$ is small.

Much larger signal is obtained near the bandhead, where many lines pile up together so that the laser line overlaps the absorption from many levels at once (see Fig. 2). Excitation in a bandhead region may be quite useful, especially for low densities of the molecule studied, although analyzing the overlap to obtain the effective fractional population monitored may present problems for accurate measurements.

3.3. Lifetime measurements

The excited molecule radiates at a characteristic rate $k_r = 1/\tau$. This is directly related to the Einstein B- and A-coefficients [Eq. (3)], and its measurement serves as a useful way to determine absorption and emission strengths for the transition. For radical species it is often difficult to obtain a high enough concentration to perform precise absorption measurements; even when one can do so, accurate knowledge of the absolute concentration often presents problems. (To determine the strength of a given band, one must combine the lifetime measurements with determinations of relative $P_{v'v''}$, as discussed in the next section.)

For lifetimes longer than the pulse length of the laser, LIF furnishes a good method of measurement. Figure 4 shows the decay of fluorescence from the v' = 1 level of the $A^3\Pi_i$ state of the NH radical under collision-free conditions.[9] Here a narrow electronic gate has been triggered initially just before the laser pulse, and its delay is scanned through the excitation (rising portion of the signal) and through the exponential decay. The data, fit to the exponential, furnish the lifetime. In the section on collisions, we will discuss quenching measurements made in this way at varying pressure of collision partner.

Lifetime measurements can furnish other information as well. In the case of NCO, the two different electronic states have very different radiative lifetimes: $\tau(A^2\Sigma^+) = 410$ ns; $\tau(B^2\Pi_i) = 63$ ns. The latter value was measured for the 000 level of the B-state. If one moves upward to the 100 level, only $\sim$ 1000 cm^{-1} higher, the decay is indistinguishable from the laser pulse time dependence. Thus, the lifetime of this higher level is $\leq$ 10 ns. The marked decrease between these two vibrational levels is likely caused by the onset of a predissociation to the $N(^2D) + CO(X^1\Sigma^+)$ limit (see Fig. 3). These lifetime

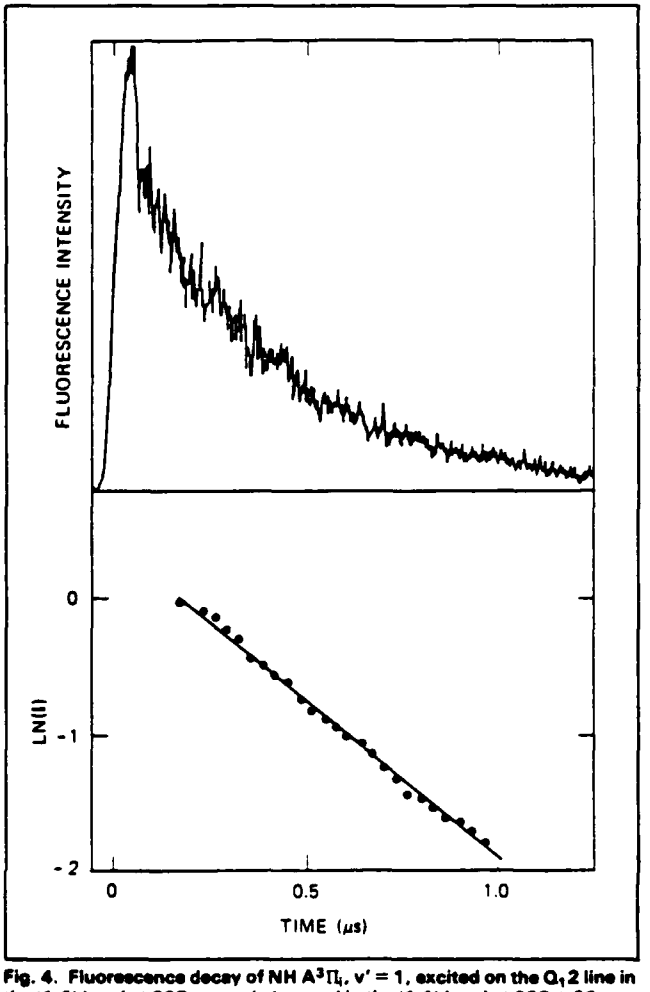

Fig. 4. Fluorescence decay of NH $A^3\Pi_i$, v' = 1, excited on the $Q_1 2$ line in the (1,0) band at 305 nm and observed in the (1,1) band at 338 ± 20 nm, at collisionless pressures. The lower, logarithmic plot of the data gives a radiative lifetime of 440 ns.

measurements thus place this dissociation limit between these levels, 0.46 eV lower than determined in an earlier study of the photodissociation of HNCO. This new determination of the dissociation limit[10] has as a consequence a higher heat of formation of both NCO and HNCO compared to the previously accepted values. The differences, nearly 10 kcal/mol, have implications concerning the role of the NCO radical in flame chemistry.

3.4. Fluorescence scans

A schematic indication of a fluorescence scan is given in Fig. 5. Here the laser is parked on one excitation. The level pumped radiates to some set of ground-state levels, for example, a series of vibrational levels. A monochromator is scanned to measure these transitions as a function of fluorescence wavelength. Under conditions where energy-transfer collisions occur before the molecule radiates, other levels are populated and can be discerned by such a scan; this phenomenon will be discussed in Sec. 4.

From each measured separation of a fluorescence wavelength from that of the pumping laser, one can obtain the separation in energy of a terminal v" level for the fluorescence from the energy of the initial absorbing level. Figure 6 shows a fluorescence scan[7] resulting from pumping the 000 level of the $B^2\Pi_i$ state of NCO. The laser line is off the chart to the left (at 315 nm). As the monochromator scans to longer wavelengths, one detects fluorescence returning to

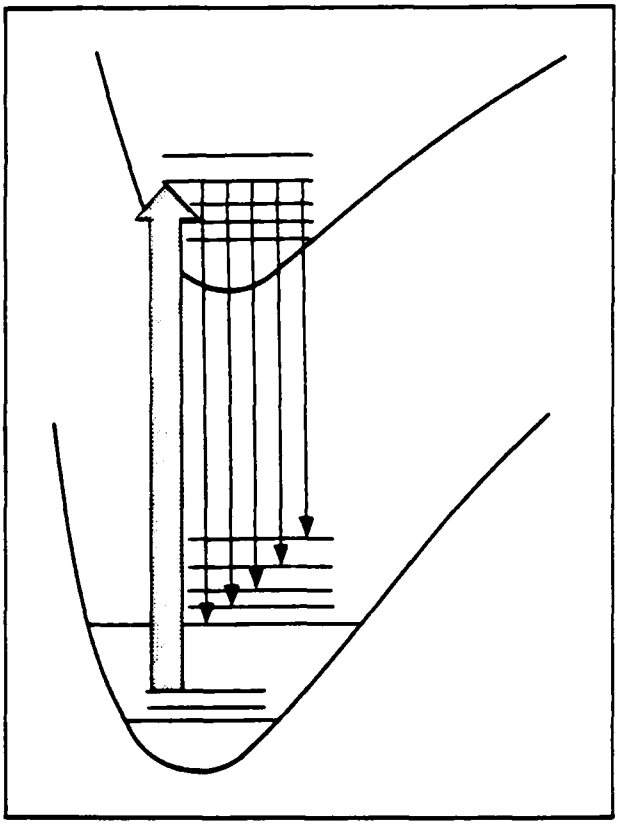

Fig. 5. Schematic representation of a fluorescence scan. The laser is tuned to a specific absorption line (shaded arrow) and the monochromator is scanned across the individual fluorescence emission lines from the excited level (small arrows).

higher v'' vibrational levels of the $X^2\Pi_i$ state. The more intense bands seen have one or more stretching vibrational quanta and $v_2'' = 0$; they are marked on the figure. Some weaker transitions (unmarked) involve $v_2'' = 2$ and 4. From a scan such as this (which extends further than is shown in the figure) one obtains the energies of the vibrational levels in ground-state NCO, which can be fit to a collection of harmonic and anharmonic vibrational constants. Previous information on NCO gas-phase spectroscopy came from absorption studies which probed only the 000 and 010 levels in the ground state, so that these results represent the first determination of these constants in the gas phase. The results may be used to understand the structure of the NCO molecule and to calculate its thermodynamic and thermochemical kinetic properties. From the standpoint of diagnostic measurements, knowledge of the wavelengths of the fluorescent transitions is needed in order to choose a suitable spectral region for detection.

Measurements of the intensities of the series of bands are also clearly important for the choice of an observation wavelength so as to maximize the available signal and or avoid interferences. They are also needed for quantitative measurements of concentrations using LIF. We shall consider for simplicity a diatomic molecule with only one vibration although the concepts are applicable to larger species, such as NCO. For a particular $v'v''$ band, the relative intensity of fluorescence $P_{v'v''}$ is given by the integral

$$P_{v'v''} = |\int \psi_{v'}(r)\, R_e(r)\, \psi_{v''}(r) dr|^2 \qquad (8)$$

over the two vibrational wave functions ψ and the electronic transition moment R_e, all expressed as functions of the internuclear distance r. $R_e(r)$ expresses the probability of the molecule making the

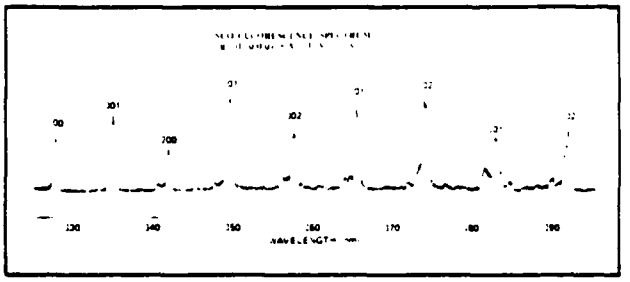

Fig. 6. Fluorescence spectrum from the 000 level of NCO $B^2\Pi_i$ excited at the R_1 head at 315 nm.

electronic transition as a function of internuclear distance. If it is constant, Eq. (8) reduces to

$$P_{v'v''} = R_e^2 |\int \psi_{v'} \psi_{v''} dr|^2 = R_e^2 q_{v'v''} , \qquad (9)$$

where $q_{v'v''}$ is simply the vibrational overlap integral, or Franck-Condon factor. For small species that have been well characterized spectroscopically, $q_{v'v''}$ is often calculable using potential curves for the pertinent electronic states constructed from the spectroscopic constants. If R_e varies with r, however, the relative $P_{v'v''}$ must be obtained from experimental intensity measurements. For larger molecules, one is generally better off using directly the empirical determinations of the $P_{v'v''}$.

An important example is the OH molecule, whose relative and absolute transition probabilities are reviewed in Ref. 11. For example, fluorescence scans[12] of the 0,0 and 0,1 bands show that $P_{01}/P_{00} = 0.004$ even though $q_{01}/q_{00} = 0.09$. The reason is that R_e decreases with increasing r, and the 0,1 band transition occurs at larger average values of r (1.22 Å) than does the 0,0 band (1.01 Å). A fit of the observed intensities for nine bands in each of OH[12] and OD,[13] using calculated values of $q_{v'v''}$, showed that $R_e(r)$ could be fit to a linear form,

$$R_e(r) = c(1 - \rho r) , \qquad (10)$$

with $\rho = 0.75$ Å^{-1}.

Transition probabilities in OH are unusual in another respect. The variation of $R_e(r)$ coupled with the high degree of centrifugal distortion present causes a significant variation in P with J. That is, the P values of Eqs. (3), (5), and (8) should be properly expressed as

$$P_{v'v'';J'J''} = |\int \psi_{v'J'}(r)\, R_e(r)\, \psi_{v''J''}(r) dr|^2 , \qquad (11)$$

with the radial variation of the rotational wavefunction included. The form of $R_e(r)$ determined from the LIF fluorescence scans, given in Eq. (10), has been combined with accurate wave functions $\psi_{v'J}(r)$ from RKR potentials to calculate $P_{v'v'';J'J''}$ for all bands of the OH $A^2\Sigma^+$-$X^2\Pi_i$ system which are of diagnostic interest.[14]

No other molecule is as well characterized as OH, and even where numerous studies exist for others, there can remain uncertainty in the results. An example is the C_2 molecule. A table of previously measured lifetime values of the $A^3\Pi_i$ state (upper level of the Swan bands) was given in the paper[15] describing the first application of optically saturated LIF in combustion, because this value was needed to analyze the experimental data. A variation of more than a factor of seven, over 17 different measurements, can be seen.

4. COLLISIONAL EFFECTS

As noted earlier, the collisions which the molecule suffers while excited can have a profound influence on both the magnitude and spectral form of LIF signals. The collisions may be of a quenching nature, reducing the overall quantum yield Φ [Eqs. (6) and (7)]. Collisions can also cause energy transfer to other v'', J'' levels of the excited state. These collisionally transferred molecules will then fluoresce at different wave-

lengths and with different intensities compared to the originally pumped level. Thus, the effective quantum yield into the detector bandpass can be affected, particularly if it is narrow.

The subject of collisional effects on LIF measurements in flames has been reviewed with coverage of the literature through early 1981, and we refer the reader to that article[2] for a comprehensive discussion. Emphasized here are the fundamental methods used to study collisional effects, and studies performed since the appearance of Ref. 2.

4.1. Quenching

Quenching rate constants k_Q for individual collision partners are generally obtained from lifetime measurements. The time dependence of the excited-state population is given by

$$N_e(t) = N_e(t = 0)\exp[-(k_r + k_Q n)t] , \quad (12)$$

where $N_e(t = 0)$ is the population initially created by the laser pulse, and n is the density of the added collision partner. A plot of the total decay rate versus pressure of added O_2 and N_2 for the 100 level of the $A^2\Sigma^+$ state of NCO is shown in Fig. 7; from the slopes we obtained k_Q for these gases.[7] In such experiments it is essential to measure all of the excited-state fluorescence. Suppose, for example, a $v' = 1$ level is pumped by the laser and the choice of fluorescence wavelengths is such that only emission from that level is detected. Then any collisional transfer to $v' = 0$ will appear as quenching, and the slope of the plot will not give the true value of k_Q.

Lifetime measurements may be used only under conditions in which the decay time is longer than the laser pulse length, typically 10 ns for the lasers used in these experiments. At a high enough pressure, the total decay time becomes shorter than this, and the population N(t) will reflect only the time dependence of the laser pulse. For some molecules k_r is already too fast, precluding quenching determinations from lifetimes. Under conditions where the number density of the molecules pumped by the laser can be controlled, fluorescence intensity measurements can yield quenching rates. An example is CO,[16] pumped by two photons at 289 nm to the $v' = 3$ level of the $A^1\Pi$ state, which has a lifetime of 10 ns. The total fluorescence intensity F, integrated over laser pulse and decay time, is compared for a given CO density, with (F) and without (F_o) an added gas at density n:

$$\frac{F_o}{F} = \frac{k_r + k_Q^{co} n_{co} + k_Q n}{k_r + k_Q^{co} n_{co}} . \quad (13)$$

A plot of this ratio for N_2 as the collision partner is given in Fig. 8; runs at three separate n_{co} values, normalized for comparison, are shown. Both k_r and k_Q^{co} must be separately measured to determine k_Q for N_2.

Of the molecules in Table I, k_Q is known for a variety of collision partners only for OH. Even here, all the previous direct measurements have been made at room temperature, where the flow systems used for the radical production operate most easily. Extensions of these rate constants to flame conditions have been made by assuming that the cross section σ_Q is constant, so that the only temperature variation in k_Q is $T^{1/2}$ from the velocity dependence. However, experiments on state-to-state energy transfer in $A^2\Sigma^+$ OH[17] suggest that attractive forces play a role in its collisional phenomena. If this is the case, one expects that σ_Q will decrease with increasing temperature,[18] so that k_Q will increase less rapidly than $T^{1/2}$.

Using our laser pyrolysis/laser fluorescence apparatus,[6] we have made measurements of k_Q for OH at temperatures in the 1100 to 1400 K region for a variety of collision partners.[19] The pulsed CO_2 laser radiation is absorpbed by SF_6, heating the gas mixture and pyrolyzing H_2O_2 to OH radicals; these are pumped by the dye laser to $v' = 0$ of the A-state at a fixed time delay after the CO_2 pulse. Measurements of the fluorescence lifetime for ten different collision partners of importance in flames have been made and show in general that the cross section is indeed smaller than at room temperature. In particular, k_Q for N_2 is anomalously small, with a value of 1.2×10^{-11} $cm^3 \cdot s^{-1}$. This is much lower than previously assumed at flame temperatures and has important implications for LIF signal strengths in air-based flames.

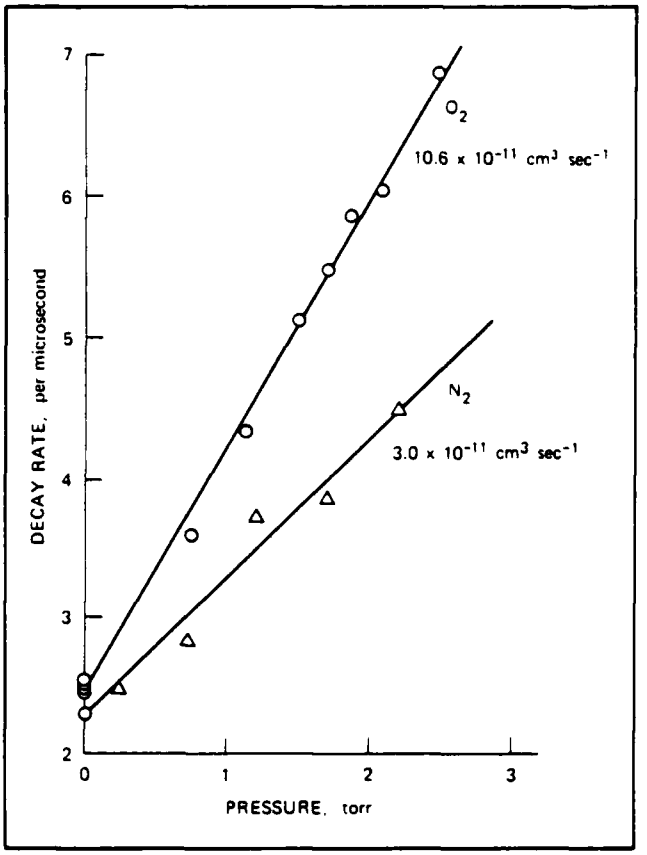

Fig. 7. Plots of the fluorescence decay rate for NCO $A^2\Sigma^+$ observed on the $\Delta v = 0$ bands after excitation of the 001 level as a function of added pressure of oxygen and nitrogen. Lines give the least-squares quenching rate constants.

The results for the other collisional partners have been examined[19] in the context of theoretical approaches which express σ_Q in terms of attractive well depths between the excited OH and its collision partner,[18] and a combination of multipole interactions.[20] The trends in σ_Q with the characteristics of the collision partner confirm the conclusion from the temperature comparison that attractive forces are important in the quenching process. Further examination of OH and other excited radicals will be important not only for LIF diagnostic development but also to establish a fundamental understanding of collisional mechanisms.

Results for k_Q for a variety of gases, both directly measured and estimated from these correlations, have been combined with profiles of major species (the predominant quenchers) published for a number of low pressure flames. The results[21] indicate little variation in the total quenching rate Q through the flame. This is in agreement with direct determinations of Q by lifetime measurements in low pressure flames for both OH[22] and CH,[23] which show a relatively constant value (within 20%) through the flame fronts.

4.2. Energy transfer

Collisions may also transfer the excited molecule among v'J' levels of the upper state. This phenomenon is studied by making fluorescence scans at controlled pressures of added gas. An example[24] for S_2 is shown in Fig. 9. Here changes in the fluorescence spectrum* from the

*The actual scan from which this figure was made employed as an excitation source a Zn atomic lamp, one of whose lines coincidentally overlapped an S_2 line, but the experiment could be performed (actually more easily) using laser e...ation.

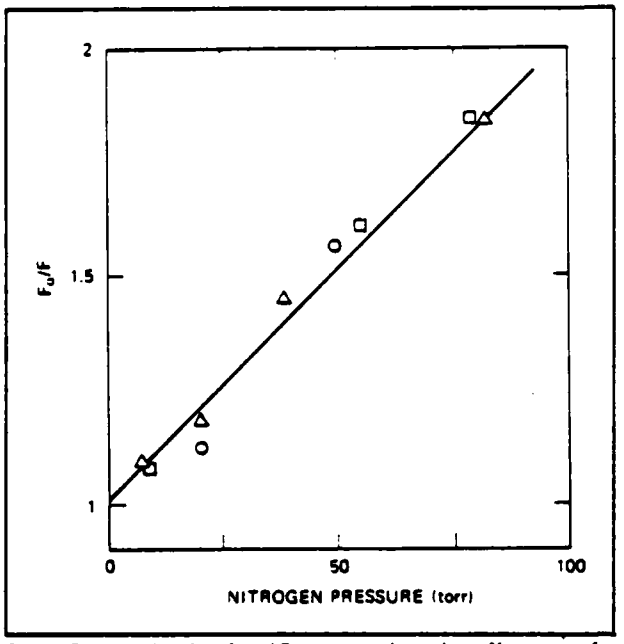

Fig. 8. Comparative plot of total fluorescence intensity vs N_2 pressure for CO $A^1\Pi$ excited to v' = 3. Data are shown for three separate runs. The ordinate ratio F_0/F, given by Eq. (13) in the text, is the fluorescence intensity without and with added N_2. The CO pressures are: circles and squares, 20.1 Torr; triangles, 23.8 Torr.

$B^3\Sigma_u^-$ state, upon addition of successively higher pressures of Ar, are seen. First rotational transfer occurs within the initially pumped v' = 4 level, and then the molecule undergoes vibrational relaxation with the population piling up largely in v' = 0 and 1.

The degree to which such thermalization within the excited state occurs depends on the relative rates of quenching Q and rotational (R) or vibrational (V) energy transfer. If Q << R, V, the molecule will relax before being quenched. However, if Q >> R, V, then the single level pumped by the laser will not be transferred before being quenched from the excited state. The resulting upper-state population distribution will be highly peaked and nonthermal, a situation that has been termed arrested relaxation, or frozen excitation. Studies made in flames indicate an intermediate situation, so that partial relaxation occurs. Fluorescence scans have been made after pumping several levels in OH, which show rotational[11,25] and vibrational relaxation,[26] and both effects were seen for a single level pump in CN.[5] The results on OH exhibit distinct state-dependent features[11,26]; that is, both the rate and magnitude of the transfer are dependent on the initial level pumped. These effects must be accounted for to obtain quantitative determinations of temperatures and concentrations from LIF measurements.[27] Thus, knowledge of state-to-state transfer propensities is needed for LIF diagnostic development, especially for the important OH molecule.

Such experiments are performed much in the manner illustrated in Fig. 9, using the spectral resolution necessary to distinguish rotational and, or vibrational levels, depending on which phenomenon is to be studied. Except at the lowest pressures, multiple collisions can occur (as evident in Fig. 9), and these effects must be incorporated into the data analysis to obtain true state-specific rates. In general, it is found that multiple-quantum ($|\Delta v|$ or $|\Delta J| > 1$) jumps can occur on single collisions although the probability falls off with increasing separation of the initial and final levels.

4.3. Polarization phenomena

Most laser radiation is linearly polarized; that is, its electric vector

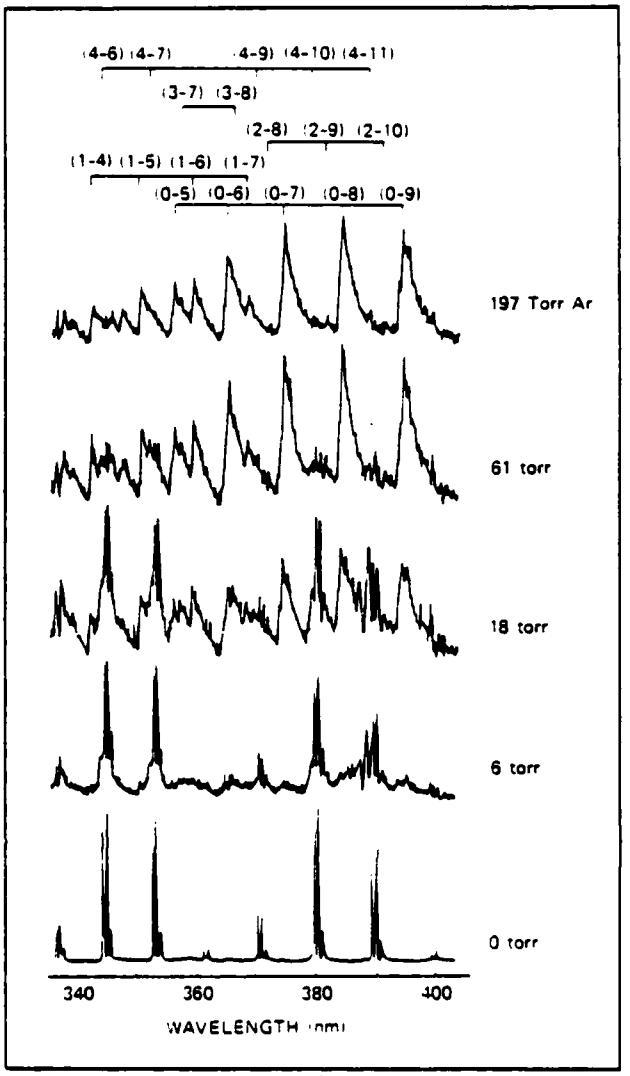

Fig. 9. Fluorescence spectra of S_2 $B^3\Sigma_u^-$ initially excited in v' = 4, J' = 41, at various pressures of added argon gas. As pressure is increased, rotational energy transfer first populates other J' levels in v' = 4, broadening the bands. At higher pressures, vibrational energy transfer populates other v' levels. Other bands with lower v' appear as those with v' = 4 decrease in intensity.

has a particular relationship to laboratory-fixed axes. This electric field interacts with the transition dipole moment in the molecule, which in turn bears a fixed relationship to the internal molecular axes. The result is that the excited-state molecule has a definite orientation in space (described quantum mechanically by a particular distribution over over m_J magnetic sublevels), and the fluorescent emission from the isolated molecule will have an anisotropic spatial distribution. This is manifested as a polarization of the fluorescence which varies with viewing direction. For a simple dipole oscillator this anisotropy is total; that is, no light is emitted in the direction of the original laser electric field. In the case of a molecule, the rotation reduces the degree of polarization. However, because the rotational angular momentum, which is a constant of the motion, bears a definite relationship to the molecular axes, a significant degree of polarization can remain.

If, as in a flame, collisions take place before the molecule emits, the degree of polarization will be reduced still further. Collisions

causing vibrational and rotational transfer can at the same time scramble the orientation; in addition, elastic depolarizing collisions (at a rate D) can alter the orientation of the molecule in space while leaving it in the initially pumped level. The degree of resulting polarization of light emitted by the pumped level is then governed by the ratio $D/(Q+V+R)$, while that of light emitted by collisionally populated levels is dependent on the amount of disorientation that occurs during such a process.

The first direct evidence of polarization of LIF in flames was obtained by the observation of apparent differences in rotational line strengths in OH,[28] in qualitative accord with earlier calculated predictions.[29] We have made measurements of the degree of polarization of OH LIF in the burnt gases of a series of methane/oxygen flames in N_2, Ar, or He diluent.[30] Surprisingly, the degree of polarization is very high, nearly that which would be found for a collision-free case; this indicates that $D << Q+R+V$. Even more surprising is the fact that the polarization of the fluorescence emitted by nearby levels populated by rotational energy transfer is also quite high; that is, such collisions alter the magnitude of the rotational angular momentum without randomizing its direction in space. Vibrational transfer collisions, on the other hand, scramble the orientation, in accord with a picture of attractive forces and long-lived collisions as the responsible factors. Polarization has also now been observed in OH with LIF under optical saturation conditions.[31]

Calculations[29,30] indicate that these effects are most pronounced when the fluorescence is rotationally resolved. Since P- and R-branches exhibit polarization opposite to that of the Q-branches, a sum over the entire band reduces these effects to a few percent.

5. CONCLUSIONS

In this paper we have attempted to provide a feel for the necessary experiments that make up the spectroscopic and collisional data base needed for quantitative detection of reaction intermediates in flames using LIF. Such research is being performed in our laboratory and elsewhere, and we reemphasize that this is not intended as a comprehensive review. This data base continues to grow, especially for OH and to a lesser degree for the other species listed in Table I. As noted earlier, it is important that the needs of the user community and the capabilities of the basic spectroscopic researchers be mutually communicated, so as to direct future efforts in this area as fruitfully as possible.

6. ACKNOWLEDGMENTS

The experiments described herein which were carried out in our laboratories were the result of collaboration with a number of colleagues. It is our pleasure to thank Tom Caughey, Irv Chidsey, Paul Doherty, Mark Dyer, Paul Fairchild, Russ Lengel, and Brian Sullivan for their invaluable contributions. We are also grateful for the support for this research, which is provided by the U.S. Army Research Office, the National Science Foundation, the Department of Energy, the Air Force Wright Aeronautical Laboratories, and the National Aeronautics and Space Administration.

7. REFERENCES

1. D. R. Crosley, J. Chem. Educ. 59, 446(1982).
2. D. R. Crosley, Opt. Eng. 20(4), 511(1981).
3. D. R. Crosley, Ed., *Laser Probes for Combustion Chemistry*, Amer. Chem. Soc. Symposium Series, Vol. 134 (Aug. 1980).
4. M. J. Dyer and D. R. Crosley, Opt. Lett. 7, 382(1982).
5. W. R. Anderson, L. J. Decker, and A. J. Kotlar, Comb. Flame 48, 179(1982); W. R. Anderson, J. A. Vanderhoff, A. J. Kotlar, M. A. Dewilde, and R. A. Beyer, J. Chem. Phys. 77, 1677(1982); J. A. Vanderhoff, R. A. Beyer, A. J. Kotlar, and W. R. Anderson, Comb. Flame 49, 197(1983).
6. P. W. Fairchild, G. P. Smith, and D. R. Crosley, 19th Symp. (Int.) on Combustion, 107(1982).
7. B. J. Sullivan, G. P. Smith, and D. R. Crosley, to be published.
8. R. N. Dixon, Philos. Trans. R. Soc. London A252, 165(1960).
9. P. W. Fairchild, G. P. Smith, and D. R. Crosley, to be published.
10. B. J. Sullivan, G. P. Smith, and D. R. Crosley, Chem. Phys. Lett. 96, 307(1983).
11. G. P. Smith and D. R. Crosley, 18th Symp. (Int.) on Combustion, 1151(1981).
12. D. R. Crosley and R. K. Lengel, J. Quant. Spectrosc. Radiat. Transfer 15, 579(1975).
13. D. R. Crosley and R. K. Lengel, J. Quant. Spectrosc. Radiat. Transfer 17, 59(1977).
14. I. L. Chidsey and D. R. Crosley, J. Quant. Spectrosc. Radiat. Transfer 23, 187(1980).
15. A. P. Baronavski and J. R. McDonald, Appl. Opt. 16, 1897(1977).
16. B. J. Sullivan and D. R. Crosley, Bull. Amer. Phys. Soc. 27, 882(1982).
17. R. K. Lengel and D. R. Crosley, Chem. Phys. Lett. 32, 261(1975); J. Chem. Phys. 68, 5309(1978).
18. H. M. Lin, M. Seaver, K. Y. Tang, A. E. W. Knight, and C. S. Parmenter, J. Chem. Phys. 70, 5442(1970).
19. P. W. Fairchild, G. P. Smith, and D. R. Crosley, Paper 82-004, Western States Meeting of the Combustion Institute, Livermore, Calif. (Oct. 1982); J. Chem. Phys. In press.
20. D. L. Holtermann, E. K. C. Lee, and R. Nanes, J. Chem. Phys. 77, 5327(1982).
21. D. R. Crosley, unpublished calculations.
22. D. Stepowski and M. J. Cottereau, Comb. Flame 40, 65(1981).
23. R. J. Cattolica, D. Stepowski, D. Puechberty, and M. Cottereau, Paper 82-41, Western States Combustion Meeting, Salt Lake City, Utah (April 1982).
24. T. A. Caughey and D. R. Crosley, J. Chem. Phys. 69, 3379(1978).
25. C. Chan and J. W. Daily, Appl. Opt. 19, 1357(1980).
26. G. P. Smith and D. R. Crosley, Appl. Opt., 22, 1428(1983).
27. D. R. Crosley and G. P. Smith, Comb. Flame 44, 27(1982).
28. D. Stepowski and M. J. Cottereau, J. Chem. Phys. 74, 6674(1981).
29. D. R. Crosley, to be published.
30. P. M. Doherty and D. R. Crosley, Bull. Amer. Phys. Soc. 27, 44(1982).
31. R. P. Lucht, N. M. Laurendeau, and D. W. Sweeney, Appl. Opt. 21, 3729(1982).

RATE CONSTANTS FOR USE IN MODELING

D. M. Golden and C. W. Larson
Department of Chemical Kinetics
SRI International, Menlo Park, CA 94025

ABSTRACT

The current status of quantitative understanding of reaction rate constant data for use in combustion mdeling is discussed. It is pointed out that simple bimolecular and unimolecular reactions can be tabulated as functions of various physically meaningful parameters over wide ranges of temperature and pressure. We also discuss the more complicated problems of complex surfaces and their manifestations. A major emphasis is on the underlying framework for critical evaluation of rate data.

We point out that currently used values for $2CH_3 \xrightarrow{k} + C_2H_5 + H$ are incorrect and that the temperature dependence of the branching ratio $H + N_2O \begin{cases} \rightarrow NH + NO \\ \rightarrow OH + N_2 \end{cases}$ can be understood as consequence of angular momentum conservation.

---

*This work was supported by the U.S. Army Research Office, Contract No. DAAG29-80-K-0049.

INTRODUCTION

Computer-based modeling of chemical reaction systems is becoming very common.[1] The computational frontiers are constantly being pushed ahead and greater numbers of scientists have taken advantage of standard codes that have been developed.

Many modelers and compilers of combustion kinetic data have developed the habit of abstracting the literature for the necessary model inputs without critical analysis. Unfortunately, given the great difficulty of performing and understanding experiments, values that are both suspect on physical grounds and internally inconsistent often find their way into the data base.

As these chemical models are adapted for larger systems, the need increases for an internally consistent method for critical evaluation of the rate constants that make up a given model, as well as for intercomparison of models. Rate constants must be correct not only in absolute magnitude at a given temperature, but also with respect to their temperature, pressure, and environmental (i.e., nature of the colliding partners) variations. Furthermore, since complex chemical mechanisms invariably contain competing steps and the branching ratios evolving from these competitions may carry the mechanism in distinctly different directions, it is crucial to have a consistent treatment of competing pathways.

This paper reviews the guidelines already well established[2] for a framework in which to evaluate rate data. We will also discuss those areas

where this framework needs further substantiation. In addition, we will present some development of the treatment of that increasingly ubiquitous class of reactions that appear to proceed via a bound intermediate.

It is our hope to enable modelers to have the courage, based on knowledge, to extend individual rate parameters for elementary chemical reactions and chemical mechanisms beyond the range of current measurement. Indeed, this is a modeling requirement since most of the kinetic laboratory studies are performed at temperatures less than 1000 K and most of the flame temperatures of interest are between 1200 and 2000 K.

GROUND RULES

Framework

The model for elementary reactions based on the transition state theory (TST) is discussed in most text books. The entirety of chemical reactions is limited to two basic classes: (1) Simple bimolecular reactions, such as described by the potential surface in Fig. 1(a), and (2) simple unimolecular reactions, such as described by the potential surface in Fig. 1(b).

The barrier, denoted by E, could be as small as zero, and often is. Reactions that follow pathways such as depicted in Fig. 1(b) are pressure and temperature dependent, and depend on the nature of the colliding partners, whereas those that follow potentials of the type in Fig. 1(a) are only temperature dependent. According to the principle of detailed balancing, bimolecular processes that are the reverse of a unimolecular decomposition are subject to exactly the same pressure and partner dependence. The complex surfaces (Figs. 1(c), 1(d), and 1(e)) are combinations of the simple surfaces and are discussed later in this paper.

Simple Bimolecular Reactions

In TST the thermal (canonical) rate constant is expressed in terms of a single parameter, $\Delta G^{\ddagger}_{T}$, , the free energy difference between transition state and reactants at the temperature T:

$$k = \frac{k_B T}{h} \exp\left(-\Delta G^{\ddagger}_{T} / RT\right) \qquad (1)$$

Choice of units for k implies choice of standard state for $\Delta G^{\ddagger}_{T}$. $\Delta G^{\ddagger}_{T}$ is a function of temperature. This, along with the explicit first power of T in the transition state formula, implies that over any reasonable temperature range the rate constant should be described by at least three parameters:

$$k = AT^{B} \exp(-C/T). \qquad (2)$$

It is clear that these parameters may be understood in terms of molecular models for reactant and transition state and the nature of breaking and forming bonds; thus, the parameters are subject to evaluative criteria beyond the bounds of any particular experiment. Furthermore, physically reasonable parameters should enable rate constants to be extrapolated beyond the measured temperature range.

The parameters most easily subject to evaluative criteria are A and B which are related to $\Delta S^{\ddagger}$ and $\Delta C^{\ddagger}_{p}$ and thus to reactant and transition state structure. The parameter C, related to $\Delta H^{\ddagger}$, requires potential surface information, but can often be judged based on comparison of similar reactions.

As has been stated many times previously, $\Delta S^{\ddagger}$ ab initio evaluation requires potential surface information, but limiting ranges can be deduced by chemical common sense, and comparison of homologous series forces a certain order.

As an example, consider the reaction:

$$O(^3P) + CH_4 \rightarrow OH + CH_3 \qquad (3)$$

This process has been well studied[3] up to ~ 2000 K from ~ 300 K. (Caution should be exercised concerning results from the low temperature experiments, since very small amounts of higher hydrocarbon impurities

would consume significant quantities of O-atoms.) This process has also been the subject of analysis by transition state theory[2d,3] and the agreement on rate constant parameters is universal:

$$[k/(cm^3\ mole^{-1}\ s^{-1})] = 10^{7.07}\ T^{2.08}\ \exp(-\ 3840/T) \qquad (4)$$

On an Arrhenius plot (ln k vs T^{-1}), this expression produces a strongly curved line that yields values of k at 2000 K that are a factor of ten higher than would have been predicted by extrapolation of a straight line, two-parameter, Arrhenius fit to the data in the 300 to 800 K range.

It would be inconsistent then, when considering the reaction $O(^3P) + C_2H_6 \rightarrow C_2H_5 + OH$, to use a two-parameter expression determined in the low temperature range. Consistency demands that a model transition state be described, based to some extent on $O + CH_4$, which, when its parameters are fit to the low temperature data, will automatically produce a curved Arrhenius plot that should be described with at least three parameters.

Of course, in a particular model study, the computed property of interest may not be sensitive to the curvature in the Arrhenius plot of any particular rate constant. Nevertheless, if the model is to be extrapolated to a different problem, the temperature dependences of the rate constants should be consistent with what is understood from TST.

Two sets of bimolecular rate constant parameters for the reactions of O-atom, hydroxyl radical and methyl radical with ethane have recently been tabulated as follows: (There are others in the literature as well.)

		Set I[4]			Set II[1]		
		A	B	C	A	B	C
(a)	$O + C_2H_6 \rightarrow OH + C_2H_5$	1.82E13	0	3070	1.5E13	0	3201
(b)	$HO + C_2H_6 \rightarrow H_2O + C_2H_5$	6.31E13	0	1812	8.7E9	1.05	911
(c)	$CH_3 + C_2H_6 \rightarrow CH_4 + C_2H_5$	5.5 E14	0	10820	5.5E-1	4.0	4167

The rate constants one calculates from each of these parameter sets agree to within a factor of two between 1000 and 2000 K. However, the direction of decrease of A-factors in parameter set I is inverted from the TST prediction. A-factors should decrease in this series of reactions in going from the atom to the diatom to the polyatomic species because the loss of rotational entropy accompanying formation of the series of transition states increases in this order. There are many examples in the modeling literature where relations among rate constant parameters of bimolecular reactions are inconsistent with simple TST constraints. In most cases where these constraints have been tested, they have been remarkably useful.[5]

Simple Unimolecular Reactions

Reactions that follow potential energy surfaces such as depicted in 1(b) may be described by the Lindemann mechanism:[6]

$$A + M \underset{-1}{\overset{1}{\rightleftharpoons}} A^* + M \qquad (5)$$

$$A^* \xrightarrow{2} \text{Products}$$

These reactions are always the result of energy transfer by collision of the reactant A with both gas M (step 1 and -1) and the spontaneous decomposition of the energized molecules (A^*).

In the so-called "high pressure limit", the unimolecular rate constant may be described by TST in the same manner as were bimolecular reactions; values of the A-factors and activation energy may be evaluated by consideration of the changes that occur upon formation of the transition state from the reactants. In general, the temperature dependence of the rate constant may also be represented by three parameters, but often two will suffice (see Fig. 3). Reverse bimolecular association processes may always be computed from the overall equilibrium constant. Adequate representation of the temperature dependence of the equilibrium constant will usually require at least three parameters as ΔC_p for the reactions is not usually zero.

The unimolecular reactions of interest may not be at their "high pressure limits", because spontaneous reaction of energized reactant (process 2) might be much faster than the collisional energizing process; thus, at lower pressures an equilibrium population would not be maintained. Under this condition canonical TST does not apply and the rate constant for unimolecular dissociation (and the reverse bimolecular association) becomes pressure dependent (fall-off).

According to standard unimolecular rate theory,[6] the observable rate constant $k_{uni}(T,M)$, may be evaluated by averaging the microcanonical specific rate of spontaneous decomposition of energized reactant, k(E), over the appropriate non-equilibrium distribution function:

$$k_{uni}(T,M) = \int_0^\infty k(E) \frac{\omega}{\omega + k(E)} B(E)\, dE \qquad (6)$$

The effective rate of strong collisions of reactant with bath gas is denoted by ω, and B(E) is the normalized Boltzman distribution of reactant.

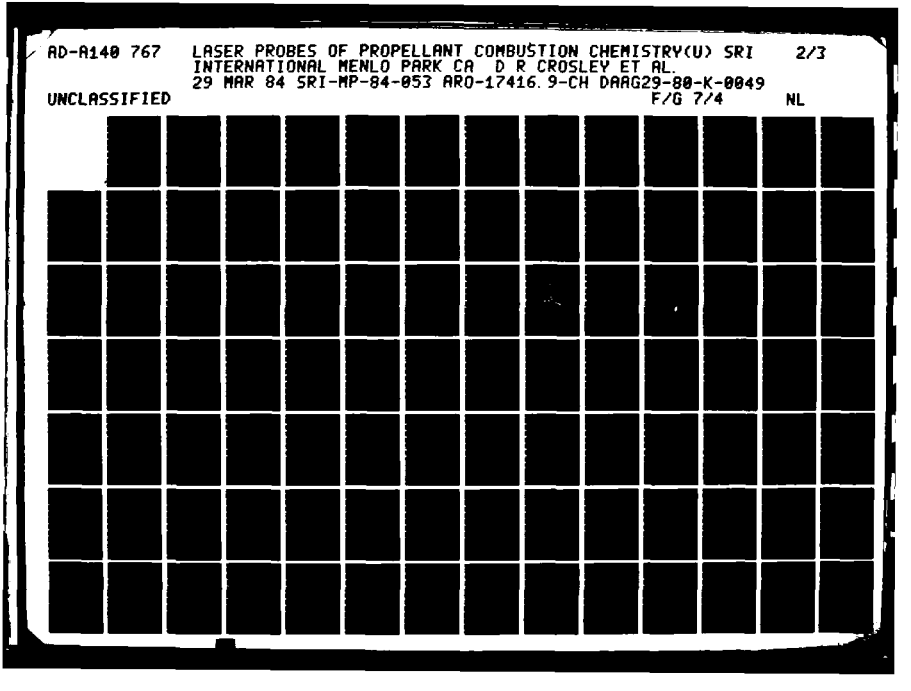
AD-A140 767 LASER PROBES OF PROPELLANT COMBUSTION CHEMISTRY(U) SRI 2/3
INTERNATIONAL MENLO PARK CA D R CROSLEY ET AL.
29 MAR 84 SRI-MP-84-053 ARO-17416.9-CH DAAG29-80-K-0049
UNCLASSIFIED F/G 7/4 NL

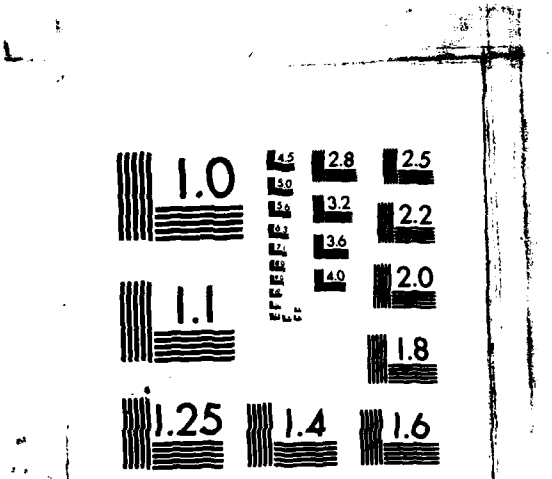

The microcanonical rate constant, k(E), may be evaluated quantum statistically (RRKM theory) but simpler approximations of the pressure dependence will usually suffice for modeling purposes (see below).

In Fig. 2, actual "fall-off" curves for butane and octane at 1000 K (on a reduced basis) are compared with the Lindemann fall-off curve. The Lindemann fall-off curve, obtained by solution of the three differential rate equations of the Lindemann mechanism, has a particularly simple form explicit in pressure, viz.,

$$k_{uni}^{Lindemann}/k_\infty = (1 + k_\infty/k_o M)^{-1} \qquad (7)$$

The constants, k_o and k_∞ , are functions only of temperature; $k_o M$ and k_∞ are the actual values of the unimolecular rate constant in the low-pressure ($M \to 0$) and high-pressure ($M \to \infty$) limit. The temperature dependence of k_o and k_∞, shown in Fig. 3 for a variety of hydrocarbon fuel pyrolysis reactions, may be represented adequately by three-parameter expressions of the same form as has been used for simple bimolecular reactions, equation (2).

Troe[7] has demonstrated that accurate empirical relationships between the Lindemann and actual fall-off curves exist, viz.,

$$k_{uni}^{actual}(T,M) = k_{uni}^{Lindemann}(T,M) \quad F(T,M) \qquad (8)$$

Troe shows that the "broadening factor", F(T,M), may be written in a variety of universal pressure explicit forms of varying accuracy, the most simple of which is:

$$\log F(T,M) = 1 - (\log k_o M/k_\infty)^{2\,-1} \quad \log F_c(T). \qquad (9)$$

In all of Troe's pressure explicit forms, the temperature dependence of F(T,M), is carried entirely by $F_c(T)$, the broadening factor at the center of the fall-off, Fig. 3.

Fig. 4 shows $F_c(T)$ for a variety of fuel pyrolysis reactions; $F_c(T)$ may be adequately described by a three parameter function, viz.,

$$F_c(T) = a \exp(-b/T) + \exp(-T/c). \qquad (10)$$

This is slightly different than suggested by Troe. In the limits of zero or infinite temperature or pressure, all unimolecular reactions approach Lindemann behavior and $F_c(T)$ and F(T,M) approach unity.

Values of the broadening factor in regimes of pressure and temperature relevant to combustion processes (e.g., 1-atm and 1000 K to 2000 K) are unity for all small molecule fuels with energy thresholds around 100 kcal mol^{-1} (e.g., CH_4, NH_3, CH_2O) because unimolecular pyrolysis for these small molecules (a process important to initiation of combustion) is in its low pressure limit, $k_{uni} = k_o M$, Fig. 5. Pyrolysis of larger molecule fuels (with thresholds around 80 kcal/mol^{-1}, e.g., butane and larger molecules) also have unity broadening factors because $k_{uni} = k_\infty$. At 1-atm pressure and 1500 K, ethane pyrolysis is at the center of the fall-off, and its center broadening factor, also the maximum braodening factor, is around 0.2.

It seems proper then to take into account our physical understanding of these processes by tabulating data for modeling purposes to be consistent with Troe's expressions. We suggest, in complete analogy to the tabulation of pressure-dependent association reactions by the NASA Stratospheric Rate Constant Evaluation Panel, that for a given reaction, values of the two sets of three parameters that will describe k_∞ and k_o, as well as

the three parameters that are defined in equation (10), be tabulated. These nine parameters used with equations (8) and (9) describe k(M,T) for the process well enough for the modeling exercise. It must be reiterated that these formulae allow cosiderable extrapolation far from the reported conditions.

Complex Elementary Processes

In its simplified form a chemical mechanism consists of a number of sequential and consecutive elementary reactions. It is usual to treat these independently in a model, describing each with k(T) or k(P,T) as appropriate (see previous discussion). There are, however, some oft-occurring instances in which elementary reactions cannot be separated in the usual way. Consider the reaction proceeding along the surface depicted in Fig. 1(c). (The barriers E_1 and/or E_2 may be as low as zero.) Such a surface describes three processes: the unimolecular decomposition of substance Y via two pathways, the bimolecular reaction of A and B to form C and D (and possibly Y), or the reverse bimolecular reaction. In each case different non-thermal energy distributions (Chemical Activation) may obtain and simple canonical TST is not applicable. However, if the pressure is sufficiently high so that substance Y is present in thermal equilibrium, the competing unimolecular processes

$$Y \overset{1}{\rightleftharpoons} A + B \qquad (11)$$

$$Y \overset{2}{\rightleftharpoons} C + D \qquad (12)$$

may be separately described by their respective k_∞ values, or the bimolecular process,

$$A + B \rightarrow C + D, \tag{13}$$

can be written as the sum of the two reactions

$$A + B \longrightarrow Y \tag{14}$$

$$Y \longrightarrow C + D \tag{15}$$

It is important to recognize that these simplifications do not apply for nonthermal distributions where the lifetime of Y is pressure dependent![2d] In these cases the rate constants k_1, k_{-1}, and k_2 must be specified at the microcanonical level and the overall rate constant and branching ratios are pressure as well as temperature dependent.

For example, for the overall bimolecular reaction between methyl radicals,

$$CH_3 + CH_3 \xrightarrow{k_{bi}} C_2H_5 + H, \tag{16}$$

We may depict this process by the scheme:

$$CH_3 + CH_3 \underset{k_1}{\overset{k_{-1}}{\rightleftharpoons}} C_2H_6^* \xrightarrow{k_2} C_2H_5 + H \tag{17}$$

$$C_2H_6^* \xrightarrow{k_3[M]} C_2H_6$$

Under conditions where $k_2(E) \ll k_1(E)$, which apply here since the overall process is ten kcal mol^{-1} endothermic, it is easily shown[6] that at all pressures $k_{bi} = K_{eq}\, k_2^\infty$ where K_{eq} is the overall equilibrium constant. Thus, we have a simple means of including experimental determinations of

k_{bi}, since all the appropriate values of molecular parameters required to know k_2^{∞} and K_{eq} are known or can be easily estimated.

Production of H-atoms by the methyl-methyl reaction has been advocated as an important contributor to the dominant pathways in methane combustion. The temperature dependence of the rate constant used in current modeling[1,4] ($10^{14.9}$exp - 26.5/RT cm^3 mol^{-1} sec^{-1}) is in substantial disagreement with our calculation ($10^{11.3}$ exp - 10.0/RT) which agrees with new experimental evidence.[8] Thus, although the absolute value of the rate of the methyl-methyl reaction currently in use is correct at 1000 K, it is a factor of 16 too large at 1500 K and 64 too large at 2000 K. The consequences of this observation may impact strongly on the methane combustion model, especially at higher temperatures, where initiation and H-atom propagation reactions dominate the properties of the youngest parts of a flame.

When complex surfaces, such as depicted in Fig. 1(c) give rise to situations in which $k_2(E) \approx k_1(E)$, the overall reaction may exhibit pressure as well as temperature dependence. The temperature dependence can easily give rise to a negative activation energy if the ratio $k_1(E)/k_2(E)$ increases with temperature.[2d] At this writing we have no simple suggestions as to general tabulation of the data concerning these processes.

Multi-Channel Bimolecular Processes-Branching

The potential energy surface shown in Fig. 1(d) is the result of recent state-of-the-art theoretical calculation for the H + N_2O system[9] and exemplifies a class of multi-channel bimolecular processes with branching that are common in combustion chemistry.

The kinetics of the overall bimolecular reactions, viz.,

$$H + N_2O \xrightarrow{k_{bi2}} OH + N_2 \qquad (i8)$$

$$H + N_2O \xrightarrow{k_{bi3}} NH + NO \qquad (19)$$

may be deduced through analysis of the unimolecular reactions of intermediate HNNO.

Measures of the branching ratio, $R = k_{bi3}/k_{bi2}$, have been inferred at ~2000 K by direct observation of laser induced fluorescence from HN and OH in a H_2/N_2O flame and at 873 K in a static system.[10] The weak temperature dependence of R ($R_{2000K} \sim 0.04$ and $R_{873K} \sim 0.004$) yields an apparent activation energy difference of only about 7 kcal/mol^{-1}, less than half the difference between the critical energy thresholds of the branches, 17 kcal/mol^{-1}. Fig. 1(d).

The modeling of the observation of the very weak temperature dependence of branching requires use of a hindered Gorin model transition state for reaction channel 3. Properties of the hindered Gorin model have been studied in the past[11] in connection with radical-radical recombinations and their reverse unimolecular bond scission. Thus, considering channel 3 from the point of view of the NO + NH interaction, the system geometry is characterized as a prolate symmetric top as the N-N interfragment distance decreases. The minor external rotational degree of freedom of this symmetric top is active and strongly coupled to the internal rotation about the N-N axis; its moment of inertia does not change as the N-N distance

decreases. By contrast, the two major external rotational degrees of freedom are adiabatic. Their moments of inertia decrease drastically with decreasing interfragment distance.

It has been customary to evaluate the effect of momentum conservation constraints by use of the quasi-diatomic model.[6] Thus, an "effective" potential energy surface may be defined at any given temperature which conserves the overall rotational quantum number, Fig. 1(e). On this surface, the dissociation energy of HNNO is less than its value at the absolute zero by the amount $(I^+/I - 1)RT$, where I^+/I is the ratio of the moments of inertia of activated complex to molecule. In addition to this temperature dependent centrifugal energy effect, a temperature dependent hindrance parameter, η, causes the entropy of the transition modes in the hindred Gorin model to decrease with temperature.[11] In this case the transition modes are the two overall rotations in the separated diatomics which become hindered internal rotors in the activated complex.

The empirical Gorin model hindrance parameter, is defined in terms of a ratio of A-factors, $A_H/A = (100 - \eta)/100$, where A_H and A are A factors for the hypothetical high pressure unimolecular reaction for the hindred and unhindered model.

In the case of the Channel 3 reaction, a hindrance parameter that varies between 84 and 99% (1000 K-2000 K) has been required to fit the observed branching ratio, k_{bi3}/k_{bi2}. The radical-radical interactions modeled in the past have also required values between 85 and 99.5% (220 K-1200 K). Thus, the ideas embraced by the hindered Gorin model, with $A_H/A \sim 0.2$ to 0.005, are appropriate for description of reactions involving simple bond fission. The consequence of use of the hindered Gorin model to

predict the pressure and temperature dependence of k_{b13} is to produce a nearly pressure independent Arrhenius plot whose activation energy and A-factor decrease with increasing temperature.

CONCLUSIONS

This work is meant to exemplify the current status of the overview that is applicable to the critical evaluation of chemical rate data for combustion modeling. Specifically:

1. Simple bimolecular reactions should all be tabulated as a function of temperature alone. Three parameters are required. The parameters should be evaluated keeping in mind the relative values of appropriate physical quantities, such as $\Delta S^{\ddagger}$, $\Delta H^{\ddagger}$, and $\Delta C_p^{\ddagger}$.

2. Simple unimolecular reactions should be tabulated as a function of temperature and pressure. It is convenient to characterize the temperature dependence of both high and low pressure-limiting rate constants by three parameters. The fall-off curve can then be reproduced by a parameterization due to Troe that requires three additional parameters.

3. Complex surfaces must be recognized and apparent bimolecular processes must be distinguished from simple bimolecular processes. The possibilitiues for both pressure dependence and negative activation energies for the former must be accounted for correctly. A simple formalism is not yet available. Each process needs to be considered in some detail.

4. The existence of multi-channel surfaces must be taken into account. It appears that appropriate branching ratio calculations will require use of models that take into account angular momentum conservation restrictions. A simple formalism for expressing these reaction rate constants is not yet available. Each process needs to be considered in some detail.

5. We have bypassed discussion of the important problem of energy transfer. Collisional rate constants and their temperature dependences must be expressed terms of the average energy transferred per collision.[12] In general, only empirical relationships currently exist.

REFERENCES

1. Westbrook, C. W. and Dryer, F. L.: Prog. Energy Comb. Sci. (in press).

2. (a) Benson, S. W.: Thermochemical Kinetics, 2nd Ed., John Wiley and Sons, Inc., 1976.
   (b) Golden, D. M.: Fourteenth Symposium (International) on Combustion, p. 121, The Combustion Institute, 1973.
   (c) Golden, D. M.: Dynamics and Modeling of Reactive Systems, (W. F. Stewart, W. H. Ray, C. C. Conley, Eds.), p. 315, Academic Press, 1980.
   (d) Golden, D. M.: J. Phys. Chem. 83, 108 (1979).

3. Michael, J. V., Keil, D. G., and Klemm, R. B.: Int. J. Chem. Kinetics 15, 705 (1983), and references therein.

4. Levy, J. M. and Sarafim, A. F.: Combustion and Flame 53, 1 (1983).

5. (a) Cohen, N.: Int. J. Chem. Kinetics 14, 1339 (1982).
   (b) Cohen, N.: Nineteenth Symposium (International) on Combustion, p. 31, The Combustion Institute, 1983.

6. (a) Forst, W.: Theory of Unimolecular Reactions, Academic Press, 1973.
   (b) Robinson, P. J., and Holbrook, K. A.: Unimolecular Reactions, John Wiley and Sons, Inc., NY, 1972.

7. (a) Troe, J.: J. Phys. Chem. 83, 114 (1979), and references therein.
   (b) Troe, J.: Ber. Bunsenges. Phys., Chem. 87, 167 (1983).

8. Keifer, J. H. and Budach, K. A.: Int. J. Chem. Kinetics 16, 0000 (1984).

9. Melius, C. F. and Binkley, J. S.: Private communication (1983).

10. (a) Cattolica, R., Snooke, M., Dean, A.: A Hydrogen-Nitrous Oxide Flame Study, Paper presented at the 1982 Fall Meeting of the Combustion Institute, Sandia National Laboratories, Livermore, CA, 11-12 October 1983, Paper WSS/CI 82-95.
    (b) Baldwin, R. R., Gethin, A., Plaistowe, J., Walker, R. W., Trans. Faraday Soc. I, 6, 1265 (1975).

11. (a) Smith, G. P. and Golden, D. M.: Int. J. Chem. Kinetics 10, 489 (1978).
    (b) Baldwin, A. C., Lewis, K. E., and Golden, D. M.: Int. J. Chem. Kinetics 11, 529 (1979).

12. Barker, J. R.: J. Pys. Chem. 88, 0000 (1984).

FIGURE CAPTIONS

Figure 1 Schematic potential energy surfaces for:

(a) simple bimolecular,

(b) simple unimolecular, and

(c) complex elementary processes at zero degrees Kelvin. Processes without barriers (E = 0) at OK are constrained at higher temperatures to follow surfaces which allow momentum conservation.

Figure 2 Comparison between actual fall-off and Lineman fall-off, on a reduced basis: reduced pressure = $P_r = k_o M/k_\infty$ and reduced rate constant = $k_r = k_{uni}/k_\infty$. At the center of the fall-off, $P_r = 1$, $k_r^{Lindeman} = 0.5$, and $F_c = 0.5/k_r^{actual}$.

Figure 3 Temperature dependence of k_o and k_∞ for several fuel pyrolysis reactions.

Figure 4 Temperature dependence of the center broadening factor for several fuel pyrolysis reactions.

Figure 5 The pressure at the fall-off center, P_c, as a function of temperature for several fuel pyrolysis reactions and the combustion window, 1-10 atm and 1000 - 2000 K. Around 1 atm pressure, butane and larger molecular pyrolyze near their high pressure limit and methane and smaller molecular pyrolyze in their low pressure limit.

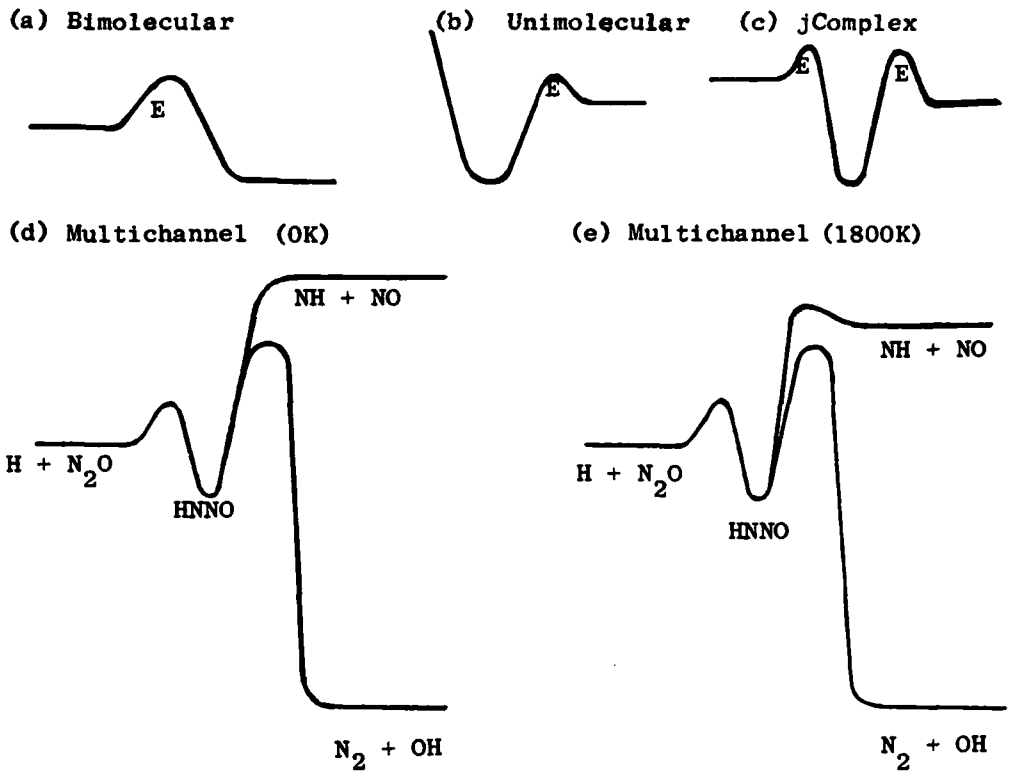
(a) Bimolecular
E
(b) Unimolecular
E
(c) jComplex
E
E
(d) Multichannel (0K)
NH + NO
H + N2O
HNNO
N2 + OH
(e) Multichannel (1800K)
NH + NO
H + N2O
HNNO
N2 + OH

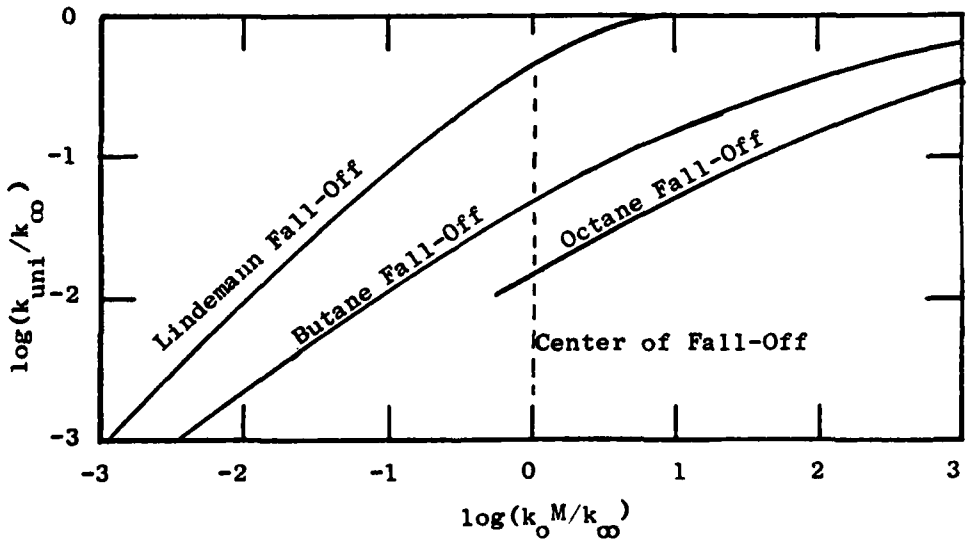
0
-1
-2
-3
log(kuni/k∞)
Lindemann Fall-Off
Butane Fall-Off
Octane Fall-Off
Center of Fall-Off
-3
-2
-1
0
1
2
3
log(koM/k∞)

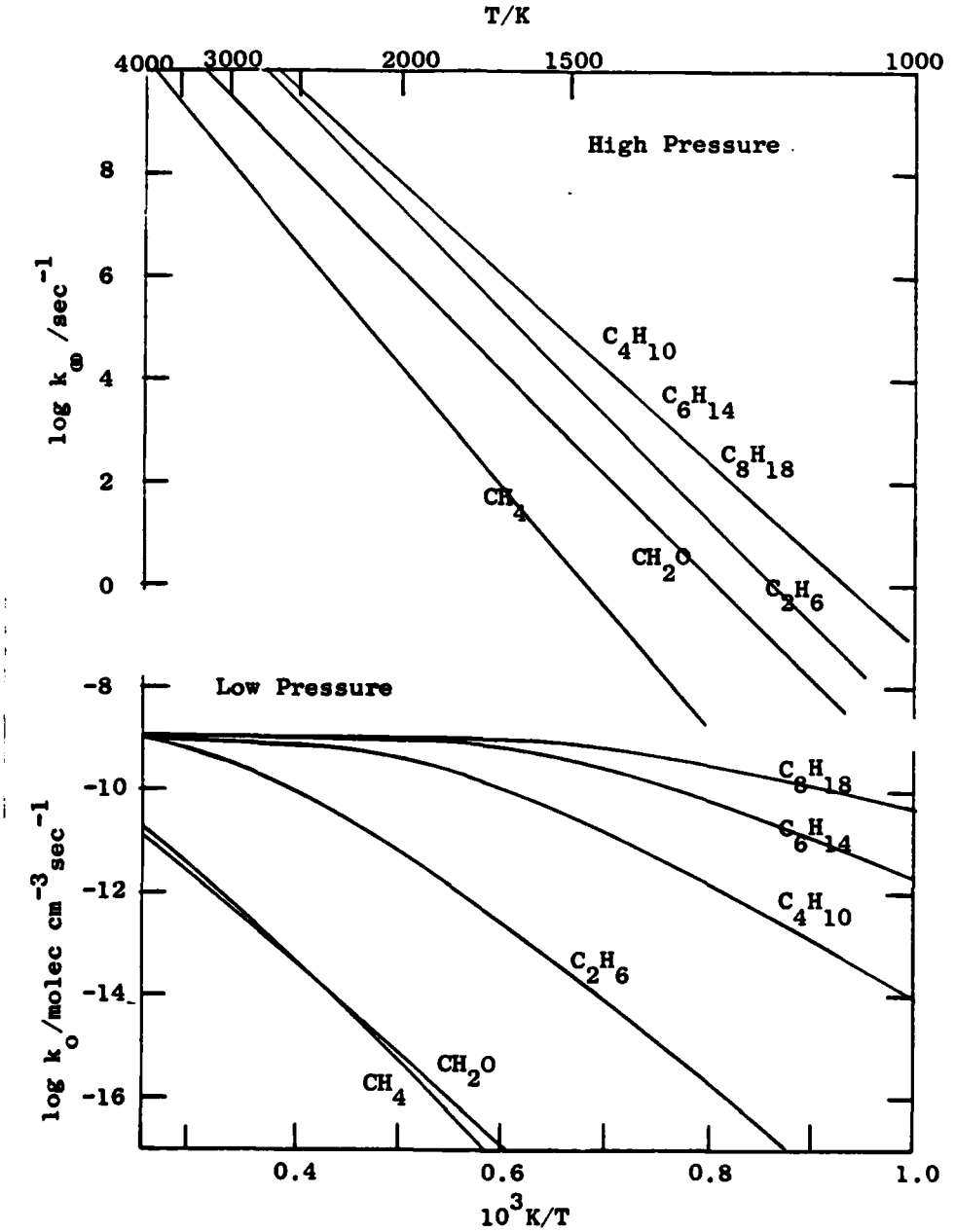
T/K
4000
3000
2000
1500
1000
High Pressure
log k∞ /sec-1
8
6
4
2
0
C4H10
C6H14
C8H18
CH4
CH2O
C2H6
Low Pressure
-8
-10
-12
-14
-16
log k0 /molec cm-3 sec-1
C8H18
C6H14
C4H10
C2H6
CH2O
CH4
0.4
0.6
0.8
1.0
10^3 K/T

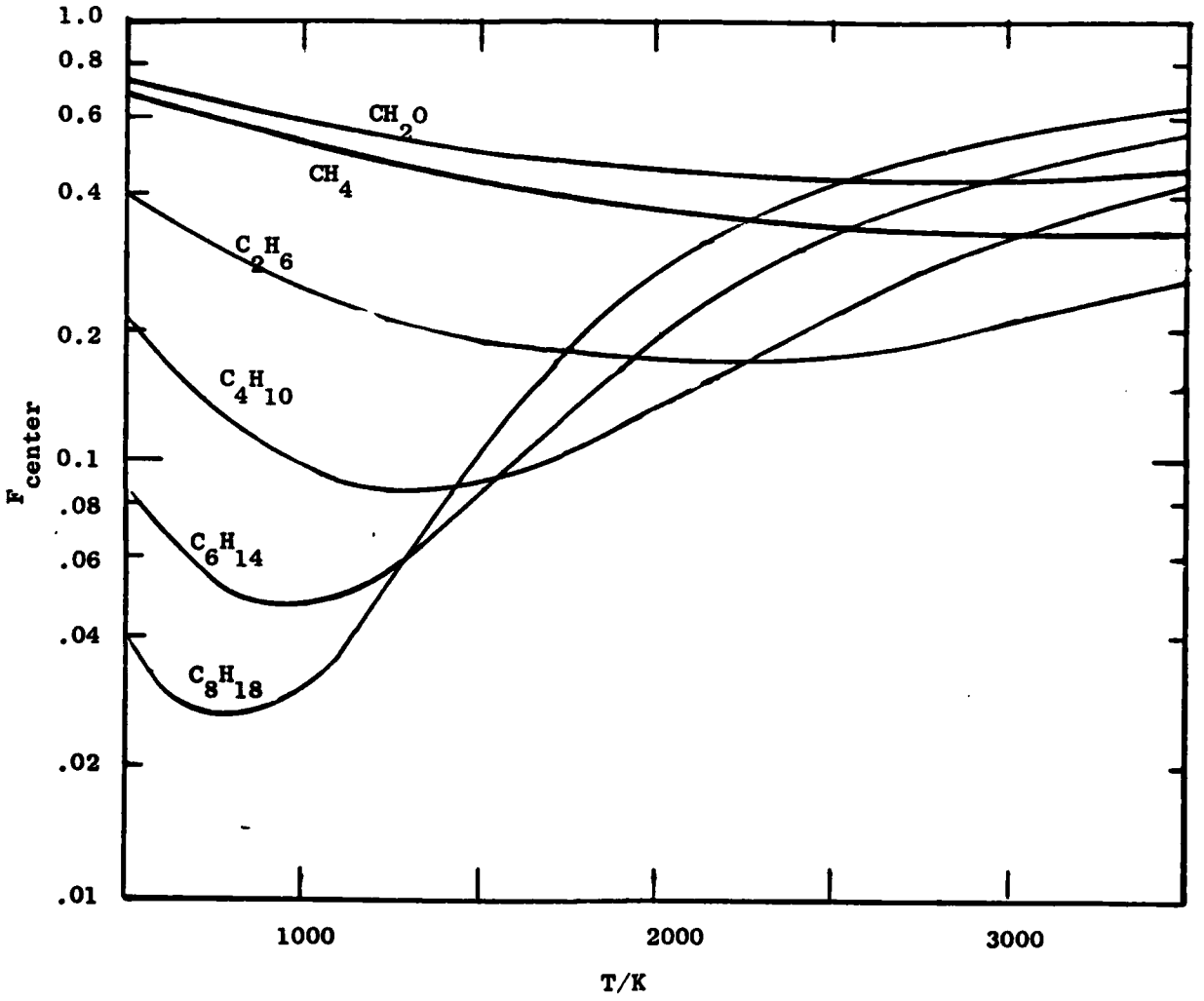
1.0
0.8
0.6
0.4
0.2
0.1
.08
.06
.04
.02
.01
F_{center}
CH_2O
CH_4
C_2H_6
C_4H_{10}
C_6H_{14}
C_8H_{18}
1000
2000
3000
T/K

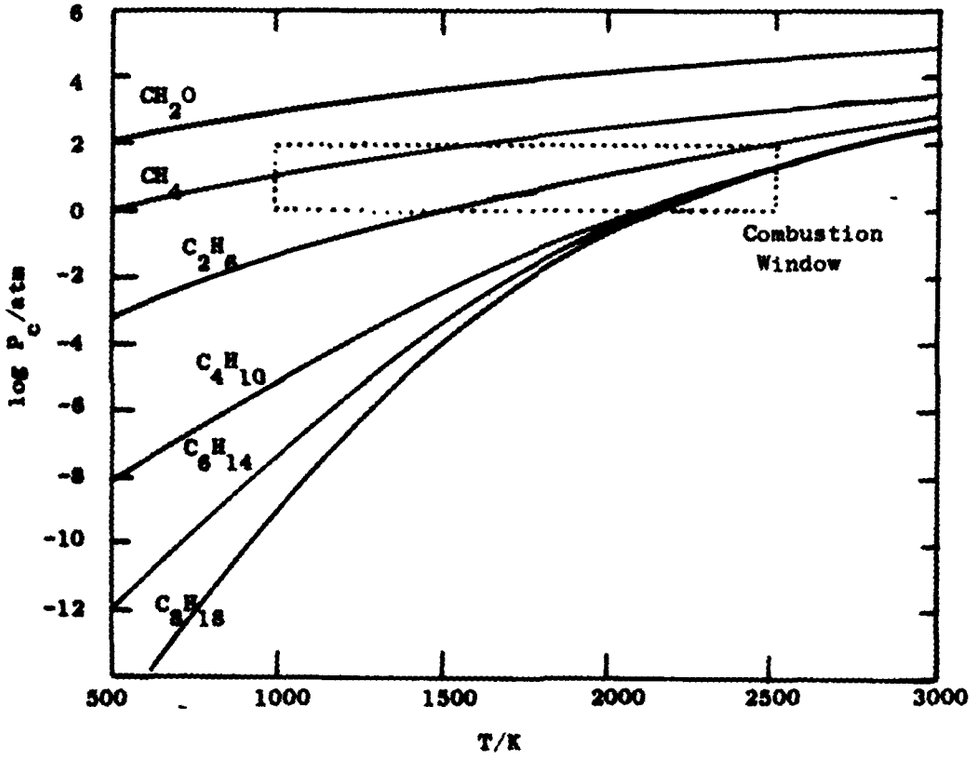
6
4
2
0
-2
-4
-6
-8
-10
-12
log P_c/atm
CH_2O
CH_4
C_2H_6
C_4H_{10}
C_6H_{14}
C_8H_{18}
Combustion
Window
500
1000
1500
2000
2500
3000
T/K

LASER-INDUCED FLUORESCENCE SPECTROSCOPY OF NCO AND NH_2 IN ATMOSPHERIC PRESSURE FLAMES

Richard A. Copeland, David R. Crosley and Gregory P. Smith
Chemical Physics Laboratory
SRI International
Menlo Park, California 94025

Laser-induced fluorescence (LIF) is a powerful method for the sensitive detection of trace species in flames, so as to gain insight into the combustion chemistry mechanisms. However, LIF has been applied almost exclusively to diatomic radicals whereas the chemical networks contain many species of larger size whose presence can signal definite mechanistic paths. We describe here a comprehensive survey of the LIF spectroscopy of the NCO molecule in a CH_4/N_2O flame and the NH_2 molecule in NH_3/N_2O and NH_3/O_2 flames, all burning rich at atmospheric pressure. NCO was excited in the B-X and A-X systems in the ultraviolet and blue, respectively; the latter is much more intense and can be more easily made free of strong interfering transitions due to diatomics. NH_2 was excited in the $\tilde{A} - \tilde{X}$ transition. Excitation and fluorescence wavelengths furthest to the red minimize background interference due to underlying, unidentified absorption features and flame emission. Prescriptions for detecting these two species are presented, including a table of excitation and detection wavelengths, as well as some general conclusions which should be useful in extending flame LIF detection to other triatomic and larger radicals.

MP84-005

Introduction

Laser-induced fluorescence (LIF)[1] is the member of the family of laser spectroscopic probes[2,3] best suited for the detection of trace radical species in combustion systems. It possesses high sensitivity and selectivity coupled with spatial and temporal resolution and a non-intrusive nature. Such information is valuable for obtaining qualitative insight into the mechanisms of the combustion chemistry, and provides sensitive data for comparison with quantitative predictions from detailed computer models of that chemistry in simple laboratory flames.

Consider as the atomic constituents of naturally occuring fuels H, C, N, O and S. All of these atoms and the 15 diatomic molecules formed from them have been observed by LIF in low pressure discharge flows or static cells, and two of the atoms plus ten of the diatomics have been detected in flames by LIF (for the atoms, and H_2, N_2 and CO one must use two-photon excitation because their first absorption bands lie in the vacuum ultraviolet). However, only a few of these diatomics have yet been meaningfully fit into chemical kinetic schemes, and the flame chemistry involves many larger radicals as well.

Therefore it is important to extend LIF flame detection capability to larger species. Of the 35 triatomics which can be formed from these atoms (not counting the chemically and spectroscopically distinct isomers such as CCN and CNC), 14 have been observed in LIF in cells or flows and another 13 are definite or possible candidates on spectroscopic grounds. However, only four have been detected by LIF in flames. SO_2[4] and NO_2[5] have been detected over wide wavelength regions but in each case the complexity of the absorption spectrum and the laser wavelengths and bandwidth used resulted in near-continuum-like excitation precluding definitive spectroscopic assignment.

NCO[6] has been cleanly excited and studied, via the coincidental overlap of one of its absorption lines with one of the fixed-wavelength lines of an Ar^+ laser. NH_2, with a well-known LIF signature under low pressure conditions, has escaped LIF detection in atmospheric pressure flames in previous experiments in this laboratory as well as elsewhere,[7] although unpublished results indicate it can be excited weakly with the frequency-doubled line of a Nd:YAG laser.[8] However, while it can be very convenient, such fixed-frequency excitation does not permit optimization of detection under a variety of conditions including potential intefering absorptions, and cannot be relied on as general for other molecules. NH_2 has also been detected in atmospheric pressure flames by absorption of laser radiation directly[9] and optoacoustically[10] but these methods do not have the pointwise spatial resolution attribute of LIF.

We have performed a survey of the LIF spectroscopy of the NCO and NH_2 molecules in atmospheric pressure flames, using lasers and detection systems tunable over a wide range of wavelengths. The burners and gas mixtures were chosen to optimize conditions for the spectroscopic studies, but the detection strategies developed can be later used on burners better suited for obtaining profiles for comparison with theoretical models.

NCO and NH_2 were chosen for study for two reasons. One is the existence of considerable spectroscopic information from previous studies, both in conventional spectroscopy and LIF experiments. This has not only facilitated initial detection but also permitted more general conclusions and extensive comparison. (In this connection, it is noteworthy that <u>all</u> the species, regardless of size, which have been detected by LIF were first studied spectroscopically in flame or plasma discharge emission or in flash photolysis absorption.) On the other hand, the use of LIF in flames has provided new

spectroscopic information for NCO not previously attainable, as described below.

The other reason is the intrinsic potential importance of these radicals in certain combustion chemical networks. NCO has been postulated as an intermediate in the formation of NO_x from fuel-nitrogen[11] and was found to be present in copious quantity in CH_4/N_2O flames,[6] pertinent to nitramine combustion. NH_2 has been suggested as an intermediate in the production of prompt-NO[12] and in the ammonia de-NO_x process.[13]

We present here a description of our experiments. Because of the large amount of data on excitation and fluorescence spectra involved, we can include only a condensed version of the results. We hope that this will serve as an adequate guide to LIF detection of these two species in combustion experiments in other laboratories. In addition, we plan to assemble later in report form[14] a LIF spectroscopic atlas of the wavelength regions covered in these flames, including excitation of several diatomics whose fluorescence must be filtered out. We include some general observations from the experiments which we hope will prove useful in extension of LIF detection in flames to other triatomics and larger molecules.

Experimental set-up

Several burners were tried: a McKenna products porous plug burner, a small flat flame burner with 1 mm holes in the surface, a glassblowing torch, and a knife-edge slot burner patterned after a design explicit for laser probing.[15] This last burner, which presents a saddle-point-shaped flame and easy laser beam access underneath the reaction zone, proved the easiest to use and provided the largest signals for these spectrocopic experiments. The

flames were run rich, so as to yield larger quantities of the oxygen-poor or oxygen-free radicals of interest. The relative flow rates used in most of the experiments were: $CH_4 : N_2O : N_2 = 1.0:3.5:2.7$; $NH_3:N_2O = 5:3$; $NH_3 : O_2 = 2:1$.

The first step in each case was measurement of the emission spectrum of each flame. In addition to the spectroscopic overview provided, this served two specific purposes. The first was the selection of gas mixtures yielding strong radical emission (the ground and excited state radical concentrations are not necessarily proportional but this was a useful guide). The second was the choice of detection wavelengths minimizing interference and noise from flame emission. In the case of CH_4/N_2O, no NCO emission could be seen but there were clearly favorable regions between different vibrational sequences of the CH, CN and C_2 emission. The NH_3/N_2O spectrum, apparently not previously described, was similar to that of the NH_3/O_2 flame, and consisted of OH, NH and NH_2 bands, with the NH_2 about half as strong, compared to the diatomics, for the N_2O-based flame as in the O_2-based flame. Here, the potential interference is NH_2 itself (and perhaps unassignable NO_2 underneath); the spectra suggest it is minimized as one operates furthest to the red.

The LIF arrangement was standard, with the laser beam passing through the movable burner and the fluorescence focussed at right angles onto a spectrometer, sometimes filtered with colored glass. An XeCl-pumped dye laser with typical pulse energy $E_\ell \sim 3$ mJ, bandwidth $\Delta\tilde{\nu}_\ell \sim 0.3$ cm^{-1} and repetition rate $r_\ell \sim 100$ Hz was used for the blue (A-X) NCO excitation, and a Nd:YAG-pumped dye laser ($r_\ell = 10$ Hz) was used in the fundamental ($E_\ell = 30$ mJ, $\Delta\tilde{\nu}_\ell = 0.15$ cm^{-1}) for NH_2 and frequency-doubled ($E_\ell = 1$ mJ, $\Delta\tilde{\nu}_\ell = 0.25$ cm^{-1}) for NCO B-X. The pulse length of each laser was 10 nsec, and the signals followed the laser in time. A 0.35 m spectrometer with

dispersion 22 Å/mm and cooled EMI 9558 Q photomultiplier were used for NCO A-X; the slit was aligned parallel to the laser beam. A 0.75 m spectrometer (11 Å/mm) and uncooled 9558 or red-sensitive RCA 31034A photomultiplier were used for NCO B-X and NH_2; here the beam and slit were perpendicular.

The photomuliplier signal was amplified a factor of 100 using a Pacific video 2A50 preamp (50 Ω in and out) and fed to a gated boxcar integrator with a 20 nsec gate. This mode of fast pulse operation was always preferable and often essential to maximize the LIF to background emission ratio, in comparison with higher input impedance (e.g., 1MΩ) and a longer gate (1 μsec). Even so, care had to be taken to keep the photomultiplier operating voltage low enough that the tube did not saturate under the continuous flame emission current. An oscilloscope proved useful for signal searching and monitoring. The boxcar output was then fed to a scanning stripchart recorder. The laser beam energy was continually monitored in a second boxcar channel.

During some of the NH_2 runs, where absorption due to unidentified bands and/or species appeared present, a half-inch microphone was mounted near the burner to optoacoustically[10] monitor the total absorption.

NCO radical

The NCO LIF spectrum over the range of one laser dye is illustrated in Figure 1. The top two scans are noise-free at this sensitivity, and concomitant excitation of CH, CN and C_2 in this region is not seen due to the choice of fluorescence wavelength. The top scan shows the overall pattern, increasing sharply in intensity as one scans to shorter wavelengths through the electronic origin (000-000) near 440 nm. The transition from 000 to the

first allowed excited vibrational level (100) of $A^2\Sigma^+$ occurs at 416 nm; the observed fluorescence for $\lambda < 437$ nm thus is hot bands, originating from vibrationally excited levels in the ground state. Because the laser power is beginning to drop for $\lambda < 430$ nm, the bands in this region appear much less intense in Fig. 1 than they actually are.

A 4 nm portion showing the four heads of the 000–000 band (marked by arrows) as well as other bands, is presented in the middle panel. In turn, a 0.45 nm section of this, exhibiting individual rotational lines of the $^oP_{12}$ satellite branch, is given in the bottom scan. Interestingly, the $^oP_{12}$ head, which occurs for J near 70, is barely discernable in room temperature flow system LIF spectra[16] (see Ref. 1 for a comparable scan) but is very marked in the flame.

The overall excitation spectrum throughout this region is clearly congested and complex, due largely to the significant fractional populations in vibrationally excited levels of the ground state at flame temperatures. In order to make quantitative measurements of NCO concentrations (even relative) it is necessary to have individual, assigned rotational lines at the level of resolution of those in the bottom panel of Fig. 1, due to the variation with temperature of population in a given v, J level. We have mapped a portion of the region $\lambda < 440$ nm but have concentrated attention for hot flames on bands to the red, involving vibrationally excited levels whose excitation spectra are much less congested.

The vibrational level structure in the X, A and B states of NCO is illustrated in Fig. 2. A brief structural and spectroscopic description of NCO follows. (Details may be found elsewhere.[14,16-19]) It is a linear molecule with two stretching (v_1 and v_3) and one degenerate bending vibration

(v_2). The electronic orbital angular momentum of the ground Π state couples with the vibrational angular momentum ℓ of the bend ($\ell = v_2, v_2-2, v_2-4, \ldots, 0$ or 1 as v_2 is even or odd), yielding a total angular momentum K exclusive of spin. The states of different ℓ split according to the so-called Renner-Teller interaction. This yields states of Π symmetry for v_2=0, Π and Φ for v_2=2; and Σ and Δ for v_2=1. The spin angular momentum of this doublet molecule then interacts to produce spin-orbit-split components. In states where v_2=0, this yields $^2\Pi_{3/2}$ and $^2\Pi_{1/2}$ components like those in OH. In the transition to the upper $A^2\Sigma^+$ state the $^2\Pi_{1/2}$ spin-orbit component yields four discernible rotational branches branches, $^oP_{12}$, $P_2 + {}^PQ_{12}$, $Q_2 + {}^QR_{12}$ and R_2 with two heads; the $^2\Pi_{3/2}$ component has the P_1, $Q_2 + {}^QP_{21}$, $R_1 + {}^RQ_{21}$ and $^SR_{21}$ branches with two heads (see Figs. 1 and 3). Transitions originating from the Σ levels where v_2=1 have only P and R branches; two heads arising from excitation out of the higher Σ level (labelled $\kappa^2\Sigma^-$) are seen in Fig. 3. Transitions from higher Σ,Π and Δ levels have also been observed but will not be described here.

Figure 3 exhibits an excitation scan of the 000 ← 100 band which appears the most convenient for flame diagnostic measurements. Individual lines of this and of other bands were readily assigned from the 000-000 absorption spectra of Dixon.[17] The R_2 and Q_2 branches at 466 nm are the best individually resolved for quantitative measurements whereas the intense P_2 head is the best for signal searching. Line strengths[14] may be calculated form standard diatomic-like $^2\Sigma^+$-$^2\Pi$ formulae. Radiative lifetimes and Franck-Condon factors, needed for vibrational band intensities, have been separately measured.[16]

The excitation scan of Fig. 3 was made with a monochromator bandpass of 4 nm centered on the 000 ← 000 emission at 400 nm. This relatively narrow

bandpass is needed to filter out flame emission and strong fluorescence from laser-excited C_2 in this same region. The need for careful setting of the monochromator, and the dual selectivity of LIF with variable excitation and detection wavelengths, is shown in Fig. 4. The bottom scan shows the $^oP_{12}$ and P_2 heads, plus Q_2 and R_2 lines of the 000 ← 001 band observed via 000 → 000 emission. When the monochromator is tuned to the 010 → 010 emission band only 5 nm away, the 001 excitation greatly decreases whereas the P_1 and P_2 heads of the 010 ← 011 $\kappa^2\Sigma^-$ transition near 478.5 nm, and the 010 ← 011 $^2\Delta_{5/2}$ component near 478.2 stand out (top scan). (Here, the $^oP_{12}$ head is still rather apparent; it involves high-J levels emitting Q and R branches at shorter wavelengths.)

Table I lists the excitation bands which have been observed for the A-X system and the emission bands furnishing the strongest signals free of interference from any diatomic LIF with excitation lines in the same region.

Previous conventional room temperature absorption spectra[17,19] originating from the lowest levels (000 and 010) have been of key importance enabling the present LIF search. However, the combination of the laser excitation and flame environment has also furnished new high-resolution spectroscopic information in excited vibrational levels of $X^2\Pi_i$. The band-head separations P_2-Q_1 depend largely on the spin-orbit splitting constant A whereas the $^oP_{12}$-P_2 separation furnishes a measure of the rotational constant B. The actual wavelengths were calibrated by changing the observation wavelength so as to excite previously measured or readily calculated bands of CH, CN or C_2 in the same wavelength region of the laser. We find by fitting the band heads that the magnitude of A (in cm^{-1}, with typical 0.3 cm^{-1} error) decreases with v_1 and increases with v_3 : A_{000} = -95.5; A_{100} = -90.0; A_{200} = -71.8; A_{001} = -97.3; A_{101} = -92.6. The Renner-Teller splitting also

varies with stretching vibrations. To our knowledge, this represents the largest range of vibrationally-dependent A-values for a triatomic. A full fit and the results will be separately published;[20] we note these values to illustrate the spectroscopic potential of LIF in flames.

The B-X system[18] of NCO appears attractive for diagnostic purposes due to the shorter lifetime of the $B^2\Pi_1$ state[21] although its fluorescence is spread over many bands[16] in contrast to that from the $A^2\Sigma^+$ state which is concentrated in a few. Scans through the 000-000 band near 315 nm showed it to actually be decidedly inferior to A-X. The B-X fluorescence was very weak by comparison and only the R_1 and R_2 heads, with indefinite J-values, could be discerned. Within the 1.5 nm region around these heads are also strongly interfering excitations in the 0,0 and 1,1 bands of OH A-X, the 1,0 and 2,1 bands of NH A-X and a band of CN B-X. We recommend the A-X system for flame diagnostic purposes.

NH_2 radical

The ground $\tilde{X}^2B_1$ state of NH_2 is a bent, assymetric top with an angle of 103° while the $\tilde{A}\ ^2A_1$ state may be described as linear, corresponding to a Π electronic level. This large difference in equilibrium geometries leads to large changes in the bending quantum v_2 for intense bands. v_3 must change by two units due to symmetry considerations, leading to bands too far to the red to be seen here. In the ground state, the rotational levels (ignoring spin) are described by the total angular mementum N and its projections: K_a along the axis parallel to the H-N-H linear axis and K_c perpendicular to the molecular plane. In the excited state, K_a is (as in $X^2\Pi$ NCO) the sum of one unit of electronic orbital angular momentum plus the vibrational angular

momentum; it thus takes on even values (0,2,...) for odd v_2' and odd values for even v_2'. The selection rules are $\Delta K_a = \pm 1$, and ΔK_c = even with zero the strongest. The most intense features are the $^{P}Q_{1N}$ heads of the so-called Σ bands (odd v_2') and the $^{R}Q_{ON}$ heads of the Π bands (even v_2'). These produce 3 and 4 emission branches respectively. Because of electronic spin, each branch is double, and nuclear spin statistics produce a 1:3 population ratio in alternate ground state levels.

Figure 5 exhibits the vibrational levels pertinent to flame diagnostic LIF. The basic spectroscopic source for NH_2 is the absorption study of Dressler and Ramsay,[22] and there are several useful recent conventional spectroscopic[23] and flow system LIF[24-27] studies. The emission and LIF spectrum extends throughout the entire visible region, with a maximum intensity near 590 nm.

In the flames studied, the absolute NH_2 signal level has been adequate but major noise sources are posed by background flame emission and a complex, thus far unidentified, LIF excitation spectrum (perhaps NO_2 and/or hot bands of NH_2, also observed optoacoustically) underlying the assigned features. Most of our effort has been devoted to optimizing the desired signal in the midst of this background. Of course in other flames such as hydrocarbon-air, different interference problems may be present. Figure 6 shows a typical excitation spectrum and a scan of flame emission in the same band. Interference from flame emission can be minimized by using narrow temporal, spatial, and wavelength resolved detection of LIF in the redder bands. Altogether we have investigated 8 excitation bands between 570 and 660 nm. The most intense fluorescence, about 2/3 of the total, occurs in the $v_1v_20 \rightarrow 000$ band in each case; the remainder is typically spread over the terminal $\tilde{X}\ ^2B_1$ 010, 100, and 020 states with a smaller amount in 030. When

the $v_1v_20 \leftarrow 000$ band is excited, observation in the same band requires narrower spectrometer slits to discriminate against the the laser scatter, so that only one of the fluorescing rotational branches may be detected at one time. The NH_2 appears not to undergo significant energy transfer while in the upper state, but emits primarily from the pumped level (see below). Thus the coarse rotational structure of the transiton means that R or P branch fluorescence following Q-excitation will occur at different wavelengths for different N', requiring scanning of the spectrometer together with the laser for an excitation scan. This phenomenon was observed for 090 excitation.

The underlying background LIF, and total absorption measured optoacoustically, makes it inadvisable to obtain flame profiles for NH_2 by simply parking on one excitation; rather a scan through the head as in Fig. 6 should be made at each position. Observation of the bands red of the laser is generally preferable, so as to reduce flame emission interference. This also permits wider slits centered on a Q-head, and eliminates the double-scanning problem noted above. Excitation of v_1v_20 from 010 or 100 and observation of $v_1v_20 \rightarrow 000$ yields comparable intensities to the opposite scheme but flame emission is worse when observing the bands at shorter wavelength. In general it appears best to both excite and observe as far to the red as possible to avoid the background problems, even though the band intensities become weaker for lower v_2'. We recommend excitation of 080 or 070 for flame diagnostic purposes.

Figure 7 exhibits a scan of the $070 \rightarrow 010$ fluorescence following $070 \leftarrow 000$ excitation. Here the laser pumps overlapped lines of one of each doublet component of the 5_{05} and 3_{03} upper state levels. It can be seen from the resolved $^{P}P_{1,N-1}$ branch that only the pumped levels emit. The lack of transfer to the 4_{04} level is a symmetry-forbidden collisional propensity[24-26]

but transfer to the allowed 1_{01} level is not seen either. A similar scan of the 090 band, however, does show evidence of limited rotational energy transfer from the 3_{03} upper state level. More detailed examination of several levels is in progress.

In the flames studied, the concentration of NH_2 is likely high[9], between 10^{14} - $10^{15} cm^{-3}$, and comparable to [OH] in these rich flames. The NH_2 peaks at the flame front whereas the OH persists into the burnt gases. As a rough guide to overall signal levels, we have compared optoacoustic total absorption and LIF intensities for exciting the 1,0 band of OH ($P_1 7$) and the 0, 10, 0 band of NH_2 ($^R Q_{ON}$ head). The appropriate oscillator strength for the NH_2[9] is about 1/3 of that for OH.[28] LIF is observed in the 0,0 Q-head region of OH (~ 80% of total emission) and 0,10,0 → 0,2,0 (~ 10%) for NH_2. Normalized to unit laser pulse energy, the OH optoacoustic signal (absorption) is about 40 times that of NH_2 and the OH LIF is about 250 times larger. This suggests similar fluorescence quantum yields in these flames. NH_2 is known to undergo fast quenching even by He[24], while OH has rapid quenching rates for NH_3, N_2O and H_2O as collision partners.[29] Raman signals for NH_3 and H_2O comparable to the weaker NH_2 fluorescence bands were observed high and low in the flame, respectively.

Acknowledgement

This rsearch was supported by the U.S. Army Research Office, under contract DAAG29-80-K-0049.

References

1. Crosley, D. R., and Smith, G. P., Opt. Engr. 22, 545 (1983).

2. Crosley, D. R., Ed., Laser Probes for Combustion Chemistry, Amer. Chem. Soc. Symposium Series Vol. 134, 1980.

3. Bechtel, J. H., Dasch, C. J., and Teets, R. E., "Combustion Research with Lasers," to appear in Laser Applications (R. K. Erf and J. F. Ready, Eds.), Academic Press, New York, 1983.

4. Muller, C. H. III, Schofield, K., and Steinberg, M., in ref. 1, p. 103.

5. Barnes, R. H., and Kircher, J. F., Appl. Opt. 17, 1099 (1978).

6. Anderson, W. R., Vanderhoff, J. A., Kotlar, A. J., Dewilde, M. A., and Beyer, R. A. J. Chem. Phys. 77, 1677 (1982).

7. Morley, C., Comb. Flame 47, 67 (1982).

8. Dasch, C. J., private communiation, November 1983.

9. Chou, M. S., Dean, A. M., and Stern, D., J. Chem. Phys. 76, 5334 (1982).

10. Smith, G. P., Dyer, M. J., and Crosley, D. R., Appl. Opt. 22 3995 (1983).

11. Haynes, B. S., Iverach, D., and Kirov, N. Y., Fifteenth Symposium (International) on Combustion, p. 1103, The Combustion Institute, 1975.

12. Fenimore, C. P., Seventeenth Symposium (International) on Combustion, p. 661, The Combustion Institute, 1979.

13. Dean, A. M., Hardy, J. E., and Lyon, R. K., Nineteenth Symposium (International) on Combustion, p. 97, The Combustion Institute, 1982.

14. Copeland, R. A., Crosley, D. R., and Smith, G. P., to be published.

15. Beyer, R. A., and Dewilde, M. A., Rev. Sci. Instr. 53, 103 (1982).

16. Sullivan, B. J., Crosley, D. R., and Smith, G. P., to be published.

17. Dixon, R. N., Phil. Trans. Roy. Soc. London A252, 165 (1960).

18. Dixon, R. N., Can. J. Phys. 38, 10 (1960).

19. Bolman, P. S. H., Brown, J. M., Carrington, A., Kopp, I., and Ramsay, D. A., Proc. Roy. Soc. London A343, 17 (1975).

20. Copeland, R. A., and Crosley, D. R., to be published.

21. Sullivan, B. J., Smith, G. P., and Crosley, D. R., Chem. Phys. Lett. 96, 307 (1983).

22. Dressler, K., and Ramsay, D. A., Phil. Trans. Roy. Soc. London A251, 69 (1959).

23. Johns, J. W. C., Ramsay, D. A., and Ross, S. C., Can. J. Phys. 54, 1804 (1976).

24. Halpern, J. B., Hancock, G., Lenzi, M., and Welge, K. H., J. Chem. Phys. 63, 4808 (1975).

25. Kroll, M., J. Chem. Phys. 63, 319 (1975).

26. Dixon, R. N., and Field, D., Proc. Roy. Soc. London A366 (1979).

27. Merienne-Lafore, M. F., and Vervloet, M., Mol. Phys. 44, 1229 (1981).

29. Smith, G. P., and Crosley, D. R., Eighteenth Symposium (International) on Combustion, p. 1511, The Combustion Institute, 1981.

29. Fairchild, P. W., Smith, G. P., and Crosley, D. R., J. Chem. Phys. 79, 1795 (1983).

Table I. EXCITATION AND FLUORESCENCE WAVELENGTHS

NCO BAND	λ (P_2 HEAD)	λ (OBSERVE)	NH_2 BAND	λ(Q-HEAD)	λ(OBSERVE)[b]
000←000	440.35	465.0	0,10,0←000	571.0	620[c], 687, 697
000←100	466.42	440.0	090←000	597.9	656[d], 726, 740[e]
000←001	481.09	440.0	0,11,0←010	591.0	543[f]
000←200	495.60	437.5	0,12,0←020	607.2	516[f]
000←101	511.71	437.5	080←000	630.2	695, 774[e], 790[e]
010←010 $\mu^2\Sigma^+$	435.06	462.5	170←100	651.2	538[f]
010←010$^2\Delta$	437.56	462.5	0,11,0←100	655.7	543[f]
010←010 $\kappa^2\Sigma^-$	438.48	462.5	070←000	662.1	735, 824[e],
010←020$^2\Pi^-$	444.80[a]	435.0			
010←010 $\mu^2\Sigma^+$	448.35	440.0			
010←110 $\mu^2\Sigma^+$	460.61	435.0			
010←110$^2\Delta$	462.22	435.0			
010←110 $\kappa^2\Sigma^-$	464.56	435.0			
010←011 $\mu^2\Sigma^+$	474.36[a]	435.0			
010←011$^2\Delta$	477.37	435.0			
010←011$\kappa^2\Sigma^-$	478.16[a]	435.0			

[a]Preliminary identification; final confirmation awaits a detailed rotational analysis.

[b]Bands listed are emission to 010, 020, and 100 respectively except where noted.

[c]Emission at 575 also usable (0,10,0←000)

[d]Emission at 603 also usable (090←000).

[e]Calculated wavelength, but not studied in this work.

[f]v_1v_20←000 fluorescence wavelength.

Figure 1. LIF scans for A-X system of NCO in CH_4/N_2O flame. Fluorescence is collected at 465 nm with a 4 nm bandpass. Top scan: total excitation spectrum over the full range of one laser dye (Coumarin 440), not normalized to laser power. Middle: 4 nm portion covering the 000-000 band, with Q_1, P_1, P_2 and $^oP_{12}$ heads (left to right) marked by arrows, and hot bands at shorter wavelengths. Bottom: region from P_2 to $^oP_{12}$ head (0.45 nm) showing rotationally resolved $^oP_{12}$ branch.

Figure 2 Pertinent vibrational levels of the B, A and X states of NCO. Note the breaks in the energy scale. Levels are arranged for clarity according to value of v_2. Those with $v_2 = 0$ have $^2\Pi$ symmetry ($^2\Pi_{1/2}$ and $^2\Pi_{3/2}$) in the X and B states and $^2\Sigma^+$ in the A state. For v_2=1 in X, there are 4 levels: $^2\Sigma^+$, $^2\Delta_{3/2}$ and $^2\Delta_{5/2}$ (not separated in the figure), and $^2\Sigma^+$ in order of decreasing energy. For v_2=2 in X, there are also 4 levels: $^2\Pi^-$, $^2\Phi_{7/2}$ and $^2\Phi_{5/2}$, and $^2\Pi^+$. In the A state, v_2=1 has $^2\Pi$ symmetry and v_2=2 has $^2\Sigma^+$, $_2\Sigma^-$ and $^2\Delta$, all close together.

Figure 3 Excitation scan, detecting at 440 nm with 4 nm bandpass, through the red end of the 000-100 band. The two heads of the 010←110κ $^2\Sigma^-$ transition are also marked.

Figure 4 Excitation scans with detection wavelengths as marked and 4 nm bandpass, showing the difference depending on observation region. Bottom: 000←001 band seen observing 000→000 emission: $^oP_{12}$ and P_2 heads plus R_2 and Q_2 branches as the laser wavelength is decreased. Top: tuning to 010→010 emission to pick out 010←011 transitions originating from $\kappa^2\Sigma^-$ near 478.5 nm and from $^2\Delta_{3/2}$ near 478.2 nm. The $^oP_{12}$ head decreases less than the P_2 compared to the bottom scan because it occurs at higher J levels which emit more to the blue. Running throughout the spectrum are some small unidentified lines belonging to neither of these transitions.

Figure 5 Vibrational structure in NH_2: the 6 lowest levels having v_3=0 in $\tilde{X}\ ^2B_1$, and the 7 levels in $\tilde{A}\ ^2A_1$ for which LIF was observed in this study. Note the break in energy scale.

Figure 6 Top: LIF excitation scan through the most intense portion of the 080–000 band with several lines marked. Each is present as a doublet due to the spin-doubling; note that the upper state perturbations render the doublet splitting irregular with N'. Bottom: flame emission spectrum in the same region, using 25 μm slits in the 3/4-m spectrometer.

Figure 7 Fluorescence scan of the 070–010 band following excitation near 660 nm in the 070–000 band. The laser is overlapping one doublet component of the 5_{05}←5_{15} transition and the other component of 3_{03}←3_{13} in that band, so the fluorescence seen here consists of branches from each level. Note the absence of significant rotational energy transfer as evidenced by the presence of only two lines in the $^PP_{1,N-1}$ branch.

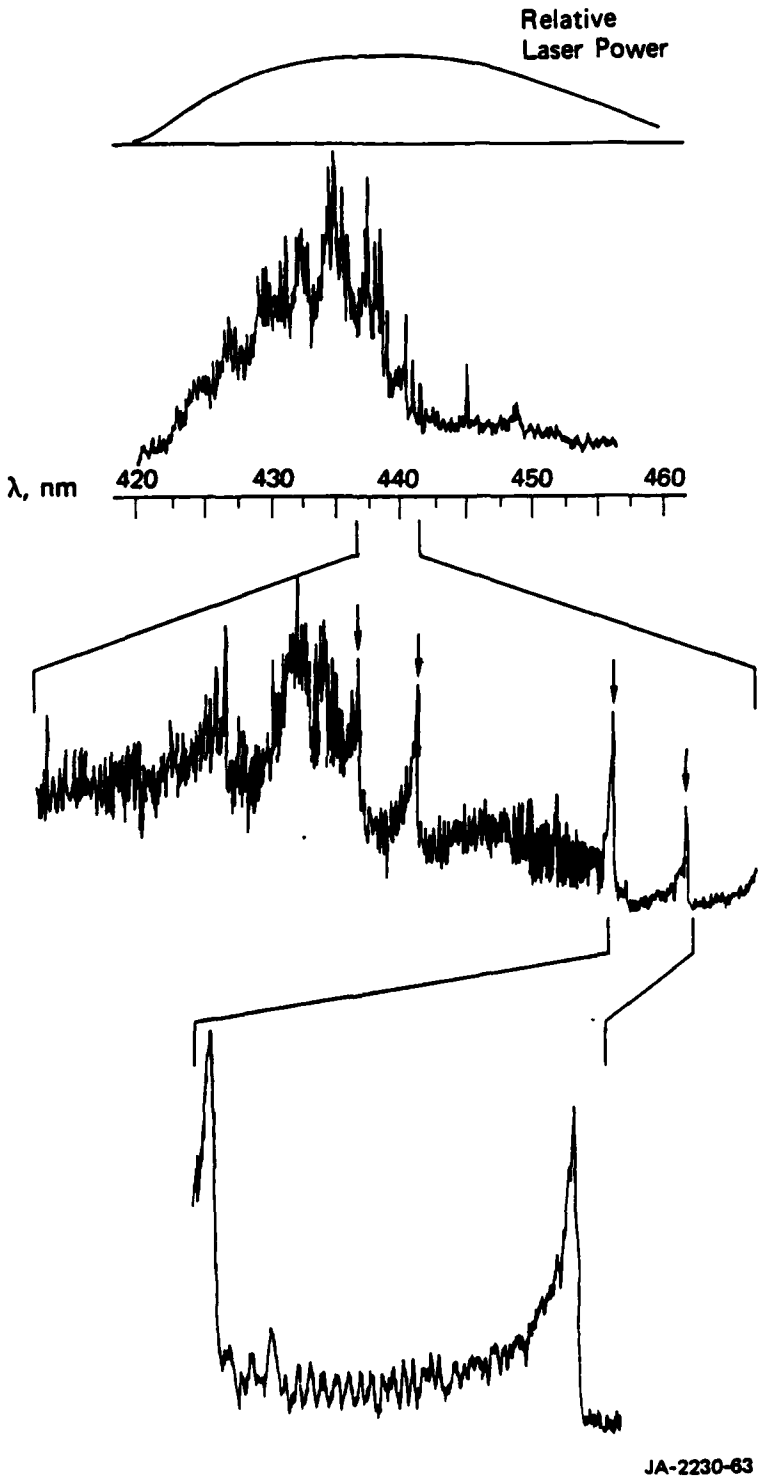
Relative
Laser Power
λ, nm
420
430
440
450
460
JA-2230-63

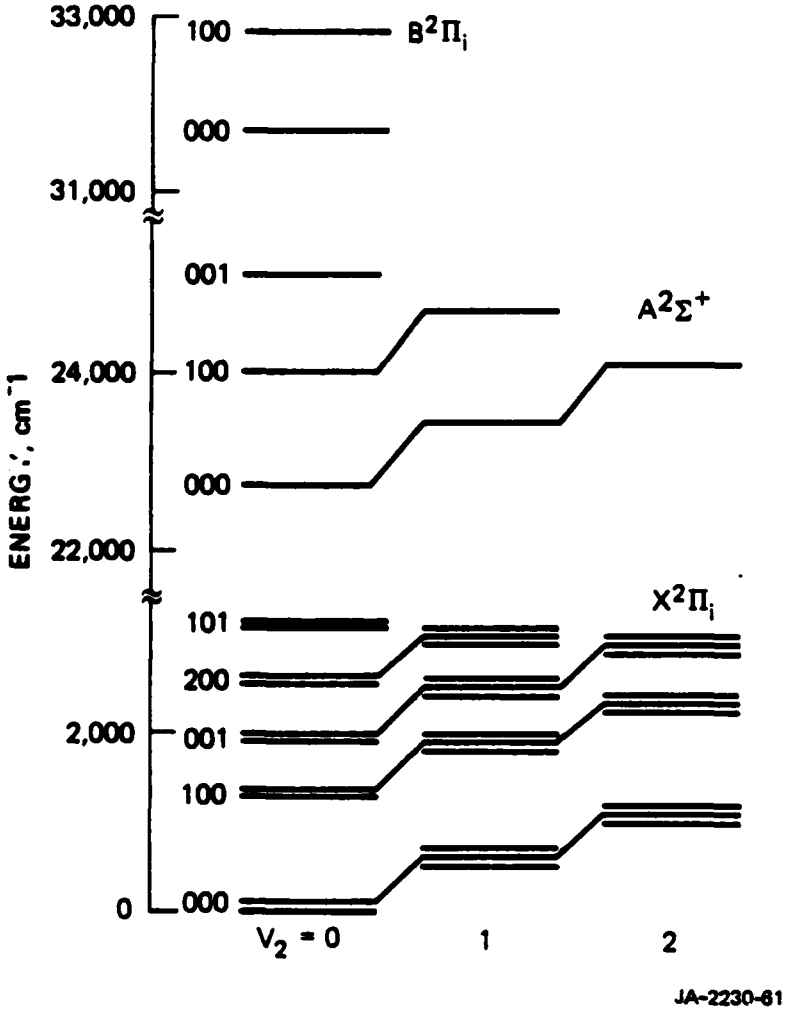
33,000
31,000
24,000
22,000
2,000
0
ENERG', cm⁻¹
100
000
001
100
000
101
200
001
100
000
B²Π_i
A²Σ⁺
X²Π_i
V₂ = 0
1
2
JA-2230-61

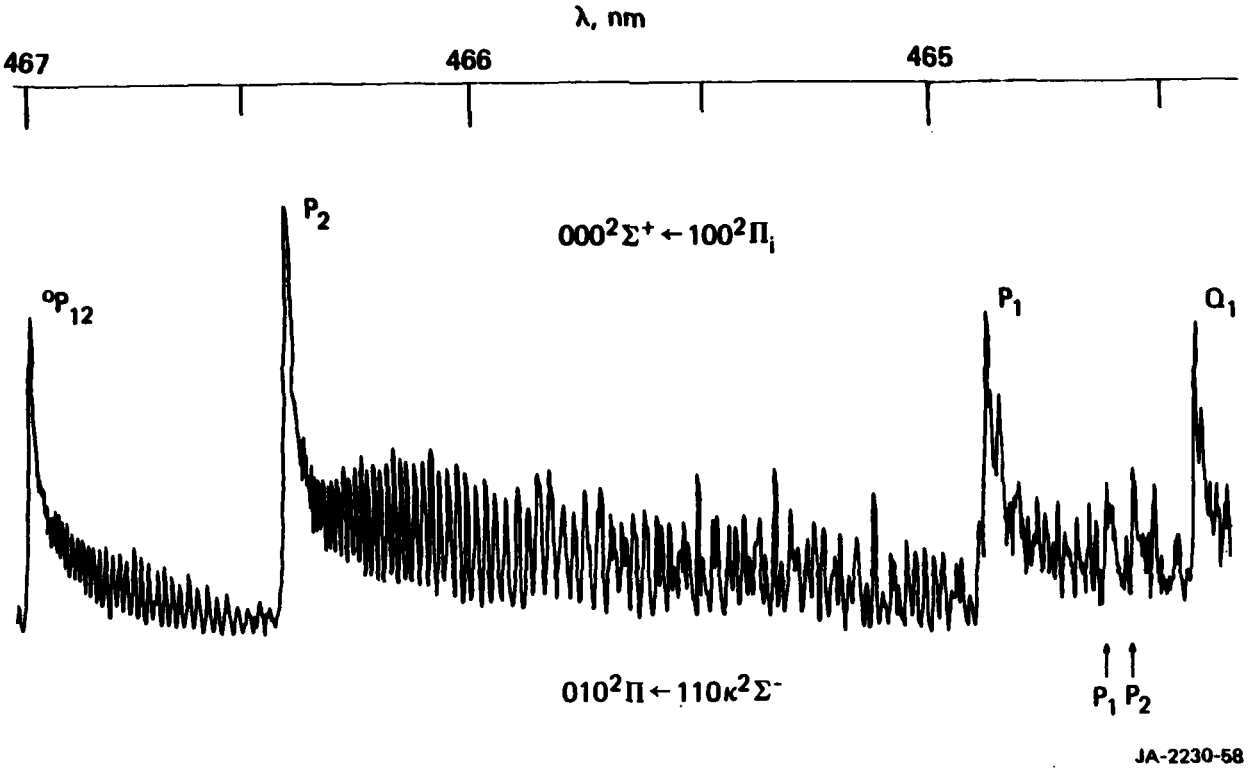
λ, nm
467
466
465
P2
000²Σ⁺ ← 100²Πi
oP12
P1
Q1
010²Π ← 110κ²Σ⁻
P1 P2
JA-2230-58

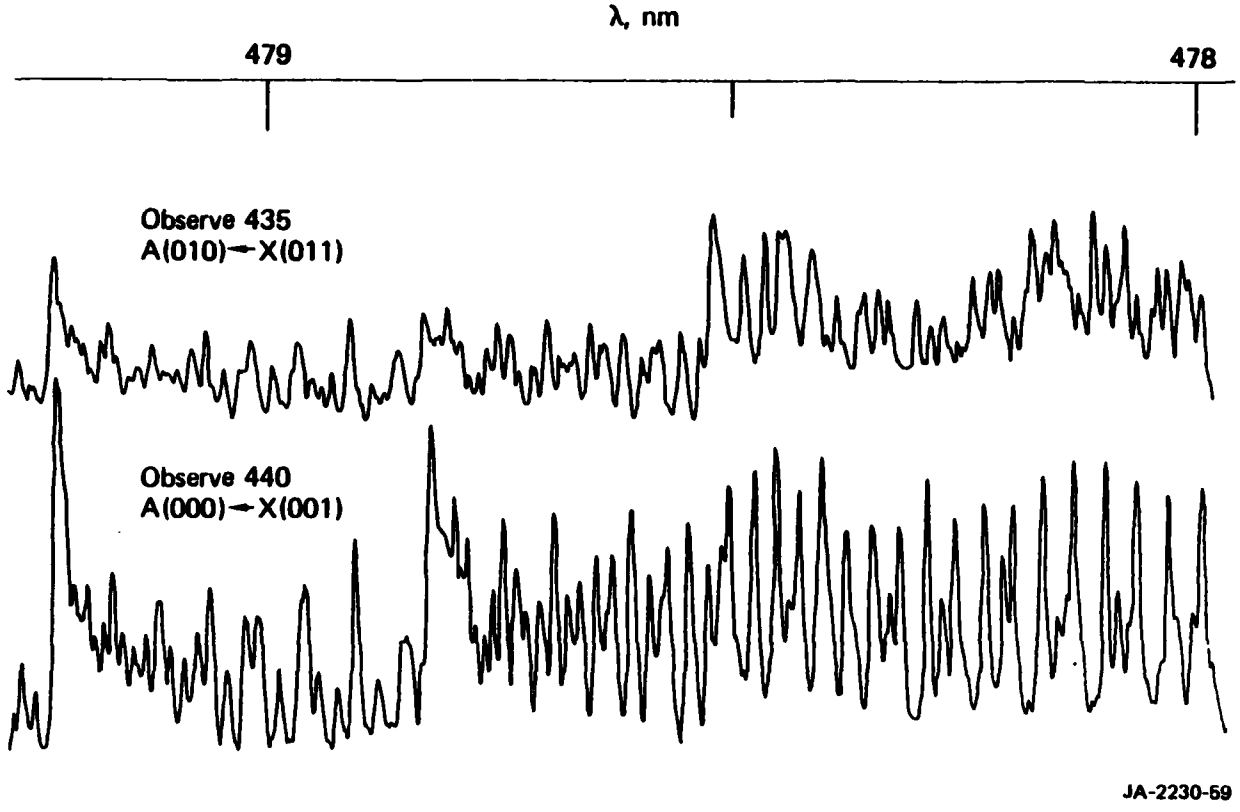
λ, nm
479
478
Observe 435
A(010)→X(011)
Observe 440
A(000)→X(001)
JA-2230-59

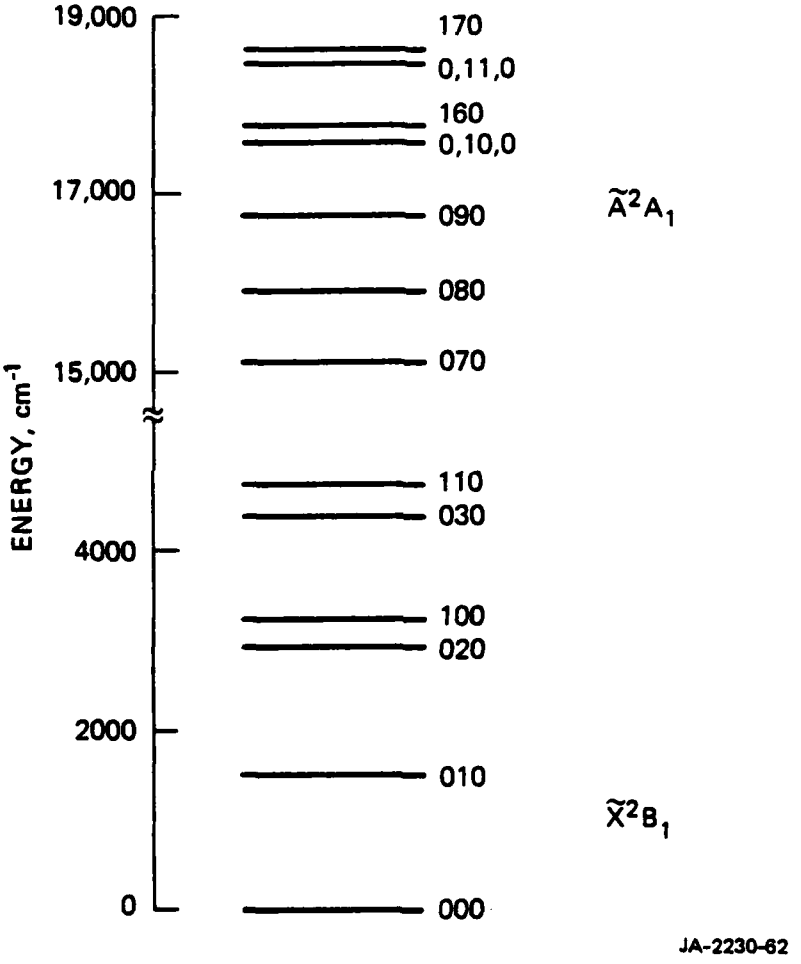
19,000
17,000
15,000
4000
2000
0
ENERGY, cm-1
170
0,11,0
160
0,10,0
090
080
070
110
030
100
020
010
000
$\tilde{A}^2A_1$
$\tilde{X}^2B_1$
JA-2230-62

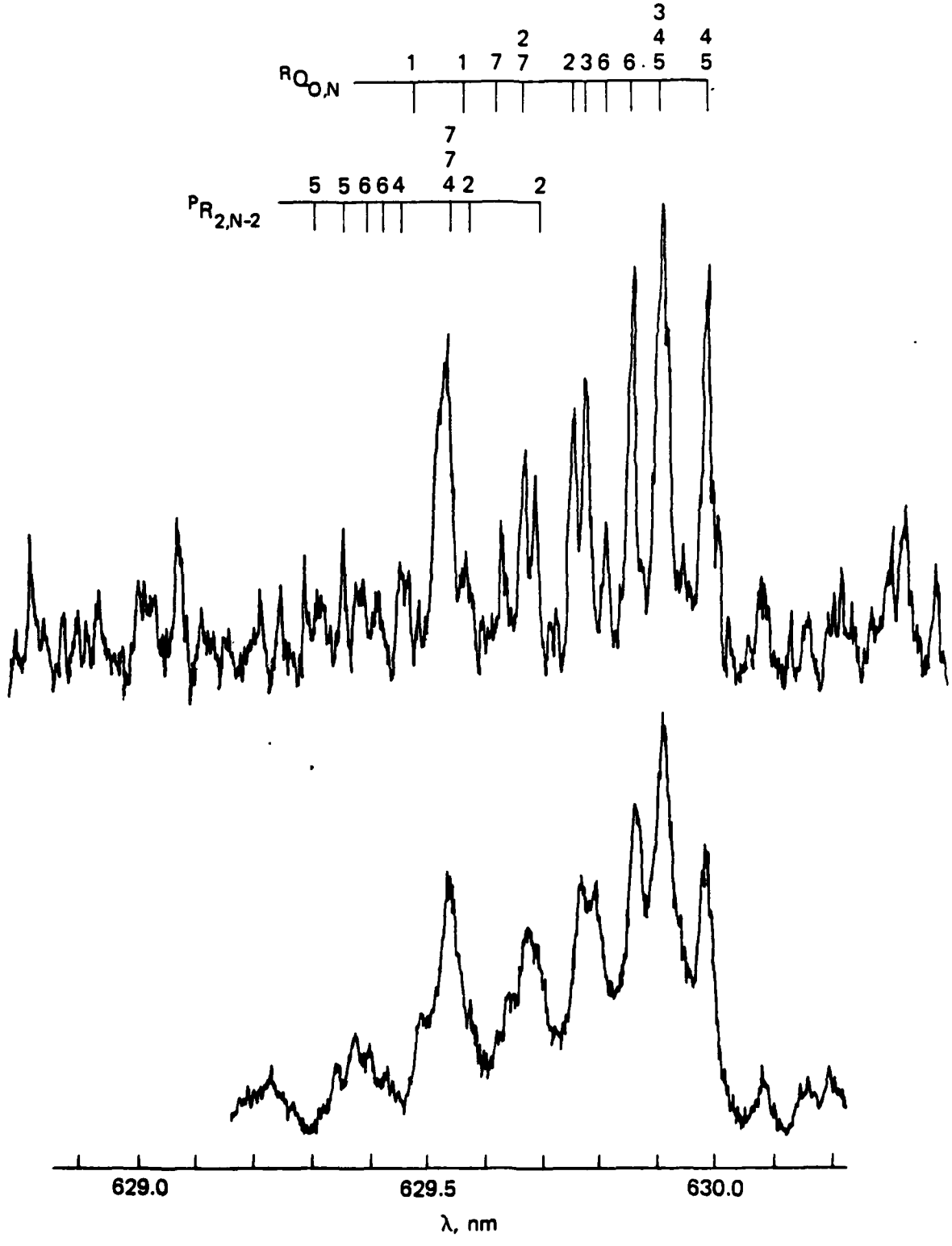

JA-2230-55

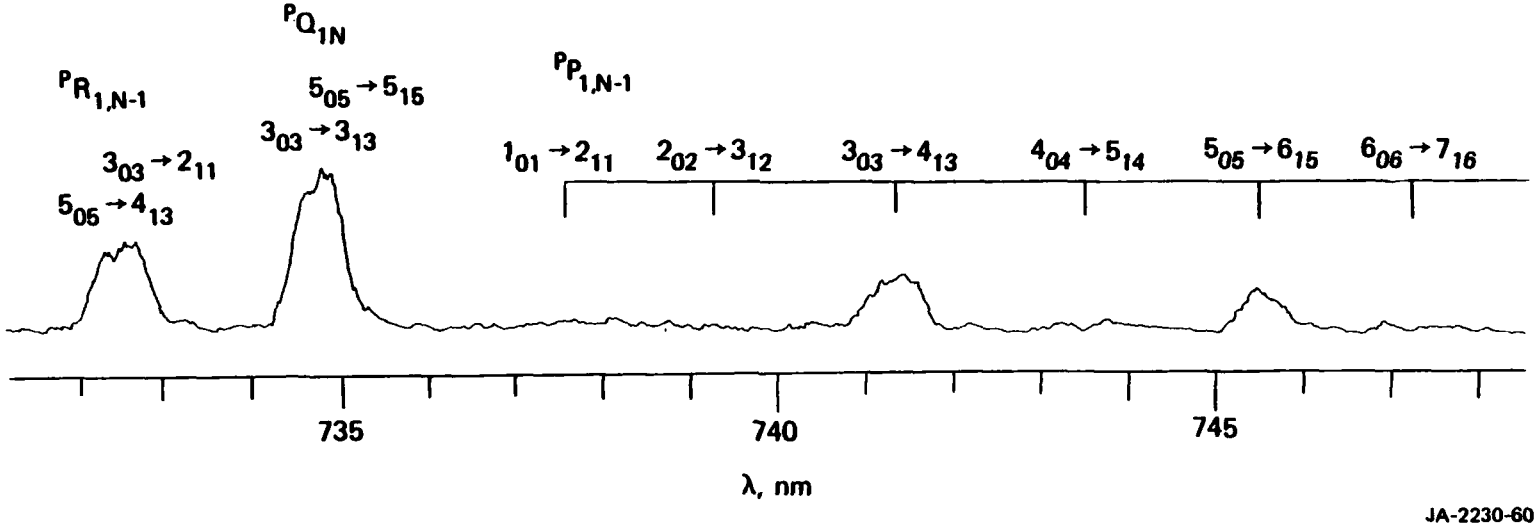
$^{P}Q_{1N}$
$^{P}R_{1,N-1}$
$5_{05} \rightarrow 5_{15}$
$^{P}P_{1,N-1}$
$3_{03} \rightarrow 3_{13}$
$1_{01} \rightarrow 2_{11}$
$2_{02} \rightarrow 3_{12}$
$3_{03} \rightarrow 4_{13}$
$4_{04} \rightarrow 5_{14}$
$5_{05} \rightarrow 6_{15}$
$6_{06} \rightarrow 7_{16}$
$3_{03} \rightarrow 2_{11}$
$5_{05} \rightarrow 4_{13}$
735
740
745
λ, nm

JA-2230-60

PRESSURE AND TEMPERATURE DEPENDENCE OF UNIMOLECULAR PROCESSES: AN APPROACH FOR COMBUSTION MODELERS*

C. William Larson, Roger Patrick, and David M. Golden
Department of Chemical Kinetics
SRI International, Menlo Park, CA 94025

ABSTRACT

There exists a well recognized need for a critical overview of the rate data that goes into combustion modeling. Modelers should be able to consult tables of parameters for combustion-relevant reactions that would enable the calculation of relevant rate constants as a function of temperature and pressure over the entire range of interest: 1000 K to 2500 K and 0 atm to 100 atm. A complete tabulation would include both uni- and bimolecular reactions; in this paper we focus on the analysis of unimolecular reactions. The approach is illustrated with unimolecular "fall-off" calculations for formaldehyde, methane, ethane, butane, hexane, and octane.

*This work was supported by the Army Research Office, Contract No. DAAG29-80-K-0049.

I INTRODUCTION

The unimolecular pyrolysis reactions of hydrocarbon molecules and radicals that occur in combustion depend on temperature and pressure in a complex manner dictated by (1) the complexity or size of the molecule or radical, (2) the threshold energy for reaction, and (3) the details of the intermolecular energy-transfer processes.

In the simplest model of unimolecular reactions, the Lindemann-Hinshelwood reaction scheme, energization by collisions, is followed by reaction of energized species, A^*,

$$A + M \rightleftarrows A^* + M$$

$$A^* \rightarrow \text{Products} \quad .$$

Solution of the differential rate equations in the steady-state approximation produces a particularly simple expression relating the reduced unimolecular rate constant, k_r, to the reduced pressure, M_r:

$$k_r = M_r / (1 + M_r) \qquad (1)$$

Here, k_r is the ratio of the unimolecular rate constant at pressure M to its value as $M \rightarrow \infty$: $k_r = k/k_\infty$. Also, $M_r = \left(k_0/k_\infty \right) M$, where $k_0[M]$ is the value of the unimolecular rate constant as $M \rightarrow 0$.

Since the Lindemann-Hinshelwood model neglects the pressure dependence of the relative populations of the manifold of energy eigenstates of A^*, as well as the differential depletion of these populations by reaction of A^*, it predicts that k_r will "fall off" from its high-pressure limiting

value more slowly than is observed. The quantum statistical RRKM theory corrects this deficiency.

Troe[1] has developed an approach for modeling the pressure and temperature dependence of unimolecular reactions of ethane and smaller molecules based on use of a "corrected" Lindemann-Hinshelwood model. In the Troe approach, the corrected reduced unimolecular rate constant is defined by:

$$k_r = \frac{M_r}{1 + M_r} F \qquad (2)$$

Thus, Troe calculated values of k_r, k_o, and k_∞ using a RRKM model, and developed simple formulae for expressing the "broadening factor," F, as a function of temperature and pressure. The value of the Troe approach lies in its retention of the simplicity of the Lindemann-Hinshelwood form and the ease with which it may be used to model unimolecular reactions of molecules important in combustion.

In this paper we have applied the Troe approach to the study of the temperature and pressure dependence of unimolecular reaction by fission of the central carbon-carbon bond in ethane, butane, hexane and octane and of the carbon-hydrogen bond in methane and formaldehyde. We have not, as of this writing, carried out the important calculational studies of the effects of inefficiencies in collisional energy transfer, but we will discuss some aspects of this problem qualitatively at the end of the paper.

II METHOD OF CALCULATION

For the calculation of the reduced unimolecular rate constant as a function of temperature and pressure, we have used the RRKM quantum statistical model. Molecular vibrational eigenstate densities were calculated

with use of the Whitten-Rabinovitch[2] approximation, and anharmonic corrections were made according to the procedure developed by Haarhof.[3] Vibrational eigenstate sums for the activated complex were calculated with use of an exact count routine. Overall rotational degrees of freedom were treated as adiabatic.

Frequency assignments for alkanes were based on the generalized normal-mode study of C_2 to C_{12} saturated hydrocarbons of Schachtschneider and Snyder[4] as adapted for use in RRKM calculations by Chua and Larson.[5]

Frequency assignments for activated complexes were made so as to fit high-pressure limit A-factors: $\log A_\infty = 16.3$. One 950 cm^{-1} C-C stretch frequency was deleted from the alkane assignment (reaction coordinate) and 5 frequencies in the alkane (4-bending modes and 1-torsion which are associated with the breaking C-C bond and which become overall rotations and realtive translations in the products) were lowered, until the correct valve for A_∞ was obtained. Figure 1 shows how the calculated k_∞ for ethane compares to determinations reported in the literature.[6-11]

Collision frequencies were calculated based on a Lennard-Jones model; collision diameters of 5 to 6 Å and a value of ε/k of 173 K were used for the N_2-alkane mixtures.

Threshold energies for central C-C bond rupture of butane, hexane, and octane were fixed at 80.0 kcal mol^{-1}, for ethane at 87.7 kcal mol^{-1}, for methane at 105 kcal mol^{-1} and for formaldehyde at 90 kcal mol^{-1}.

III RESULTS

Arrhenius plots of the RRKM calculated high- and low-pressure rate constants, k_∞ and k_o, are shown by Figure 2 for the ethane through octane

series. The characteristic curvature in the low-pressure plots is especially pronounced for the larger molecules; the low-pressure rate constant for octane is nearly temperature independent at high temperature. By contrast, the high pressure Arrhenius plots are only slightly curved upward; thus, high pressure activation energies between 1000 K and 2500 K increase by only about one kcal mol^{-1}.

Figure 3 shows a comparison between the Lindemann-Hinshelwood fall-off curve and those calculated with the RRKM model for octane and butane at 1000 K. The broadening factor at the center of the fall of curve, F_c, is defined at $M_r = 1$ as the ratio of the k_r calculated by RRKM to k_r calculated with the Lindemann model.

Figure 4 illustrates the pressure dependence of the fall-off broadening parameter of octane at 1500 K and 2500 K. The asymmetric "Gaussian-like" shape is typical of all molecules and the minimum value of F is found only slightly to the low pressure side of the "fall off" center: $F_c \approx F_{minimum}$. Also, the pressure range over which the deviations from Lindemann fall-off behavior are significant spans several orders of magnitude.

Figure 5 shows the temperature dependence of the central broadening parameter, $F_c(T)$ for the five alkanes and formaldehyde. The figure shows, and the Troe approach predicts, that the central broadening factor approaches unity at the zero and infinite temperature limits. Also, $F_c(T)$ for the larger molecules passes through a minimum near 1000 K; the minimum deepens and moves to lower temperatures as the moleculer size increases.

IV DISCUSSION

The temperature dependences of high and low pressure-limiting rate constants, $k_o(T)$ and $k_\infty(T)$, illustrated by Figure 2, and the temperature/pressure dependences of the Troe broadening factor, F(T,M), illustrated by Figure 4, provide all the information required to write parameterized analytical functions that enable facile calculation of the unimolecular rate constant, k(T,P).

High and Low Pressure Limits

The limiting rate constants are easily written in the customary way as 3-parameter functions of temperature:

$$k_o(T) = AT^n \exp -B/T \qquad (3)$$

and

$$k_\infty(T) = CT^m \exp -D/T \qquad (4)$$

Figure 2 shows that C and D are very close to the high-pressure Arrhenius A-factor and activation energy, respectively, and that $m \approx 0$.

The curvature in the Arrhenius plot for k_o, which is more pronounced for larger molecules, is representable to within 1% by the nonlinear, 3-parameter expression. Table 1 summarizes the results of parameter evaluation from least squares fits of these expressions to the k_o and k_∞ calculated from RRKM theory. The nonlinear regression algorithm given by Bevington[12] was used in this evaluation.

Table 1

VALUES OF PARAMETERS FOR REPRESENTATION OF HIGH AND LOW PRESSURE RATE CONSTANTS

[$k_o(T)$ molecule-cm^{-3}-sec^{-1}, and $k_\infty(T)$, sec^{-1}]

1000-3000 K

Molecule	ln A	n	$B/10^3$ (K)	ln C	m	$D/10^3$ (K)
Ethane	85.57	-11.22	207	38.37	0.246	185
Butane	131.39	-17.15	180	38.84	0.028	167
Hexane	97.74	-13.52	124	38.84	0.028	167
Octane	43.12	- 7.28	66	38.84	0.028	167

Broadening as a Function of Pressure

Troe presents three forms as successive levels of approximation to express the pressure dependence of F in terms of F_c:

(1) Symmetric broadening about $M_r = 1.0$:

$$\log F_1 = \left(1 + \left[(\log M_r)\right]^2\right)^{-1} \log F_c \qquad (5)$$

(2) Including width broadening:

$$\log F_2 = \left(1 + \left[\left(\frac{\log M_r}{0.9 - \log F_c}\right)\right]^2\right)^{-1} \log F_c \qquad (6)$$

(3) Including width plus asymmetric broadening:

for $M_r > 1$:

$$\log F_3 = \left(1 + \left[\left(\frac{\log M_r - 0.12}{0.85 - 0.67 \log F_c}\right)\right]^2\right)^{-1} \log F_c \qquad (7)$$

for $M_r < 1$:

$$\log F_3 = \left(1 + \left[\frac{\log M_r - 0.12}{0.65 - 1.87 \log F_c}\right]^2\right)^{-1} \log F_c \qquad (8)$$

Figure 6 shows how the broadening factor from Troe's highest level approximation, F_3 (Troe), compares to the RRKM calculated broadening, F (RRKM). The figure shows that the Troe expression predicts F (M) to within 30% for all molecules over the pressure and temperature ranges studied. The simpler expressions (Eq (6) or (7)) are less satisfactory and, since they are not significantly easier to use, they are not recommended.

Center Broadening as a Function of Temperature

Troe has suggested a 4-parameter expression to describe the temperature dependence of F_c as follows:

$$F_c(T) = \exp(-T^{**}/T) + \exp(-T/T^{***}) + a\left(\exp(-T/T^{*})-\exp(-T/T^{***})\right) \qquad (9)$$

We have evaluated the performance of a similar 3-parameter, 2-term expression,

$$F_c(T) = a\left(\exp(-b/T) + \exp(-T/c)\right) , \qquad (10)$$

and find that a, b, c values listed in Table 2 reproduce the RRKM calculated $F_c(T)$ shown by Figure 5 to within better than 15%.

Table 2

VALUES OF PARAMETERS FOR REPRESENTATION OF $F_c(T)$, 1000-3000 K

Molecule	a	b (K)	c (K)
Formaldehyde	0.348	301	811
Ethane	0.352	1966	616
Butane	4.95	7618	465
Hexane	2.88	5504	306
Octane	2.61	4613	141

Thus, the 6 parameters of equations (3) and (4) (A, n, B, C, m, D) contain the information required to construct Lindemann fall-off curves and the three parameters of equation (10) contain the information required to correct the Lindemann fall-off to the more realistic fall-off predicted by the RRKM model.

Weak Collisional Energy Transfer

In the preceding calculations, we have made use of the strong collision approximation. In order to model weak collision processes, it is necessary to make two specifications: (1) the form of the function relating the probability of energy transfer during a collision to the amount of energy transfer and (2) the average amount of energy transfer per collision.

Troe has examined weak collision models for a variety of molecules amd found that the center-broadening factor in weak collider fall-off was related to the strong collider fall-off by the empirical approximation

$$F_c^{wc} = \beta^{0.14} F_c^{sc}$$

Here, β is the collisional efficiency, defined by $\beta = k_o^{wc}/k_o^{sc}$, where k_o^{wc} is the low pressure-limiting rate constant for the weak collider. Thus, β becomes a scaling factor in the reduced pressure appropriate to weak collider fall-off:

$$p_r^{wc} = k_o^{wc} M/k_\infty = \beta\, p_r^{sc} \quad .$$

Troe's approximation shows that computed fall-off behavior in weak-collider systems is much more sensitive to the absolute value of β used as a scaling factor in p_r^{wc} than to the additional broadening brought about by the weak collision model.

Relevance to Combustion

As a first approximation to weak collision fall-off calculations, we may ignore weak collision broadening. The more important parameter, β, as a scaling factor in p_r, is retained and, in a "Lindemann-like" approximation, the weak collider model reduces to a quasi-strong collider model where the probabilities that a collision will be either strong or elastic are β and $1 - \beta$, respectively.

The evidence on the temperature dependence of β is mixed[13] and, for the moment, we will ignore this very imporant aspect of the problem.

Figure 7 shows the relationship between temperature and weak collider pressure at the center of the fall-off P_c^{wc}, for each of the molecules studied. To define the pressure axis, the quasi-strong collider model with $\beta = 0.1$, independent of temperature, is used.

A "combustion window" may be defined by the pressure range (1-100 atm) and temperature range (1000-2500 K), which are relevant to combustion processes. Thus, a molecule whose P_c vs. T curve passes through the combustion window exhibits its maximum deviation from Lindemann behavior within this important pressure and temperature range. At pressures two to three orders of magnitude above or below their P_c vs. T curve, the molecules are in their high- or low-pressure limits.

Larger molecules enter the window at higher temperatures where their F_c values are larger. Thus, values of F_c within the "combustion window" are greater than ~ 0.2 for all molecules of the current study. For molecules larger than butane, fall-off need be considered at temperatures greater than about 2000 K. Below 1500 K, the larger molecules are in their high-pressure limit. For methane and ethane, maximum broadening occurs at about 1500 K, and fall-off considerations are important at all combustion temperatures. For formaldehyde at 1500 K, a weak collider pressure of ~ 100 atm would be required to bring its decomposition to the center of the fall-off. At 1 atm, formaldehyde pyrolysis is in its second-order limit at temperatures greater than 1000 K.

Competitive Multiple Reaction Channels

Ethane and the higher alkanes contain multiple dissociation channels for C-C and C-H bond rupture which have not been considered in the present calculations. Generally, C-H rupture is 10-20 kcal mol^{-1} more endothermic than C-C rupture. Under conditions where C-H and C-C rupture are both in the high-pressure limit, C-H rupture (per C-H bond) may amount to as much as one-half percent of C-C rupture (per bond) at 1000 K. At 3000 K, the C-H rate approaches 20 percent of the C-C rate on a per-bond basis.

In the fall-off and low-pressure limits, C-H rupture would tend to be less competitive with C-C rupture. However, it is important to note that at pressures lower than the high-pressure limit, different dissociative channels cannot be treated as if they were independent of one another. For example, in the dissociation of ethane, two processes that require consideration are:

$$C_2H_6 \rightarrow 2\ CH_3 \qquad (a)$$

$$C_2H_6 \rightarrow C_2H_5 + H \qquad (b)$$

It would be inappropriate to use a "fall-off" curve for channel (b) that was derived in the manner described here for a single-channel process, since at pressure below the high-pressure limit, competition by channel (a) would lower the rate constant below that predicted by such a treatment. A more correct treatment for multi-channel processes is currently being developed.

Computer Code for Inclusion of Unimolecular Fall-Off

The computer codes for solution of the coupled differential equations which are generated by a chemical mechanism requires the elementary reactions and their rate constants. The value of retention of the Lindemann form for unimolecular processes is made apparent in the simple code it generates for computing both the temperature and pressure dependence of these reactions. Thus, in the case of ethane, we would write:

(1) $C_2H_6 \rightarrow CH_3 + CH_3$ $\qquad k_{diss} = k_\infty\left(1 - P_r^{-1}\right)^{-1} F$

(2) $CH_3 + CH_3 \rightarrow C_2H_6$ $\qquad k_{rec} = k_\infty\left(1 - P_r^{-1}\right)^{-1} F \cdot K_{eq}$

The "fall-off" behavior of the rate constant for the reverse recombination, $k_{rec}(T,P)$, is related to $k_{diss}(T,P)$ by detailed balancing, $K_{eq} = k_{diss}/k_{rec}$.

Conclusions

The initiation of combustion is governed by the reaction that produces an H-atom, i.e., the unimolecular decomposition of the fuel. These calculations indicate that both methane pyrolysis ($CH_4 \rightarrow CH_3 + H$) and ethane pyrolysis ($C_2H_6 \rightarrow CH_3 + CH_3$) are near their maximum pressure sensitivities at combustion temperatures. A simple computer code is presented to include the pressure and temperature dependence of these important reactions in terms of 9-parameters and the collision efficiency, β:

$$k_{diss} = k_\infty \left(1 + P_r^{-1}\right)^{-1} F$$

3 parameters — 6 parameters — 9 parameters

$$k_\infty = CT^m \exp^{-D/T} \qquad p_r = p_r(\beta k_o[M], k_\infty) \qquad F = F\left(p_r, F_c\ (\beta, a, b, c)\right)$$

$$k_o = A\,T^n \exp^{-B/T}$$

The Lindemann model generates the maximum sensitivity of k_{diss} to pressure and requires 6-parameters and β. Application of the RRKM correction causes fall-off to occur over a broader pressure range and thus, desensitizes k_{diss} to pressure. If weak collider-broadening corrections are also applied (by Troe's $\beta^{0.14}$ factor), k_{diss} is even less sensitive to pressure.

Finally, the fall-off behavior of the reverse combination reaction may be coded with three additional parameters (S, ℓ, H) to specify the equilibrium constant, $k_{eq} = S\,T^{\ell}\,e^{-H/T}$.

References

1. (a) J. Troe, J. Phys. Chem., 1979, 83, 114-126.
   (b) J. Troe, Ber. Bunsenges. Phys. Chem., 1983, 87, 167-177 extends the treatment to larger molecules: methyl and propyl-cyclohexatriene, toluene, etc.

2. G. Z. Whitten and B. S. Rabinovitch, J. Chem. Phys., 1963, 38, 2466.

3. P. C. Haarhof, Mol Phys., 1963, 6, 101.

4. J. H. Schachtschneider and R. G. Snyder, Spectrochim. Acta., Part A, 1963, 19, 117; 1965, 21, 169.

5. C. W. Larson, P. T. Chua, and B. S. Rabinovitch, J. Phys. Chem., 1972, 76, 2507-2517.

6. E. B. Skinner and W. E. Ball, J. Phys. Chem., 1972, 64, 1462.

7. P. D. Pacey and J. H. Purnell, J. Chem. Soc. Faraday I, 1972, 68, 1462.

8. D. B. Olson and W. C. Gardiner, J. Phys. Chem., 1979, 83, 922.

9. E. B. Skinner and R. A. Ruehrwein, J. Phys. Chem., 1959, 63, 1736.

10. M. C. Lin and M. A. Back, Can. J. Chem., 1966, 44, 2537.

11. C. P. Quinn, Proc. Roy. Soc. 1963, (A)275, 190.

12. P. R. Bevington, Data Reduction and Error Analysis, McGraw Hill, New York, 1969, p. 237.

13. J. R. Barker and R. E. Golden, Western States Combustion Symposium, Los Angeles, 1983.

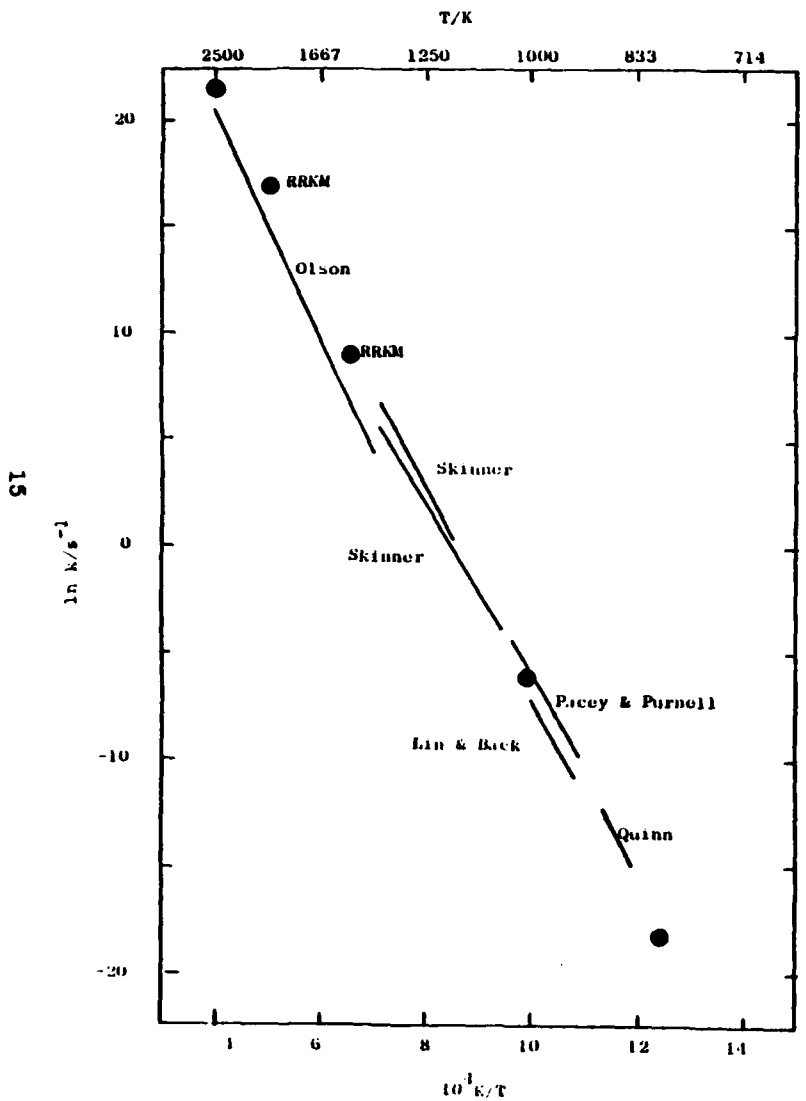

Figure 1 - Comparison Between Calculated and Measured High Pressure Rate Constants - Ethane

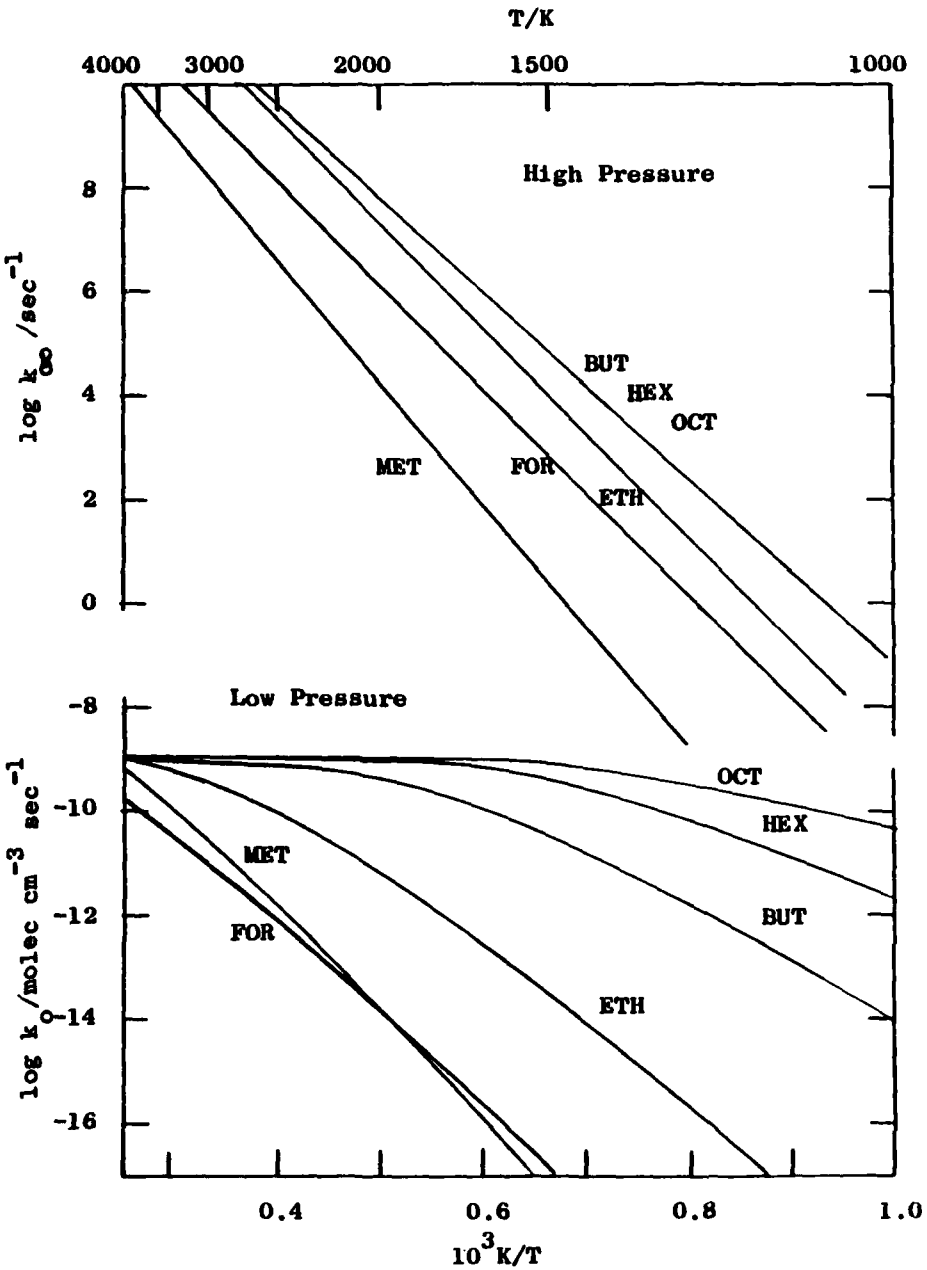

Figure 2 - Computed Arrhenius Behavior of High and Low Pressure Rate Constants.

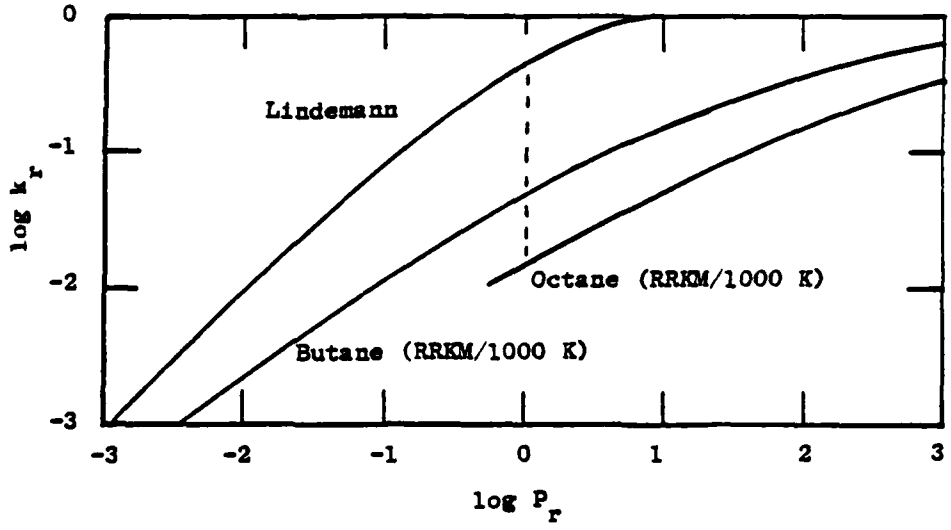

Figure 3 - Comparison of Lindemann Fall-Off to RRKM Fall-Off for Butane and Octane at 1000 K

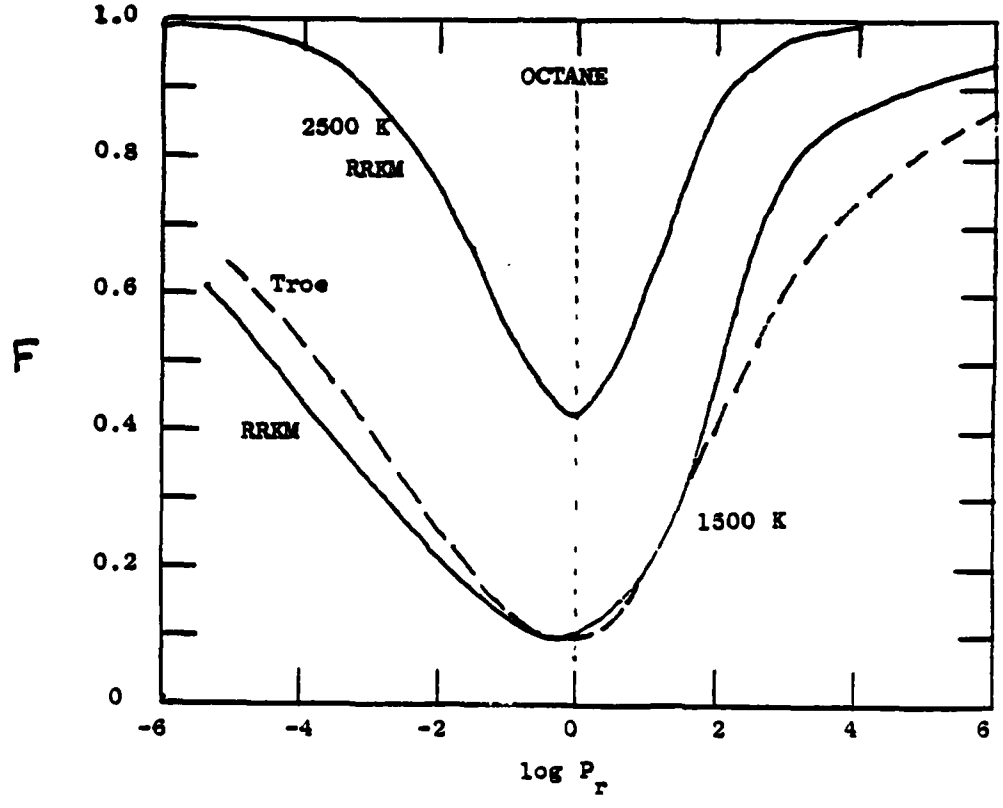

Figure 4 - Broadening Factor as a Function of Reduced Pressure and Comparison with Troe Approximation - Octane

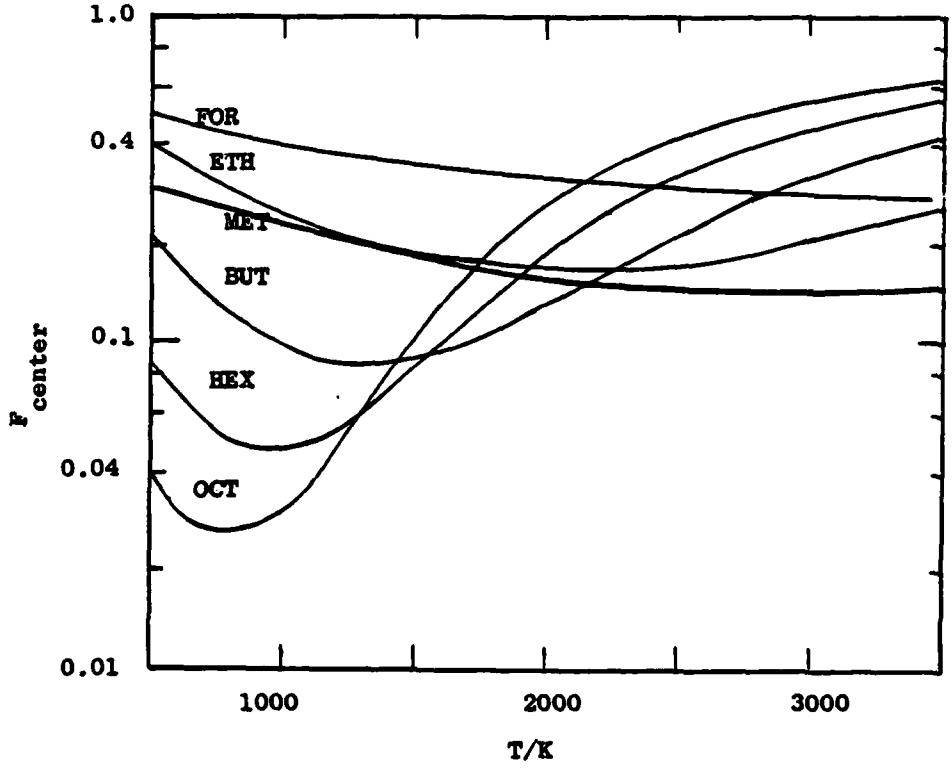

Figure 5 - Temperature Dependence of Central Broadening Factor

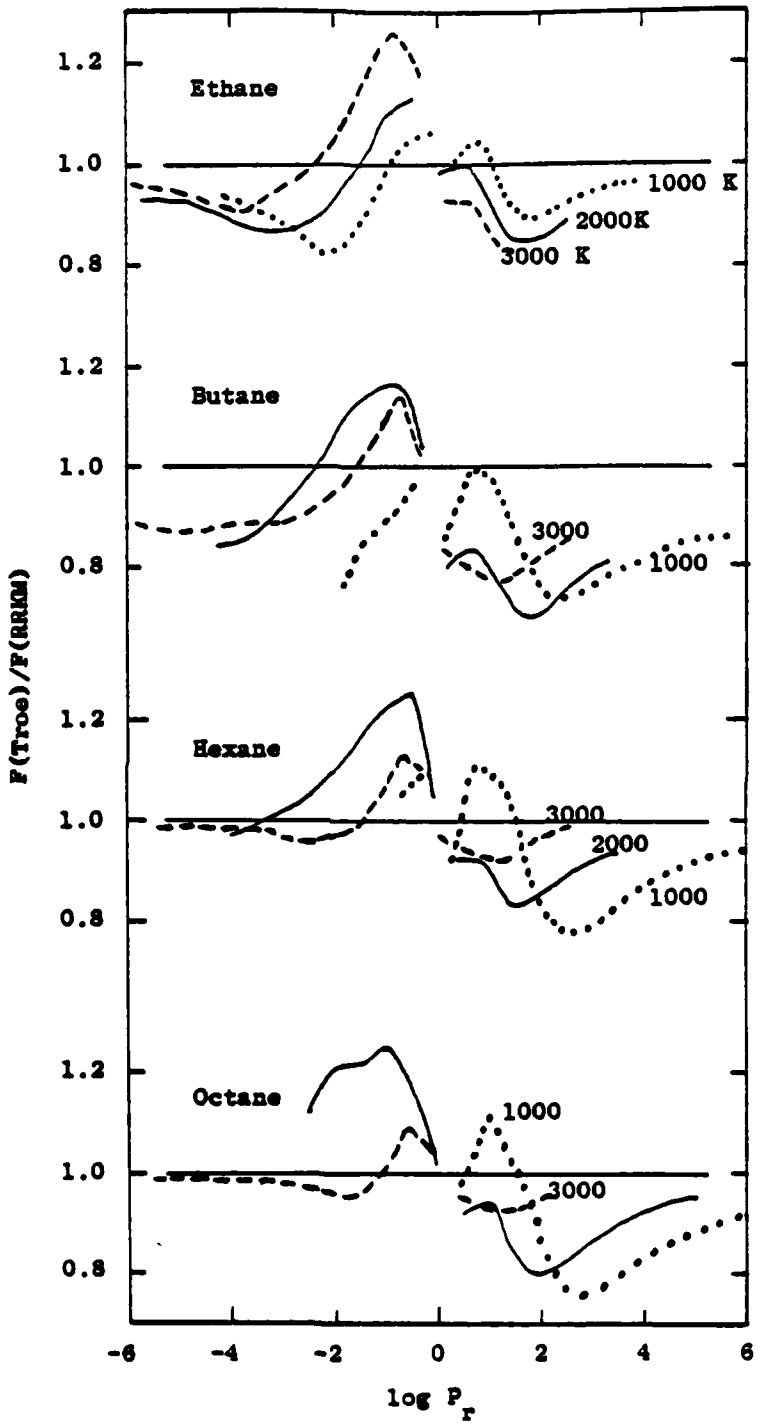

Figure 6 - Comparison Between Calculated and Approximate Fall-Off Broadening.

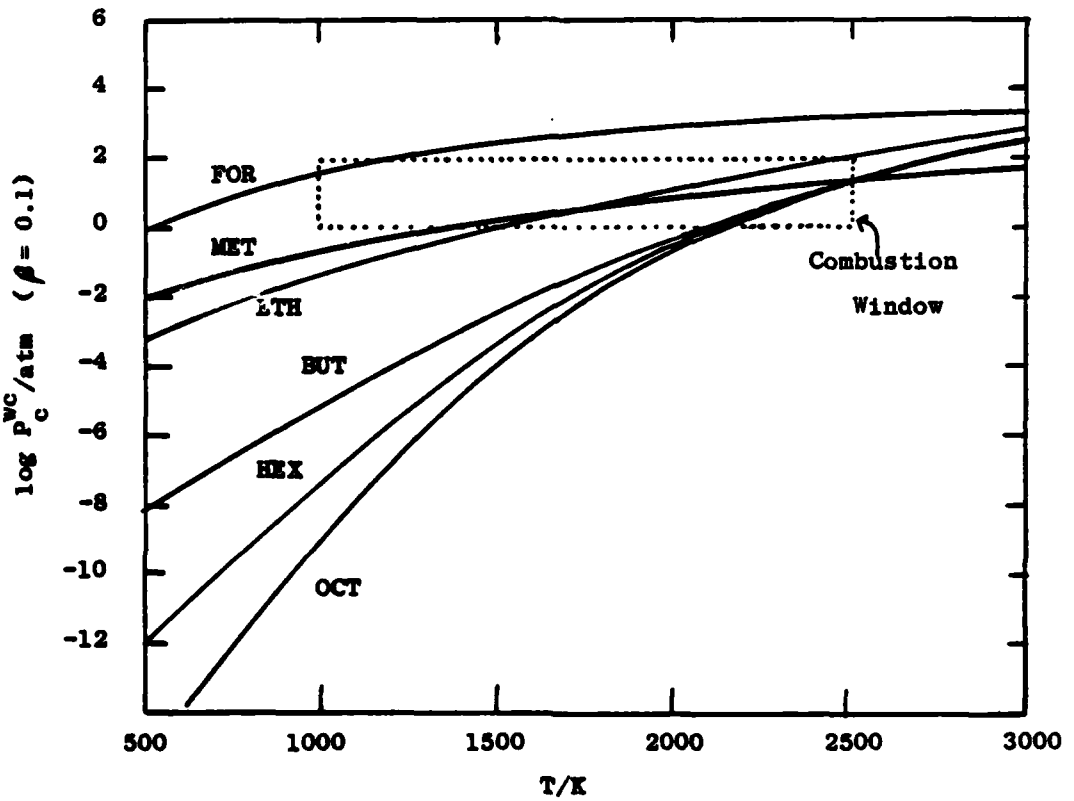

Figure 7 - The Combustion Window and Relations Between Temperature and Pressure at the Center of the Fall-Off

MODELING THE CHEMICAL NETWORK OF THE N_2O/CH_2O FLAME

C. William Larson and David M. Golden

Abstract

In this paper we consider a chemical network for the N_2O/CH_2O flame. Two reaction branches, initiated by H-atom attack on the oxidant, are described:

C/H/O Branch

$$H + N_2O \rightarrow NNOH \rightarrow N_2 + OH \qquad (3)$$

C/H/N/O Branch

$$H + N_2O \rightarrow HNNO \rightarrow NO + NH \qquad (20)$$

Reaction simulations of the C/H/O branch at 2500 K with a mechanism of 17-elementary reactions showed that reaction (3) consumes almost all the oxidant and releases the majority of the chemical energy.

Recent laser probes of H_2/N_2O and CH_4/N_2O flames at ~ 2000 K have revealed NH in concentrations near 4% of the OH.

An approach is described for modeling the NH/OH branching through HNNO and NNOH intermediates and includes isomerization of postulated intermediate: $HNNO \rightleftharpoons NNOH$.

Production of NH by reaction (20) precipitates a complex chemistry involving N-containing species. Production of the C-N linkage occurs through NH addition to the unsaturation in CO:

$$NH + CO \rightarrow HNCO^{*} \qquad (21)$$

Isocyanic acid may be collisionally stabilized and undergo reactions with the radical pool or react by competitive unimolecular reactions to generate a variety of carbon-nitrogen species (e.g., NCO, CNO, CN, HOCN) that are sensitive to laser probe techniques.

I INTRODUCTION

The N_2O/CH_2O flame is the most simple flame containing all of the four most important elements of combustion chemistry: H, N, C, and O. The model of its chemical network is an important basic element of the more extensive networks one would create to model the ignition and propagation properties of nitramine propellants. As part of this research, we have considered the elementary reactions plausible for this flame. This document summarizes some preliminary ideas.

The N_2O/CH_2O flame chemistry is composed of two main branches. Most of the oxidation/reduction occurs through a C/H/O network that Dean, Johnson, and Steiner[1] (DJS) have modeled with an elementary reaction set composed of 19 reactions and 13 species (see Table I). The model fits data obtained from shock tube experiments (1600 to 3000 K) on formaldehyde loss, carbon dioxide production, and oxygen atom concentration profile between 1 and 60 μs. Also, both oxygen and nitrous oxide oxidant were studied in various dilute argon mixtures.

With the DJS model (extrapolated to a stoichiometric flame mixture at 1 atmosphere pressure), almost all the oxidant is consumed through reaction (3):

$$H + N_2O \rightarrow N_2 + OH \qquad (3)$$

even though the value of k_3 used is eight times lower (at 2000 K) than the widely used value published in the review by Baulch and co-workers

(BDHL).[2] Most recently, Cattolica and co-workers[3] used the BDHL value to model experimental results from an N_2O/H_2 flame, for example. In addition, the DJS model uses rate constants for fuel-consuming reactions:

$$CH_2O + M \rightarrow HCO + H + M \qquad (9)$$

and

$$CH_2O + OH \rightarrow HCO + H_2O \qquad (4)$$

which are also at least ten times lower than the values previously used to model methane oxidation.[4,5]

Compelling evidence for the existence of the second branch of N_2O/CH_2O flame chemistry was recently obtained by Cattolica and co-workers (CSD).[3] In the CSD research, NH amounting to about 4% of the OH was measured with laser probe of the H_2/N_2O flame. The NH production was attributed to

$$H + N_2O \rightarrow NH + NO \qquad (20)$$

The branching ratio, $R_b = k_{20}/k_3$, derived from the model of the chemical network was 0.04 at 2000 K.

Previously, Baldwin and co-workers (BGPW)[6] studied the H_2/N_2O system in a batch experiment at 813 and 873 K and, through analysis of a simple model, derived $R_b = 0.0041 \pm .005$. Coupling of the flame study to the batch study yields an "apparent" activation energy difference of 7 kcal mol^{-1}:

$$R_b \propto \exp - 7000/RT.$$

Additional evidence supporting the existence of reaction (20) may be found in the laser probe experiments by Anderson and co-workers (ADK)[7] on the N_2O-supported methane flame. Here, in the flame region where NH and OH concentrations were maximum, concentration ratios of NH to OH of about 0.04 were measured.

II SIMULATIONS OF THE C/H/O BRANCH

The DJS model of the C/H/O branch is composed of reactions (1) through (19) as summarized in Table I. The reaction of a stoichiometric mixture of N_2O and CH_2O at 1 atm pressure and 2500 K was simulated on a computer using this 19-step mechanism. All reverse reactions were included in the simulation. Reverse rate constants were computed from the tabulated equilibrium constants[8] and the DJS values of the forward rate constants.

Figure 1 shows the rate of each reaction as a function of reaction time. Table 1 lists the reactions in order of decreasing reaction rate as computed at 0.8 μs, near the time where the reaction is proceeding at its maximum rate.

The figure and table provide a picture of the role of the various reactions in initiation and propagation of the N_2O/CH_2O flame. Initiation occurs by pyrolysis of the oxidant:

$$N_2O + M \rightarrow N_2 + O + M \qquad (5)$$

and branching occurs by O-atom reaction with the fuel:

$$O + CH_2O \rightarrow HCO + OH \qquad (6)$$

By contrast, in O_2-oxidant systems, initiation by fuel pyrolysis produces H-atoms and branching occurs by H-atom reaction with oxidant. For

Table 1. LIST OF REACTIONS OF THE C/H/O BRANCH[a]

Reaction	Rx[b] Type	Rate[c] at T_r = 0.8 μs	ΔH[d]	log K_{eq}^{c} [e]
Fuel and Oxidant Reactions				
1. $M + HCO = H + CO + M$	P	6000	19.9	-1.60
2. $H + H_2CO = HCO + H_2$	P	4500	-19.9	2.67
3. $H + N_2O = OH + N_2$	P	3200	-67.59	7.01
4. $OH + CH_2O = HCO + H_2O$	P	2400	-34.4	3.36
5. $M + N_2O = O + N_2 + M$	I	850	39.5	-1.68
6. $O + CH_2O = OH + HCO$	B	550	-17.7	2.85
7. $OH + HCO = CO + H_2O$	T	480	-103.9	7.60
8. $H + HCO = CO + H_2$	T	280	-89.4	6.91
9. $M + CH_2O = HCO + H + M$	I	180	89.3	-5.84
10. $O + HCO = OH + CO$	P	73	-87.2	7.09
11. $O + N_2O = N_2 + O_2$	T	25	-83.0	7.31
12. $O + N_2O = NO + NO$	T	25	-39.8	4.86
Reversible Reactions				
13. $OH + H_2 = H + H_2O$	P	620	-14.5	0.69
(13R) ($H_2O + H = H_2 + OH$)	(P)	(30)		
14. $O + H_2 = H + OH$	B	180	2.2	0.18
(14R) ($H + OH = H_2 + O$)	(T)	(26)		
15. $OH + CO = H + CO_2$	P	120	-20.0	-0.10
(15R) ($H + CO_2 = CO + OH$)	(P)	(0.3)		
16. $OH + OH = O + H_2O$	T	48	-16.7	0.51
(16R) ($O + H_2O = OH + OH$)	(B)	(15)		
17. $OH + O = H + O_2$	T	10	-15.4	0.31
(17R) ($H + O_2 = OH + O$)	(B)	(.8)		
Reactions Important With O_2 Oxidant				
18. $O + CO + M = CO_2 + M$	T	0.007	-127.0	8.59
19. $O_2 + CO = CO_2 + O$	I	0.002	-4.6	-0.40

[a]Rate constants for simulations were taken from Ref. 1.

[b]Initiation, Propagation, Branching, Termination.

[c]Units are 10^{-4} mol-cm^{-3}-sec^{-1}, Ref. 8.

[d]kcal mol^{-1}, Ref. 8.

[e]Concentration units, mol cm^{-3}.

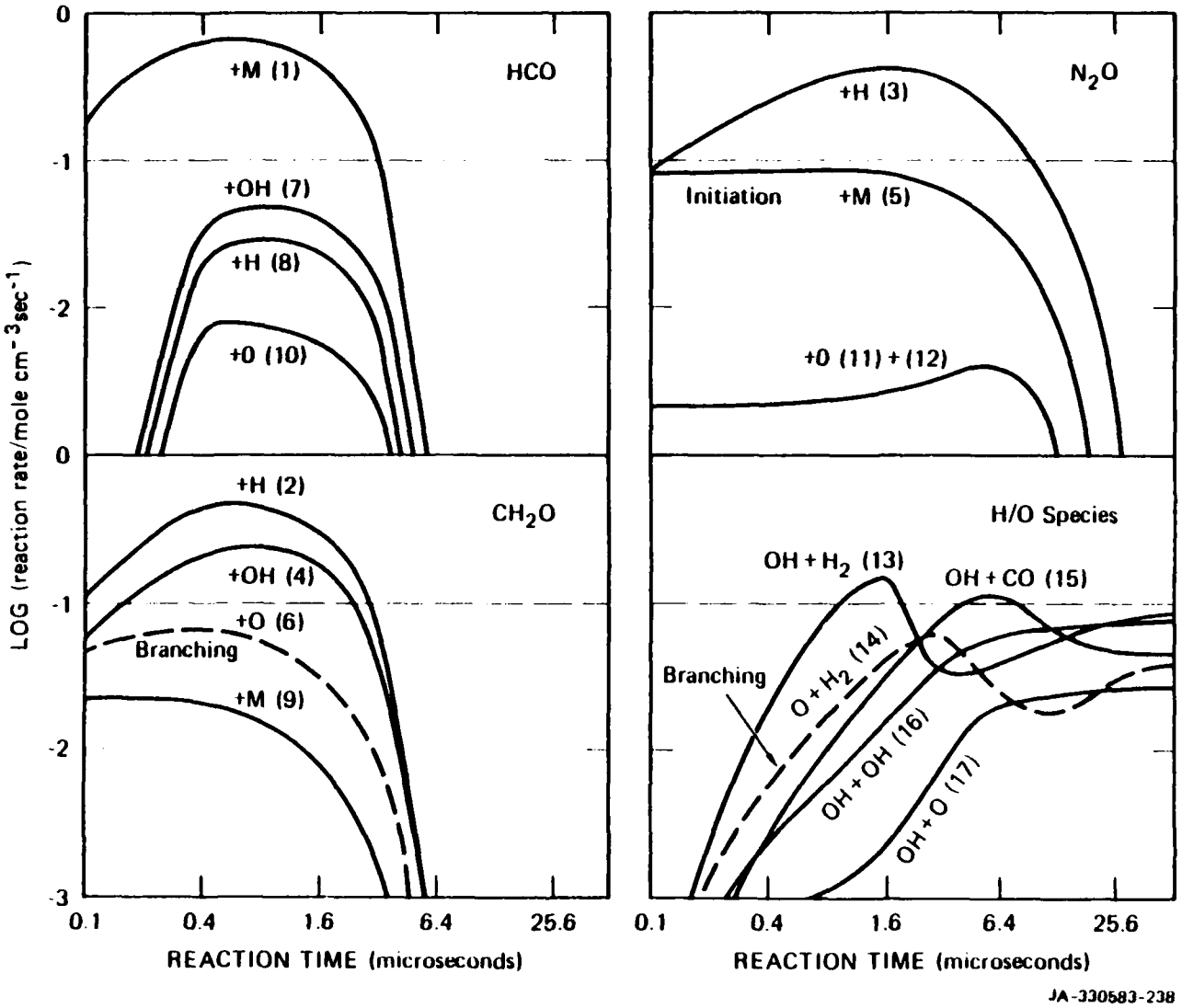

FIGURE 1 REACTION RATES AS A FUNCTION OF TIME IN THE SIMULATION OF THE C/H/O REACTION BRANCH

example, in the oxidation of methane by oxygen, initiation by $CH_4 + M \rightarrow CH_3 + H + M$ is followed by branching via $H + O_2 \rightarrow OH + H$. Thus, in a N_2O-supported flame, branching would be enhanced by a <u>richer</u> mixture, whereas in an oxygen-supported flame, branching would be enhanced by a <u>leaner</u> mixture. This difference between the effects of stoichiometry would also show up in the initiation properties.

Branching through O-atom reaction with H_2

$$O + H_2 \rightarrow OH + H \qquad (14)$$

plays a secondary role in both N_2O- and O_2-supported flames. Formyl radical pyrolysis, reaction (1), is so rapid at this temperature that its concentration is likely to be too low to enable detection.

The figure and table show that about 50 to 80% of N_2O is consumed by H-atom via reaction (3). The rates of the N_2O-consuming reactions at 0.8 μs are as follows:

Reaction	Rate (mol cm^{-3} s^{-1})	
$N_2O + H \rightarrow OH + N_2$	0.32	(3)
$N_2O + M \rightarrow N_2 + O + M$	0.085	(5)
$N_2O + O \rightarrow NO + NO$	0.0025	(12)
$N_2O + O \rightarrow O_2 + N_2$	0.0025	(11)

Thus, if the branching ratio for NH production by $H + N_2O$ is near 0.04 as the H_2/N_2O flame study indicates, the net yield of NH that becomes available for reaction with the radical pool is 2 to 3% of the amount of oxidant.

A simulation that includes a C/H/N/O reaction branch is planned to determine the effects of processing this large amount of material on the C/H/O branch. Because the NH radical may strongly perturb the concentration relationships among OH, H, and O and because NH may consume the material from which it is produced (NH + N_2O → N_2 + HNO), the amount of material processed in the C/H/O branch of the network may be significantly reduced. The low rate constants, which are required in the unperturbed C/H/O branch to fit the DJS data, will be raised by an amount that depends on their sensitivity to the NH perturbation.

Reverse reactions that reform fuel or oxidant are unimportant in the model. However, equilibria among the various O/H species (O, H, OH, O_2, H_2, H_2O) must be included, reactions (13R) through (17R) in Table 1. Oscillations in the rates of the faster (forward) components of these equilibria are apparent in the latter stages of the simulation, Figure 1. These oscillations are possibly an artifact of the calculation that will vanish when the time increment between the successive solutions to the tightly coupled differential equations is shortened.

Species Profiles from Simulation of the C/H/O Branch

Figure 2 shows the concentration profiles for the 13 species of the C/H/O branch. The figure shows results from three hypothetical models: Model 1 is a 19-step mechanism without reverse reactions; Model 2 is a 19-step mechanism with reverse reactions; and Model 3 is a 19-step mechanism, with reverse reactions, that includes a series of steps to synthesize NH. In Model 3, NH is produced by 3-body recombination of H-atom and NO, followed by H + HNO → NH + OH as has been estimated by Tunder and co-workers.[9]

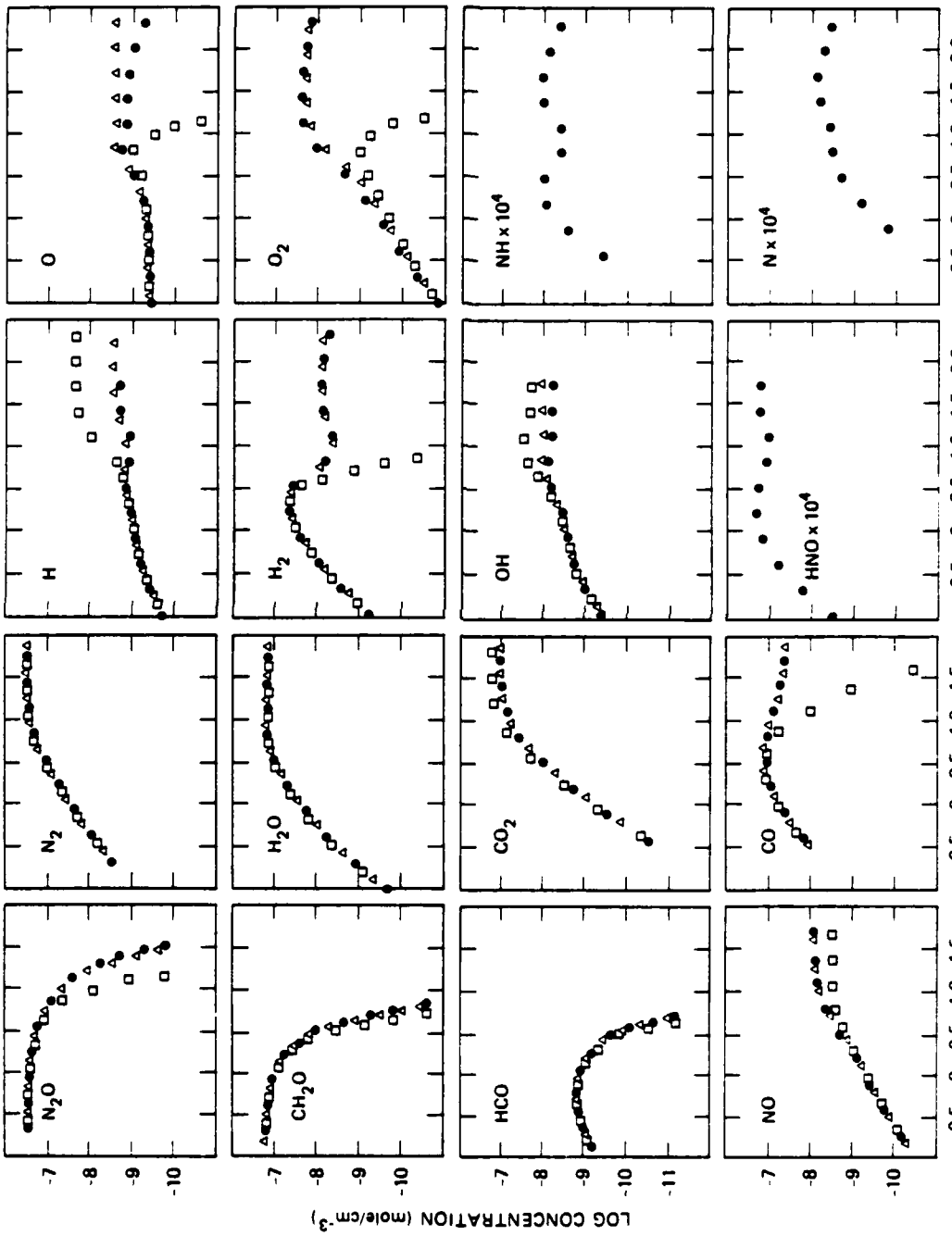

FIGURE 2 SPECIES PROFILES IN THE SIMULATION OF THREE MODELS. MODEL 1-SQUARES, MODEL 2-TRIANGLES AND MODEL 3-FILLED CIRCLES

The figure shows that failure to include reverse reactions (Model 1) leads to unstable solutions for the profiles of CO, O, H_2, and O_2. This instability in the first model does not show up in shock tube simulations where the fuel/oxidant is diluted to about 1 to 4% of the total pressure of 1 atm. The effect of dilution is to proportionately reduce the rates of bimolecular reactions while leaving unimolecular reaction rates unchanged.

The profiles of the nitrogen-containing species (NH, N, and HNO), introduced in the third model, show that the quantity of NH synthesizable through H + HNO → HN + OH (whose rate constant was estimated by Tunder et al[9]) is far too small to account for the observations of NH in N_2O-supported flames.

III ELEMENTARY REACTIONS IN THE C/H/N/O BRANCH

Potential Energy Surface for H + N_2O Branching

Although the minor reaction path for H-atom consumption of N_2O probably contributes little to bulk flame properties (e.g., temperature profiles, heat release, flame speed), it nevertheless is probably the only important reaction leading to the nitrogen-containing species that could or already have been observed or measured by laser probe techniques. An understanding of the temperature and pressure dependences of the branching ratio is crucial to the calibration of the behavior of the nitrogen-containing species that might be used as flame diagnostics.

A potential energy surface for the dual-channel reaction of H-atoms with N_2O may be estimated as shown in Figure 3 and as described below.

Table II lists the values of thermochemical parameters (heats of formation, ΔH_f^o, bond dissociation energies, D°, and activation energies, E_{act}) that may be used to establish a potential energy surface for the two channels:

$$H + N_2O \rightarrow N_2 + OH \qquad (3)$$

$$H + N_2O \rightarrow NH + NO \qquad (20)$$

The CSD flame study (2000 K) and BGPW bulb study (873 K) of the H_2/N_2O system establish an apparent activation energy for the branching ratio, k_{20}/k_3, as follows:

$$E_{act}\ (\text{apparent}) = R\frac{d[\ln(k_{20}/k_3)]}{d[1/T]} = 7.3\ \text{kcal mol}^{-1}$$

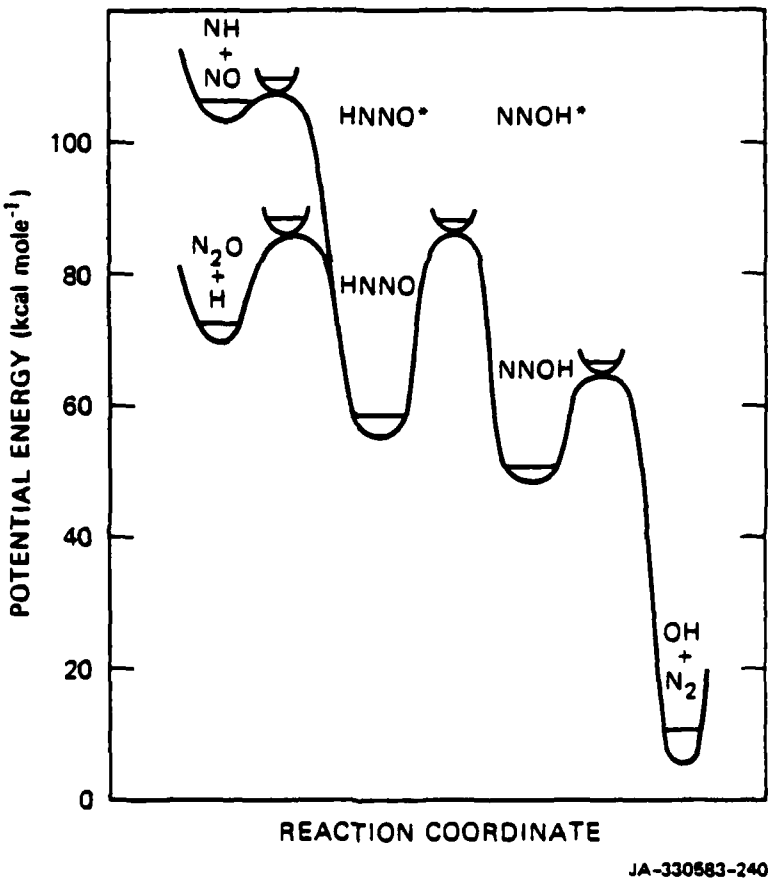

FIGURE 3 ENERGY SURFACE FOR DUAL CHANNEL REACTION OF H-ATOM WITH N_2O

Table II. THERMOCHEMICAL PARAMETERS FOR ESTIMATION OF $H + N_2O$ SURFACE, ($kcal\text{-}mol^{-1}$)

Species	ΔH^{o}_{f298}	Ref.
NH	84.3	12
NO	21.6	11
OH	9.3	11
H	52.1	11
N_2O	19.6	11
HNNOH	32.4	10
(HNNOH)*	(-6 to 30)*	(14)
HNNO	59.1	This estimate
(NNOH)*	(40.1)*	(This estimate)
NNOH	51.8	This estimate

Bond	D^{o}_{298}	Ref.
H-ONO	78.8	11
H-NNH	71.5	10
(H-NNH)*	(59.8)*	(12)
H-NNOH	71.5	This estimate
H-ONNH	78.8	This estimate

Reaction	E_{act}	Ref.
$H + N_2O \rightarrow OH + N_2$	15.1	2
$(H + N_2O \rightarrow OH + N_2)$*	(22.0)*	(1)
$NH + NO \rightarrow H + N_2O$	2.0	13

*These values are alternatives, but they were not used to estimate the potential energy surface.

It may not be possible to reconcile these measured high and low temperature branching ratios by any means because the difference between reaction thresholds, $E_{20} - E_3$ is about 21 kcal mol^{-1}:

$$E_{20} - E_3 = \Delta H_f^o (NH + NO) + E_{act} (NH + NO \rightarrow N_2O + H)$$

$$-(\Delta H_f^o (N_2O + H) + E_{act} (H + N_2O \rightarrow N_2 + OH)$$

$$= 21 \text{ kcal mol}^{-1}$$

The CSD flame model lists values of the rate constants as follows:

$$k_3 = 7.60 \times 10^{13} \exp - 15100/RT \text{ cm}^3 \text{ mol}^{-1} \text{ s}^{-1},$$

$$k_{20} = 3.80 \times 10^{14} \exp - 34500/RT \text{ cm}^3 \text{ mol}^{-1} \text{ s}^{-1}.$$

If the BGPW experiment has been properly interpreted, the branching ratio in the CSD model will not show the correct temperature dependence.

Casewit and Goddard[10] have performed generalized valence bond-configuration interaction calculations on various isomers of NH_2NO. The heat of formation of the most stable isomer, a near linear molecule:

was computed to be ΔH_f^o (HNNOH) = 32.4 kcal mol^{-1}.

Heats of formation of the two intermediates may be estimated by equating the N-H and O-H bonds of HNNOH to those of trans-diimide and trans-nitrous acid, respectively:

$$\Delta H_f^o \text{ (NNOH)} = \Delta H_f^o \text{ (HNNOH)} - D^\circ\text{(H-NNH)} = 51.8 \text{ kcal mol}^{-1}$$

$$\Delta H_f^o \text{ (HNNO)} = \Delta H_f^o \text{ (HNNOH)} - D^\circ\text{(H-ONO)} = 59.1 \text{ kcal mol}^{-1}$$

Thus, stable intermediate species may be established on the potential energy surface. The apparent activation energy for branching depends on the way that the isomers interconnect and on the details of their formation from $H + N_2O$.

Figure 3 shows the surface that is most likely to produce an apparent activation energy for branching which is significantly less than the difference between the threshold energies of the branches, $E_{20} - E_3$.

The formation of NNOH directly from reactants is excluded. The reaction sequence may be visualized:

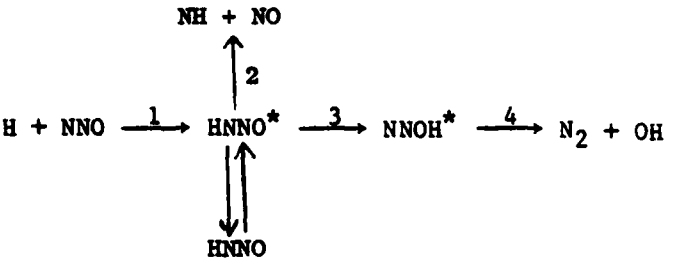

Because the isomerization (3) occurs at an energy level where the specific rate constant for isomerization is nearly energy independent, the activation energy for formation of $N_2 + OH$, a composite energy quantity, is principally determined by the threshold energy required to from $HNNO^*$ from $H + N_2O$. The details of the reactions on this surface may be analyzed by performing RRKM calculations on the three-channel competitive unimolecular decomposition of HNNO. Whereas the average energy of the $HNNO^*$ formed by $H + N_2O$ is at the same level as HNNO

molecules which would decompose (to H + N_2O) in the high pressure limit, the average energies of the HNNO that decomposes through channels 2 and 3 correspond to the substantially lower activation energies in the low pressure limit.

REFERENCES

1. A. M. Dean, R. L. Johnson, and D. C. Steiner, Combustion and Flame, 37, 41 (1980).

2. D. L. Baulch, D. D. Drysdale, D. G. Horne and A. C. Lloyd, Evaluated Kinetic Data on High Temperature Reactions, Vol. 2 Butterworths, London, (1972-73).

3. R. Cattolica, M. Smooke, and A. Dean, "A Hydrogen-Nitrous Oxide Flame Study," Presented at 1982 Fall Meeting of the Combustion Institute, Sandia National Laboratories, Livermore, CA, October 11-12, Paper WSS/C1 82-95.

4. D. B. Olson and W. C. Gardiner, Jr., Combustion and Flame, 32, 151 (1978).

5. D. E. Jensen and G. A. Jones, Combustion and Flame, 32, 1 (1978).

6. R. R. Baldwin, A. Gethin, J. Plaistowe and R. W. Walker, Trans. Far. Soc. I, 6, 1265 (1975).

7. W. R. Anderson, L. J. Decker, and A. J. Kotlar, Technical Report ARBRL-TR-02406, Ballistic Research and Development Command, Aberdeen, MD, (October 1982).

8. V. S. Engleman, "Survey and Evaluation of Kinetic Data on Reactions in Methane/Air Combustion," Environmental Protection Technology Series, EPA-600/2-76-003, USEPA, Research Triangle Park, NC 27111.

9. R. Tunder, S. Mayer, E. Cook and L. Schieler, Thermochemical Research Department, Aerospace Corporation, Report No. TR-1001 (9210-02)-1, AD813485 (1967).

10. C. J. Casewit and W. A. Goddard, III, J. Am. Chem. Soc., 104, 3280, 1982.

11. JANAF Thermochemical Tables, Dow Chemical Company, CFSTI Department of Commerce, Springfield, VA and supplements to 1982.

12. S. N. Foner and R. L. Hudson, J. Chem. Phys., 68, 5017, 1981.

13. T. R. Roose, R. K. Hanson and C. H. Kruger, Proceedings of the Eleventh International Shock Tube Symposium (University of Washington Press, Seattle, WA, 1977), p. 245.

14. J. A. Miller, M. C. Branch, and R. J. Kee, Combustion and Flame, 43, 81, 1981.

DETECTION OF O AND N ATOMS BY TWO-PHOTON LASER INDUCED FLUORESCENCE

W. K. Bischel, B. E. Perry, D. R. Crosley
Molecular Physics Laboratory
SRI International, Menlo Park, Ca 94025

(415) 859-5129

ABSTRACT

Oxygen and nitrogen atoms in a low-pressure flow have been detected by observing near-IR fluorescence (845-870 nm) from states excited by two-photon absorption. The uv exciting radiation was provided by coherent anti-Stokes Raman scattering from a doubled dye laser. Relative two-photon cross sections, excited state lifetimes and quenching rates have been determined.

Conf Lasers & Elec Opt WAC, June 19[illegible]

W. K. Bischel, et al.
Molecular Physics Laboratory
SRI International
Menlo Park, CA 94025

(415) 859-5129

DETECTION OF O AND N ATOMS BY TWO-PHOTON LASER INDUCED FLUORESCENCE*

SUMMARY

The sensitive detection of ground-state atomic species under non-ideal experimental conditions, such as those found in combustion research or plasmas, has been a problem for many years. Single photon detection techniques such as resonance fluorescence are not applicable since the medium is generally opaque at vuv wavelengths. We describe here a new general detection scheme for atomic species based on two-photon excitation using wavelengths which will be transmitted, and its application to the detection of oxygen[1] and nitrogen atoms.

Oxygen and nitrogen atoms at $\sim 10^{14}$ cm^{-3} concentration were produced in a flowing microwave discharge and were excited on the two-photon transitions $O(^3P \rightarrow 3p\,^3P)$ and $N(^4S^o \rightarrow 3p\,^4D^o)$. The required uv laser wavelengths were 225 nm and 211 nm respectively. The exciting uv radiation was provided by stimulated Raman scattering (third anti-Stokes order in H_2) from a frequency doubled dye laser. Detection of the near ir fluorescence emission (845-870 nm) from the excited state formed the observed signal. For oxygen, the two-photon absorption cross section was measured to be the same for each ground state fine structure component, (summed over the final state fine structure). For nitrogen, the relative two-photon absorption

cross sections from the ground $^4S^\circ$ state to the four fine structure components of the $^4D^\circ_J$ excited state were in the ratio of 4:3:2:1: for the J = 7/2, 5/2, 3/2, and 1/2 states, respectively. These values are in agreement with a simple theory based on angular momentum coupling rules.

In addition, radiative lifetimes and quenching rates for the excited states have been determined. For oxygen, the radiative lifetime of the $3p^3P$ excited state was determined to be 34 nsec in agreement with past measurements, and the rate constant for collisional quenching by N_2 was found to be $2 \times 10^{-10} cm^3 sec^{-1}$. For nitrogen, the radiative lifetime of the $^4D_{7/2}$ excited state was determined to be 30 nsec, and the rate constant for collisional quenching by N_2 was found to be approximately the same as that for O atoms.

In summary, the atom detection technique demonstrated here provides a promising new way to sensitively determine atom concentrations. Scaling from the signal levels in these experiments indicated that a modest improvement in the laser intensity to ~1 mJ/pulse would allow atom concentrations on the order of 10^{11} cm^{-3} to be detected under low pressure conditions.

*Supported in part by the U.S. Army Research Office and in part by internal research and development funds of SRI International.

[1]W. K. Bischel, B. E. Perry, and D. R. Crosley, Bull. Amer. Phys. Soc. 26, 23 (1981).

Chemical Education

Laser-Induced Fluorescence in Spectroscopy, Dynamics and Diagnostics

avid R. Crosley

Molecular Physics Laboratory
SRI International
333 Ravenswood Avenue
Menlo Park, CA 94025
(415) 859-2395

x x

Physicist

SRI International

x

J. Chem. Ed.

LASER-INDUCED FLUORESCENCE IN SPECTROSCOPY, DYNAMICS AND DIAGNOSTICS* David R. Crosley, Molecular Physics Laboratory, SRI International, Menlo Park, CA 94025

The phenomenon of laser-induced fluorescence (LIF) occurs when a laser, tuned to match an absorption line of some atom or molecule, elevates the species to an emitting electronically excited state. Using a sufficiently narrow laser bandwidth, a single rotational-vibrational level in the upper state can be excited. Detection of all the fluorescent emission, as the laser is tuned through a series of absorption lines, (a so-called excitation scan), yields population distributions over ground state internal levels, whereas a scan of the dispersed fluorescence, while the laser pumps a single level, provides information about the excited state. The clean state preparation afforded by LIF has significant advantages for spectroscopic studies and the investigation of state-specific collisional behavior. As a diagnostic tool, LIF provides considerable species selectivity coupled with high spatial and temporal resolution and a non-intrusive nature; it is especially well suited for the measurement of small free radicals present in flames, plasmas, and the atmosphere. The recent availability of powerful tunable lasers in the visible and ultraviolet, coupled with stimulated Raman frequency shifting, makes possible the excitation of a wide variety of species spanning the wavelength range from the vuv to the near ir. These attributes of LIF will be discussed, using as examples spectroscopic studies on S_2, energy transfer measurements in OH, two-photon excitation of O and N atoms, and the detection of transient radical species in flames.

*The author's research in this area is supported by the U.S. Army Research Office and the National Science Foundation (Engineering Energetics).

Eastern Section of the Combustion Institute
Pittsburgh, Pennsylvania
October 1981

LASER-INDUCED FLUORESCENCE STUDIES OF THE NCO MOLECULE

Brian J. Sullivan, Gregory P. Smith, David R. Crosley and Graham Black
SRI International
Menlo Park, California 94025

Introduction

Laser-induced fluorescence (LIF) is the laser spectroscopic probe technique[1] suitable for measurement of the transient species which are the intermediates in combustion chemistry. To date, two dozen such molecules have been detected, in flames and/or flow systems, using LIF. The high sensitivity afforded by LIF follows from the participation of a real electronically excited state; this also means that the spectral form and magnitude of the signals are affected by collisions, whose influence must be known for a fully quantitative measurement.[2] Nonetheless there exist many cases in which the detection of some given species, at an appropriate concentration level, can provide significant clues as to the chemical mechanism involved in the combustion process.

We report here the results of LIF studies on the $A^2\Sigma^+ - X^2\Pi_i$ and the $B^2\Pi_i - X^2\Pi_i$ systems of the NCO molecule, performed in a discharge flow system at low pressure. NCO has been proposed as an intermediate in the oxidation of HCN and production of NO in nitrogen-containing fuels,[3] and in the C_2N_2/O_2 flame,[4] although it was not measured in those cases. It has also been suggested[5] as a potential intermediate in hydrocarbon/N_2O flames. Recently, NCO has been identified[6] using LIF in the reaction zone of CH_4/N_2O flames. The excitation was by an Ar^+ laser at fixed wavelengths, which overlap lines in hot bands of the A-X system. The present work provides some of the spectroscopic characterization necessary for semi-quantitative estimates of NCO concentrations from LIF signals in flames.

Both absorption and emission in gas-phase NCO have been previously observed. Dixon, using absorption data from flash photolysis experiments, performed an extensive rotational analysis on the A-X system[7] and a less complete survey of the B-X system.[8] These have served as a key starting point for our investigations and assignments. LIF in the A-X system has previously been studied[9] for NCO deposited on an Ar matrix at 4° K, and that work has also provided a useful guide.

MP 81-140
07/31/81

Experimental

NCO is produced by the gas-phase reaction F + HNCO and/or HOCN. The acid vapor is formed in a small reaction vessel containing KOCN and stearic acid at ~ 100° C,[10] and is injected into a glass flow system of moderate pumping speed. F atoms are created using a microwave discharge on CF_4 or SF_6 in ~ 1 torr He. Pressures are measured with a Baratron gauge.

The exciting radiation for the A-X excitation is provided by a Nd:YAG-pumped tunable dye laser which has been frequency shifted by stimulated Raman frequency conversion in ~ 10 atm of H_2. The second order antistokes shifted radiation, displaced to the blue from the input by twice the H_2 vibrational spacing, falls in the appropriate wavelength region using rhodamine dyes in the laser; it has a bandwidth of ~ 0.15 cm^{-1} and pulse length of ~ 8 nsec. For the B-X excitation, we use a frequency doubled dye laser containing rhodamine.

The fluorescence emitted at right angles to the laser beam is focussed through a filter onto a photomultiplier tube wired for fast response. In a few runs the filter was an interference-filter/color-glass-filter combination but for most of the measurements a 0.35 m monochromator was used, with about a 40 Å bandpass. The slit was narrowed to a 5 or 10 Å bandpass for several runs in which the fluorescence spectra at fixed excitation wavelength were measured. Signals were read out using a boxcar integrator (operated in the scanning mode for lifetime runs) and a chart recorder; typically a 1-2 second (10-20 pulses) averaging time was used.

Results and Discussion

Four vibrational levels of $A^2\Sigma^+$ have been pumped in transitions originating from the 000 level of $X^2\Pi_i$ (the 030 excitation was too weak to permit experiments beyond its observation). An excitation scan (fixed detection wavelength while the laser is tuned) of the 001-000 band has been rotationally assigned following Dixon's analysis;[7] lines up to N ~ 40 in each of the eight observable rotational branches could be seen. Using line strengths calculated from standard $^2\Sigma - {}^2\Pi$ equations with Dixon's spectral constants, rotational level populations in the ground state could be determined. The results from the $R_1 + {}^RQ_{21}$ branch yield a temperature of 310° K, in accord with expectations for this room temperature experiment. The results from the R_2 and the $Q_2 + {}^QR_{12}$ branches yield a much lower temperature (200° K), perhaps indicating a detector spectral bias.[11] The other three bands, though not rotationally analyzed in detail, show the expected features and general structure.

Upper state lifetimes were measured for each vibrational level (except 030), both with and without added gases. In a plot of the decay rate vs. added gas pressure, the intercept yields the radiative lifetime τ while the slope yields the collision-induced decay rate k_Q. The results are listed in Table 1.

Table 1

Level $\nu_1\nu_2\nu_3$	λ(exc) nm	τ nsec	$k_Q(N_2)$ 10^{-11} cm sec^{-1}	$k_Q(O_2)$
001	399	410 ± 15	3.0 ± 0.2	10.6± 0.2
030	403	---	---	---
020	413	430 ± 20	0.56 ± 0.10	---
100	417	300	---	---

The quoted error bars are statistically determined from fits to the lifetime runs, and do not include estimates of possible systematic errors; only an approximate τ has been obtained for the 100 level. The background gases He, SF_6, and CF_4 were found not to noticeably influence the decay rate at the pressures used.

The radiative lifetime of ~ 430 nsec is considerably longer than the value of 180 nsec obtained in the matrix study.[9] A comparison[9] of spectral constants from the gas phase and matrix investigations shows that the matrix does not greatly alter the potential curves, so that it would not be expected to affect the transition moment. Thus the difference is likely a quenching effect due to the matrix environment.

The measured k_Q could be the sum of both quenching back to the ground state and transfer to other vibrational levels of the excited state. Fluorescence scans were made at zero added gas pressure and with the addition of N_2. Several bands could be identified in the emission from each vibrational level but in no case was the spectrum altered noticeably upon the addition of N_2. Thus $k_Q(N_2)$ can be ascribed entirely to collisional quenching. In particular, transfer downward to 000 of the A-state, a strong emitter, is not seen. The 100 and 020 levels are in Fermi resonance,[7] and the fluorescence spectra in the matrix study[9] showed very rapid transfer between these two levels. The present work demonstrates that gas-phase collisional coupling between these levels is not enhanced by the existence of the Fermi resonance.

Excitation of the 000-000 band of the B-X system near 315 nm has also been performed. The fluorescence spectrum shows a long progression, to nearly 500 nm, in the bending vibration. Preliminary lifetime measurements indicate a τ(B) of 50 nsec, considerably shorter than τ(A).

Conclusions

From the radiative lifetime, calculated line strengths, and Franck-Condon factors estimated from the fluorescence runs, one may calculate approximate absorption coefficients for the A-X bands excited here of $k_Q \sim 5 \times 10^{-14}$ N cm^{-1} where N is the number density (cm^{-3}) per absorbing level. However, the possibility of collisionless state mixing in triatomics, exemplified by NO_2[12], can cause a stronger apparent absorption than indicated by the radiative lifetime and such a situation cannot be ruled out here.

The lack of energy transfer means that emission from laser-excited $A^2\Sigma^+$ NCO will occur from the vibrational level pumped, and not from lower-lying levels as is often the case for diatomics in flames; this fact then dictates that appropriate detector wavelengths for NCO monitoring correspond to emission from the level directly excited. From the ratio of τ and k_Q values, the fluorescence quantum yield would be $\sim 0.2\%$ in room temperature air for 001 excitation but may be higher for 020 excitation.

The 000–000 band of the B–X system falls in a convenient wavelength region for laser excitation. Although the long progression in the fluorescence spectrum leads to a smaller effective quantum yield for a given spectral bandpass, the shorter lifetime indicated in the preliminary measurements would mean stronger absorption and less collisional influence. Hence this system may be a better choice for LIF measurements of NCO.

Acknowledgments

We thank M. J. Dyer for assistance with the experiments. This work was supported by the U. S. Army Research Office.

References

1. D. R. Crosley, Ed., "Laser Probes for Combustion Chemistry," Amer. Chem. Soc. Symposium Series, Vol. 134, 1980.

2. D. R. Crosley, Opt. Eng. 20, 511 (1981).

3. B. S. Haynes, D. Iverach, and N. Y. Kirov, Fifteenth Symposium (International) on Combustion, 1975, p. 1103; C. P. Fenimore, Comb. Flame 26, 249 (1976); C. Morely, Comb. Flame 27, 189 (1976); B. S. Haynes, Comb. Flame 28, 113 (1977); C. P. Fenimore, Seventeenth Symposium (International) on Combustion, 1979, p. 611; C. Morely, Eighteenth Symposium (International) on Combustion, 1981, p. 23.

4. J. N. Mulvihill and L. F. Phillips, Fifteenth Symposium (International) on Combustion, 1975, p. 113.

5. G. P. Smith, unpublished.

6. J. A. Vanderhoff, R. A. Beyer, W. R. Anderson, and A. J. Kotlar, Thirty-Sixth Symposium on Molecular Spectroscopy, Columbus, Ohio, June 1981; W. R. Anderson, J. A. Vanderhoff, A. J. Kotlar, L. J. Decker, and R. A. Beyer, Eastern Section Meeting of the Combustion Institute, Pittsburgh, Pennsylvania, October 1981.

7. R. N. Dixon, Phil. Trans. Roy. Soc. London, A262, 165 (1960.

8. R. N. Dixon, Can. J. Phys. 38, 10 (1960).

9. V. E. Bondybey and J. H. English, J. Chem. Phys. 67, 2868 (1977).

10. W. P. Drozdoski, A. P. Baronavski, and J. R. McDonald, Chem. Phys. Lett. 64, 421 (1979).

11. D. R. Crosley and G. P. Smith, Comb. Flame, in press.

12. A. E. Douglas, J. Chem. Phys. 45, 1007 (1966); V. M. Donnelly and F. Kaufman, J. Chem. Phys. 66, 4100 (1977).

Physical Chemistry

Laser-Induced Fluorescence In Combustion Chemical Kinetics

David R. Crosley

Molecular Physics Laboratory x x
SRI International
333 Ravenswood Avenue
Menlo Park, CA 94025
(415) 859-2395 Physicist

ACS Membership number MUST be indicated for at least one author (Please use number as it appears on C&EN mailing label)

SRI International

LASER-INDUCED FLUORESCENCE IN COMBUSTION CHEMICAL KINETICS* David R. Crosley, Molecular Physics Laboratory, SRI International, Menlo Park, California 94025

In laser-induced fluorescence (LIF), the absorption of a laser photon promotes a molecule to an electronically excited state which then radiates. For those molecules which can be made to fluoresce, LIF is an extremely sensitive and selective means of their detection. Into this category fall some 20 species (atoms, diatomic and triatomic free radicals) which are intermediates in combustion chemistry. The number continues to expand with further spectroscopic studies (e.g., NCO), new lasers and frequency conversion methods such as Raman shifting, and the use of two-photon absorption as for O and N atoms. LIF has thus become a key tool for the understanding of combustion chemistry through the nonintrusive measurement of flame intermediates. In addition to probing flames themselves, LIF can also be used in related kinetics studies. An example is measurement LIF of the time dependence of radical concentrations in isothermal laser pyrolysis. Here, a pulsed CO_2 laser is absorbed in a sample seeded with SF_6, causing rapid heating to temperatures of combustion interest, with the production and subsequent reaction of the radicals. For example, H_2O_2 dissociates to OH radicals at T > 1000K, and the OH reaction rates can then be measured at high temperature. LIF's capabilities and limitations (chiefly the need to account for collisional processes in the excited state) in both flames and combustion chemistry experiments, will be discussed.

*Research supported by the Army Research Office, National Science Foundation, Department of Energy, and Wright Aeronautical Laboratories.

LASER-INDUCED FLUORESCENCE STUDIES OF THE A-X AND B-X SYSTEMS OF THE NCO RADICAL

Brian J. Sullivan, Gregory P. Smith, and David R. Crosley

NCO was produced in a low-pressure flow system by reacting HNCO with F atoms generated in a discharge in CF_4/He. Utilizing a Nd:YAG-pumped dye laser, excitation spectra of the $A^2\Sigma^+ - X^2\Pi_i$ system and the $B^2\Pi_i - X^2\Pi_i$ system were obtained between 4400-3980 Å and 3156-3142 Å respectively. Signals were read out using a boxcar intergrator, which was operated in a scanning mode for lifetime runs. A small monochromator, capable of 1 Å resolution, was used to obtain fluorescence spectra.

Five vibrational levels (0,0,0; 0,1,0; 1,0,0; 0,2,0; 0,0,1) of the A state were probed, and assignments could be made following Dixon (1). The radiative lifetime was found to be 410 nsec and was insensitive to vibrational level. Quenching rates determined for N_2 and O_2 are 3.0×10^{-11} and 11×10^{-11} cm^3 sec^{-1} respectively.

The R_1 and R_2 heads of the (0,0,0 - 0,0,0) band of the B-X system (2) were pumped, and the resulting fluorescence spectra showed a long progression in ground state stretching modes. These spectra allowed us to extract a set of constants describing these stretching vibrations in $X^2\Pi_i$:

$\omega_1^o = 1286$ cm^{-1} $\omega_3^o = 1925$ cm^{-1} $X_{13} = -27.8$ cm^{-1}

$X_{11} = -10.3$ cm^{-1} $X_{33} = -11.6$ cm^{-1}

The radiative lifetime obtained for the B state was 63 nsec. Quenching rates for N_2 and O_2 were found to be 1.3×10^{-10} and 2.0×10^{-10} cm^3 sec^{-1} respectively.

(1) R. N. Dixon, Phil. Trans. Roy. Soc. London, A262, 165 (1960).
(2) R. N. Dixon, Can. J. Phys. 38, 10 (1960).

This work was supported by the U. S. Army Research Office.

LASER FLUORESCENCE SPECTROSCOPY OF NCO. Brian J. Sullivan, Gregory P. Smith, and David R. Crosley, SRI International, Menlo Park, CA 94025.

Laser-induced fluorescence of the NCO $A^2\Sigma^+ - X^2\Pi$ and the $B^2\Pi - X^2\Pi$ systems was investigated between 440-398 nm and 316-314 nm, respectively. Excitation spectra, fluorescence spectra, radiative lifetimes, and quenching rate constants were studied.

NCO has been proposed as an intermediate in the oxidation of nitrogen-containing fuels, and has recently been observed in the reaction zone of a CH_4/N_2O flame.[1] The present work provides some of the spectroscopic characteristics necessary for semi-quantitative estimates of NCO concentrations from LIF signals in flames.

NCO is produced by the gas-phase reaction F + HNCO and/or HOCN. The acid vapor is formed in a small reaction vessel containing KOCN and stearic acid at ~ 100°C, and is injected into a glass flow system of moderate pumping speed. F-atoms are created using a microwave discharge on CF_4 or SF_6 in ~ 1 torr He.

The exciting radiation for the A-X excitation is provided by a Nd:YAG-pumped tunable dye laser which has been frequency-shifted by stimulated Raman frequency conversion in ~ 10 atm of H_2. Coumarin dyes and second-order anti-stokes shifted radiation from rhodamine dyes were used. The laser has a bandwidth of ~ 0.15 cm^{-1} and pulse length of ~ 8 nsec. For the B-X excitation, we use a frequency doubled dye laser containing rhodamine 640.

The fluorescence emitted at right angles to the laser beam is focussed onto the slits of a .35 m monochromator with a 40 Å bandpass for excitation spectra, and a 1-10 Å bandpass for several runs in which the fluorescence spectra at fixed excitation wavelength were measured. A boxcar integrator and a chart recorder, with 2 second (20 pulse) averaging time, were used for signal processing.

Transitions from the ground (0,0,0) level of the $X^2\Pi$ state to five vibrational levels (0,0,0; 0,1,0; 1,0,0; 0,2,0; 0,0,1) of the $A^2\Sigma^+$ state were pumped; excitation scans (fixed fluorescence detection wavelength while the laser is tuned) have been obtained for such upper state vibration level

XV Informal Conf. on Photochem.) . . 1982

studies. These spectra can be rotationally assigned following Dixon's analysis.[2]

Emission lifetimes were measured for such vibrational levels, both with and without added gases, to obtain radiative lifetimes (t) and collisional quenching rates. The radiative lifetime is 410 nsec and is relatively insensitive to vibrational level. Our measured radiative lifetimes agree well with those of Reisler, Mangir, and Wittig[3], but is considerably longer than the value of 180 nsec in an Ar matrix[4] study. Collisional quenching rate constants for the 0,0,1 level are 3.0×10^{-11} and 1.1×10^{-10} cm^3 sec^{-1} for N_2 and O_2, respectively. Similar rates were measured for the other levels. Helium was found to have a small collisional quenching rate ($\leq 1.5 \times 10^{-12}$ cm^3 sec^{-1}). The fluorescence spectra also indicate no significant collisional population of other vibrational levels of the A-state prior to quenching or fluorescence.

Fluorescence spectra (laser-fixed, monochromator-scanned) were obtained for excitation at band heads in all levels. The wavelengths of the observed bands agree with previous determinations of $X^2\Pi$ vibrational level energies.[4,5] The $A^2\Sigma^+(0,1,0) \leftarrow X^2\Pi(0,0,0)$ transistion is electronically forbidden, but weakly allowed due to vibronic interaction. Figure 1 shows a portion of the

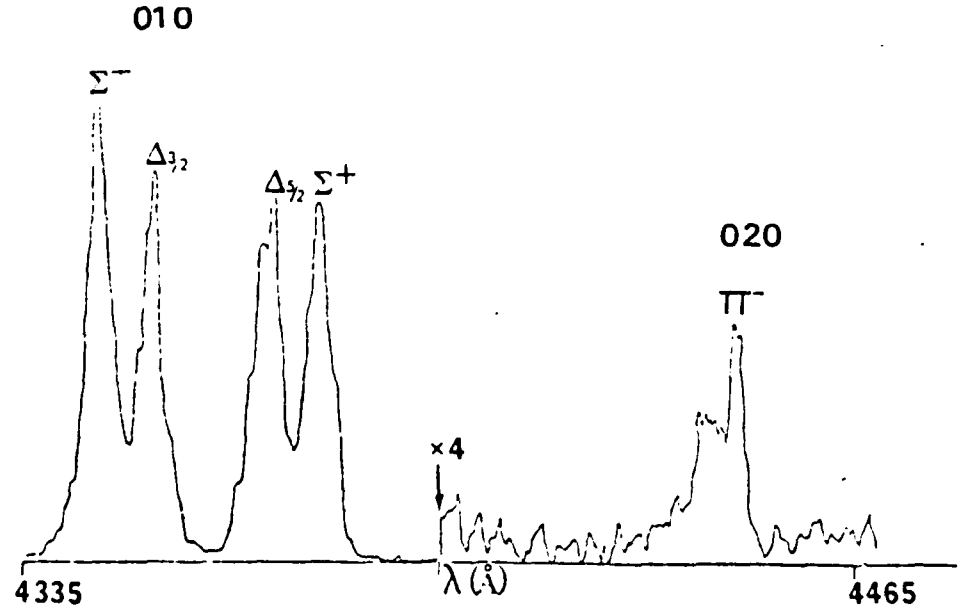

high resolution (1 Å) spectra of the $A^2\Sigma^+(0,1,0) \rightarrow X^2\Pi_i(\nu_1,\nu_2,\nu_3)$ fluorescence. The four vibronic components, which are due to Renner-Teller and spin-orbit interactions, of the 0,1,0 level of the ground state, were easily seen. The lack of observable $A^2\Sigma^+(0,1,0) \rightarrow X^2\Pi_{1/2}(0,0,0)$ fluorescence indicates this transition is at least an order of magnitude weaker than the $A^2\Sigma^+(0,1,0) \rightarrow X^2\Pi(0,1,0)$ transition. Several $A^2\Sigma^+(0,1,0) \rightarrow X^2\Pi_i$ $(\nu_1,2,\nu_3)$ fluorescence bands were also observed, but only emission to the Π^- vibronic component was seen. Fluorescence from the 0,0,0 level of the $A^2\Sigma^+$ state shows similar behavior. Possible explanations for this phenomenon are being pursued.

An excitation spectrum of the (0,0,0)-(0,0,0) band of the $B^2\Pi_i - X^2\Pi_i$ system was obtained between 3156-3142 Å. The rotational structure is very congested[6], and only the R_1 and R_2 heads are easily discernible. A radiative lifetime of 63 nsec was measured for the $B^2\Pi_i$ state, considerably shorter than the $A^2\Sigma^+$ state lifetime. No fluorescence to the A-state, or A-X emission upon B-state excitation was observed. Quenching rate constants for N_2 and O_2 are 1.3×10^{-10} and 2.0×10^{-10} cm^3 sec^{-1}, respectively. The fluorescence spectra show long progressions in the ground-state stretching modes. Derived ground-state vibration constants are: $\omega^o_1 = 1286$ cm^{-1}, $\omega^o_3 = 1925$ cm^{-1}; $X_{11} = -10.3$ cm^{-1}, $X_{33} = -11.6$ cm^{-1}, $X_{13} = -27.8$ cm^{-1}. Attempts are underway to derive potential surface information from the fluorescence spectrum intensities.

This work was supported by the U.S. Army Research Office.

References

1. J. A. Vanderhoff, R. A. Beyer, W. R. Anderson, and A. J. Kotlar, Thirty-Sixth Symposium on Molecular Spectroscopy, Columbus, Ohio, June 1981; W. R. Anderson, J. A. Vanderhoff, A. J. Kotlar, L. J. Decker, and R. A. Beyer, Eastern Section Meeting of the Combustion Institute, Pittsburgh, Pennsylvania, October 1981.

2. R. N. Dixon, Phil. Trans. Roy. Soc., London, A262, 165 (1960).

3. H. Reisler, M. Mangir, and C. Wittig, Chem. Phys., 47, 49-58 (1980).

4. V. E. Bondybey and J. H. English, J. Chem. Phys., 67, 2868 (1977).

5. D. E. Milligan and M. E. Jacox, J. Chem. Phys., 47, 5157 (1967).

6. R. N. Dixon, Can. J. Phys., 38, 10 (1960).

LASER PYROLYSIS STUDIES OF UNIMOLECULAR AND BIMOLECULAR REACTIONS OVER 1000 K: ORGANOMETALLIC BOND ENERGIES, OH REACTIONS

G.P. Smith K. E. Lewis, D.M. Golden
P. W. Fairchild, and D. R. Crosley

SRI International
Menlo Park, California 94025 USA

• ABSTRACT

A pulsed CO_2 laser was used to heat a 50 torr gas mixture of bath gas, SF_6 absorber, and reactant molecules to 1000-1500 K. The unimolecular decomposition kinetics of metal carbonyls, such as $Fe(CO)_5$, were measured using either other known decomposition reactions or bath gas infrared fluorescence as a thermometer. First, bond dissociation energies for these organometallics were determined from these competitive kinetics measurements. Bimolecular reactions, such as $OH + CH_4$, were also measured by the laser pyrolysis method. Hydroxyl is formed by laser pyrolysis of H_2O_2, and its temporal evolution is monitored by laser-induced fluorescence using a variable delay pulsed dye laser. Both temperature and decay rate at set methane pressures were determined, thus furnishing bimolecular rate constants. The general features, advantages, and limitations of this new high-temperature kinetic method will be discussed.

AD-A140 767 LASER PROBES OF PROPELLANT COMBUSTION CHEMISTRY(U) SRI INTERNATIONAL MENLO PARK CA D R CROSLEY ET AL. 29 MAR 84 SRI-MP-84-053 ARO-17416.9-CH DAAG29-80-K-0049 3/3

UNCLASSIFIED F/G 7/4 NL

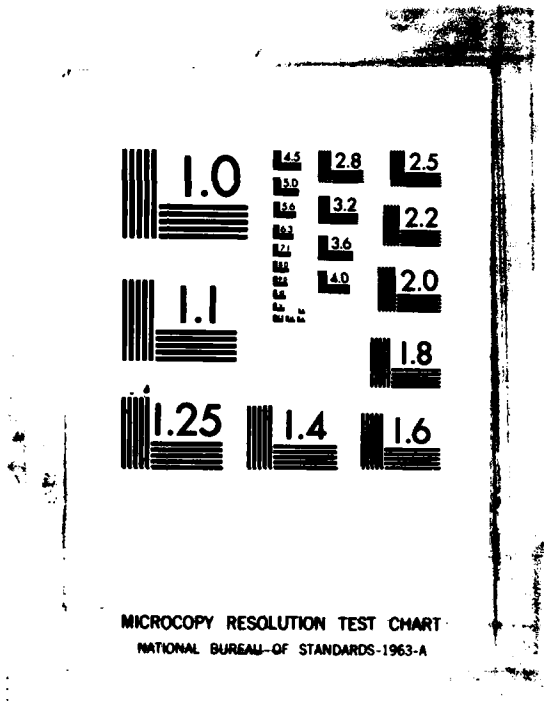
1.0
1.1
1.25
1.4
1.6
2.8
3.2
3.6
4.0
2.5
2.2
2.0
1.8
MICROCOPY RESOLUTION TEST CHART
NATIONAL BUREAU OF STANDARDS-1963-A

SRI International

BIMOLECULAR QUENCHING RATE CONSTANTS FOR OH AT HIGH TEMPERATURE

Paul W. Fairchild, Gregory P. Smith
and David R. Crosley
Molecular Physics Laboratory
SRI International
Menlo Park, California 94025

Rate constants k_Q for collisional quenching of the $A^2\Sigma^+$ state of the OH molecule have been measured in the temperature range 800-1500K. The OH is produced and detected in a laser pyrolysis/laser fluorescence experiment, in which a mixture of SF_6, H_2O_2 and the collision partner M is heated by a pulsed CO_2 laser. Thermal decomposition of H_2O_2 produces some OH. Following dye laser excitation of the OH, the real-time decay of the fluorescence signal is measured. Measurements were made for a variety of gases M found in flames. The high temperature values of k_Q are generally smaller than expected for a cross section independent of temperature. This result, the size of k_Q, and its dependence on M suggest that attractive forces are important in the quenching collisions, and the results have been examined with the objective of extablishing a theoretical foundation for describing the variation of k_Q.

MP 82-124
10/20/82

Western States Section of the Combustion Institute Fall Meeting, Livermore, CA October 1982

SRI International
333 Ravenswood Ave. • Menlo Park, CA 94025
(415) 859-6200 • TWX: 910-373-2046 • Telex: 334 486

Abstract for an Invited Paper
for the Philadelphia Meeting of the
American Physical Society
3-5 November 1982

Laser-Induced Fluorescence Spectroscopy in Combustion Research*.
DAVID R. CROSLEY, Molecular Physics Laboratory, SRI International.

Laser-induced fluorescence (LIF), which involves the absorption of tunable laser radiation and detection of the resulting fluorescent emission, is one of several laser spectroscopic probe techniques recently developed as a tool in combustion research. Possessing high sensitivity and selectivity, it is especially well suited for the measurement of the transient free radicals which are intermediates in combustion chemistry. About 20 atomic, diatomic and triatomic species fall into this category; the number continues to grow with new spectroscopic studies (e.g., NCO), new lasers and frequency conversion methods such as Raman shifting, and the use of two photon excitation as for O, N and CO. Most LIF measurements have been made on a point-resolved basis with high spatial resolution, but recently a two-dimensional, single-shot image of LIF in OH in a flame has also been obtained. This imaging can provide spatially correlated measurements in a time varying combustion system such as a turbulent flame. In addition to measurements directly in flames, LIF can be used for related chemical kinetics studies, for example a laser pyrolysis/LIF measurement of OH reactions with hydrocarbons in the 800-1400K range. Collisions undergone by the laser-excited species while in the upper electronic state both reduce the fluorescence yield and alter the spectral form of the signals. In order to obtain quantitative measurements, these collisional effects must be addressed, often on a state-to-state basis. The spectroscopic and collisional aspects of LIF as a combustion research tool will be discussed.

*Research in the area supported by Army Research Office, National Science Foundation, Department of Energy, and Wright Aeronautical Laboratories.

June 13-17, 1983

PAUL W. FAIRCHILD, GREGORY P. SMITH, AND DAVID R. CROSLEY

Rate constants for collisional quenching of the v'=0 level of the $A^2\Sigma^+$ state of the OH molecule have been measured at temperatures in the range 1000-1400 K. The OH was produced at these temperatures by a laser pyrolysis method,[1] in which a mixture of SF_6, H_2O_2 and the collision partner was irradiated by a pulsed CO_2 laser. The SF_6 absorbed the infrared radiation, rapidly heating the mixture and pyrolyzing the peroxide to OH radicals. The OH was pumped to the N'=6, J'=6 1/2, v'=0 level of the $A^2\Sigma^+$ state by a 10 nsec-long frequency doubled dye laser pulse fired 30 μsec after the CO_2 laser. Quenching rate constants were measured by the added gas pressure dependence of the fluorescence decay time.

The results, given as thermally averaged cross sections (A^2) at 1100 K are:

CO^*	H_2O^*	CH_4	NH_3	O_2^*	H_2^*	NO	N_2O	N_2^*	SF_6	CO_2^*
21	36	16	43	12	11	28	34	0.7	0.14	13

No significant temperature dependence was observed over the limited range covered, in agreement with expectations. However, the values are lower than room temperature literature values (which exist for colliders marked with an asterisk), except for H_2. The values for N_2 and SF_6 are conspicuously low.

Cross sections have been calculated with a collision complex model, where multipole attractive forces and a repulsive rotational barrier dominate the potential, a reformulation of an approach used for SO_2.[2] The experimental results for the first eight of the collision partners listed agree well (±25%) with the calculation, assuming 0.45 probability of quenching per capture collision.

This research was supported by the U.S. Army Research Office.

[1] P. W. Fairchild, G. P. Smith and D. R. Crosley, Nineteenth Symposium (International) on Combustion, The Combustion Institute, Pittsburgh, 1983, in press.

[2] D. L. Holtermann, E.K.C. Lee and R. Nanes, J. Chem. Phys. 77, 5327 (1982).

Address of Fairchild, Smith, and Crosley: Molecular Physics Laboratory, SRI International, Menlo Park, CA 94025

Time required: 15 min.

Session in which paper is recommended for presentation: 6 or 4

Abstract for an Invited Paper
for the San Francisco Meeting of the
American Physical Society
21-23 November 1983

Laser-Induced Fluorescence for Combustion Chemistry*

DAVID R. CROSLEY, Molecular Physics Laboratory, SRI International

In laser-induced fluorescence (LIF), the absorption of tunable laser radiation elevates a molecule to an electronically excited state which then emits. For those molecules which can be made to fluoresce, LIF is an extremely sensitive and highly selective means of detection. This category includes some 25 atomic, diatomic and triatomic free radicals which are reactive intermediates in combustion chemistry; the number continues to grow with new spectroscopic studies, the use of two-photon excitation, and the extension of lasers into the ultraviolet and infrared. Most LIF measurements in flames are made on a point-resolved basis, but planar, instantaneous images of OH in flames can also be obtained. Recently this method has been extended to provide two sequential images 100 μsec apart. In addition to detection of radicals directly in flames, LIF can be used for related chemical kinetics studies, as in a laser pyrolysis/LIF measurement of OH reactions with various hydrocarbons in the 800-1400 K temperature range. The status of LIF, and aspects of the underlying spectroscopic and collisional studies needed to provide quantitative measurements of flame radicals, will be discussed.

* Research in this area supported by the Army Research Office, National Science Foundation, Department of Energy, Wright Aeronautical Laboratories, and the National Aeronautics and Space Administration.

No. 229A

LASER FLAME DIAGNOSTICS

D. R. Crosley, Molecular Physics Laboratory, SRI International, Menlo Park, California 94025

The measurement of species concentrations and temperatures in combustion processes is one of the many research areas in which the use of laser techniques has had a large impact. In flames themselves, laser probes offer excellent spatial and temporal resolution and are highly species selective. They are nonintrusive in nature, so that neither the gas flow nor chemistry is perturbed, and can be used in hostile environments.

Several methods involving the absorption of tunable radiation can be used to measure with high sensitivity the transient species, often free radicals, which are present at low concentration in flames. These molecules, the intermediates in the combusion chemical networks, provide the crucial information for understanding the details of that chemistry. The most prominent of these techniques is laser-induced fluorescence (LIF), in which the absorption of laser radiation elevates the molecule to an electronically excited state which then emits. About 25 atomic, diatomic and triatomic free radical combustion intermediates have been detected by LIF in flames and/or flow systems. Optoacoustic detection of the absorbed laser energy, or subsequent laser ionization from the electronically excited state, form alternative means of detection of the selectively absorbed laser radiation in special cases in which the molecule does not fluoresce efficiently. The number of detectable species, and the types of combustion processes which can be probed, continues to grow with advances in laser techniques, such as multiphoton excitation and the extension of usable regimes of wavelength and pulse width.

The use of a planar sheet of radiation, formed with a cylindrical lens, permits two-dimensional images of the OH radical concentation throughout a flame to be obtained on a single laser pulse; this is in contrast to the customary beam configuration furnishing single-point measurements and it can be very useful in rapidly time-varying systems such as turbulent flames. Recently this method has been extended to provide two sequential images 100 μsec apart. In addition to detection of radicals directly in flames, LIF can also be used for related chemical kinetics studies, for example in discharge flow tubes and in a laser pyrolysis/LIF measurement of rate constants for the reaction of OH with various hydrocarbons in the 800-1400K temperature range. The present and likely future status of LIF and related methods for the measurement of flame radicals will be discussed.

Research in this area supported by Army Research Office, National Science Foundation, Department of Energy, Wright Aeronautical Laboratories and National Aeronautics and Space Adminstration.

LASER-INDUCED FLUORESCENCE MEASUREMENT OF SPIN-ORBIT SPLITTINGS IN EXCITED VIBRATIONAL LEVELS OF NCO ($X^2\Pi_i$)*

RICHARD A. COPELAND AND DAVID R. CROSLEY

In this study on NCO we use the combination of laser excitation and a CH_4/N_2O atmospheric pressure flame to furnish new high resolution spectroscopic information on a ground state transient molecule in excited vibrational levels. The linear NCO molecule is of interest both spectroscopically, since the $X^2\Pi_i$ state has a Renner-Teller split bending vibration with possible Fermi resonances, and chemically, as an intermediate in several combustion mechanisms.

We have undertaken a detailed investigation of these NCO ground state levels $0v_20$, $1v_20$, $2v_20$, $0v_21$, and $1v_21$ where v_2 varies from 0 to 2 in some cases. Spin-orbit splitting constants A, rotational constants and vibrational band origins are extracted for several previously unobserved vibrational levels. A preliminary fit to band head positions shows that the magnitude of A (in cm^{-1}, with typical 0.3 cm^{-1} error) decreases with v_1 and increases with v_3: A_{000}=-95.5; A_{100}=-90.0; A_{200}=-71.8; A_{001}=-97.3; A_{101}=-92.6. The Renner-Teller splitting also changes with stretching vibrations. Similar variations in the spin-orbit coupling constants are seen in $BO_2(X^2\Pi_g)$[1] and $NCS(A^2\Pi_i)$[2]. These molecules possess a strong Fermi interaction which may also contribute to the large spin-orbit splitting variations in the v_1 levels of the $X^2\Pi_i$ state of NCO.

*Supported by the U.S. Army Research Office, Contract No. DAAG29-80-K-0049.

[1]R. N. Dixon, D. Field and M. Noble, Chem. Phys. Lett. 50, 1 (1977); K. G. Weyer, R. A. Beaudet, R. Straubinger, and H. Walther, Chem. Phys. 47, 171 (1980).

[2]R. N. Dixon and D. A. Ramsay, Can. J. Phys. 46, 2619 (1968).

Address of Authors: Molecular Physics Department, SRI International, Menlo Park, CA 94025.

Time Required: 15 minutes.

*Session in which paper is recommended for presentation: Laser Spectra.

MP 84-036

ENERGY TRANSFER PATHWAYS FOR $A^2\Delta$ CH IN AN ATMOSPHERIC PRESSURE FLAME*

NANCY L. GARLAND AND DAVID R. CROSLEY

Vibrational energy transfer (V) and rotational energy transfer (R) within the $A^2\Delta$ state of CH has been studied in an atmospheric pressure CH_4/O_2 flame at ~2000 K. A laser pumps specific N' levels in v'=0 and fluorescence in the (1,0) and (0,0) bands is monitored. Excitation of N'=5 (E_N ~400 cm^{-1}) shows a partially rotationally relaxed distribution within v'=0 and very little v'=1 emission (ΔG ~2700 cm^{-1}); excitation of N'=13 (E_N ~2500 cm^{-1}) produces considerable transfer to v'=1 but less rotational redistribution than for the low rotational level. A more extensive map of relative R, V, and electronic quenching routes as a function of N' is in progress.

*Supported by the U.S. Army Research Office, Contract No. DAAG29-80-K-0049.

Address of Authors: Molecular Physics Department, SRI International, Menlo Park, CA 94025

Time Required: 15 min.

Session in which paper is recommended for presentation: Energy Transfer

MP 84-040

RATE CONSTANTS FOR USE IN MODELING

D. M. Golden and C. W. Larson
Department of Chemical Kinetics
SRI International, Menlo Park, CA 94025

ABSTRACT

The current status of quantitative understanding of reaction rate constant data for use in combustion mdeling is discussed. It is pointed out that simple bimolecular and unimolecular reactions can be tabulated as functions of various physically meaningful parameters over wide ranges of temperature and pressure. We also discuss the more complicated problems of complex surfaces and their manifestations. A major emphasis is on the underlying framework for critical evaluation of rate data.

We point out that currently used values for $2CH_3 \xrightarrow{k} + C_2H_5 + H$ are incorrect and that the temperature dependence of the branching ratio $H + N_2O \begin{cases} \rightarrow NH + NO \\ \rightarrow OH + N_2 \end{cases}$ can be understood as consequence of angular momentum conservation.

---

*This work was supported by the U.S. Army Research Office, Contract No. DAAG29-80-K-0049.

LASER-INDUCED FLUORESCENCE SPECTROSCOPY OF NCO AND NH_2 IN ATMOSPHERIC PRESSURE FLAMES

Richard A. Copeland, David R. Crosley and Gregory P. Smith
Chemical Physics Laboratory
SRI International
Menlo Park, California 94025

Laser-induced fluorescence (LIF) is a powerful method for the sensitive detection of trace species in flames, so as to gain insight into the combustion chemistry mechanisms. However, LIF has been applied almost exclusively to diatomic radicals whereas the chemical networks contain many species of larger size whose presence can signal definite mechanistic paths. We describe here a comprehensive survey of the LIF spectroscopy of the NCO molecule in a CH_4/N_2O flame and the NH_2 molecule in NH_3/N_2O and NH_3/O_2 flames, all burning rich at atmospheric pressure. NCO was excited in the B-X and A-X systems in the ultraviolet and blue, respectively; the latter is much more intense and can be more easily made free of strong interfering transitions due to diatomics. NH_2 was excited in the $\tilde{A} - \tilde{X}$ transition. Excitation and fluorescence wavelengths furthest to the red minimize background interference due to underlying, unidentified absorption features and flame emission. Prescriptions for detecting these two species are presented, including a table of excitation and detection wavelengths, as well as some general conclusions which should be useful in extending flame LIF detection to other triatomic and larger radicals.

MP84-005

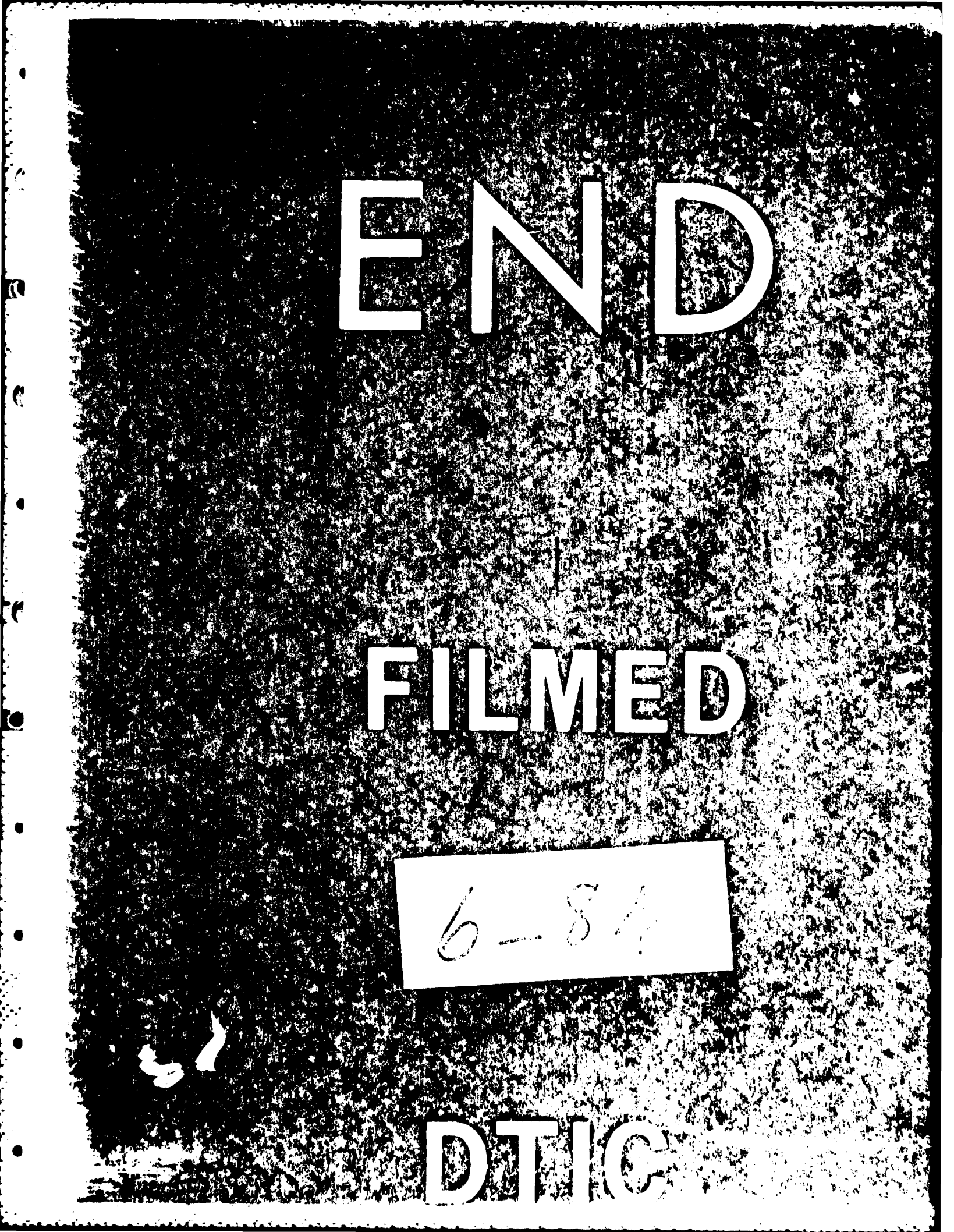
END
FILMED
6-84
DTIC